VYSOKÁ ŠKOLA CHEMICKO-TECHNOLOGICKÁ V PRAZE

Fakulta chemické technologie

Ústav polymerů

Habilitační práce

Biodegradovatelné polymery – od syntézy po degradaci

Autor: Mgr. Soňa Hermanová, Ph.D.

Praha 2019

PROHLÁŠENÍ

Prohlašuji, že jsem tuto práci vypracovala samostatně a že jsem řádně citovala veškeré informační prameny a literaturu. Byla jsem seznámena s tím, že se na moji práci vztahují práva a povinnosti vyplývající ze zákona č. 121/2000 Sb., o právu autorském, o právech souvisejících s právem autorským a o změně některých zákonů (autorský zákon). Souhlasím se zveřejněním své práce podle zákonu č. 111/1998 Sb., o vysokých školách, ve znění pozdějších předpisů.

V Praze dne 8. listopadu 2019

……..

Poděkování

Děkuji svým rodičům za celoživotní laskavou podporu a pomoc. Z kolegů patří poděkování Zdeňku Soferovi, Martinu Pumerovi a Janu Mernovi z VŠCHT za intenzivní spolupráci při společném výzkumu v oblasti imobilizací proteinů, polymerních mikromotorů a polymerů jako nosičů léčiv.

Souhrn

Alifatické polyestery, polykarbonáty a jejich kopolymery představují nejvíce studované biodegradovatelné syntetické polymery. V této habilitační práci je pozornost věnována (1) přípravě biodegradovatelných polyesterů a polykarbonátů s definovanou délkou řetězců a koncovými skupinami, (2) přípravě telechelických polymerů a amfifilních blokových kopolymerů a (3) studiu mechanismů biodegradace a abiotické degradace ve vztahu ke struktuře materiálu. Syntetizované materiály byly studovány jak z hlediska možnosti přípravy autonomně se pohybujících mikromotorů tak mikro/nanočástic se schopností enkapsulace fluorescenčních barviv a biomolekul DNA. Studie enzymatické a abiotické hydrolýzy polyesterů vedly k získání poznatků o vlivu nadmolekulární struktury a přítomnosti plniva na bázi oxidu grafitu na mechanismus degradace. V případě alifaticko-aromatických kopolyesterů byla pro biodegradaci rozhodující vedle jejich počátečního složení také přítomnost specifických mikroorganismů v prostředí kalů a kompostu.

Summary

Aliphatic polyesters, polycarbonates and their copolymers represent the most extensively studied biodegradable synthetic polymers. This Thesis is focused on (1) the preparation of biodegradable polyesters and polycarbonates with controlled chain length and chain end groups, (2) the preparation of telechelic polymers, and amphiphilic block copolymers, and (3) the study of mechanism of the biodegradation and abiotic degradation in the relation with the material structure. Synthesized materials were studied for their potential to constitute both autonomously propelling micromotors and micro/nanoparticles with the encapsulation capability of fluorescent dyes and DNA biomolecules. Studies of polyesters' abiotic and enzyme-catalysed hydrolysis afforded deeper knowledge of the impact of morphology and the presence of graphite oxide-based filler on the degradation mechanism. In the case of aliphatic-aromatic copolyesters, the presence of specific microorganisms in sludge and compost soil played an important role in addition to the starting material composition.

Obsah

1 Úvod

Alifatické polyestery a polykarbonáty a jejich kopolymery představují biokompatibilní, biodegradovatelné a resorbovatelné materiály, které mohou být syntetizovány s vlastnostmi šitými „na míru“ pro konkrétní aplikace zahrnující jak biomateriály (skafoldy, stenty, implantáty, chirurgické nitě) tak systémy nosičů léčiv a biologicky aktivních látek.[1] Dobře prostudovanou cestou pro přípravu (ko)polyesterů a polykarbonátů s řízenou mikrostrukturou a úzkou distribucí molárních hmotností je koordinační polymerace za otevření kruhu cyklických esterů/karbonátů katalyzovaná/iniciovaná organokovovými sloučeninami.[2] Od relativně jednoduchých homoleptických sloučenin cínu, zinku a hliníku byl výzkum zaměřen na přípravu takzvaných „single-site“ katalyzátorů. Můžeme je popsat obecným vzorcem L_nMX, kde M je centrální atom kovu, X nejčastěji alkoxidová skupina a L_n představuje ligandy, které se nepodílejí přímo na růstové reakci, ale stericky a elektronově ovlivňují centrální atom a brání agregaci komplexů.[3] V práci [**P1**] jsme studovali potenciál komplexu dimethylaluminia [$AlMe_2\{\kappa^2$-O,O′-[4,5-$(P(O)Ph_2)_2$tz]}] s O,O′-bidentátním 4,5-bis(difenylfosforanyl)-1,2,3-triazolovým ligandem pro polymerace ε-kaprolaktonu v přítomnosti vybraných alkoholů jako iniciátorů a ověřili jsme také možnost přípravy blokových kopolymerů za iniciace poly(ethylenoxidem), (PEO).

Vedle tradiční organokovové katalýzy vstoupila do popředí polymerací laktonů a laktidů také chemoselektivní organokatalytická polymerace za otevření kruhu.[4, 5] Hedfords a kol. v roce 2005 připravili enzymaticky katalyzovanou polymerací ε-kaprolaktonu za využití 2-sulfanylethanolu jako iniciátoru poly(ε-kaprolakton), PCL s koncovými thiolovými (-SH) skupinami.[6] Díky těmto reaktivním skupinám bylo možné vázat na polymerní řetězce nanočástice platiny, zlata a oxidů železa a připravit tak hybridní materiály polymer/kov s novými vlastnostmi.[7] V práci [**P2**] jsme se zabývali přípravou sférických nanočástic pro enkapsulaci fluorescenčního barviva - Nilské červeni (NR) a přípravou mikročástic pokrytých vrstvou platiny, vycházejíce v obou případech z PCL s koncovými hydroxy a thiolovými skupinami. Prokázali jsme, že Pt/PCL mikročástice, autonomně se pohybující v roztoku peroxidu vodíku, jsou schopny po kolizi s PCL nanočásticemi je zachytit a transportovat.

Mezi nejvíce studované kopolymery biodegradovatelných polyesterů a polykarbonátů patří amfifilní blokové kopolymery s hydrofilním blokem na bázi biokompatibilního PEO, které mají schopnost se samouspořádat ve vodě jako selektivním rozpouštědle.[8] PEO vystupuje při polymeraci za otevření kruhu cyklických esterů/karbonátů jako makroiniciátor a podle počtu koncových hydroxy skupin poskytuje nejčastěji diblokové nebo triblokové kopolymery typu

A-*b*-B nebo A-*b*-B-*b*-A. V práci [**P3**] jsme připravili sérii kopolymerů s centrálním PEO blokem a hydrofobními bloky na bázi alifatického poly(trimethylenkarbonátu), (PTMC) s rozdílnou délkou řetězců a studovali jsme vliv složení na schopnost krystalizace bloků v závislosti na tepelné a mechanické historii.

Vedle syntézy materiálu s vlastnostmi vhodnými pro konkrétní aplikaci je u biodegradovatelných polymerů značná výzkumná pozornost věnována také studiu mechanismů a kinetiky degradace z důvodu přípravy kontrolovaně rozložitelných materiálů po uplynutí jejich funkční doby za vzniku netoxických produktů. Alifatické polyestery/polykarbonáty díky přítomnosti esterových/karbonátových vazeb v řetězcích podléhají abiotické hydrolýze či enzymaticky katalyzované degradaci vedoucí ke vzniku rozpustných oligomerních produktů.[9] V polymerním vzorku nerozpustném ve vodě probíhá hydrolýza podle rychlosti difúze molekul vody do polymerní matrice buď současně v celém jeho objemu, nebo se uplatňuje pouze v povrchové vrstvě jako eroze.[10] O uplatnění daného mechanismu rozhoduje vedle vlastního chemického okolí hydrolyzované vazby především nadmolekulární struktura (obsah krystalické fáze), molární hmotnost, poměr plochy povrchu k objemu vzorku a přítomnost enzymů v degradačním médiu.[11] V pracích [**P4-P6**] jsme se věnovali studiu mechanismů (bio)degradace PCL filmů v závislosti na způsobu přípravy a odlišné morfologie, bimodální distribuci molárních hmotností a přítomnosti plniva na bázi oxidu grafitu.

Při modelových studiích se z enzymů na štěpení vazeb v řetězcích PCL a PTMC (ko)polymerů uplatňují typicky lipasy, které přirozeně katalyzují hydrolýzu triacylglycerolů na fázovém rozhraní olej/voda.[12] V případě poly(laktidu), (PLA) byla prokázána degradace aktivitou proteasy.[13] V práci [**P7**] jsme působením proteinasy K za definovaných podmínek reprodukovatelně docílili degradace nevodivého polymerního povrchu a zpřístupnění vnitřní matrice s vodivým grafenovým plnivem pro využití kompozitu PLA a grafenu ve formě 3D-vytištěných elektrod v elektrochemii.

V pracích [**P8-P10**] jsme studovali mechanismus biodegradace alifaticko-aromatických kopolyesterů na bázi použitého poly(ethylentereftalátu), (PETP) modifikovaného zabudováním laktátových jednotek. Kopolyestery byly degradovány za termofilních podmínek (55-58° C) jednak ve vyhnilém kalu a kompostu a jednak v roztocích pufrů pro vyhodnocení abiotické hydrolýzy. Biologické testy fytotoxicity laboratorního kompostu po degradaci kopolyesterů neprokázaly toxické účinky rozpustných degradačních produktů, což je naprosto zásadní předpoklad pro kompostovatelné odpadní materiály.

2 Komentář k vybraným publikacím

2.1 Syntéza polyesterů a jejich kopolymerů a příprava polymerních nanočástic

Příprava poly(ε-kaprolaktonu) s definovanými koncovými skupinami

Isopropoxidy hliníku [Al(O-*i*-Pr)$_3$] jsou známy více než čtyři desetiletí jako tradiční iniciátory koordinační polymerace laktonů za otevření kruhu.[14] Nevýhodou těchto jinak dobře dostupných a netoxických sloučenin je zejména na rozpouštědle a teplotě závislá agregace vedoucí ke vzniku trimerních (A_3) a tetramerních struktur (A_4) s rozdílnou polymerizační aktivitou.[15] Pozdější generace heteroleptických komplexních katalyzátorů obsahovaly dobře modifikovatelnou ligandovou sféru, která minimalizovala jak vznik agregátů tak nežádoucí postranní transesterifikační reakce na růstovém centru.

Mezi stabilní monometalické komplexy patřil komplex dimethylaluminia [AlMe$_2${κ^2-O,O′-[4,5-(P(O)Ph$_2$)$_2$tz]}] (**1**), který vznikl koordinací obou kyslíkových atomů 4,5-bis(difenylfosforanyl)-1,2,3-triazolového ligandu k centrálnímu kovu Al(+III) za vytvoření sedmičlenné cyklické struktury[16]. V práci [**P1**] jsme studovali aktivitu tohoto komplexu pro polymerace za otevření kruhu ε-kaprolaktonu (ε-CL) v roztoku chlorbenzenu při 40 a 60° C. Vznik polymeračně aktivní alkoxidové vazby na centrálním kovu byl docílen alkoholýzou komplexu **1** bezvodým alkoholem (1 ekv. k komplexu **1**) *in situ* v roztoku, do kterého byl po 30 min dávkován monomer (**Obr. 1**). O vzniku aktivního centra a inzerce molekuly ε-CL do alkoxidové vazby svědčil vznik polymerů zakončených methyl-, isopropyl- a benzylesterovými skupinami.

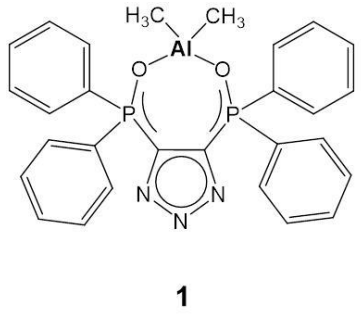

1

Koiniciátor	**Iniciátor**
MeOH	Al—O—**CH3**
i-PrOH	Al—O—CH(CH$_3$)$_2$
BnOH	Al—O—CH$_2$—C$_6$H$_5$
OH-PEO-OH	Al—O—(CH$_2$—CH$_2$—O)$_9$—H

Obr. 1 Struktura studovaného komplexu a iniciátory pro polymerace ε-CL

U studovaného systému probíhaly řízeně pouze polymerace iniciované komplexem **1** s benzyloxidovým ligandem při počáteční koncentraci monomeru 0,5 M (200 násobek monomeru k iniciátoru) a v rozmezí 40 - 60° C za vzniku polymerů s nízkou disperzitou ($Đ$ =

1.2) a molární hmotností nastavitelnou poměrem monomeru k iniciátoru a konverzí. U řady alkoxidových komplexů hliníku bylo prokázáno, že benzylalkohol (BnOH) působí jako přenašeč polymerního řetězce z růstového centra za vzniku nového iniciačního centra Al-OBn. Také v našem případě vedl dvojnásobek BnOH (2 ekv. k **1**) po 6 h polymerace ke vzniku polymeru o přibližně poloviční molární hmotnosti a nižší disperzitě (M_n = 6 kg·mol^{-1}, $Đ$ = 1,1) než při ekvimolárním poměru BnOH a komplexu **1** (M_n = 11 kg·mol^{-1}, $Đ$ = 1,2), což potvrzovalo přenosovou reakci. Vedle řízené syntézy PCL s definovanými koncovými skupinami a délkou řetězců byl pomocí komplexu **1** a makroiniciátoru dihydroxy PEO, o molární hmotnosti 400 g·mol^{-1} připraven triblokový kopolymer PCL-*b*-PEO-*b*-PCL o M_n = 37 kg·mol^{-1} a $Đ$ = 1,5.

Biodegradabilní polymerní mikromotory

PCL je biodegradovatelný a biokompatibilní alifatický polyester, který díky možnosti funkcionalizace řetězce a variabilitě tvorby od 2D lamelárních struktur, nanovláken až po mikro/nanosféry našel uplatnění v oblasti autonomně se pohybujících chemických mikro- a nonomotorů.[17] V práci [**P2**] jsme na základě chemoselektivity enzymatického katalyzátoru vůči sulfanylalkoholu při iniciaci polymerace připravili α-hydroxy-ω-thio funkcionalizovaný PCL o M_n = 10 kg·mol^{-1} a $Đ$ = 1,5. Z tohoto polymeru byly metodou odlití z roztoku připraveny tenké fólie, na jejichž povrch byla nanesena vakuovým napařováním vrstva platiny (~ 40 nm). Působením ultrazvukové lázně byl film v důsledku nízké molární hmotnosti polymeru dezintegrován na nepravidelné mikročástice dlouhé 35-125 μm s průměrnou tloušťkou 400 nm, které se zavinuly za vzniku tubulární struktury (**Obr. 2**). Jelikož Pt vrstva katalyzovala rozklad peroxidu vodíku za vzniku kyslíku, tyto mikročástice byly schopné využívat bublinky plynu jako pohon a autonomně se pohybovaly v 1% vodném roztoku H_2O_2 s rychlostí 43±14 μm·s^{-1}. Pro srovnání v dosud publikovaných studiích polymerní lamely[18] a mikrosféry[19] na bázi PCL-SH s vázanými nanočásticemi Pt dosahovaly obdobné rychlosti při 10 a 15% koncentraci H_2O_2 ve vodě. Vyšší výkon mikromotorů lze vysvětlit sférolitickou morfologií povrchu PCL filmů, která byla vytvořena krystalizací při odpařování rozpouštědla a představuje vyšší povrch pro depozici Pt než hladký, amorfní povrch.

Mezi klíčové funkce mikro- a nanomotorů patří jednak zachycení a transport biomolekul a buněk z biologických vzorků anebo naopak transport a uvolnění kontrastní látky, léčiva nebo fluorescenčního barviva v cílové tkáni nebo prostředí.[20] V naší studii byly z téhož výchozího polymeru připraveny nanosféry o velikosti 400 nm (disperzita 0,3) za enkapsulace

modelového hydrofobního barviva NR. Připravené nanosféry obsahovaly 2 μg NR/1mg PCL-SH. Tubulární mikromotory při srážce zachycovaly nanosféry chemisorpcí thiolových skupin na povrchu platiny[21] a transportovaly je dále během svého pohybu.

K uvolnění barviva dochází difúzí při hydrolytické degradaci nanosfér, která je významně urychlena enzymatickou katalýzou. Lipasy však štěpí i esterové vazby v mikromotoru, kde však degradace probíhá mnohem pomaleji díky semikrystalickému charakteru. Mikroskopické analýzy prokázaly, že nanosféry a mikromotory podstupovaly hydrolytickou degradaci působením lipasy izolované z *Rhizopus arrhizus* rozdílnou rychlostí. V naší studii byl tedy navržen a prokázán koncept biodegradovatelného mikromotoru jako nosiče biodegradovatelných nanočástic s enzymaticky řízenou rychlostí degradace.

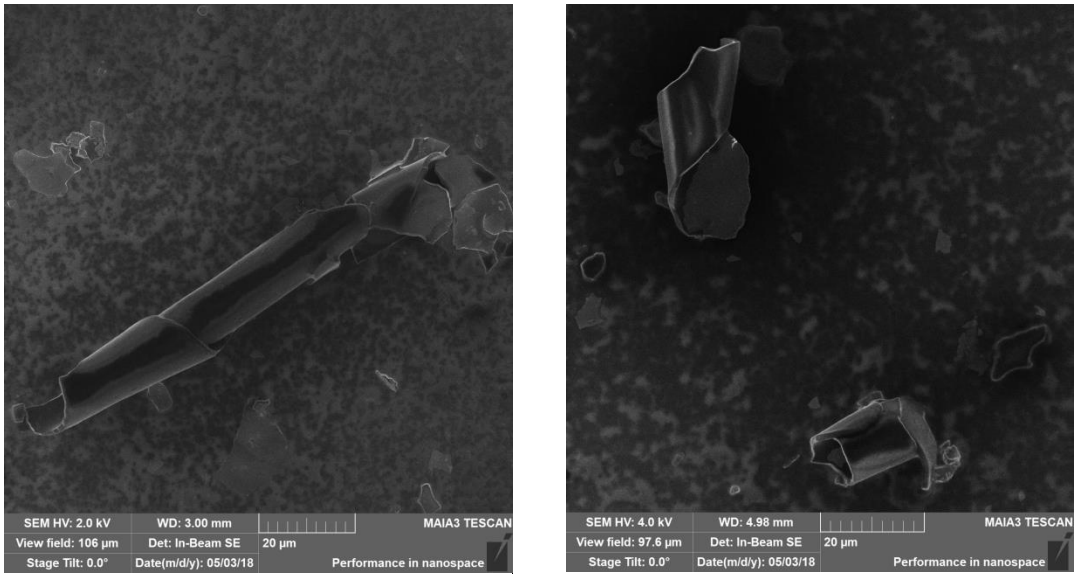

Obr. 2 SEM snímky tubulárních mikromotorů vzniklých desintegrací a svinutím PCL filmu pokrytého vrstvou Pt.

Amfifilní triblokové kopolymery

Amfifilní blokové kopolymery s polykarbonátovým hydrofobním blokem nebyly dosud tak intenzivně zkoumány jako kopolymery s polyesterovými hydrofobními bloky typicky tvořenými PCL nebo PLA.[22, 23] V práci [**P3**] jsme připravili sérii 7 triblokových kopolymerů PTMC-*b*-PEO-*b*-PTMC polymerací trimethylenkarbonátu (TMC) katalyzovanou bezvodým HCl v dietyléteru a za iniciace dihydroxy-terminovanými PEO o molárních hmotnostech 1, 2 a 4 kg·mol^{-1}. Připravené blokové kopolymery nabývaly molární hmotnosti M_n 5-9 kg·mol^{-1} a

$Đ \leq 1{,}20$ a obsahovaly v souladu se složením polymerační násady 7-67 mol. % TMC jednotek v řetězcích. U připravených kopolymerů byly studovány termické vlastnosti a zejména schopnost krystalizace, neboť krystalinita významně ovlivňuje fyzikální a chemické vlastnosti polymerního materiálu. Zatímco homopolymerní PTMC je všeobecně v odborné literatuře považován za amorfní elastomer se schopností krystalizace pod napětím, PEO je semikrystalický a jeho schopnost krystalizace v kopolymeru souvisí s celkovým zastoupením komonomerních jednotek a délkou řetězců[24].

Rentgenová prášková difrakce (WAXD) prokázala přítomnost krystalické fáze v homopolymeru PTMC (M_n =3 kg·mol^{-1}, $Đ$ = 1,20), který byl připraven jako referenční materiál za využití stejného iniciačního systému a benzylalkoholu jako iniciátoru. Na základě srovnání s difraktogramy PTMC a PEO homopolymerů byla u kopolymerů s více než 42 mol. % TMC jednotek zjištěna difrakční maxima krystalické fáze PTMC bloků. Přítomnost krystalických fází jak PTMC tak PEO bloků byla potvrzena pro kopolymer s 39 mol. % TMC jednotek a při jejich nižším poměrném zastoupení došlo ke krystalizaci pouze PEO bloku.

Výsledky diferenciální skenovací kalorimetrie prokázaly převážně amorfní charakter PTMC homopolymeru, neboť endoterm tání při 33°C (37 J·g^{-1}) patrný při prvém ohřevu, již po druhém ohřevu nebyl nalezen a materiál vykazoval teplotu skelného přechodu T_g = -25 °C. K upořádání řetězců došlo pouze při dostatečně dlouhé době krystalizace amorfní matrice PTMC. Stejně tak kopolymery obsahující 39-67 mol. % TMC jednotek byly amorfní, se schopností dokrystalizace amorfního podílu v závislosti na tepelné a mechanické historii vzorku. V souladu s výsledky rentgenové strukturní analýzy vykazovaly kopolymery obsahující 7-36 mol. % TMC jednotek v důsledku pravidelného uspořádání PEO řetězců krystalický charakter nezávisle na historii vzorku. Obsah krystalické fáze PEO bloků kopolymerů byl však vždy nižší než samotných PEO homopolymerů o stejné molární hmotnosti.

Klíčovou vlastností blokových amfifilních kopolymerů je schopnost samouspořádání se do agregátů nabývajících od sférické morfologie s hydrofobním jádrem a hydrofilním pláštěm po polymersomy, ve kterých kopolymerní membrána obaluje vnitřní kavitu vyplněnou vodou.[25] Z kopolymerů o hraničním složení komonomerních jednotek (7 a 67 mol. % TMC jednotek) byly připraveny nanosféry o velikosti do 130 nm s disperzitou ≤ 0.2 a záporným zeta-potenciálem (-30 mV). Analýzou dynamickým rozptylem světla (DLS) byla prokázána ochota

nanočástic podstupovat enzymatickou degradaci lipasou izolovanou z *Mucor miehei*, přičemž mechanismus a rychlost degradace byly ovlivněny složením kopolymeru.

Metodou odpařování rozpouštědla byl docílen vznik polymersomů, do kterých byla úspěšně enkapsulována DNA se 70% enkapsulační účinností (**Obr. 3**). Prokázali jsme tak potenciál studovaných kopolymerů jako biodegradabilních nosičů biomolekul.

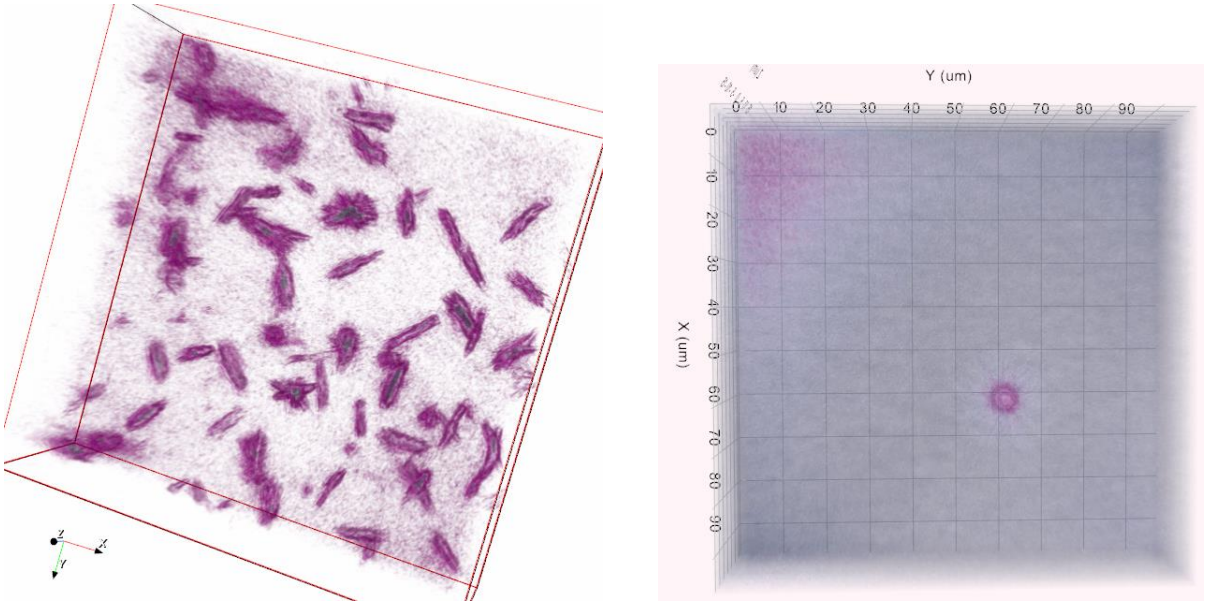

Obr. 3 Tomografické mikroskopické snímky kopolymerních vesikul s enkapsulovanou DNA (Nanolive 3D Cell Explorer)

2.2 (Bio)degradace alifatických polyesterů

Vliv morfologie povrchu a distribuce molárních hmotností na mechanismus degradace

Studie vlivu složení a struktury (ko)polymerního materiálu na mechanismus hydrolytické degradace jsou často prováděny *in vitro* v přítomnosti modelového enzymu v roztoku pufru o konstantním pH při 25-37 °C a za pravidelné výměny média s degradačními produkty.[26] Případná rozdílná reaktivita esterových vazeb v řetězcích vůči enzymatické hydrolýze by byla jasně uplatnitelná v roztoku. V pevném, ve vodě nerozpustném polymerním filmu probíhá enzymatická degradace v povrchové vrstvě na rozhraní fází, kde svoji roli hraje dostupnost vazeb v amorfních či krystalických segmentech s rozdílnou mobilitou. Mechanismus štěpení vazeb je ovlivněn i specifitou zvoleného enzymu, kdy enzym katalyzuje přednostně štěpení vazby v blízkosti konců řetězců anebo hydrolýzu vazeb náhodně podél řetězců. Proto je vedle prosté enzymatické hydrolýzy (ko)polymerní materiál laboratorně degradován za

definovaných podmínek také v médiu obsahujícím izolované mikrobiální kmeny z důvodu produkce celé řady extracelulárních enzymů s různou specifitou *in situ*.[27] Při vlastních degradačních studiích jsme tedy vycházeli z metod popsaných v literatuře za využití enzymů a mikroorganismů, které se nám jevili jako perspektivní při předběžných testech.

V práci [**P4**] jsme studovali vliv počáteční morfologie PCL filmů (M_n =18 kg·mol^{-1}, $Đ$ = 2,7) na průběh jejich degradace lipasou z *Aspergillus oryzae*. Filmy o tloušťce ~100 μm byly připraveny jednak lisováním (CM) a jednak odlitím z roztoku a odpařením rozpouštědla (SC). O uplatnění enzymatické degradace u obou typů vzorků formou eroze povrchu svědčily úbytky hmotnosti, vznik trhlin a malý pokles hmotnostně průměrné molární hmotnosti M_w o 10 % po 42 dnech inkubace. Zatímco u CM filmu došlo pravděpodobně k náhodnému štěpení esterových vazeb v amorfních doménách na povrchu filmu, u SC filmů byly přednostně štěpeny pro enzym dostupné vazby v amorfní mezivrstvě v prostoru mezi lamelami sférolitů. Interlamelární amorfní vrstva obsahuje zvýšenou koncentraci koncových karboxylových a hydroxylových skupin níže-molekulárních řetězců vyloučených z krystalizace[28], což by vysvětlovalo selektivitu působení enzymu v důsledku analogie s nízkomolekulárními substráty. Sekundární krystalizace polymerních segmentů, které původně spojovaly jednotlivé lamely, poté vedla u SC degradovaného filmu dokonce k 40% nárůstu podílu krystalické fáze.

V práci [**P5**] jsme zkoumali mechanismus hydrolytické degradace PCL s bimodální distribucí molárních hmotností (M_n ~20 kg·mol^{-1}, $Đ$ = 6,5-6,8) ve formě filmů o tloušťce ~100 μm připravených odlitím z roztoku. Laboratorní testy byly vedeny jednak za podmínek enzymatické hydrolýzy jako v předchozí práci [**P4**] a jednak působením bakteriálního kmene *Bacillus subtilis* (CCM 1999) v živném médiu. Mikroorganismus *Bacillus subtilis* produkoval extracelulární enzymy *in situ* v důsledku přídavku malého množství olivového oleje jako přirozeného substrátu s esterovými vazbami. V případě bakteriální degradace byl prokázán mechanismus náhodného štěpení esterových vazeb podél řetězců, kdy nejdelší řetězce degradují rychleji než kratší, což se projevilo snížením počáteční M_w o 70 % za vzniku monomodální distribuční křivky s novým, narůstajícím píkem oligomerních produktů štěpení.

U enzymatické degradace lipasou z *Aspergillus oryzae* vedle poklesu početně průměrné molární hmotnosti M_n o 25 % došlo naopak k vzrůstu disperzity ($Đ$ = 7,5), což svědčí o mechanismu štěpení esterových vazeb v blízkosti konců řetězců vedoucím k depolymeraci. Znamenalo by to, že kratší řetězce depolymerují rychleji než dlouhé, které nepřispívají k sekundární krystalizaci, a podíl krystalické fáze dokonce mírně klesl.

Vliv přítomnosti oxidu grafitu jako plniva na mechanismus degradace

V práci [**P6**] jsme se zabývali studiem vlivu přítomnosti plniva oxidu grafitu (GO) na mikrobiální degradaci PCL filmů (M_n = 18 kg·mol^{-1}, $Đ$ = 1,5). Disperze GO plniva byla v první kroku smíšena s roztokem PCL a po odpaření rozpouštědla byla směs lisována za vzniku filmu o tloušťce ~250 μm a s obsahem plniva 2,7 % (GO/PCL film). Termická analýza potvrdila, že GO plnivo působilo v PCL matrici jako nukleační činidlo, což vedlo ke zvýšení teploty tání i teploty krystalizace kompozitu oproti samotnému PCL.

Pro degradaci byl použit mikrobiální kmen *Bacillus subtilis*, ovšem vzorky byly degradovány za třepání v médiu obsahujícím pouze glukosu jako počáteční, dostupný zdroj uhlíku, a navíc bez pravidelné výměny média. Úbytky hmotnosti a vznik trhlin na povrchu filmů svědčily o uplatnění se abiotické i enzymatické hydrolytické degradace v povrchové vrstvě jak PCL tak GO/PCL filmu. Jelikož počáteční hodnota pH = 7 degradačního média v důsledku metabolické aktivity mikroorganismu rostla v pozdější fázi experimentu do alkalické oblasti (pH = 8,5-9,0), nešlo vyloučit synergické působení bazicky katalyzované hydrolýzy[29] vedle enzymatické degradace. Lze však konstatovat, že GO plnivo neovlivňuje mechanismus degradace PCL filmu, neboť u obou PCL i GO/PCL degradovaných filmů došlo v důsledku štěpení řetězců ke srovnatelnému posunu maxima chromatografických elučních křivek do níže-molekulární oblasti za vzniku nových píku oligomerních produktů. Na druhou stranu nižší úbytky hmotností degradovaného GO/PCL filmu oproti samotnému PCL svědčí o nižší rychlosti enzymatické hydrolýzy. Je známo, že GO umožňuje díky především hydrofobním a částečně také elektrostatickým interakcím imobilizaci řady lipas[30], které se v důsledku konformačních změn mohou stát méně přístupné pro makromolekulární substráty.

Podíl krystalické fáze u obou degradovaných filmů vzrostl. Lze shrnout, že degradace probíhala v amorfních doménách jednak za vzniku rozpustných oligomerů a jednak za vzniku nerozpustných řetězců původně nezačleněných do primárních krystalů a schopných se reorganizovat. Nárůst krystalinity byl zaznamenán u řady degradovaných biodegradabilních polyesterů a experimentální data korelují s matematickým modelem krystalizace původně amorfních řetězců indukované jejich štěpením.[31, 32]

Enzymatická degradace 3D elektrody z kompozitu poly(laktidu) s grafenovým plnivem

Filament, komerčně dostupný pod obchodním názvem Black Magic filament na bázi PLA matrice s grafenovým plnivem (8% podle výrobce), je možné technologií 3D tisku tavenou

strunou zpracovat do tvaru elektrod a senzorů. Nevýhodou těchto cenově přijatelných a na míru tvarovaných elektrod je nízká nebo nulová odezva kvůli povrchové vrstvě nevodivého polymeru. Elektrodu je možné aktivovat krátkým vystavením dimethylformamidu (DMF) za rozpuštění určitého podílu PLA.[33] DMF je však toxické výše-vroucí rozpouštědlo, které je nutné z materiálu odstranit prodlouženým sušením za vyšší teploty a sníženého tlaku. V práci [**P7**] jsme se proto zabývali povrchovou erozí PLA/grafenové elektrody připravené technologií 3D tisku působením enzymu proteinasy K (*Tritirachium album*). Elektrody byly vystaveny působení enzymu v Tris-HCl pufru o pH = 8 při 37° C za třepání a pravidelné výměny média s enzymem každých 24 h. Elektrody během počáteční 4 h fáze absorbovaly vodu, přičemž nasákavost v roztoku s enzymem byla vyšší (7 %) než v samotném kontrolním pufru (4 %), v důsledku rychlejší enzymatické hydrolýzy za vzniku hydrofilních karboxylových a hydroxylových skupin. V dalším čase již pouze u enzymaticky degradovaných vzorků docházelo ke vzniku rozpustných oligomerních produktů, které difundovaly do roztoku za celkového 4% úbytku hmotnosti vzorku (po vysušení) po 28 h. Prodloužená doba enzymatické degradace byla vyloučena, neboť po 72 h v důsledku pokračující degradace z povrchové vrstvy do celého objemu došlo ke ztrátě integrity elektrody. Enzymaticky degradovaná elektroda, testována redoxním systémem ferrokyanid/ferrikyanid vykazovala přibližně 40% nárůst rychlosti přenosu elektronů oproti elektrodě vystavené DMF rozpouštědlu. Znamená to tedy, že vytvoření porézního povrchu enzymatickou hydrolýzou vede k zachování makroskopických rozměrů, neboť probíhá pouze v povrchové vrstvě, přitom však za dosažení větší plochy měrného povrchu zpřístupněného grafenového plniva.

2.3 Biodegradace alifaticko-aromatických kopolyesterů

Zatímco alifatické polyestery podstupují abiotickou i enzymatickou hydrolýzu v relativně krátkém časovém horizontu, polyestery s aromatickými jednotkami v řetězcích jako poly(ethylentereftalát), (PETP) degradují v přírodních podmínkách velmi pomalu tak, že prakticky nejsou považovány za biodegradovatelné. Koncept alifaticko-aromatického kopolyesteru Ecoflex (BASF, Německo) získaného transesterifikačními reakcemi poly(butylentereftalátu), butan-1,4-diolu a adipové kyseliny inspiroval řadu výzkumných skupin k vývoji a výzkumu biodegradabilních materiálů za využití odpadního PETP například z lahví.[34-37] Alifaticko-aromatické kopolyestery byly připraveny buď analogicky

transesterifikačními reakcemi anebo depolymerací PETP a následnou kopolymerací s laktony, laktidy či mléčnou kyselinou. Výsledné materiály si zachovaly přijatelné mechanické a zpracovatelské vlastnosti za zvýšené ochoty podstupovat abiotickou či enzymaticky katalyzovanou hydrolýzu. Problematikou biodegradabilních kopolyesterů z použitého PETP se zabývala také výzkumná skupina doc. Prokopové působící na Ústavu polymerů VŠCHT Praha před mým nástupem se zacílením na podmínky syntézy za využití polykondenzační aparatury.[38-40]

Naše prvotní studie biodegradací modifikovaných alifaticko-aromatických kopolyesterů vycházely z použití mikrobiálních kmenů a podmínek, které jsme již úspěšně ověřili pro biodegradace alifatických polyesterových filmů.[41] Kopolyesterové fólie obsahující 42 mol. % aromatických a 58 mol. % laktátových jednotek však byly zcela inertní vůči působení lipasových enzymů izolovaných z *Candida rugosa*, *Aspergillus niger*, *Rhizopus arrhizus*, *Penicillium roqueforti*, *Mucor miehei* a *Thermomyces lanuginosus* po dobu 21 dní při teplotě 25 a 37° C. Stejně tak inkubace s půdní bakterií *Bacillus subtilis*, mikromycétním kmenem *Rhizpus arrhizus* a ligninolytickou houbou *Phanerochaete chrysosporium* nevedla k detekovatelnému hydrolytickému štěpení v povrchové vrstvě fólií. Pouze při inkubaci kopolyesterových fólií za zvýšené teploty 55° C v živném médiu se v důsledku zvýšené mobility řetězců uplatnila abiotická hydrolýza nejdelších řetězců za poklesu molární hmotnosti a to nezávisle na přítomnosti termofilního bakteriálního kmene *Geobacillus stearothermophilus*. Bylo tedy zřejmé, že biodegradační studie je nezbytné provádět v úzkém intervalu mezi teplotou degradace a T_g kopolyesterové matrice pro dostatečnou mobilitu segmentů a ideálně také v prostředí se zvýšenou koncentrací hydroxidových iontů. Z řady studií je známo, že alifatické polyestery a typicky PLA ochotně podstupují bazicky katalyzovanou abiotickou hydrolýzu v prostředí o hodnotě pH ~9.[42]

Studium biodegradace alifaticko-aromatických kopolyesterů v kalu

V práci [**P8**] jsme studovali biodegradaci čtyř kopolyesterů obsahujících tereftalátové a laktátové jednotky o molárních poměrech 41:59-60:40 připravených depolymerací PETP a následnou polykondenzací a transesterifikací oligomerních produktů a L-mléčné kyseliny. Kopolyestery byly amorfní s jedinou hodnotou T_g 63-67 °C, což dokazuje jejich náhodnou mikrostrukturu. Pro vyhodnocení mechanismu degradace byly kopolyestery lisováním převedeny na fólie o tloušťce ~700 μm (čtvercové vzorky o rozměrech 10 x 10 mm). Biodegradační studie byly prováděny (1) ve vyhnilém kalu odebraném z Ústřední čistírny

odpadních vod (ÚČOV) v Praze a (2) v takzvaném deaktivovaném kalu, který byl před biodegradačním testem vystaven tlaku 2 bar a teplotě 150° C po dobu 2 h pro potlačení mikrobiální aktivity. Deaktivovaný kal měl sloužit jako referenční abiotické prostředí, ovšem testy enzymatických aktivit v něm přesto prokázaly přítomnost lipas a esteras, i když v podstatně menší míře než ve vyhnilém kalu.

Pro posouzení vlivu enzymatické a abiotické hydrolýzy byla provedena počáteční studie nasákavosti a to pravidelným vážením zbotnalých vzorků po dobu 216 h. Vzorky byly inkubovány v prostředí anaerobně stabilizovaného, vyhnilého kalu (pH = 8), deaktivovaného kalu o pH = 8,9, fosfátového pufru (pH = 7,5) a borátového pufru (pH = 8,0) při teplotě 55° C. S rostoucím podílem aromatických jednotek v řetězcích klesal hydrofilní charakter materiálů a tedy jejich schopnost absorbovat vodu jak v kalech, tak v pufrech. U vzorků s 41-57 mol. % aromatických jednotek byla patrná podstatně vyšší absorpce vody v kalech oproti pufrům. Ve vyhnilém kalu byly hodnoty absorpce vody vyšší než v deaktivovaném, což lze přičíst enzymatickým aktivitám. U těchto fólií tedy docházelo v důsledku enzymatické degradace ke zvýšení koncentrace hydrofilních karboxylových a hydroxyskupin v povrchové vrstvě za následného zvýšení absorpce vody až ke vzniku pórů a trhlin. Naopak u vzorku s nejvyšším podílem hydrofobních aromatických jednotek (60 mol. %) a nejvyšším rozdílem mezi T_g (67° C) a teplotou média (55° C) byla schopnost absorpce vody zanedbatelná a to nezávisle na prostředí.

Analýza úbytků hmotnosti a poklesu molární hmotnosti fólií vystavených působení kalu a fosfátovému pufru po prodlouženou dobu 29 dní potvrdila zásadní roli jak výchozího složení kopolyesteru tak přítomnosti enzymů pro katalyzovanou hydrolýzu. Je zapotřebí však také zmínit, že studie byla prováděna za termofilních podmínek (55° C) pro zajištění dostatečné mobility řetězců a v alkalickém prostředí, kde se vedle enzymatické hydrolýzy uplatnila také bazicky katalyzovaná abiotická hydrolýza řetězců. Strukturní i termická analýza degradovaných materiálů potvrdily, že jsou přednostně štěpeny esterové vazby mezi alifatickými jednotkami za zachování delších aromatických sekvencí, což se projevilo částečnou krystalizací a nerozpustností reziduí fólie v běžných organických rozpouštědlech. Současně s degradační studií byla prováděna dlouhodobá inkubace po dobu 394 dní za měření produkovaného bioplynu. Kompletní biodegradace, tedy mineralizace fólií, vyjádřená jako procentuální podíl teoretického výtěžku bioplynu vypočítaného podle Buswellovy rovnice[43], dosahovala hodnot 34 - 69% v závislosti na výchozím složení materiálů.

Studium biodegradace alifaticko-aromatických polyesterů v kompostu

V práci [**P9**] jsme studovali biodegradace kopolyesterů o stejném složení jako v práci [**P8**] ve formě fólií o tloušťce 900 μm (50 x 50 mm) v modelovém, laboratorním kompostu při 58° C a v kompostu z Centrální kompostárny Brno po dobu 21 dní. Z analýzy úbytků hmotnosti a poklesu molární hmotnosti vyplývá, že rychlost degradace klesala s rostoucím podílem aromatických jednotek a ke štěpení řetězců došlo v důsledku jak bazicky tak enzymaticky katalyzované degradace v principu analogicky jako v prostředí kalů. Na druhou stranu zatímco nejvíce hydrofilní kopolyester degradoval stejně rychle bez ohledu na podmínky, fólie s vyšším podílem aromatických jednotek (57 a 60 mol. %) degradovaly podstatně více v přírodním kompostu, kde působí různá mikrobiální konsorcia v závislosti na fázi zrání kompostu. Strukturní a termická analýza prokázaly, že se během degradace štěpily hydrolyticky labilní alifatické esterové vazby za nárůstu aromatických jednotek v reziduích fólie až na 75 mol. % (centrální kompostárna). Zvýšení obsahu delších aromatických sekvencí schopných krystalizace vedlo ke ztrátě rozpustnosti v běžných rozpouštědlech pro analýzu.

Nedílnou součástí hodnocení odpadních plastových materiálů z hlediska jejich vhodnosti pro kompostování je testování toxicity produktů degradace. Normované biologické testy jsou prováděny v laboratoři za definovaných podmínek a z tohoto pohledu je jednoznačně výhodný modelový laboratorní kompost pro získání reprodukovatelných výsledků. V práci [**P10**] jsme zkoumali fytotoxicitu laboratorního kompostu s degradovanými kopolyesterovými fóliemi v návaznosti na práci [**P9**] a to hodnocením vlivu rozpuštěných produktů degradace podle normy ČSN EN 13432 na růst dvouděložných rostlin; řeřichy seté (*Lepidium sativum*) a ječmene obecného (*Hordeum vulgare*). Ke kultivaci semen byla použita speciální zemina obohacená o kompost v hmotnostních poměrech 25 a 50 %. Z testu klíčivosti semen rostlin podle normy ČSN EN 13432[44] vyplynulo, že rozpustné produkty degradace studovaných kopolyesterů nejsou fytotoxické. U rostlin nebyly pozorovány známky nekrózy či opadu listů a naopak došlo k nárůstu hmoty biomasy oproti kontrolnímu vzorku.

3 Závěr

V habilitační práci jsou shrnuty zásadní výsledky mojí práce v rámci výzkumných projektů řešených na Ústavu polymerů VŠCHT Praha a částečně na Ústavu chemie materiálů VUT v Brně. Výzkumná pozornost byla věnována přípravě alifatických polyesterů a polykarbonátů a jejich kopolymerů a studiu mechanismů jejich degradace v modelovém prostředí za přítomnosti enzymů a vybraných mikroorganismů. Vybrané (ko)polymery byly studovány z hlediska přípravy nosičových systémů látek s řízenou dobou degradace. Biodegradace modifikovaných alifaticko-aromatických kopolymerů byla studována také v prostředí reálných kompostů a kalů s vyhodnocením toxicity uvolněných degradačních produktů.

4 Seznam zkratek a symbolů

CM	polymerní film připravený lisováním
Đ	disperzita (M_w/M_n)
DLS	dynamický rozptyl světla
ε-CL	ε-kaprolakton
M_n	početně průměrná molární hmotnost
M_w	hmotnostně průměrná molární hmotnost
NR	Nilská červeň
PTMC	poly(trimethylenkarbonát)
PCL	poly(ε-kaprolakton)
PEO	poly(ethylenoxid)
PLA	poly(laktid)
PETP	poly(ethylentereftalát)
SC	polymerní film připravený odlitím z roztoku
TMC	trimethylenkarbonát

5 Literatura

1. Brannigan, R. P.; Dove, A. P., Synthesis, properties and biomedical applications of hydrolytically degradable materials based on aliphatic polyesters and polycarbonates. *Biomaterials Science* **2017,** *5* (1), 9-21.
2. Thomas, C. M., Stereocontrolled ring-opening polymerization of cyclic esters: synthesis of new polyester microstructures. *Chemical Society Reviews* **2010,** *39* (1), 165-173.
3. Jianming, R.; Anguo, X.; Hongwei, W.; Hailin, Y., Review – recent development of ring-opening polymerization of cyclic esters using aluminum complexes. *Designed Monomers and Polymers* **2014,** *17* (4), 345-355.
4. Kundys, A.; Białecka-Florjańczyk, E.; Fabiszewska, A.; Małajowicz, J., Candida antarctica Lipase B as Catalyst for Cyclic Esters Synthesis, Their Polymerization and Degradation of Aliphatic Polyesters. *Journal of Polymers and the Environment* **2018,** *26* (1), 396-407.
5. Zhu, N.; Liu, Y.; Liu, J.; Ling, J.; Hu, X.; Huang, W.; Feng, W.; Guo, K., Organocatalyzed chemoselective ring-opening polymerizations. *Scientific Reports* **2018,** *8* (1), 3734.
6. Hedfors, C.; Östmark, E.; Malmström, E.; Hult, K.; Martinelle, M., Thiol End-Functionalization of Poly(ε-caprolactone), Catalyzed by Candida antarctica Lipase B. *Macromolecules* **2005,** *38* (3), 647-649.
7. Dong, B.; Zhou, T.; Zhang, H.; Li, C. Y., Directed Self-Assembly of Nanoparticles for Nanomotors. *ACS Nano* **2013,** *7* (6), 5192-5198.
8. Kutikov, A. B.; Song, J., Biodegradable PEG-Based Amphiphilic Block Copolymers for Tissue Engineering Applications. *ACS Biomater Sci Eng* **2015,** *1* (7), 463-480.
9. Zhang, Z.; Kuijer, R.; Bulstra, S. K.; Grijpma, D. W.; Feijen, J., The in vivo and in vitro degradation behavior of poly(trimethylene carbonate). *Biomaterials* **2006,** *27* (9), 1741-1748.
10. Jain, J. P.; Yenet, W.; Domb, A. A. J.; Kumar, N., Biodegradable Polymers in Drug Delivery. In *Biodegradable Polymers in Clinical Use and Clinical Development* Domb, A. J.; Kumar, N.; Ezra, A., Eds. 2011.
11. Murthy, N.; Wilson, S.; Sy, J. C., Biodegradation of Polymers. In *Polymer Science: A Comprehensive Reference*, Matyjaszewski, K.; Möller, M., Eds. Elsevier: Amsterdam, 2012; pp 547-560.
12. Sharma, D.; Sharma, B.; Shukla, A. K., Biotechnological Approach of Microbial Lipase: A Review. . *Biotechnology* **2011,** *10* (1), 23-40.
13. Williams, D. F., Enzymic Hydrolysis of Polylactic Acid. *Engineering in Medicine* **1981,** *10* (1), 5-7.
14. Ouhadi, T.; Stevens, C.; Teyssié, P., Mechanism of ε-Caprolactone polymerization by Aluminum Alkoxides. *Die Makromolekulare Chemie* **1975,** *1* (S19751), 191-201.
15. Mecerreyes, D.; Jérôme, R., From living to controlled aluminium alkoxide mediated ring-opening polymerization of (di)lactones, a powerful tool for the macromolecular engineering of aliphatic polyesters. *Macromolecular Chemistry and Physics* **1999,** *200* (12), 2581-2590.
16. Alcántara-García, J.; Jancik, V.; Barroso, J.; Hidalgo-Bonilla, S.; Cea-Olivares, R.; Toscano, R. A.; Moya-Cabrera, M., Coordination Diversity of Aluminum Centers Molded by Triazole Based Chalcogen Ligands. *Inorganic Chemistry* **2009,** *48* (13), 5874-5883.
17. Hermanova, S.; Pumera, M., Polymer platforms for micro- and nanomotor fabrication. *Nanoscale* **2018,** *10* (16), 7332-7342.
18. Liu, M.; Liu, L.; Gao, W.; Su, M.; Ge, Y.; Shi, L.; Zhang, H.; Dong, B.; Li, C. Y., Nanoparticle mediated micromotor motion. *Nanoscale* **2015,** *7* (11), 4949-4955.

19. Liu, L.; Liu, M.; Dong, Y.; Zhou, W.; Zhang, L.; Su, Y.; Zhang, H.; Dong, B., Preparation, heat-enabled shape variation, and cargo manipulation of polymer-based micromotors. *Journal of Materials Science* **2016,** *51* (3), 1496-1503.
20. Abdelmohsen, L. K. E. A.; Peng, F.; Tu, Y.; Wilson, D. A., Micro- and nano-motors for biomedical applications. *Journal of Materials Chemistry B* **2014,** *2* (17), 2395-2408.
21. Grove, D. E., Catalysts - Myths and Realities. *Platinum Metals Review* **2003,** *47* (1), 44-44.
22. Sun, J.; He, C.; Zhuang, X.; Jing, X.; Chen, X., The crystallization behavior of poly(ethylene glycol)-poly(ε-caprolactone) diblock copolymers with asymmetric block compositions. *Journal of Polymer Research* **2011,** *18* (6), 2161-2168.
23. Zhou, D.; Shao, J.; Li, G.; Sun, J.; Bian, X.; Chen, X., Crystallization behavior of PEG/PLLA block copolymers: Effect of the different architectures and molecular weights. *Polymer* **2015,** *62*, 70-76.
24. Wang, L.; Feng, C.; Shao, J.; Li, G.; Hou, H., The crystallization behavior of poly(ethylene glycol) and poly(l-lactide) block copolymer: Effects of block length of poly(ethylene glycol) and poly(l-lactide). *POLYMER CRYSTALLIZATION* **2019,** *2* (4), e10071.
25. Egli, S.; Schlaad, H.; Bruns, N.; Meier, W., Functionalization of Block Copolymer Vesicle Surfaces. *Polymers* **2011,** *3* (1), 252-280.
26. Banerjee, A.; Chatterjee, K.; Madras, G., Enzymatic degradation of polymers: a brief review. *Materials Science and Technology* **2014,** *30* (5), 567-573.
27. Müller, R., Biodegradability of Polymers: Regulations and Methods for Testing. In *Biopolymers Online*, Steinbüchel, A., Ed. 2005.
28. Tsuji, H.; Mizuno, A.; Ikada, Y., Properties and morphology of poly(L-lactide). III. Effects of initial crystallinity on long-term in vitro hydrolysis of high molecular weight poly(L-lactide) film in phosphate-buffered solution. *Journal of Applied Polymer Science* **2000,** *77* (7), 1452-1464.
29. Rydz, J.; Sikorska, W.; Kyulavska, M.; Christova, D., Polyester-Based (Bio)degradable Polymers as Environmentally Friendly Materials for Sustainable Development. *International Journal of Molecular Sciences* **2015,** *16* (1), 564-596.
30. Hermanova, S.; Zarevucka, M.; Bousa, D.; Pumera, M.; Sofer, Z., Graphene oxide immobilized enzymes show high thermal and solvent stability. *Nanoscale* **2015,** *7* (13), 5852-5858.
31. Han, X.; Pan, J., A model for simultaneous crystallisation and biodegradation of biodegradable polymers. *Biomaterials* **2009,** *30* (3), 423-430.
32. Gleadall, A.; Pan, J.; Atkinson, H., A simplified theory of crystallisation induced by polymer chain scissions for biodegradable polyesters. *Polymer Degradation and Stability* **2012,** *97* (9), 1616-1620.
33. Manzanares Palenzuela, C. L.; Novotný, F.; Krupička, P.; Sofer, Z.; Pumera, M., 3D-Printed Graphene/Polylactic Acid Electrodes Promise High Sensitivity in Electroanalysis. *Analytical Chemistry* **2018,** *90* (9), 5753-5757.
34. Olewnik, E.; Czerwiński, W.; Nowaczyk, J., Hydrolytic degradation of copolymers based on l-lactic acid and bis-2-hydroxyethyl terephthalate. *Polymer Degradation and Stability* **2007,** *92* (1), 24-31.
35. Olewnik, E.; Czerwiński, W.; Nowaczyk, J.; Sepulchre, M.-O.; Tessier, M.; Salhi, S.; Fradet, A., Synthesis and structural study of copolymers of l-lactic acid and bis(2-hydroxyethyl terephthalate). *European Polymer Journal* **2007,** *43* (3), 1009-1019.
36. Acar, I.; Kaşgöz, A.; Özgümüş, S.; Orbay, M., Modification of Waste Poly(Ethylene Terephthalate) (PET) by Using Poly(L-Lactic Acid) (PLA) and Hydrolytic Stability. *Polymer-Plastics Technology and Engineering* **2006,** *45* (3), 351-359.

37. Acar, I.; Pozan, G. S.; Özgümüş, S., Thermal oxidative degradation kinetics and thermal properties of poly(ethylene terephthalate) modified with poly(lactic acid). *Journal of Applied Polymer Science* **2008,** *109* (5), 2747-2755.
38. Prokopová, I.; Vlčková, E.; Šašek, V.; Náhlík, J.; Soukupová-Chaloupková, V.; Skolil, J., Aromatic-aliphatic copolyesters based on waste poly(ethylene terephthalate) and their biodegradability. *e-Polymers* **2008,** *052*, 1-9.
39. Turečková, J.; Prokopová, I.; Niklová, P.; Šimek, J.; Šmejkalová, P.; Keclík, F., Biodegradable copolyester/starch blends—preparation, mechanical properties, wettability, biodegradation course. *Polimery* **2008,** *53* (9), 639-643.
40. Vitásek, J.; Šašek, V.; Prokopová, I., PET from Used Beverage Bottles: A Material for Preparation of Biologically Degradable Copolyesters. *Journal of Polymers and the Environment* **2012,** *20* (2), 618-625.
41. Voběrková, S.; Hermanová, S.; Hrubanová, K.; Krzyžánek, V., Biofilm formation and extracellular polymeric substances (EPS) production by Bacillus subtilis depending on nutritional conditions in the presence of polyester film. *Folia Microbiol* **2015,** *61* (2), 91-100.
42. Jung, J. H.; Ree, M.; Kim, H., Acid- and base-catalyzed hydrolyses of aliphatic polycarbonates and polyesters. *Catalysis Today* **2006,** *115* (1), 283-287.
43. Buswell, A. M.; Mueller, H. F., Mechanism of Methane Fermentation. *Industrial & Engineering Chemistry* **1952,** *44* (3), 550-552.
44. Standardization, E. C. f., EN-13432. Packaging - Requirements for packaging recoverable through composting and biodegradation - Test scheme and evaluation criteria for the final acceptance of packaging. 2000.

6 Seznam předložených publikací

[**P1**] Hermanova, S.; Cabrera MMM.; Vyroubalova, Z.; Vojtova, L., Novel triazole-based aluminum complex for ring-opening polymerization of lactones. *Polymer Bulletin* **2011**,67,1751-60.

[**P2**] Kroupa, T.; Hermanová, S.; Mayorga-Martinez, CC.; Novotný, F.; Sofer, Z.; Pumera, M., Micromotors as "Motherships": A Concept for the Transport, Delivery, and Enzymatic Release of Molecular Cargo via Nanoparticles. *Langmuir* **2019**, 35, 10618-10624.

[**P3**] Reinišová L.; Novotný F.; Pumera M.; Kološtová K.; Hermanová S., Nanoparticles Based on Poly(trimethylene carbonate) Triblock Copolymers with Post-Crystallization Ability and Their Degradation *in vitro*. *Macromolecular Research* **2018**,26,1026-1034.

[**P4**] Hermanová, S.; Omelková, J.; Voběrková, S.; Bálková, R.; Richtera, L.; Mravcová, L.; et al. The Effect of Processing of Polycaprolactone Films on Degradation Process Initiated by Aspergillus Oryzae Lipase. *International Journal of Polymer Analysis and Characterization* **2012**,17,465-475.

[**P5**] Hermanova, S.; Balkova, R.; Voberkova, S.; Chamradova, I.; Omelkova, J.;Richtera, L.; et al., Biodegradation study on poly(epsilon-caprolactone) with bimodal molecular weight distribution. *Journal of Applied Polymer Science* **2013**,127,4726-4735.

[**P6**] Balkova, R.; Hermanova, S.; Voberkova, S.; Damborsky, P.; Richtera, L.; Omelkova, J.; et al., Structure and Morphology of Microbial Degraded Poly(ε-caprolactone)/Graphite Oxide Composite. *Journal of Polymers and the Environment* **2014**, 22,190-199.

[**P7**] Manzanares-Palenzuela CL.; Hermanova, S.; Sofer, Z.; Pumera, M., Proteinase-sculptured 3D-printed graphene/polylactic acid electrodes as potential biosensing platforms: towards enzymatic modeling of 3D-printed structures. *Nanoscale* **2019**,11,12124-12131.

[**P8**] Hermanova, S.; Smejkalova, P.; Merna, J.; Zarevucka, M., Biodegradation of waste PET based copolyesters in thermophilic anaerobic sludge. *Polymer Degradation and Stability*. **2015**,111,176-184.

[**P9**] Vaverková, M.; Adamcová, D.; Kotrchová, L.; Merna, J.; Hermanová S., Degradation of pet copolyesters under real and laboratory composting conditions. *Journal of Material Cycles and Waste Management* **2018**,20,414-420.

[**P10**] Adamcová, D.; Vaverková, M.; Hermanová, S.; Voběrková, S., Ecotoxicity of Composts Containing Aliphatic-Aromatic Copolyesters. *Polish Journal of Environmental study* **2015**,24,1497-1505.

7 Texty publikací

Polym. Bull. (2011) 67:1751–1760
DOI 10.1007/s00289-011-0486-z

ORIGINAL PAPER

Novel triazole-based aluminum complex for ring-opening polymerization of lactones

Soňa Hermanová · Monica M. Moya Cabrera · Zdeňka Vyroubalová · Lucy Vojtová

Received: 20 January 2011 / Revised: 29 March 2011 / Accepted: 11 April 2011 /
Published online: 23 June 2011

Abstract Novel triazole-based aluminum complex {*O*,*O*′-[4,5-P(O)Ph_2tz]-AlMe_2 was studied as the catalyst for the ring-opening polymerization of caprolactone (ε-CL) in chlorobenzene. In the presence of methanol, isopropanol, and bifunctional poly(ethylene glycol), the catalytic system produced polymers with high conversion (81–85 %) but broader distribution (M_w/M_n = 1.5–1.8). The system of catalyst and benzyl alcohol produced relative monodisperse PCLs ($M_w/M_n \sim 1.2$) with defined molecular weight at 1/1ratio, 60 °C and an initial concentration of ε-CL equal to 0.5 mol/L.

Keywords Aluminum · Polycaprolactone · Ring-opening polymerization

Introduction

Biodegradable and biocompatible aliphatic polyesters have played a leading role in specialty biomedical and pharmaceutical polymer applications such as resorbable implant materials and drug delivery systems (DDS) namely since the control of their degradation rate through the composition and processing can be realized [1, 2]. From this point of view, the availability of suitable synthetic method producing polymers of the required molecular weight (according to monomer to initiator ratio) and defined chain end groups is of the utmost importance. Polymerization of di/lactones via ring-opening polyaddition (ROP) mechanism has been known as a

S. Hermanová (✉) · Z. Vyroubalová · L. Vojtová
Institute of Materials Chemistry, Faculty of Chemistry, Brno University of Technology, Purkyňova 118, 612 00 Brno, Czech Republic
e-mail: hermanova-s@fch.vutbr.cz

M. M. Moya Cabrera
Centro Conjunto de Investigación en Química Sustentable UAEM-UNAM, Carr. Toluca-Atlacomulco Km 14.5, Toluca, Estado de México 50200, México

synthetic strategy enabling fine tailoring the physico-chemical properties of polyester products [3]. Among important ROP initiators, aluminum alkoxides are particularly interesting especially because of their high selectivity, polymerization efficiency, and ability to produce the polyesters having both defined and predictable end groups. Besides classical coordination initiators based on aluminum isopropoxides [$Al(O\text{-}i\text{-}Pr)_3$] and bimetallic μ-oxo-alkoxides [4, 5] reported by Teyssié et al., a series of aluminum alkoxides (aryloxides) modified by ancillary ligands with various electronic and steric characteristics having a significant influence on the polymerization performance have been developed. Monodisperse polyesters were produced by monomeric [6] and dimeric Al complexes with O,O-bidentate ligands [7–9], (porfinato)aluminum alkoxides with N,N,N,N-donor atoms [10], Al complexes with O,N,N-tridentate [11], O,O,N-tridentate [12] or O,O,N,N-tetradentate ligands [13, 14], and phenoxyimine aluminum complexes with N,O-bidentate ligands [15–17].

The objective of our work was to study the polymerization behavior of a novel aluminum complex with O,O-bidentate ligand sphere; {O,O'-[4,5-$P(O)Ph_2$tz]-$AlMe_2$} denoted as **1** for ε-caprolactone polymerization.

Experimental

All manipulations were carried out under a dry nitrogen atmosphere (99.999%, Siad, CZ) using vacuum/inert manifold and standard Schlenk techniques. Chlorobenzene (p.a.) and ε-caprolactone (ε-CL) supplied by Lach-ner, CZ were purified with calcium hydride and freshly distilled prior to use. Anhydrous benzyl alcohol (BnOH, 99.8%), anhydrous methanol (MeOH, 99.8%), and anhydrous isopropanol (iPrOH, 99.5%) supplied by Aldrich, tetrahydrofuran (THF, p.a) supplied by Lachner, CZ, and deuterochloroform ($CDCl_3$, 99.8%) supplied by Isosar, CZ were used without further purification. Poly(ethylene glycol) 400 (PEG, bifunctional, $M_n = 400$, Fluka) was degassed at 130 °C for 8 h under vacuum prior to use.

{O,O'-[4,5-$P(O)Ph_2$tz]-$AlMe_2$} denoted as **1** was synthesized by Dr. Moya-Cabrera's group according to the published procedure [18].

Typical polymerization procedure

Polymerization reactions were carried out in a double-neck glass Schlenk flask (25 mL) with a magnetic stirring bar. To the flask containing the solution of aluminum complex **1** in chlorobenzene, the nucleophilic agent as benzyl alcohol (BnOH), methanol (MeOH), isopropanol (iPrOH), and poly(ethylene glycol) 400 (OH-PEG-OH) were added via microsyringe and the solution was stirred (600 rpm/min) for 30 min to form initiating species (I). The dosing for a particular run was as follows: **1** (31 μmol, 16 mg) and BnOH (31 μmol, 3.3 mg); **1** (42 μmol, 22 mg) and MeOH (42 μmol, 1.3 mg); **1** (23 μmol, 12 mg) and iPrOH (23 μmol, 1.4 mg), **1** (29 μmol, 15 mg) and OH-PEG-OH (29 μmol, 11.4 mg).

Afterward, a defined amount of ε-CL ($[\varepsilon\text{-CL}]_0/[I]_0 = 200$) was added keeping the ratio of solvent to monomer equal to 10 and the mixture was stirred at constant

temperature (50, 60, and 70 °C). The polymerization reaction was quenched after the prescribed time (6, 8 h) by adding a few drops of an acetic acid solution. The polymerization mixture obtained was poured into cold methanol (−10 °C) and the white precipitate formed was collected by filtration and dried under vacuum until a constant weight was obtained. The crude product was purified three times by dissolving in THF and precipitating in cold methanol (−10 °C).

Polymer characterization

^{1}H NMR spectra of the polymers were measured in $CDCl_3$ on Bruker Avance 300 MHz equipment. The chemical shift was determined with respect to residual proton signals from $CDCl_3$. Gel permeation chromatography (GPC) was performed on Agilent Technologies 1100 Series instrument equipped with a refractive index (RI) detector, two PL gel Mixed columns 300 × 7.5 mm with particle size of 5 μm using THF as an eluent at a flow rate of 1 mL/min. Molecular weight and molecular weight distribution were calculated using a series of polystyrene standards ($M_p = 316500 - 162$).

Results and discussion

Within this work, we studied the catalytic efficiency of the novel triazole-based aluminum complex (**1**) for the ring-opening polymerization (ROP) of ε-caprolactone. A series of polymerization runs was carried out using **1** as the catalyst and different alcohols with well-known ROP initiator properties; methanol, isopropanol, benzyl alcohol, and the macroinitiator—bifunctional poly(ethylene glycol) at 60 °C in chlorobenzene. The ^{1}H NMR spectra of synthesized PCLs are presented in Figs. 1, 2, 3, 4.

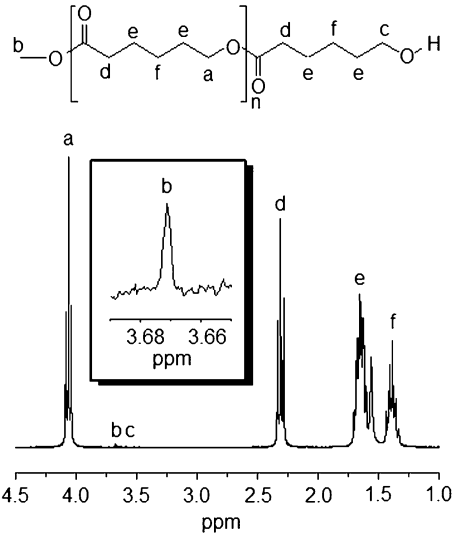

Fig. 1 ^{1}H NMR spectrum of PCL produced by **1**/MeOH in $CDCl_3$; polymerization conditions: 60 °C, chlorobenzene, 8 h. P(ε-CL) $\delta = 1.37$ ppm [m, 2H, ($-CH_2-$)], $\delta = 1.64$ ppm [m, 4H, ($-CH_2-$)], $\delta = 2.30$ ppm [t, 2H, ($-CH_2CO-$)], $\delta = 3.62$ ppm [t, 2H, ($-CH_2OH$)], $\delta = 3.67$ ppm [s, 2H, (CH_3O-)], $\delta = 4.05$ ppm [t, 2H, ($-CH_2O-$)]

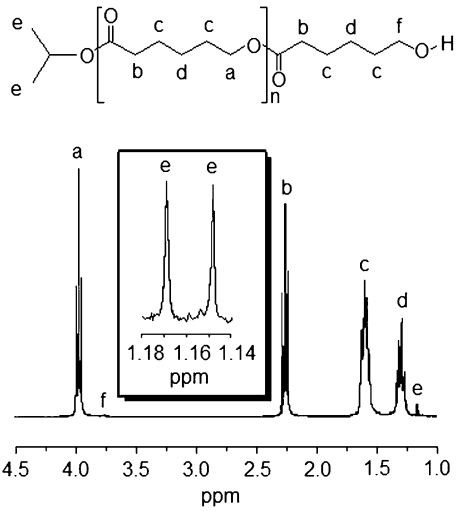

Fig. 2 ^{1}H NMR spectrum of PCL produced by **1**/iPrOH in $CDCl_3$; polymerization conditions: 60 °C, chlorobenzene, 8 h. P(ε-CL) $\delta = 1.15$ and 1.17 ppm [s, 6H, (CH_3–)], $\delta = 1.31$ ppm [m, 2H, (–CH_2–)], $\delta = 1.58$ ppm [m, 4H, (–CH_2–)], $\delta = 2.24$ ppm [t, 2H, (–CH_2CO–)], $\delta = 3.58$ ppm [t, 2H, (–CH_2OH)], $\delta = 4.00$ ppm [t, 2H, (–CH_2O–)]

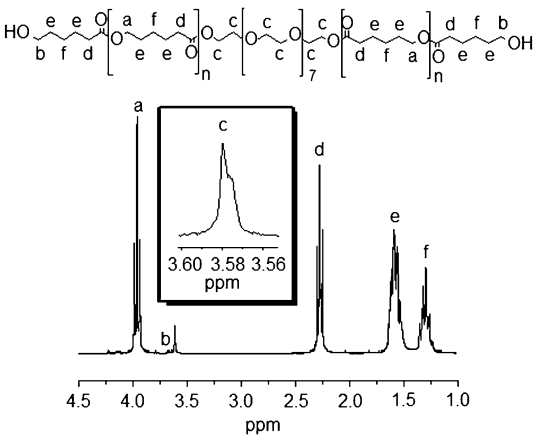

Fig. 3 ^{1}H NMR spectrum of PCL produced by **1**/PEG(400) in $CDCl_3$; polymerization conditions: 60 °C, chlorobenzene, 8 h. P(ε-CL) $\delta = 1.31$ ppm [m, 2H, (–CH_2–)], $\delta = 1.58$ ppm [m, 4H, (–CH_2–)], $\delta = 2.23$ ppm [t, 2H, (–CH_2CO–)], $\delta = 3.57$–3.59 ppm [4H, (–CH_2O–)], $\delta = 3.74$ ppm [t, 2H, (–CH_2OH)], $\delta = 4.00$ ppm [t, 2H, (–CH_2O–)]

Based on the results obtained (Table 1), one can suggest that the influence of the steric hindrance of a particular alkoxide ligand, has a significant impact on the activity of catalytic species, compared to its electronic contribution as a Lewis acidic center. Thus, both **1**/MeOH and **1**/iPrOH formed effective ROP catalytic systems with the monomer conversion of 81–88% after a polymerization period of 8 h. For **1**/OH-PEG-OH, a prolonged period of 20 h was necessary to reach a comparable conversion of 85 %. Based on well correlation between theoretical and experimental molecular weight, we can suggest the participation of both hydroxylic end groups of PEG during the initiation of ROP. The presence of the phenyl ring close to the polymerization active center of the **1**/BnOH probably led to poorer access of monomer molecules resulting in both the decrease of the polymerization rate as well as the inhibition of side reactions.

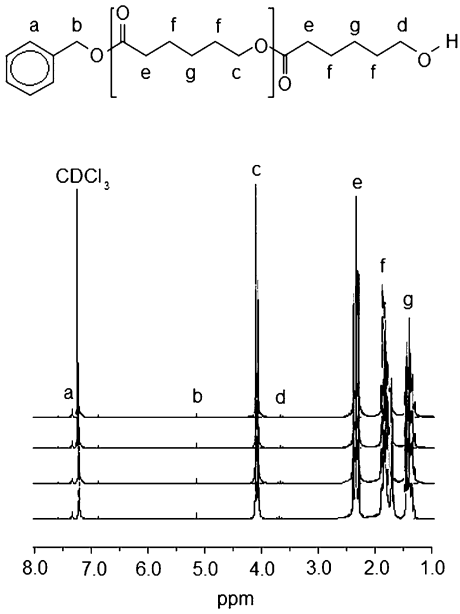

Fig. 4 ^{1}H NMR spectrum of PCL produced by **1**/BnOH in $CDCl_3$; polymerization conditions: 60 °C, chlorobenzene, 8 h. P(ε-Cl) $\delta = 1.27$ ppm [m, 2H, ($-CH_2-$)], $\delta = 1.63$ ppm [m, 4H, ($-CH_2-$)], $\delta = 2.29$ ppm [t, 2H, ($-CH_2CO-$)], $\delta = 4.05$ ppm [t, 2H, ($-CH_2O-$)], $\delta = 3.63$ ppm [t, 2H, ($-CH_2OH$)], $\delta = 5.10$ ppm [s, 2H, ($-CH_2OBn$)], $\delta = 7.25$ ppm [s, $CDCl_3$]

Moreover, the triazole-based aluminum complex **1** produced the polymer ($M_n = 25{,}000$, $M_w/M_n = 1.5$) in 6 h of polymerization performed under identical conditions even in absence of alcohol initiator. However, the yields were very low (of about 3–5%) with poor reproducibility, hence chain end-group NMR analysis was not carried out. Most probably, the monomer insertion took place either in a small portion of the aluminum-carbon(methyl) bonds or in Al–O bond of the ligand sphere, which has been already reported for some complexes [19].

Furthermore, polymerization study focused on the promising system of benzyl alcohol along with **1** as catalyst was performed in order to find the best conditions for producing polymers with the well-defined molecular weight (consistent with monomer to initiator ratio), predicted end groups, and a relative narrow polydispersity ($M_w/M_n \leq 1.2$).

The ^{1}H NMR spectra of the PCLs (Fig. 4) synthesized using ratio of **1**/BnOH = 1/1 (Table 1) confirmed the presence of the methylene signals from both benzylalkoxyl ($\delta = 5.1$ ppm) and hydroxyl ($\delta = 3.63$ ppm) chain ends, which correlate well with the expected character of active species. Thus, we assumed that the initiation step proceeds through a monomer insertion into the Al–O bond of the aluminum benzylalkoxide intermediate, which is formed "in situ" with the concomitant evolution of methane (Fig. 5). Monomer molecules are subsequently cleaved in a way that maintains the growing chains having benzylalkoxide dead end attached to the aluminum atom through an alkoxide bond. Consequently, the quenching of these aluminum active bonds by hydrolysis results in the hydroxyl end group.

Regarding the discrepancy between the actual values of molecular weights of the polyesters and those determined by GPC using polystyrene standards, ^{1}H NMR

Table 1 Screening of ROP efficiency of **1**

Run	ROH	t (h)	Yield[a] (%)	M_n[b] (GPC)	M_n[c] (NMR)	M_n[d] (Theor.)	M_w/M_n (GPC)
1	MeOH	8	88	53,000	25,000	20,000	1.8
2	iPrOH	8	81	42,000	16,000	18,000	1.7
3	OH-PEG-OH	20	85	37,000	25,000	20,000	1.5
4[e]	BnOH	8	60	26,000	11,000	14,000	1.3
5[e]	BnOH	8	66	24,000	11,000	15,000	1.2
6[e]	BnOH	8	67	25,000	15,000	15,000	1.2
7[e]	BnOH	8	67	24,000	9,000	15,000	1.2

Polymerization conditions: $T = 60$ °C, chlorobenzene, $[\varepsilon\text{-CL}]_0 = 0.7$ mol/L, $[1]_0/[\text{ROH}]_0/[\varepsilon\text{-CL}]_0 = 1/1/200$

[a] Isolated yield

[b] GPC values according PS standards

[c] M_n value was estimated by the ^{1}H NMR spectrum based on the intensity of the methylene protons at the PCL chain ($\delta = 4.05$ ppm) and that of protons derived from BnOH ($\delta = 5.10$ ppm) according to the equation: $M_n(\text{PCL}) = [(c/b + 1) \times M(\varepsilon\text{-CL})] + M(\text{BnOH})$, where c and b are the integral intensities of peaks at 4.05 ppm and 5.1 ppm, respectively. In case of $PCL_n/PEG_9/PCL_n$ copolymer, the presence of one PEG molecule per one copolymer molecule was assumed. In one PEG monomer unit (–CH_2–CH_2–O–), there are four hydrogens, so the total number of hydrogens per one PEG molecule with polymerization degree equal to 9 was calculated to be 36. Consequently, the signal integral for methylene protons of PEG ($\delta = 3.58$ ppm) was set to represent 36 hydrogens. The intensity of the methylene protons at the PCL chain ($\delta = 4.00$ ppm) was used to calculate relative number of PCL protons (2n) per one $PCL_n/PEG_9/PCL_n$ copolymer molecule. Since the intensity signal at $\delta = 4.00$ ppm is related to only two hydrogens, the ratio of signal integrals should be multiplied by 18 instead of 36. Molecular weight of the copolymer was calculated according to the equation $M_n(\text{PCL/PEG/PCL}) = [(a/c \times 18) \times M(\varepsilon\text{-CL})] + M(\text{PEG})$, where a and c are the integral intensities of peaks at 4.00 and 3.58 ppm, respectively

[d] Calculated from initial molar ratio $[\varepsilon\text{-CL}]_0/[\text{ROH}]_0 \times 114.15 \times$ conversion yield, considering one active alkoxide (RO-) group per Al complex. In case of OH-PEG-OH, the theoretical molecular weight of triblock copolymer was calculated using the same equation, since the composition at quantitative conversion is expected to be $PCL_{100}/PEG_9/PCL_{100}$

[e] $[\varepsilon\text{-CL}]_0 = 0.5$ mol/L

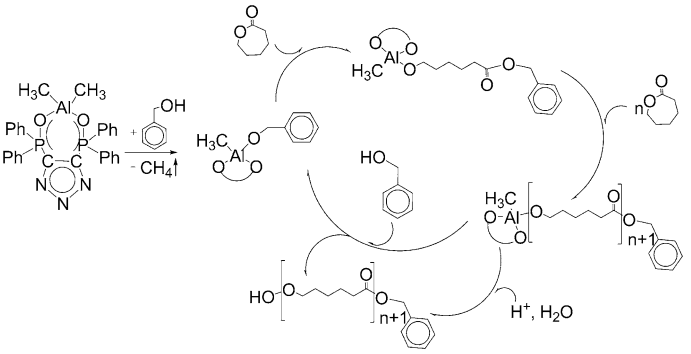

Fig. 5 Suggested mechanism for the ROP initiated by **1**/BnOH system

spectra of the PCLs synthesized under identical conditions (60 °C, chlorobenzene, 8 h, $[\varepsilon\text{-CL}]_0 = 0.5$ mol/L) were used as well to determine their actual chain lengths (Fig. 4). By comparison of M_n values obtained using GPC and those calculated from certain intensities of the proton signals of PCL in NMR spectra [19], the correction factor of 0.58 was estimated. Consequently, the values of M_n (GPC) of the PCLs produced were multiplied by this factor to give the actual values denoted as M_n (corr).

The evaluation of data from the runs performed simultaneously at the same conditions (runs 4–7 in Table 1) confirmed a high reproducibility of PCL yields, which was estimated to be of about 3%. However, the deviations of values of molecular weight and polydispersity index determined by GPC method could be ascribed to its accuracy.

To understand better the role of BnOH in the polymerization system, the different ratios to **1** (0.5 and 2 equiv. to Al) were examined (see in Table 2). In the case of the 0.5/1.0 ratio of BnOH/**1**, PCLs were obtained in high yield (92–93 %) after 6 and 8 h of polymerization (runs 4 and 5, respectively, in Table 2). The increase in polydispersity ($M_w/M_n \geq 1.6$) can be ascribed both to the occurrence of side reactions at high monomer conversions and to the participation of different active species in the polymerization process. The aluminum complex **1** which was in excess, could participate on the polymer chain growth along with the **1**/BnOH initiating system.

On the other hand, the polymerization with two equivalents of BnOH to **1** (Run 5 in Table 2) produced PCL in a low yield of only 21%. Taking into account the good correlation between the theoretical and experimental molecular weights (calculated according to the ratio of $[\varepsilon\text{-Cl}]_0/[\text{BnOH}]_0$), we can suggest the benzyl alcohol functions as a chain transfer agent. Reversible exchange of growing polymer chain between BnOH and active aluminum-alkoxide center resulted in participation of all

Table 2 Effect of the Al-complex (**1**) to BnOH ratio

Run	$[1]_0/[\text{BnOH}]_0/[\varepsilon\text{-CL}]_0$	t (h)	Yield[a] (%)	M_n[b] (GPC-corr)	M_n (NMR)	M_n[c] (Theor.)	M_w/M_n (GPC)
1	1/0/200	6	3	15,000	n.a.	–	1.5
2	1/1/200	6	45	11,000	9,000	10,000	1.2
3	1/1/200	8	67	15,000	14,000	15,000	1.2
4	2/1/200	6	92	12,000	17,000	21,000	1.6
5	2/1/200	8	93	15,000	n.a.	21,000	1.7
6	1/2/400	6	37	6,000	n.a.	8,000	1.1
7	1/2/400	8	21	3,000	4,000	5,000	1.4

Polymerization conditions: $T = 60$ °C, chlorobenzene, $[\mathbf{1}]_0 = 0.003$ mol/L, $[\varepsilon\text{-CL}]_0 = 0.5$ mol/L

[a] Isolated yield

[b] Corrected values in the brackets obtained according to the equation $M_n(\text{Corr}) = 0.58 \times M_n$ (GPC)

[c] Calculated from initial molar ratio $[\varepsilon\text{-CL}]_0/[\text{BnOH}]_0 \times 114.15 \times$ conversion yield, considering one active benzoxide group per Al complex

Table 3 Effect of polymerization temperature and initial concentration of ε-caprolactone

Run	T (°C)	$[\varepsilon\text{-CL}]_0$[a]	Yield[b] (%)	Mn[c] (GPC-corr)	M_n (NMR)	M_n[d] (Theor.)	M_w/M_n (GPC)
1	40	0.5	5	3,000	n.a.	1,000	1.1
2	50	0.5	23	6,000	8,000	5,000	1.2
3	60	0.5	45	11,000	9,000	10,000	1.2
4	60	0.7	72	16,000	12,000	17,000	1.4
5	60	1.4	99	23,000	n.a.	23,000	1.8
6	70	0.5	95	16,000	17,000	22,000	1.8

Polymerization conditions: initial molar ratio $[\varepsilon\text{-CL}]_0/[\text{Al}]_0/[\text{BnOH}]_0 = 200/1/1$, chlorobenzene, activation period 30 min, $[\mathbf{1}]_0 = 0.003$ mol/L, $t = 6$ h

[a] Initial molar concentration of ε-caprolactone [mol/L]

[b] Isolated yield

[c] Corrected values in the brackets obtained according to the equation $M_n(\text{Corr}) = 0.58 \times M_n$ (GPC)

[d] Calculated from initial molar ratio $[\varepsilon\text{-CL}]_0/[\text{BnOH}]_0 \times 114.15 \times$ conversion yield, considering one active benzyl alkoxide group per Al complex

BnOH molecules in ROP initiation. Furthermore, the overall polymerization rate decreased since the chain transfer reaction competed with the propagation step.

Moreover, the overall polymerization rate increased with the temperature (Table 3). Every temperature increase by 10 °C in the range of 50–70 °C resulted in almost a double increment with regard to the previous polymer yield. However, the polydispersity increase at 70 °C ($M_w/M_n = 1.8$) indicated possible occurring undesired transfer reactions. In the same manner, the increase on the original monomer concentration in the polymer mixture caused higher yields accompanied with lower control over the propagation step as expressed by a rise in the polydispersity (Runs 3–5 in Table 3).

The conditions during which relative monodisperse PCLs (~ 1.2) were synthesized were considered as 60 °C, initial concentration of ε-CL equal to 0.5 mol/L, and equivalent ratio of **1**/BnOH = 1/1. The subsequent polymerization experiments performed at selected conditions confirmed a living character of the process due to both a linear dependency of M_n on conversion and a relative narrow polydispersity of PCLs prepared ($M_w/M_n = 1.2$–1.3) (Fig. 6).

Regarding the synthesis of PCL with the lowest polydispersity index ($M_w/M_n = 1.1$) at 40 °C, we can expect the proceeding of polymerization process at 30 °C in the living manner as well. However, the polymerization period should be prolonged over 24 h to obtain yields comparable with those produced at higher temperatures.

On the basis of the results, ROP of ε-CL catalyzed by the novel aluminum complex **1** proceeded in a controlled manner with high catalytic efficiency under optimized conditions producing PCLs with defined molecular weight. The catalytic efficiency of **1**/BnOH for ROP of ε-CL at 60 °C and the excess of monomer of 200 to **1** estimated on the bases of [Mn(Theor.)/(Mn(NMR)] is close to 1, which is comparable with the efficiencies of aluminum amine bis(phenolates)/BnOH under similar conditions [12].

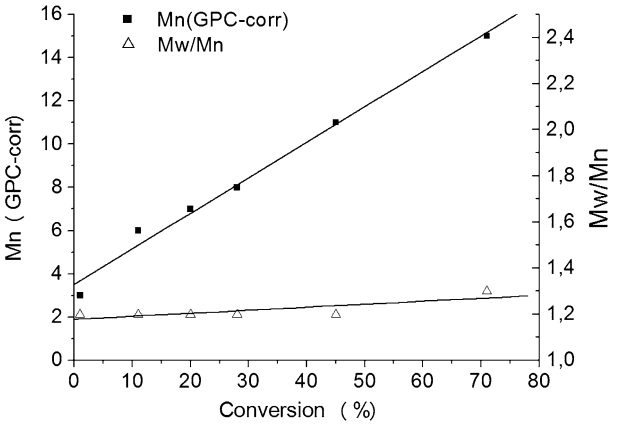

Fig. 6 The relationship between M_n (GPC-corr (*filled square*)) and its distribution (M_w/M_n) (*open triangle*) and the conversion for **1**/BnOH/ε-Cl = 1/1/200 system. Polymerization conditions: $[\varepsilon\text{-CL}]_0 = 0.5$ mol/L, chlorobenzene, 60 °C

Conclusions

In conclusion, an efficient system based on novel aluminum complex **1** and benzyl alcohol for ROP of ε-caprolactone was obtained. The living character of the polymerization process was supported by the low polydispersity index ($M_w/M_n = 1.2$) of the PCL at certain conditions. Further details of the character of active species and the relationship between the alkylgroup attached to the Al-complex and the alcohol are under investigation.

Acknowledgments This work was supported by the Ministry of Education of the Czech Republic under the project no. MSM 0021630501 and by the CONACyT (grant 058484). The authors thank J. Alcántara and N. Zavala for their technical assistance.

References

1. Gref R, Minamitake Y, Peracchia MT, Trubetosky V, Trochilin V, Langer R (1994) Biodegradable long-circulating polymeric nanospheres. Science 263:1600–1603. doi:10.1126/science.8128245
2. Allen C, Han J, Yu Y, Maysinger D, Eisenberg AJ (2000) Polycaprolactone-b-poly(ethylene oxide) copolymer micelles as a delivery vehicle for dihydrotestosterone. Control Rel 63:275–286. doi:10.1016/S0168-3659(99)00200-X
3. Jérome Ch, Lecomte P (2008) Recent advances in the synthesis of aliphatic polyesters by ring-opening polymerization. Adv Drug Deliv Rev 60:1056–1076. doi:10.1016/j.addr.2008.02.008
4. Ouhadi T, Stevens C, Teyssié P (1975) Mechanism of ε-caprolactone polymerization by aluminum alkoxides. Makromol Chem Suppl 1:191–201. doi:10.1002/macp.1975.020011975112
5. Hamitou A, Teyssié P (1977) Soluble bimetallic μ-oxoalkoxides. IX. ε-caprolactone and β-propiolactone block copolymerization. J Polym Sci Polym Chem Ed 15:1035–1041. doi:10.1002/pol.1977.170150502
6. Akatsuka M, Aida T, Inoue S (1995) Alcohol/methylaluminium diphenolate systems as novel, versatile initiators for synthesis of narrow molecular weight distribution polyester and polycarbonate. Macromolecules 28:1320–1322. doi:10.1021/ma00108a075

7. Ko BT, Lin CC (1999) Efficient "living" and "immortal" polymerization of lactones and diblock copolymer of ε-CL and δ-VL catalyzed by aluminium alkoxides. Macromolecules 32:8296–8300. doi:10.1021/ma991055s
8. Chen HL, Ko BT, Huang BH, Lin Ch-Ch (2001) Reactions of 2,2′-methylenebis(4-chloro-6-isopropyl-3-methylphenol) with trimethylalumium: highly efficient catalysts for the ring-opening polymerization of lactones. Organometallics 20:5076–5083. doi:10.1021/om010425+
9. Liu YCH, Ko BT, Lin ChCh (2001) A highly efficient catalyst for the "living" and "immortal" polymerization of ε-caprolactone and L-lactide. Macromolecules 34:6196–6201. doi:10.1021/ma0104579
10. Endo M, Aida T, Inoue S (1987) "Immortal" polymerization of ε-caprolactone initiated by aluminium porphyrin in the presence of alcohol. Macromolecules 20:2982–2991. doi:10.1021/ma00178a005
11. Lewinski J, Horeglad P, Dranka M, Justyniak I (2004) Simple generation of cationic aluminium alkyls and alkoxides based on the pendant arm tridentate schiff base. Inorg Chem 43:5789–5791. doi:10.1021/ic049337i
12. Chen ChT, Huang ChA, Huang BH (2004) Aluminium complexes supported by tridentate aminophenoxide ligand as efficient catalyst for ring-opening polymerization of ε-caprolactone. Macromolecules 37:7968–7973. doi:10.1021/ma0492014
13. Chen ChT, Huang ChA, Huang BH (2003) Aluminium metal complexes supported by amine bisphenolate ligands as catalysts for ring-opening polymerization of ε-caprolactone. Dalton Trans 2003:3799–3803. doi:10.1039/b307365c
14. Amgoune A, Lavanant L, Thomas ChM, Chi Y, Welter R, Dagorne S, Carpentier JF (2005) An aluminium komplex supported by a fluorous diamino-dialkoxide ligand for the highly productive ring-opening polymerization of ε-caprolactone. Organometallics 24:6279. doi:10.1021/om050512s
15. Nomura N, Aoyama T, Ishii R, Kondo T (2005) Salicylaldimine-aluminium complexes for the facile and efficient ring-opening polymerization of ε-caprolactone. Macromolecules 38:5363–5366. doi:10.1021/ma050606d
16. Iwasa N, Fujiki M, Nomura K (2008) Ring-opening polymerization of various cyclic esters by Al complex catalysts containing a series of phenoxy-imine ligands: effect of the imino substituents for the catalytic activity. J Mol Catal A 292:67–75. doi:10.1016/j.molcata.2008.06.009
17. Iwasa N, Katao S, Liu J, Fujiki M, Furukawa Y, Nomura K (2009) Notable effect of fluoro substituents in the imino group in ring-opening polymerization of ε-caprolactone by Al complexes containing phenoxyimine ligands. Organometallics 28:2179–2187. doi:10.1021/om8011882
18. Moya-Cabrera M et al (2009) Coordination diversity of aluminum centers molded by triazole based chalcogen ligands. Inorg Chem 48:5874–5883. doi:10.1021/ic900166u
19. Milione S, Grisi F, Centore R, Tuzi A (2006) Neutral and cationic heteroscorpionate aluminium complexes: synthesis, structure, and ring-opening polymerization of ε-caprolactone. Organometallics 25:266. doi:10.1021/om050902e

LANGMUIR Article
Cite This: Langmuir 2019, 35, 10618−10624
pubs.acs.org/Langmuir

Micromotors as "Motherships": A Concept for the Transport, Delivery, and Enzymatic Release of Molecular Cargo via Nanoparticles

Tomáš Kroupa,[†] Soňa Hermanová,[†,‡] Carmen C. Mayorga-Martinez,[‡] Filip Novotný,[‡] Zdeněk Sofer,[‡] and Martin Pumera*[,‡,§,⊥]

[†]Department of Polymers, Faculty of Chemical Technology, University of Chemistry and Technology Prague, Technická 5, 16628 Prague, Czech Republic

[‡]Center for Advanced Functional Nanorobots, Department of Inorganic Chemistry, Faculty of Chemical Technology, University of Chemistry and Technology Prague, Technická 5, 16628 Prague, Czech Republic

[§]Department of Chemical and Biomolecular Engineering, Yonsei University, 50 Yonsei-ro, Seodaemun-gu, Seoul 03722, Korea

[⊥]Future Energy and Innovation Laboratory, Central European Institute of Technology, Brno University of Technology, Purkyňova 656/123, Brno, CZ-616 00, Czech Republic

Supporting Information

ABSTRACT: Nano/micromotors based on biodegradable and biocompatible polymers represent a progressively developing group of self-propelled artificial devices capable of delivering biologically active compounds to target sites. The majority of these machines are micron sized, and biologically active compounds are simply attached to their surface. Micron-sized devices cannot enter cells, but they provide rapid velocity, which scales down with the size of the device; nanosized devices can enter cells, but their velocity is negligible. An advanced hierarchical design of the micro/nanodevices is an important tool in the development of functional biocompatible transport systems and their implementation in real in vivo applications. In this work, we demonstrate a "mothership" concept, whereby self-propelled microrobots transport smaller cargo-carrying nanorobots that are released by enzymatic degradation.

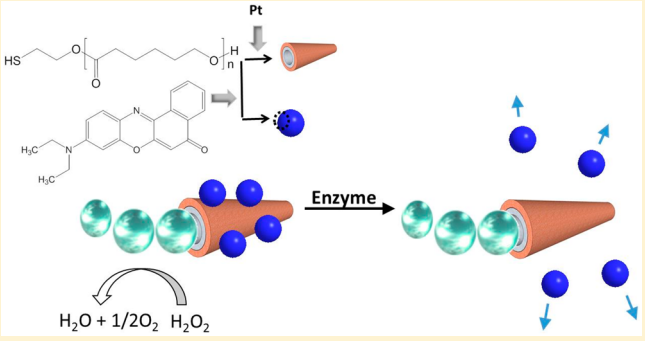

INTRODUCTION

Self-propelled micro- and nanomachines are at the forefront of research on materials. These machines have been intended as carriers in a new possible form of drug delivery and for biomedical applications.[1−5] Micro/nanomotors composed of biodegradable and biocompatible materials are of particular interest because they have potential applications in environmental remediation[6] and chemical cargo transport under physiological conditions, respectively.[7−10] Polymers are among the most promising materials for construction of micro/nanomotors as they offer elasticity and stimulus−response motion behavior.[11,12] Moreover, asymmetric polymer-based micromotors are capable of both, aggregating and leaving the swarm dynamically, depending on fuel conditions.[13]

Such microrobots were fabricated from poly(ε-caprolactone) (PCL), which is a highly valued polymer in biomedical research due to its biodegradability, biocompatibility,[14] and feasibility of further functionalization.[15,16] This allows surface-functionalized thin films, nanoparticles (NPs), and polymer lamellae to be decorated with metal nanoparticles.[16] Multifunctional micromotors composed of single PCL crystals and Pt, Au, and Fe_3O_4 NPs attached to the crystals surface were first introduced by Li and co-workers in 2013.[17] Various asymmetric PCL sheet-like and nonregular sphere-like micromotors have been previously fabricated.[13,18−20]

Here, we present a novel concept that uses an enzymatically degradable microrobot (mothership) to deliver cargo-carrying nanospheres. Nile Red was chosen as a fluorescent hydrophobic probe for visualization of loading of the nanoparticles by the polymeric mothership. Both the cargo and micromotors are susceptible to hydrolytic scission by the action of lipase isolated from *Rhizopus arrhizus* (RA) but at different rates. This allows the design of a biodegradable delivery system (Scheme 1).

Received: April 23, 2019
Revised: June 20, 2019
Published: July 19, 2019

DOI: 10.1021/acs.langmuir.9b01192
Langmuir 2019, 35, 10618−10624

Scheme 1. Fabrication Process and Enzymatically Triggered Disintegration of Micromotors Loaded with Polymer Particles[a]

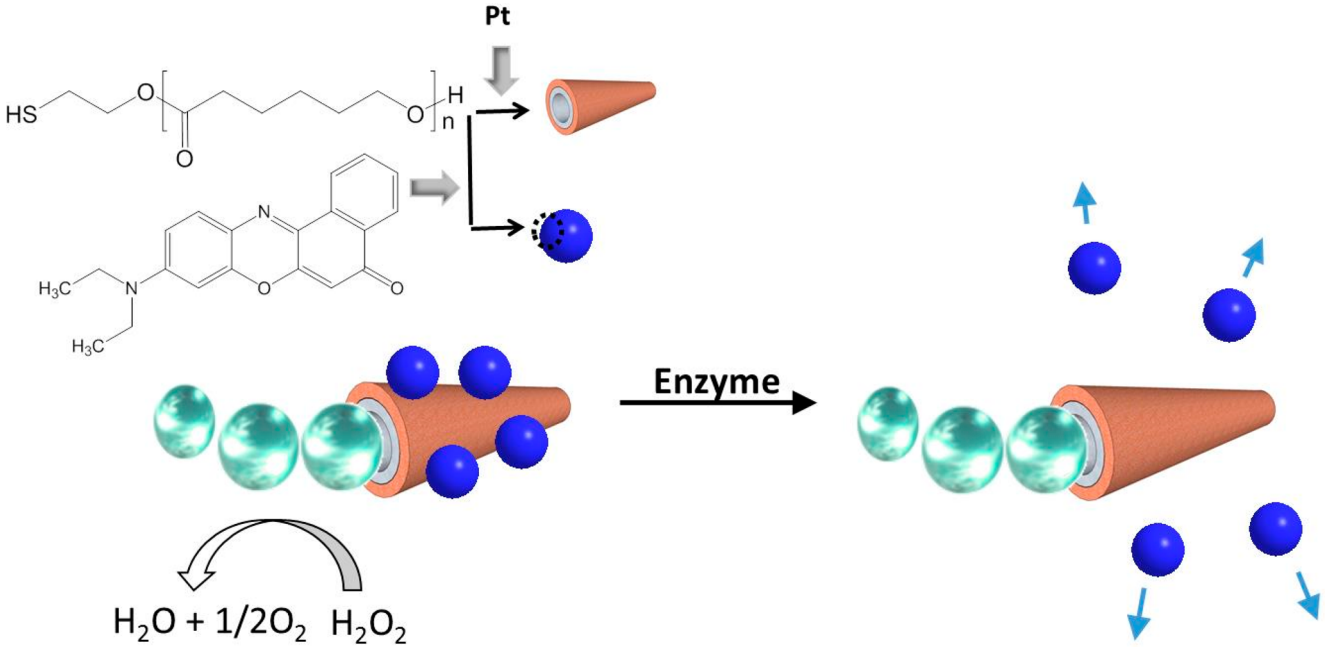

[a]Thiol-functionalized poly(ε-caprolactone), PCL was drop-cast and Pt-covered making sheet-like and tubular micromotors after sonication. The PCL-based cargo nanospheres with Nile red incorporated were obtained by the single emulsion. The cargo was loaded by the contribution of thiol-platinum and hydrophobic interactions. Both the cargo and micromotor were hydrolysed by lipase from *Rhizopus arrhizus*.

MATHERIALS AND METHODS

Materials. Immobilized lipase from *Candida antarctica* (CALB, Novozyme 435) with an activity of 2.5 $U \cdot mg^{-1}$ and lipase from *R. arrhizus* with an activity of 2 $U \cdot g^{-1}$ were obtained from Fluka and used as received. Poly(vinyl alcohol) (PVA) with a Mw of 31 $kg \cdot mol^{-1}$, 2-mercaptoethanol (99%), hydrogen peroxide (30%), and sodium dodecyl sulfate (SDS, 98.5%) were obtained from Sigma-Aldrich. Monomer, ε-caprolactone (99%) was supplied by Across Organics, dried with CaH_2, and freshly distilled prior to polymerizations.

Procedures. Enzymatically catalyzed ring-opening polymerization of ε-caprolactone was performed according to published procedure.[21] For micromotor preparation, an aqueous solution of PVA (1%, 300 μL) was deposited on the surface of a coverslip. Then, a solution of PCL-SH in dichloromethane (150 μL, 1 $mg \cdot mL^{-1}$) was drop-cast on the PVA layer. The bilayer structure was left to dry for 2 h. In the second step, a platinum (99.99%) layer was deposited on top of the thiol-functionalized polymer film by e-beam vacuum evaporation at a pressure of 1×10^{-5}mbar. The thickness of the deposited Pt layer was controlled by a quartz crystal microbalance (QCM) monitor. The deposition was performed at ambient temperature, and the temperature did not exceed 40 °C during the evaporation procedure. The slide with the as-prepared layered structure was then immersed in deionized water and sonicated for 25 min to disintegrate upon dissolution of the PVA layer.

PCL-SH nanospheres were prepared by single emulsion and solvent evaporation methods. Thiol-functionalized PCL (10 mg) and Nile Red (0.1 mg) were dissolved in 1 mL of dichloromethane and emulsified into 10 mL of 0.2% w/v aqueous PVA solution using a high-speed homogenizer (Ultra Turrax T, 18). After complete solvent evaporation, the nanospheres were collected by centrifugation (10000 rpm, 10 min) and rinsed with demineralized water. This was repeated three times to remove any nonencapsulated dye.

The encapsulation efficiency of the dye in nanospheres was evaluated using UV−vis spectroscopy (Avantes).

For micromotor propulsion experiments, Pt/PCL-SH micromotors in the presence of 9% H_2O_2 solution and 3% SDS were used. For cargo transport demonstration, volume aliquots of NR PCL-SH nanospheres (5 μL) were added to the micromotors' suspension.

To perform enzymatic degradation of the micromotors, a solution of lipase from *R. arrhizus* in phosphate buffer at pH 7.0 (0.4 mL, 9.3 $mg \cdot mL^{-1}$) was added to the suspension of Pt/PCL-SH micromotors (0.6 mL). The suspension was shaken at room temperature for 6 days. Afterward, the supernatants were collected by centrifugation and the solid residues were rinsed, with buffer solution and demineralized water, and subjected to microscopic analyses.

The course of enzymatic degradation of the PCL-SH nanospheres was followed by measuring *Z*-averaged and light scattering intensity of the polymer particles in time according to the procedure reported in the literature.[22] A lipase solution in phosphate buffer at pH 7.0 (80 μL, 9.3 $mg \cdot mL^{-1}$) was added to the dispersion of copolymer particles in water (120 μL, 1 $mg \cdot mL^{-1}$) in a cuvette. The measurement was performed directly in the cuvette at 37 °C. The relative light scattering value derived from the count rate (RLS) was calculated as follows: RLS = DCRt/DCR0, where DCRt is the derived count rate of the sample in a specific measurement interval and DCR0 is the derived count rate of the sample at time = 0 h.

Characterization of Micromotors and Particles. The morphology and height profiles of the micromotors were analyzed by an optical profilometer (Senofar S neox) using the confocal method. The morphology of the micromotors and particles was examined by a scanning electron microscope (SEM) with an FEG electron source (Tescan MAIA3 Triglav) using an in-lens secondary electron detector (5 kV beam) and a transmitted electron detector (7 kV beam). Elemental composition and mapping were performed by using an energy dispersive spectroscopy (EDS) analyzer (X-MaxN) with a 150 mm^2 silicon drift detector (Oxford Instruments) and AZtecEnergy software. SEM-EDS analysis was carried out using a 10 kV electron beam in analysis mode (not using the field immersion).

The motion of the Pt/PCL-SH micromotors in aqueous solutions of H_2O_2 of various concentrations and SDS as surfactant (1% w/v) was recorded by an Olympus BX43 microscope equipped with a FastCam mini camera. Motion analysis of the captured video was done by using NIS-Elements AR software.

DOI: 10.1021/acs.langmuir.9b01192
Langmuir 2019, 35, 10618−10624

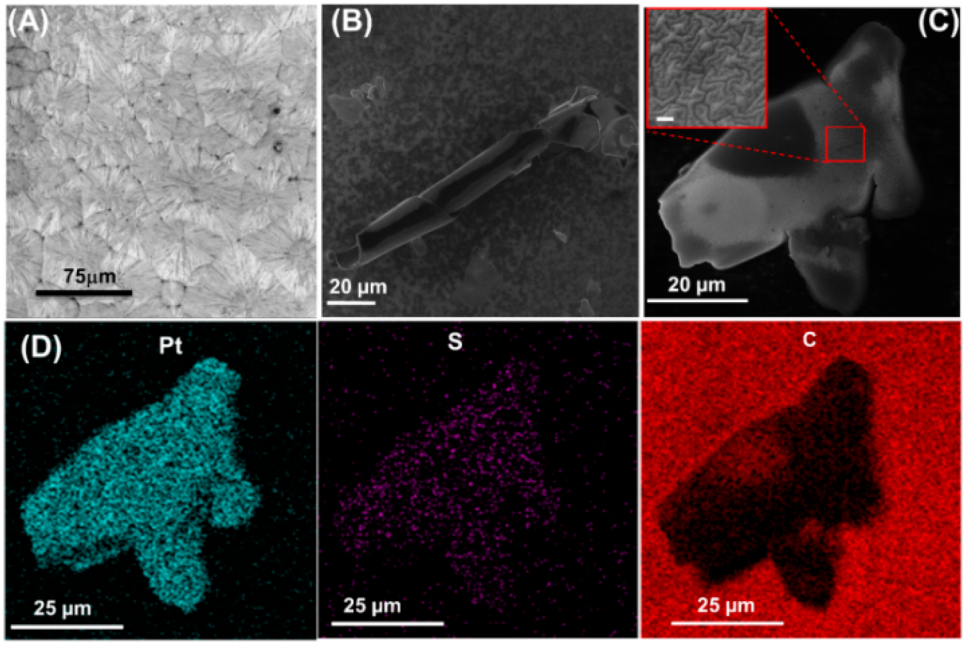

Figure 1. Microscopic analyses of PCL-based micromotors: (A) optical profilometer image of starting PCL-SH film without platinum layer (view of film's top side). (B and C) SEM images of representative PCL-SH/Pt micromotors. (D) energy-dispersive X-ray mapping from SEM images.

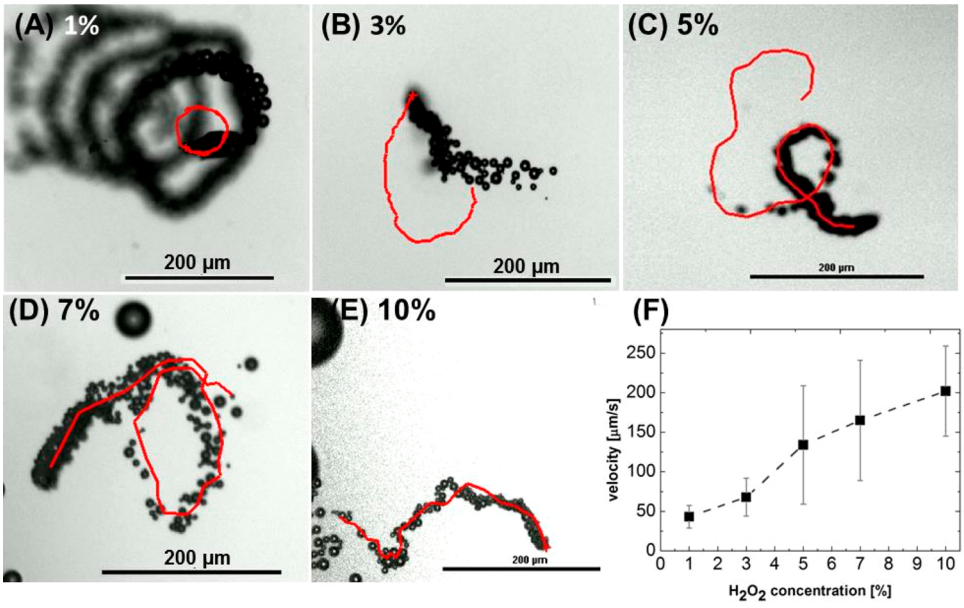

Figure 2. (A–E) Trajectories of PCL-SH/Pt micromotors at different H_2O_2 concentrations. (F) Correlation of micromotor velocity as a function of H_2O_2 concentration. Error bars indicate the standard deviation of 20 micromotors. All videos were recorded in the presence of 1 wt % SDS. Scale bar = 200 μm.

To measure PCL particles size, dynamic light scattering (DLS) was applied (Malvern Instruments Zetasizer Nano ZS with 633 nm laser and 175° detection optics) at 25 °C.

To confirm the loading of PCL with Nile Red, an inverted fluorescence microscope (Olympus IX73) was used with a Chroma 51003 filter cube and a X-Cite 120 Q 120W broadband light source. The fluorescence images of the Nile Red-loaded PCL were taken with a Retiga R1 camera.

■ RESULTS AND DISCUSSION

We fabricated micromotors and nanosphere-based cargo from biodegradable and biocompatible poly(ε-caprolactone) (PCL). Fabrication of the micromotors and cargo, loading release, and disintegration processes are illustrated in Scheme 1. Thiol-functionalized poly(ε-caprolactone) (PCL-SH) was synthesized by green ring-opening polymerization, achieving a molar mass of 10 kg·mol^{-1} and 60 mol % of thiol end groups. Polymerization and thermal analysis results are summarized in the Supporting Information, Table S1. Figure S1 shows the ^{1}H NMR spectrum of the polymer, confirming the structure of PCL and the presence of the introduced thiol groups. Once we obtained the PCL sheets, the PCL-SH/Pt micromotors were fabricated. PCL-SH powder was first dissolved in dichloromethane and deposited by drop-casting onto a PVA-modified glass slide to create a film layer (Figure 1A). This layer was

DOI: 10.1021/acs.langmuir.9b01192
Langmuir 2019, 35, 10618–10624

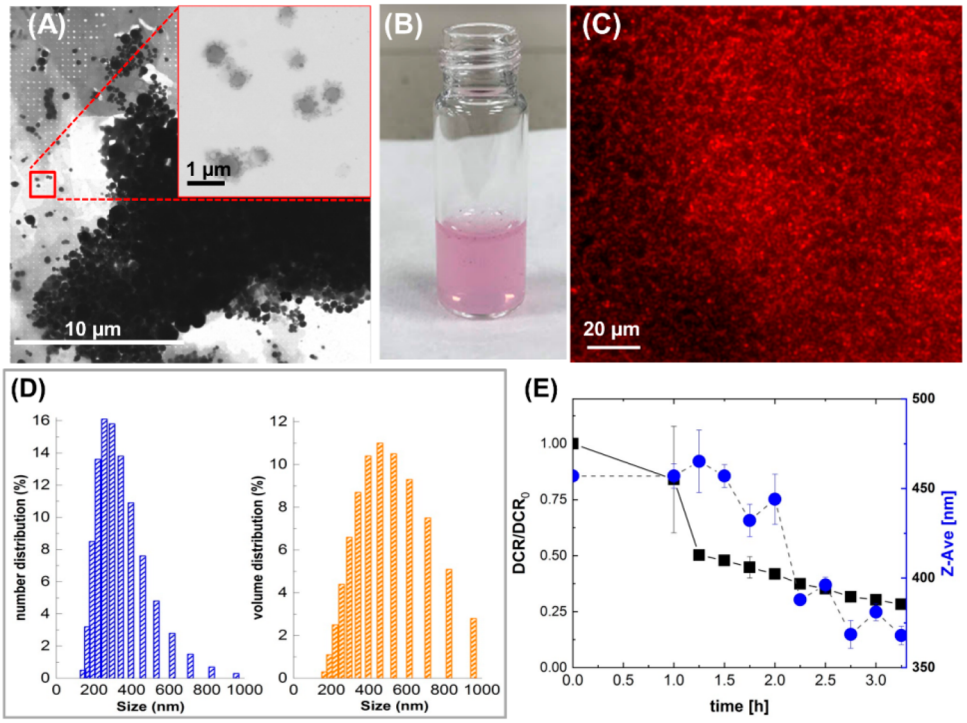

Figure 3. Microscopic images of NR-loaded PCL-SH spheres. (A) STEM image of the PCL deposited on a carbon-coated TEM grid at different resolution. (B) Polymer particles dispersion in water. (C) Fluorescence microscopy image of the deposited PCL particle loaded with Nile Red. (D) Size distribution of PCL particles according to DLS analysis. (E) Time profile of DLS analysis for NR-loaded PCL-SH spheres incubated with lipase from *R. arrhizus* (black squares = derived count rate ratio calculated as DCR_t/DCR_0; blue circles = *Z*-Average of spheres).

then coated with Pt via evaporation to deposit a compact layer (40 nm).

Afterward, the glass slide was sonicated in water, and the PCL-SH/Pt bilayer structure was disintegrated into sheet-and tubular-like micromotors with lengths from 35 to 125 μm (see SEM images, Figures 1B and 1C) and an average thickness of 400 nm. The height profile obtained by the optical profilometer is shown in Figure S2, and the representative images are shown in Figure S3. Tubular micromotors were formed by the self-rolling of platinum-PCL bilayer microsheets due to internal stress resulting from nonhomogenous Pt coating on one side. This is advantageous since rolled-up tubular micro/nanomotors have exhibited a high catalytic performance and a capability to be tailored for the performance of specific tasks.[23] In addition, the tubular micromotors are formed by their self-rolling directly in situ; this has the potential of being a simple economical template-free approach to microrocket fabrication. Qiang He et al. have recently reported the preparation of rolled-up microrockets by a template-free approach based on the combination of layer-by-layer (LbL) assembly and microcontact printing.[24] This combination of methods ensured the production of defined LbL micromotors with the capability to transport the cells.

Interestingly, a wrinkled morphology was observed on the Pt surface (inset Figure 1C), which was attributed to the spherulitic pattern of the starting PCL-SH film (Figure 1A) formed during evaporative crystallization. The surface of the self-rolled tubular micromotors appeared smooth since this was the bottom face of the starting film, which was in contact with the PVA layer on the substrate.

The presence of thiol groups and the formation of a Pt layer on the micromotors' surface was confirmed by EDX analysis (Figure 1D). The occurrence of platinum−thiol interaction between the polymer and Pt was assumed to prevent Pt leaching during the micromotors' washing, storage, or motion analysis.

Motion performance of the obtained micromotors was studied in a hydrogen peroxide aqueous solution containing the sodium dodecyl sulfate (SDS) surfactant. Representative trajectories of the micromotors at H_2O_2 concentrations varying from 1 to 10 wt % are presented in Figures 2A−E and Supporting Information Videos S1 and S2 recorded at 1 and 10 wt % H_2O_2, respectively. Movement of the micromachines by bubble propulsion can be clearly observed. The average velocities were calculated from the motion of 20 different micromotors at different concentrations of H_2O_2 (0−10%).

Lipase from *R. arrhizus* was used to demonstrate the biodegradability of PCL-SH micromotors. Both PCL-SH microsheets and PCL-SH/Pt micromotors were subjected to incubation with lipase for 6 days. It is well-known that enzymatic hydrolysis takes place first in amorphous regions of the polymeric film surface. As degradation progressed, the microsheets disintegrated into lamellar-like structures as a consequence of hydrolytic scission occurring preferentially in the loosely chain-packing domains of the spherulitic surface. The degradation progress is depicted in Figures S4. The increase in intensity of the absorption band at 1185 cm^{-1} in ATR-IR spectra (data not shown) of the degraded samples confirmed the degradation in the amorphous phase as compared with that in the spectra of the starting material. This was later utilized when well-guided and detectable micromotors were disassembled into daughter ships upon reaching the target location.

To create biocompatible and biodegradable cargo compatible with PCL-SH/Pt micromotors, the same polymeric material was used to fabricate soft nanospheres. These

DOI: 10.1021/acs.langmuir.9b01192
Langmuir 2019, 35, 10618−10624

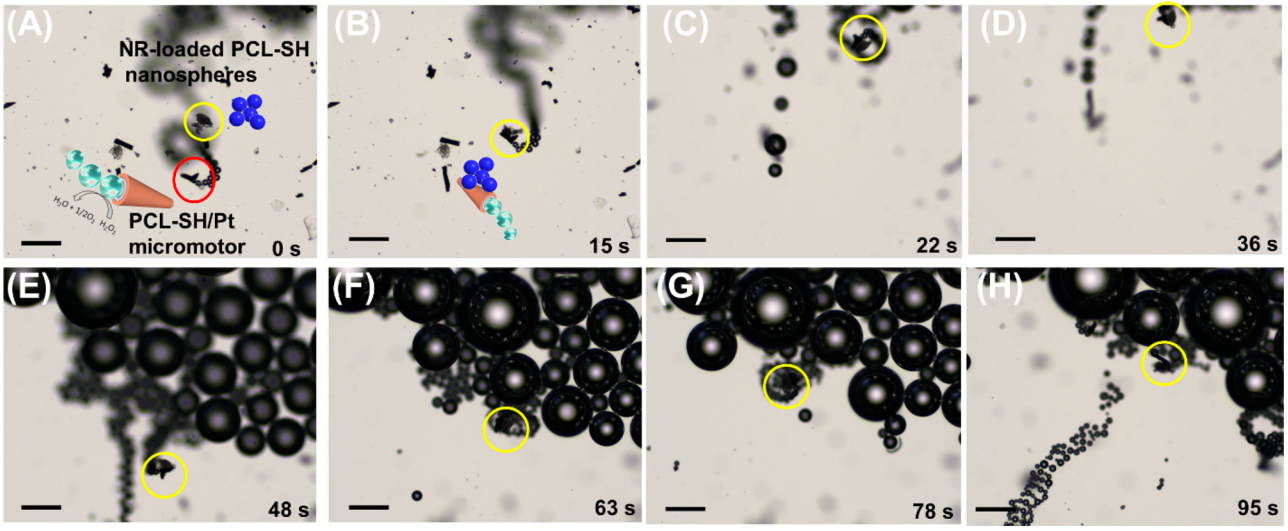

Figure 4. Consecutive image frames of the loading (A and B) and transport (B–H) of NR-loaded PCL-SH nanospheres (objects inside yellow circle in Figure 4A) by PCL-SH/Pt micromotors (objects inside red circle in Figure 4A). Experimental conditions: 1 wt % H_2O_2 and 1 wt % SDS. Scale bar = 53 μm.

nanospheres were loaded with a fluorescent compound, Nile Red (NR). The spherical shape of the NR-loaded PCL-SH nanospheres was demonstrated by SEM images (Figure 3A and inset). The presence of NR in the nanospheres (Figure 3B) was verified by fluorescence microscopy (Figure 3C). These nanospheres had a hydrodynamic size of 440 nm and a polydispersity index (PdI) of 0.3 according to dynamic light scattering (DLS) analysis. Figure 3D shows the size distribution of PCL particles according to DLS analysis in demineralized water. The particle size obtained by the DLS measurements was in agreement with the results obtained from analysis of the SEM images. Moreover, encapsulation efficiency of NR in PCL-SH nanospheres was estimated to be 20% (according to UV–vis analysis) with a loading of 2 μg of NR per 1 mg of PCL-SH polymer.

To evaluate enzymatic digestion of the nanospheres by lipase from *R. arrhizus*, a dispersion of the nanospheres was mixed with aliquots of the lipase solution directly in a cuvette and changes in Z-averaged and derived count rate (DCR) were followed in time. A decrease of the DCR was clearly observed, which can be attributed to the decreasing amount of the nanospheres. Concomitantly, the size of nanospheres decreased during the 3 h period, confirming the occurrence of surface erosion (Figure 3E).

The capability of the PCL-SH/Pt micromotors of cargo loading and transport was evaluated in an aqueous solution containing 1 wt % of H_2O_2 and 1 wt % of SDS at room temperature. Supporting Information Videos S3 and S4 show the micromotors before the cargo loading and during the cargo transport, respectively. Consecutive image frames of loading and transport of NR-loaded PCL-SH nanospheres (objects inside yellow circle in Figure 4A) by a PCL-SH/Pt micromotor (object inside red circle in Figure 4A) are presented in Figure 4 (A–H).

Efficient loading started 15 s after addition of the NR-loaded PCL-SH nanospheres to the solution containing the micromotors (Figures 4A,B). Interestingly, the micromotors were able to transport and collect additional polymer spheres during the next 80 s (Figures 4C–H). Moreover, the high catalytic activity of PCL-SH/Pt micromotors in H_2O_2 decomposition to O_2 for self-propelling was demonstrated by massive bubble production (Figure 4E–H). A successful loading of polystyrene microspheres onto Pt/PCL micromotors via magnetic or hydrophobic interactions at increased temperature have been currently reported.[19]

In this work, the contribution of the thiol–platinum interaction to efficient loading is suggested as polymer spheres had thiol groups on their surface and micromotors possessed a Pt layer on one side.

To demonstrate enzymatically triggered disassembly of the micromotors, nanosphere release, and degradation of the whole transport system, the micromotors loaded with nanospheres were exposed to lipase. More specifically, the PCL-SH/Pt micromotors were incubated with NR-loaded PCL-SH nanospheres for 2 min. The images in Figure 5A show that the NR-loaded PCL-SH nanospheres were successfully attached to the micromotors. After that, an aliquot of the lipase solution was added to obtain a final concentration of 20 mg/mL and the system was incubated for 22 h. Figure 5B shows that complete degradation of the nanospheres occurred. After 88 h of continuous incubation, just small pieces of PCL-SH/Pt micromotors were observed, confirming their disintegration (Figure 5C).

It is worth noting that in these experiments, lipase concentration was increased compared with that in enzymatic degradation of micromotors without cargo (Figure S4 in SI). Accelerated enzymatic hydrolysis resulted in the desired degradation pattern of the amorphous nanospheres into soluble oligomers. For micromotors, which are on a micrometer scale and comprise a semicrystalline polymer layer, the disintegration occurred as a consequence of the hydrolysis by surface erosion and scission of chains in the amorphous regions.

■ CONCLUSION AND OUTLOOK

In this study, we prepared a thiol-functionalized polymer for the design and fabrication of biocompatible and biodegradable micromotors and nanospheres used as transport devices for a dye-based cargo. The successful functionalization of poly(ε-caprolactone) and Nile Red dye loading was demonstrated by

DOI: 10.1021/acs.langmuir.9b01192
Langmuir 2019, 35, 10618–10624

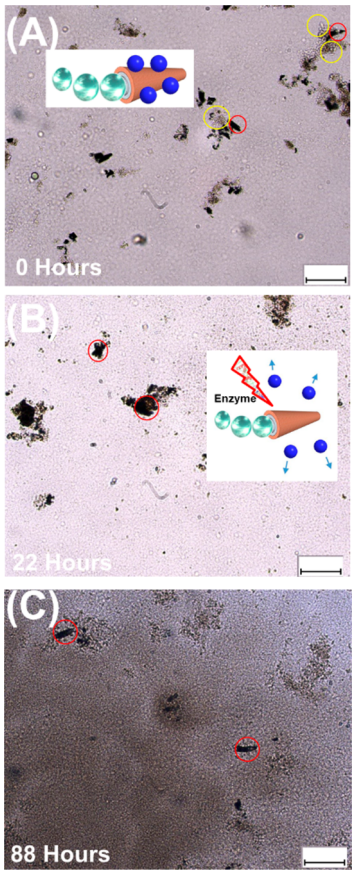

Figure 5. (A) NR-loaded PCL-SH nanospheres attached to PCL-SH/Pt micromotors after 2 min. (B) Complete degradation of NR-loaded PCL-SH nanospheres after 22 h. (C) PCL-SH/Pt micromotor disintegration after 88 h. The experiments in (B) and (C) were carried out in the presence of lipase enzyme in PBS (pH 7.0, concentration of enzyme in final solution 20 mg/mL). Scale bar = 100 μm.

^{1}H NMR and UV−vis spectroscopic analyses, respectively. The prepared PCL-SH/Pt micromotors showed good performance in terms of velocity. The conditions of enzymatic degradation of the PCL-SH-based transport vehicles were optimized to enzymatically trigger dye release and micromotor disintegration. In summary, we reported on the design of a biocompatible micromotor and cargo system with a desired degradation pattern. This represents a proof-of-concept for a transport system that uses enzymatically triggered drug release and micromotor disassembly.

Autonomously propelled micro- and nanomotors are considered as advanced drug delivery platforms, which offer passage across tumor environments, overcoming elevated interstitial fluid pressure, or across body fluids with varying viscosity. When they reach a target location, efficient release of cargo should occur thus providing bioavailability. From this point of view, the rational design of biodegradable cargo and micro/nanomotors, which undergo degradation at a time that coincides with the time of payload delivery, is a challenging issue to be addressed. Enzyme-triggered release using disease-associated enzymes or external enzymes added on purpose represents a prospective concept for therapeutic and diagnostic (theranostics) applications.

■ ASSOCIATED CONTENT

Supporting Information

The Supporting Information is available free of charge on the ACS Publications website at DOI: 10.1021/acs.langmuir.9b01192.

Polymerization results, ^{1}NMR spectrum of OH-PCL-SH, images of micromotors taken by optical profilometer (PDF)

Representative trajectories of the micromotors at H_2O_2 concentration of 1 wt % (MP4)

Representative trajectories of the micromotors at H_2O_2 concentration of 10 wt % (MP4)

Micromotors before the cargo loading (MP4)

Micromotors during the cargo transport (MP4)

■ AUTHOR INFORMATION

Corresponding Author

*E-mail: martin.pumera@vscht.cz.

ORCID

Carmen C. Mayorga-Martinez: 0000-0003-3687-0035

Zdeněk Sofer: 0000-0002-1391-4448

Martin Pumera: 0000-0001-5846-2951

Author Contributions

The manuscript was written through contributions of all authors.

Notes

The authors declare no competing financial interest.

■ ACKNOWLEDGMENTS

This work was supported by the project Advanced Functional Nanorobots (reg. no. CZ.02.1.01/0.0/0.0/15_003/0000444 financed by the EFRR) and from specific university research (MSMT No 21-SVV/2019).

■ ABBREVIATIONS

PCL, poly(ε-caprolactone); (NR), Nile Red; SDS, sodium dodecyl sulfate

■ REFERENCES

(1) Medina-Sánchez, M.; Xu, H.; Schmidt, O. G. Micro- and nanomotors: the new generation of drug carriers. *Ther. Delivery* **2018**, *9* (4), 303−316.

(2) Fischer, P.; Pumera, M.; Wang, J. Micro- and Nanomachines on the Move. *Adv. Funct. Mater.* **2018**, *28* (25), 1801745.

(3) Chen, X.-Z.; Hoop, M.; Mushtaq, F.; Siringil, E.; Hu, C.; Nelson, B. J.; Pané, S. Recent developments in magnetically driven micro- and nanorobots. *Applied Materials Today* **2017**, *9*, 37−48.

(4) Luo, M.; Feng, Y.; Wang, T.; Guan, J. Micro-/Nanorobots at Work in Active Drug Delivery. *Adv. Funct. Mater.* **2018**, *28* (25), 1706100.

(5) Li, J.; Esteban-Fernández de Ávila, B.; Gao, W.; Zhang, L.; Wang, J. Micro/nanorobots for biomedicine: Delivery, surgery, sensing, and detoxification. *Science Robotics* **2017**, *2* (4), eaam6431.

(6) Maric, T.; Moo, J. G. S.; Khezri, B.; Sofer, Z.; Pumera, M. Black-phosphorus-enhanced bubble-propelled autonomous catalytic microjets. *Applied Materials Today* **2017**, *9*, 289−291.

(7) Jurado-Sánchez, B.; Pacheco, M.; Maria-Hormigos, R.; Escarpa, A. Perspectives on Janus micromotors: Materials and applications. *Applied Materials Today* **2017**, *9*, 407−418.

(8) Tu, Y.; Peng, F.; André, A. A. M.; Men, Y.; Srinivas, M.; Wilson, D. A. Biodegradable Hybrid Stomatocyte Nanomotors for Drug Delivery. *ACS Nano* **2017**, *11* (2), 1957−1963.

DOI: 10.1021/acs.langmuir.9b01192
Langmuir 2019, 35, 10618−10624

(9) Wang, X.; Chen, X.-Z.; Alcântara, C. C. J.; Sevim, S.; Hoop, M.; Terzopoulou, A.; de Marco, C.; Hu, C.; de Mello, A. J.; Falcaro, P.; Furukawa, S.; Nelson, B. J.; Puigmartí-Luis, J.; Pané, S. MOFBOTS: Metal−Organic-Framework-Based Biomedical Microrobots. *Adv. Mater.* **2019**, 1901592.
(10) Peters, C.; Hoop, M.; Pané, S.; Nelson, B. J.; Hierold, C. Degradable Magnetic Composites for Minimally Invasive Interventions: Device Fabrication, Targeted Drug Delivery, and Cytotoxicity Tests. *Adv. Mater.* **2016**, *28* (3), 533−538.
(11) Magdanz, V.; Guix, M.; Hebenstreit, F.; Schmidt, O. G. Dynamic Polymeric Microtubes for the Remote-Controlled Capture, Guidance, and Release of Sperm Cells. *Adv. Mater.* **2016**, *28* (21), 4084−4089.
(12) Wang, X.; Qin, X.-H.; Hu, C.; Terzopoulou, A.; Chen, X.-Z.; Huang, T.-Y.; Maniura-Weber, K.; Pané, S.; Nelson, B. J. 3D Printed Enzymatically Biodegradable Soft Helical Microswimmers. *Adv. Funct. Mater.* **2018**, *28* (45), 1804107.
(13) Liu, L.; Liu, M.; Su, Y.; Dong, Y.; Zhou, W.; Zhang, L.; Zhang, H.; Dong, B.; Chi, L. Tadpole-like artificial micromotor. *Nanoscale* **2015**, *7* (6), 2276−2280.
(14) Labet, M.; Thielemans, W. Synthesis of polycaprolactone: a review. *Chem. Soc. Rev.* **2009**, *38* (12), 3484−3504.
(15) Wang, D.; Zhao, G.; Chen, C.; Zhang, H.; Duan, R.; Zhang, D.; Li, M.; Dong, B. One-Step Fabrication of Dual Optically/Magnetically Modulated Walnut-like Micromotor. *Langmuir* **2019**, *35* (7), 2801−2807.
(16) Zhou, T.; Dong, B.; Qi, H.; Lau, H. K.; Li, C. Y. One-step formation of responsive ″dumbbell″ nanoparticle dimers via quasi-two-dimensional polymer single crystals. *Nanoscale* **2014**, *6* (9), 4551−4554.
(17) Dong, B.; Zhou, T.; Zhang, H.; Li, C. Y. Directed Self-Assembly of Nanoparticles for Nanomotors. *ACS Nano* **2013**, *7* (6), 5192−5198.
(18) Liu, M.; Liu, L.; Gao, W.; Su, M.; Ge, Y.; Shi, L.; Zhang, H.; Dong, B.; Li, C. Y. A micromotor based on polymer single crystals and nanoparticles: toward functional versatility. *Nanoscale* **2014**, *6* (15), 8601−8605.
(19) Liu, L.; Liu, M.; Dong, Y.; Zhou, W.; Zhang, L.; Su, Y.; Zhang, H.; Dong, B. Preparation, heat-enabled shape variation, and cargo manipulation of polymer-based micromotors. *J. Mater. Sci.* **2016**, *51* (3), 1496−1503.
(20) Liu, M.; Liu, L.; Gao, W.; Su, M.; Ge, Y.; Shi, L.; Zhang, H.; Dong, B.; Li, C. Y. Nanoparticle mediated micromotor motion. *Nanoscale* **2015**, *7* (11), 4949−4955.
(21) Hedfors, C.; Östmark, E.; Malmström, E.; Hult, K.; Martinelle, M. Thiol End-Functionalization of Poly(ε-caprolactone), Catalyzed by Candida antarctica Lipase B. *Macromolecules* **2005**, *38* (3), 647−649.
(22) Reinišová, L.; Novotný, F.; Pumera, M.; Kološtová, K.; Hermanová, S. Nanoparticles Based on Poly(trimethylene carbonate) Triblock Copolymers with Post-Crystallization Ability and Their Degradation in vitro. *Macromol. Res.* **2018**, *26*, 1026.
(23) Zha, F.; Wang, T.; Luo, M.; Guan, J. Tubular Micro/Nanomotors: Propulsion Mechanisms, Fabrication Techniques and Applications. *Micromachines (Basel)* **2018**, *9* (2), 78.
(24) Hu, N.; Sun, M.; Lin, X.; Gao, C.; Zhang, B.; Zheng, C.; Xie, H.; He, Q. Self-Propelled Rolled-Up Polyelectrolyte Multilayer Microrockets. *Adv. Funct. Mater.* **2018**, *28* (25), 1705684.

DOI: 10.1021/acs.langmuir.9b01192
Langmuir 2019, 35, 10618−10624

Macromolecular Research

Article

DOI 10.1007/s13233-019-7007-6 www.springer.com/13233 pISSN 1598-5032 eISSN 2092-7673

Nanoparticles Based on Poly(trimethylene carbonate) Triblock Copolymers with Post-Crystallization Ability and Their Degradation *in vitro*

Lucie Reinišová[1]
Filip Novotný[2]
Martin Pumera[2]
Katarína Kološtová[3]
Soňa Hermanová*[,1]

[1] Department of Polymers, Faculty of Chemical Technology, University of Chemistry and Technology Prague, Technická 5, 16628 Prague, Czech Republic
[2] Center for the Advanced Functional Nanorobots, Department of Inorganic Chemistry, Faculty of Chemical Technology, University of Chemistry and Technology Prague, Technická 5, 16628 Prague, Czech Republic
[3] Faculty Hospital Kralovské Vinohrady, Center of Applied Bioimplantology, Šrobárova 50, Prague 10, 10043 Prague, Czech Republic

Received March 27, 2018 / Revised May 13, 2018 / Accepted June 7, 2018

Abstract: Aliphatic polycarbonate-based block copolymers have received considerable attention as carriers for targeted drug and gene delivery because of their biocompatibility and biodegradability. However, there is little understanding of their phase behaviour and physicochemical characterization of the particles made from them. Here, we prepared a series of well-defined poly(trimethylene carbonate) (PTMC)-based copolymers with molar masses of 3-9 kg·mol^{-1} by metal-free ring-opening polymerization using dihydroxy-terminated poly(ethylene oxide) as a macroinitiator. Micellar nanoparticles self-assembled from copolymers had a size of less than 130 nm. They were degraded by the action of a model lipase from *Mucor Miehei* at 37 °C, which is of high importance for biodegradability in the living organism. X-ray diffraction and differential scanning calorimetry proved that amorphous copolymers with more than 39 mol% of carbonate units and representative particles were prone to the rearrangement of PTMC chains during storage and to thus undergo post-crystallization. Our findings can contribute to the comprehensive characterization of polycarbonate biomaterials for medical applications.

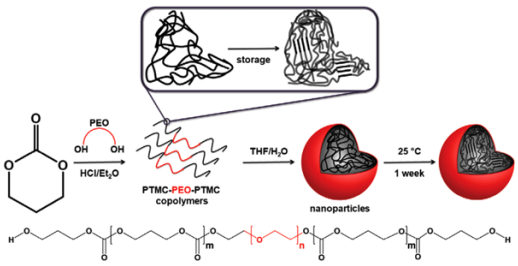

Keywords: amphiphilic copolymers, crystallization, self-assembly, enzyme degradation.

1. Introduction

Poly(trimethylene carbonate), PTMC, and its copolymers are biocompatible resorbable aliphatic polycarbonates and polyester carbonates applicable in the regeneration of soft tissues and drug delivery.[1-6] PTMC is a promising candidate for drug delivery vehicles because it is hydrolysed into nonacidic degradation products (1,3-propanediol and carbon dioxide) when subjected to *in vivo* conditions due to enzymatically induced surface erosion.[7-9] For the purpose of transporting various payloads, PTMC was formed into particles, disks, and gels.[10,11]

To extend delivery potential, amphiphilic copolymers composed of hydrophobic PTMC block and hydrophilic, mostly poly(ethylene oxide), PEO, block were synthesized. Cytotoxicity study proved that such copolymers are nontoxic biomaterials to chondrocytes.[12] Biocompatible hydrophilic PEO moiety increased the vehicles' resistance towards non-specific adsorption of proteins and cells compared to PTMC-based hydrophobic particles.[13-15] Moreover, core-shell type particles or polymersomes made from these copolymers [16-18] are particularly attractive due to their capability to accommodate poorly water-soluble drugs with high encapsulation efficiency (around 90%).[19,20]

The morphology and crystallinity of block copolymers are known to significantly influence degradation rate of polymer matrix and drug release profile.[21,22] Until now, there is little understanding to the crystallization properties of PTMC-*b*-PEO di- and triblock copolymers. Simplified cases were mostly considered. For example, PTMC block is amorphous and PEO block can crystallize when the fraction of TMC units is less than 63.5 mol%.[15] The possibility of PTMC phase crystallization in diblock copolymer; $mPEO_3$-$PTMC_{11}$, was suggested by Zhang *et al.* relating to the occurrence of a broad single melting endotherm with the heat of fusion higher than that corresponding only to the PEO block.[19]

In the present study, morphology and physicochemical properties of a series of triblock PTMC-*b*-PEO-*b*-PTMC copolymers were studied in order to obtain a comprehensive image of their phase behavior. The copolymers were assembled into micellar nanoparticles with the core formed by PTMC hydrophobic matrix (Scheme 1). To understand the effects of PTMC block length on the physicochemical properties of nanoparticles, representative samples were extensively characterized using scanning electron microscopy (SEM), dynamic light scattering (DLS), nanoparticle tracking analysis (NTA), thermal analysis

Acknowledgment: This work was supported by the project Advanced Functional Nanorobots (reg. No. CZ.02.1.01/0.0/0.0/15_003/0000444 financed by the EFRR) and from specific university research (MSMT No 21-SVV/2018).

***Corresponding Author:** Soňa Hermanová (sona.hermanova@vscht.cz)

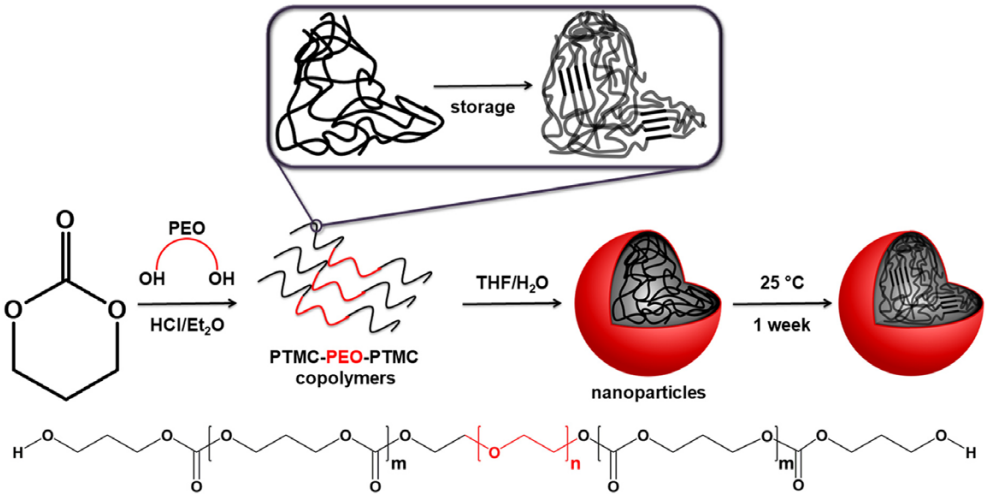

Scheme 1. Preparation of polycarbonate copolymer-based micellar nanoparticles with hydrophobic PTMC core and hydrophilic PEO shell.

(DSC) and powder diffraction (WAXD). Enzymatic degradation of particles *in vitro* was evaluated by the action of lipase from *Mucor miehei*.

2. Experimental

Trimethylene carbonate (TMC) was purchased from Labso Chimie, France, and twice recrystallized from diethyl ether. Dihydroxy-terminated PEOs (M_n=1000, 2000, 4000 g·mol^{-1}) were purchased from Sigma Aldrich. All PEOs were dissolved in dichloromethane, precipitated in diethyl ether and dried under vacuum before polymerization. Dichloromethane (DCM) was supplied by Penta, CZ and was dried over CaH_2 prior to use. Phosphate buffer (PB, pH=6.9, 56 mM) was prepared according to standard procedure.

2.1. Synthesis of copolymers and characterization of their constitution

Polymerization reactions were performed according to a procedure reported by Hyun *et al.*[23] Reference PTMC homopolymer was synthesized by ring opening polymerization of TMC (14.7 mmol; 1.5 g) initiated by benzyl alcohol (0.3 mmol; 29 μL) and HCl in diethylether (0.3 mmol; 150 μL) in dichloromethane (7.4 mL) for 24 h.

^{1}H and ^{13}C{^{1}H}-NMR spectroscopy analyses of prepared copolymers were performed on Bruker Avance III^{TM} at 500 MHz and Bruker 600 Avance^{III} at 126 MHz respectively. The analyses were performed at 25 °C in $CDCl_3$. The ^{1}H and ^{13}C NMR spectra of PTMC-*b*-PEO-*b*-PTMC copolymers were interpreted according to the studies of Feng *et al.*[18] and Liao *et al.*,[24] respectively. Representative proton signals are as follows:

^{1}H NMR of PTMC-*b*-PEO-*b*-PTMC, $CDCl_3$: δ=1.92 ppm [p, 2H, (-CH_2-)], δ=2.05 ppm [p, 2H, (-CH_2-)], δ=3.64 ppm [t, 2H, (-CH_2O-)], δ=3.73 ppm [t, 2H, (-CH_2OH)], δ=4.24 ppm [t, 4H, (-OCH_2-)], δ=4.30 ppm [t, 2H, (-CH_2-)].

^{13}C{^{1}H}-NMR of PTMC-*b*-PEO-*b*-PTMC, $CDCl_3$: δ=28.04 ppm (-O-*C*H_2-CH_2-*C*H_2-O-CO-), δ=31.56, 31.64ppm (HO-CH_2-*C*H_2-*C*H_2-O-CO-), δ=58.97 ppm (HO-*C*H_2-CH_2-CH_2-O-CO-), δ=64.29 ppm (-CH_2-*C*H_2-CH_2-CO-), δ=67.07, 67.87, 68.89 ppm (-O-CO-O-*C*H_2-*C*H_2-O-), δ=70.58 ppm (-*C*H_2-*C*H_2-O-), δ=154.91 ppm (-*C*=O).

The ^{1}H NMR and ^{13}C{^{1}H}-NMR spectra of prepared copolymers are presented in Supporting information. Attenuated Total Reflectance-Fourier Transform Infrared (ATR-FTIR) spectra of copolymers were obtained on Nicolet 6700 FTIR spectrometer (Thermo-Nicolet, USA) equipped with a diamond ATR accessory GladiATR (PIKE, USA). Spectra were recorded at 4 cm^{-1} resolution for 64 scans in the scan range of 4000-400 cm^{-1}.

SEC analysis was employed to determine M_w, weight-average molar mass, M_n, number-average molar mass, and dispersity $Đ$ (M_w/M_n). Measurements were performed on SEC Waters Breeze chromatograph equipped with two PSS Lux LIN M 5 μm (7.8 mm×300 mm) columns and refractive index detector (RI 880 nm). The mobile phase (THF) flow was 1 mL·min^{-1} and the analysis temperature was 35 °C. Polystyrene standards were used for calibration.

2.2. Particles preparation and characterization of dispersions

To have particles with different composition and comparable hydrodynamic sizes solvent displacement method was applied. THF solution (1 mL) containing 10 or 25 mg of copolymer sample was emulsified in 10 mL of ultrapure water under stirring (5000 rpm^{-1}) for 2 h. Residual THF was distilled off under vacuum (Büchi rotary evaporator, 35 °C).

The particle size was analysed by dynamic light scattering (DLS) method (Malvern Instruments Zetasizer Nano ZS, 633 nm red laser, 175° detection optics) at 25 °C, using the refractive index of PEO=1.456. To measure zeta potential the micellar dispersions were transferred to a folded capillary cell (DTS1061, Malvern Instruments) and measured at 25 °C with an applied voltage of 150 V (Malvern Instruments Zetasizer Nano ZS).

Nanoparticle Tracking Analysis (NTA) was applied to characterize copolymer particles using Nanosight NS300 instrument equipped with a green laser device (532 nm) and an intensified sCMOS camera. For the measurement, camera shutter and gain were manually adjusted as follows. The camera aperture settings were set to camera shutter 391 and camera gain 99,

detection threshold (DT) was set to 14. Maximal capture time of 215 s was selected.[25] The temperature during the acquisition was held at 25 °C. The software used for capturing and analyzing was NTA version 3.2.

The dispersion of sample 1 (1 mg·mL^{-1}) was diluted 100-fold and 200-fold for the measurement, whereas dispersion of sample 7 (1 mg·mL^{-1}) was measured undiluted and 2-fold diluted. The NTA software analysis resulted in particle size distribution, mode size (main peak), mean size and its standard deviation values. The values are presented as an average of five measurements performed under the same capturing settings and conditions directly exported from the software.

2.3. Characterization of phase composition and morphology

The phase composition was evaluated by wide-angle X-ray diffraction (WAXD) on an XRD PANanalytical X´Pert PRO diffractometer using CuKα radiation (40 kV, 30 mA) at 25 °C with step size 0.0390° 2θ and 5.0187-59.9307° 2θ angle range. Glass-transition temperatures (T_g) and melting points (T_m) along with the heat of fusion (ΔH_m) were measured by differential scanning calorimetry (DSC) on Q200 Differential Scanning Calorimeter (TA Instruments) under nitrogen flow (50 mL·min^{-1}) at scanning rate of 5 and 10 °C·min^{-1}.

Synthesized copolymers were subjected to analyses directly after drying. Oligomeric PEOs used as macroinitiators showed melting transition during the first heating with the maxima as follows: PEO 1000, T_m=31 °C (144 J·g^{-1}); PEO 2000, T_m=49 °C (163 J·g^{-1}) and PEO 4000, T_m=58 °C (167 J·g^{-1}).

To analyse the phase composition and thermal properties of the particles, their dispersions (1 mg trehalose/1 mg polymer) were immersed in liquid nitrogen and then freeze-dried overnight (L4-110 PRO freeze dryer, Gregor Instruments). Lyophilized samples were retrieved from fresh dispersions and dispersion incubated at 25 °C for 7 days and characterized. DSC thermogram of threhalose is shown in Supporting information. The morphology of the particles was examined by scanning electron microscope (SEM) with a FEG electron source (Tescan MAIA3 Triglav™). The images were acquired at 7 kV beam energy in high-resolution immersion mode using in-beam secondary electron detector.

2.4. Genomic DNA encapsulation

The procedure was adopted from a published study.[26] Briefly, 50 μL of human genomic DNA in RNase-free water (43 ng·μL^{-1}) was emulsified in a DCM solution of copolymer sample 1 (5 mg·mL^{-1}) by sonication for 5 s (Bandelin Sonorex). The emulsion was transferred into 3 mL of ethanol under moderate stirring. After 10 s, 3 mL of ultrapure water was added. The dispersion was stirred for 10 min, followed by evaporation under vacuum for 1 h (Büchi rotary evaporator, 37 °C). The dispersion was centrifuged for 30 min (Universal 320 R centrifuge, Hettich, 14,000 rpm, 4 °C), the supernatant was removed and particles were re-suspended in 2 mL of PBS. The concentration of DNA in the supernatant was determined using NanoDrop ND 1000 spectrophotometer (Thermo Scientific). The re-suspended polymersomes were directly analyzed along with the original dispersion by tomographic microscopy (Nanolive 3D Cell Explorer) using the associated STEVE software.

2.5. Enzymatic hydrolysis of particles

The occurrence of enzymatic hydrolysis was analysed by measuring Z-Average and light scattering intensity of polymer particle suspension in time according to a procedure reported by Trousil *et al.*[27] and Li *et al.* [28] A lipase solution was added to the dispersion of copolymer particles in water (1 mg·mL^{-1}) to achieve final lipase concentration of 1610 U·mL^{-1}. The measurement was performed directly in a cuvette at 37 °C. Relative light scattering value from derived count rate (RLS) was calculated as follows: RLS=DCR$_t$/DCR$_0$, where DCR$_t$ is derived count rate of the sample in a specific time of the measurement t; DCR$_0$ means derived count rate of the sample in time t=0 h.

3. Results and discussion

3.1. Physicochemical characterization of prepared copolymers

A series of triblock PTMC-based copolymers with central PEO block (M_n=1000, 2000, 4000 g·mol^{-1}) was synthesized by controlled ring-opening polymerization of TMC monomer according to the literature.[23] Molar ratios of the EO:TMC units in almost all

Table 1. Ring-opening polymerizations of TMC initiated by dihydroxy-terminated PEO and HCl/Et$_2$O catalyst

Sample No.	PEO[a] (kg·mol^{-1})	TMC:EO feed[b]	TMC:EO copol[c]	M_n (NMR)[d] (kg·mol^{-1})	M_n (SEC)[e] (kg·mol^{-1})	$Đ$[e]
PTMC	-	100:0	100:0	3	3	1.20
1	1	63:37	67:33	6	5	1.17
2	1	62:38	56:44	4	4.5	1.13
3	2	40:60	42:58	5	6	1.23
4	2	40:60	39:61	5	6	1.16
5	2	39:61	36:64	6	9	1.08
6	4	20:80	23:77	7	7.5	1.14
7	4	10:90	7:93	5	6.5	1.09

[a]Macroinitiators: PEOs with molar mass M_n of 1, 2, and 4 kg·mol^{-1}. [b]EO=ethylene oxide units, mol fractions of TMC and EO in the feed. [c]mol fractions of TMC and EO in copolymer determined by ^{1}H NMR spectroscopy ($CDCl_3$). [d]M_n (NMR) was calculated according to integral ratio of peaks at 2.05 and 3.64 ppm according to the formula as follows: $M_n=(I_{2.05}/I_{3.64}\cdot x\cdot 102)+M_n$ (PEO)+204, where x means number of PEO hydrogen atoms. [e]M_n (SEC), apparent number-average molar mass and dispersity $Đ$ were determined by SEC analysis with RI detector, based on polystyrene standards.

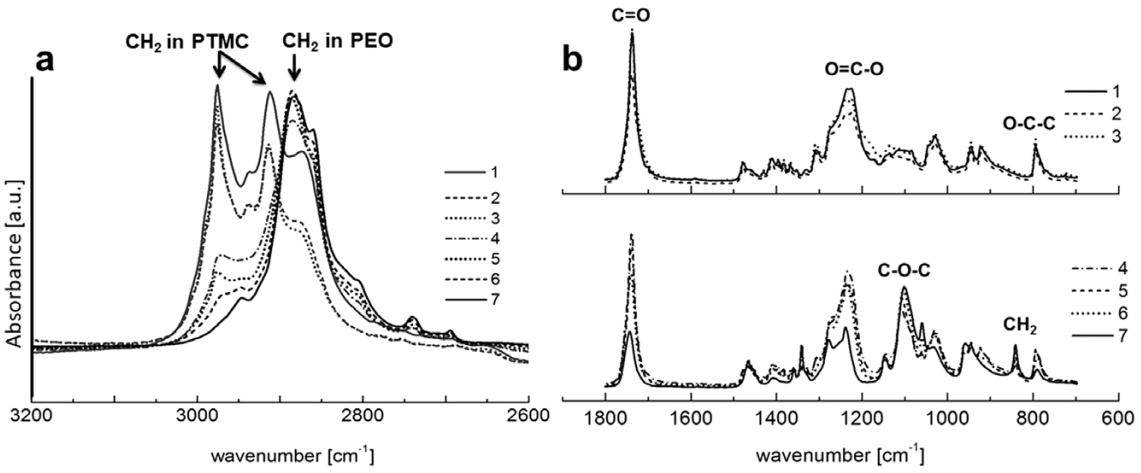

Figure 1. ATR-IR spectra of synthesized copolymers 1-7; (a) C-H stretching region; (b) the region of 1800-700 cm^{-1}.

copolymers corresponded well with the feed ratio and prepared dried samples showed narrow dispersity of 1.08-1.23 (Table 1).

ATR-IR spectra of synthesized copolymers are shown in Figure 1. The peaks at 2976 cm^{-1} and 2912 cm^{-1} corresponded to the C-H bonds of PTMC units, whereas absorption band at 2883 cm^{-1} was attributed to the C-H bonds of PEO block (Figure 1(a)). Strong absorption of carbonyl group at 1737 cm^{-1}, stretch vibration of carbonate C-O group at 1225 cm^{-1} and stretching vibrations of O-C-C at 794 cm^{-1} were associated to PTMC units in copolymer.[29] Ether stretch at 1110 cm^{-1} and CH_2 rocking at 842 cm^{-1} were assigned to PEO in copolymer. The latter was suggested as an evidence of crystalline PEO phase (Figure 1(b)).[30] Appeared absorption bands associated with both carbonate monomeric units and PEO blocks confirmed desired block structure.

To reveal the crystallization capability of the covalently linked blocks, resulting copolymers were analyzed by X-ray powder diffraction (WAXD). According to literature, higher-molecular PTMC homopolymer is assumed as an amorphous elastomer whereas PEO is a semicrystalline polyether with crystalline peaks at 19° and 23° (2θ) in the WAXD pattern.[31,32] The occurrence of crystalline PEO phase in samples with 93-64 mol% of EO units (samples 5, 6, 7) was evidenced by diffraction maxima corresponding to starting PEOs' pattern (Figure 2(a)).

For copolymers with 58-33 mol% of EO units (samples 1, 2, 3), diffraction maxima at 15.8°, 20.7°, and 26.6 °(2θ) were observed reflecting the regular arrangement of PTMC blocks. The diffraction maxima for PEO almost disappeared and the diffraction pattern obtained corresponded with that of a comparative PTMC homopolymer. For the sample with the ratio of 61:39 mol% EO:TMC units (sample 4) both blocks were found out to contribute to an amorphous halo, which prevailed in the diffraction pattern, and slightly to crystalline phases.

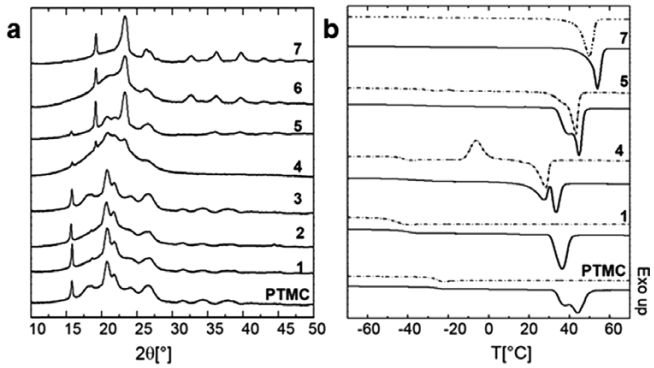

Figure 2. Characterization of physical structure; (a) WAXD patterns of synthesized PTMC and PTMC-*b*-PEO-*b*-PTMC copolymers; (b) DSC thermograms of representative samples; solid line=1st heating, dash line= 2nd heating.

Differential scanning calorimetry (DSC) was employed to study the intrinsic thermal behaviour of copolymers with regard to obtained crystallographic data. DSC results are summarized in Table 2 and thermograms of chosen samples are presented in Figure 2(b). Crystallization of the PEO block occurred in copo-

Table 2. Thermal properties of copolymers

Sample No.	$T_g{}^a$ (°C)	$T_m{}^b$ (°C)	$\Delta H_m{}^b$ (J·g^{-1})	$T_m'{}^c$ (°C)	$\Delta H_m'{}^c$ (J·g^{-1})
PTMC	-25	33	37	-	-
1	-36	36	35	-	-
2	-40	36	17	-	-
3	-43	38	44	-	-
4	-43	27/33	17/19	-	-
5	-30	45	87	43	54
6	-33	46	87	44	73
7	n.d.	54	129	50	111

[a]Glass transition temperature, T_g was determined according to the 2nd heating run. [b]Melting temperature, T_m and heat of fusion ΔH_m were determined according to the 1st heating run. [c]Melting temperature, T_m' and heat of fusion $\Delta H_m'$ were determined according to 2nd heating run at heating rate 5 °C·min^{-1}.

lymers with EO molar fraction higher than 61 mol% (samples 5, 6, 7) as it was documented by melting endotherms observed during both the first and the second heating runs. Such results do not correspond with those of Zhang, who determined crystalline PEO blocks by DSC in the copolymer with 15.6 wt% of PEO.[16]

The discrepancy could be ascribed to the influence of PTMC chains' length, which is another important parameter in addition to molar ratio. During the first heating of copolymers with 67-42 mol% of TMC units (samples 1-3) melting endotherms (T_m=36-38 °C) were detected and no crystallization occurred after cooling the melt during DSC analysis. According to literature PTMC with molar mass lower than 12 kg·mol^{-1} was shown to crystallize displaying T_m of 36 °C with a small heat of fusion (4.5-10 J·g^{-1}).[33] For the copolymers no. 1-3 the creation of crystalline domains could be explained by the impact of sufficient storage time during which an arrangement of PTMC chains took place.

Altogether, both PEO and PTMC blocks hindered regular arrangement of each other as documented by lower both T_m and heat of fusion of copolymers in comparison with those of starting PEOs (experimental section) and comparative PTMC (Table 2).

Glass transition temperature, T_g, was determined from the second heating scan to avoid the effect of thermal history.[15] Almost all copolymers showed only one T_g, which was between those of homopolymers. One value of T_g could mean partial miscibility of blocks, but in our case it would be suggested for mostly amorphous samples. The reason is that for highly crystalline PEOs glass transition is difficult to be observed by conventional DSC.

3.2. Physicochemical characterization of particles

Utilizing the precipitation method two types of particles from the copolymer with the highest (sample 1) and lowest (sample 7) TMC unit content were prepared and characterized by DLS and SEM. The size of particles was 124 nm with zeta-potential, (ζ), -32 mV starting with copolymer 1. Copolymer 7 afforded particles with the size 128 nm and (ζ) -22 mV. The polydispersity index (PdI) was 0.12 and 0.21 for sample 1 and sample 7, respectively. Such hydrodynamic size and negative surface charge are advantageous for medicinal applications since particles with size less than 200 nm are prevented against an uptake[34] by the reticuloendothelial system and against nonspecific electrostatic interaction with blood cells, respectively.[35] According to SEM observation the particles with fusiform shape had slightly larger size about 300 nm as could be seen in Figure 3. However, the copolymer with higher TMC unit content was more favourable to form solid nanoparticles than that with dominating PEO content during SEM analysis due to vacuum applied causing water evaporation. This implies that long hydrophobic PTMC block providing kinetically frozen core enables the creation of nanospheres with greater stability than micellar nanoparticles composed of copolymers with shorter PTMC block.[36] On the other hand, copolymeric nanoparticles with low PEO density are known to form larger aggregates upon freeze-drying,[37] which explains almost twice fold higher size of copolymeric spheres (Figure 3)

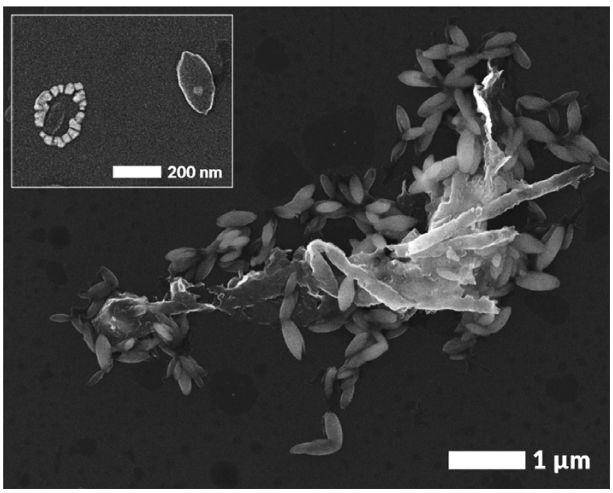

Figure 3. SEM images of particles made from copolymer 1; inset: particle detail.

in comparison to that obtained by DLS.

Water dispersions of copolymer particles were characterized by nanoparticle tracking analysis (NTA) method, which combines laser light scattering microscopy with a charge-coupled device (CCD) camera analyzing Brownian motion of illuminated particles in real-time.[38,39]

Before starting the measurement, the camera-level (CL) *i.e.* shutter speed and camera gain, and the detection threshold (DT) are suggested to be optimized for observation of the particles.[25,40] On the base of screening measurements and comparison of size distributions obtained by DLS and NTA methods, NTA measurement parameters were set-up to evaluate whole populations of particles (Supporting information). The resulting size distributions are presented in Figure 4. The distributions of particle sizes obtained by DLS and NTA measurement were comparable for both copolymer samples. However, the absolute size values of the distribution obtained by NTA were shifted towards larger particle size. The main peaks (modes) in the NTA obtained distributions were 131 and 147 nm for samples 1 and 7, respectively, in comparison to approx. half value of 79 nm for both samples obtained by DLS. The overall distribution was shifted towards larger sizes as opposed to corresponding DLS measurements. Such results can be ascribed to the underrepresentation of particles under 100 nm in the overall NTA distribution, thus shifting modes towards larger sizes.

This is caused by the lower contrast of refractive indices of polymer particles and water in comparison with, for example, the RI difference between gold and water.[38,41]

To evaluate the possibility of overrepresentation of larger particles, the samples were filtered through 0.45 µm filter and diluted by mixing equivalent volumes of their dispersions with ultrapure water. Figure 5 shows that number distribution of an undiluted dispersion divided by two corresponded well with that of twice diluted. It shows that higher concentration of particles in the sample cannot be directly linked to the peak shift and the obtained results can be compared among dispersions with various concentrations.

To reveal an occurrence of the crystallization in copolymer particles they were freeze-dried and analyzed by DSC and pow-

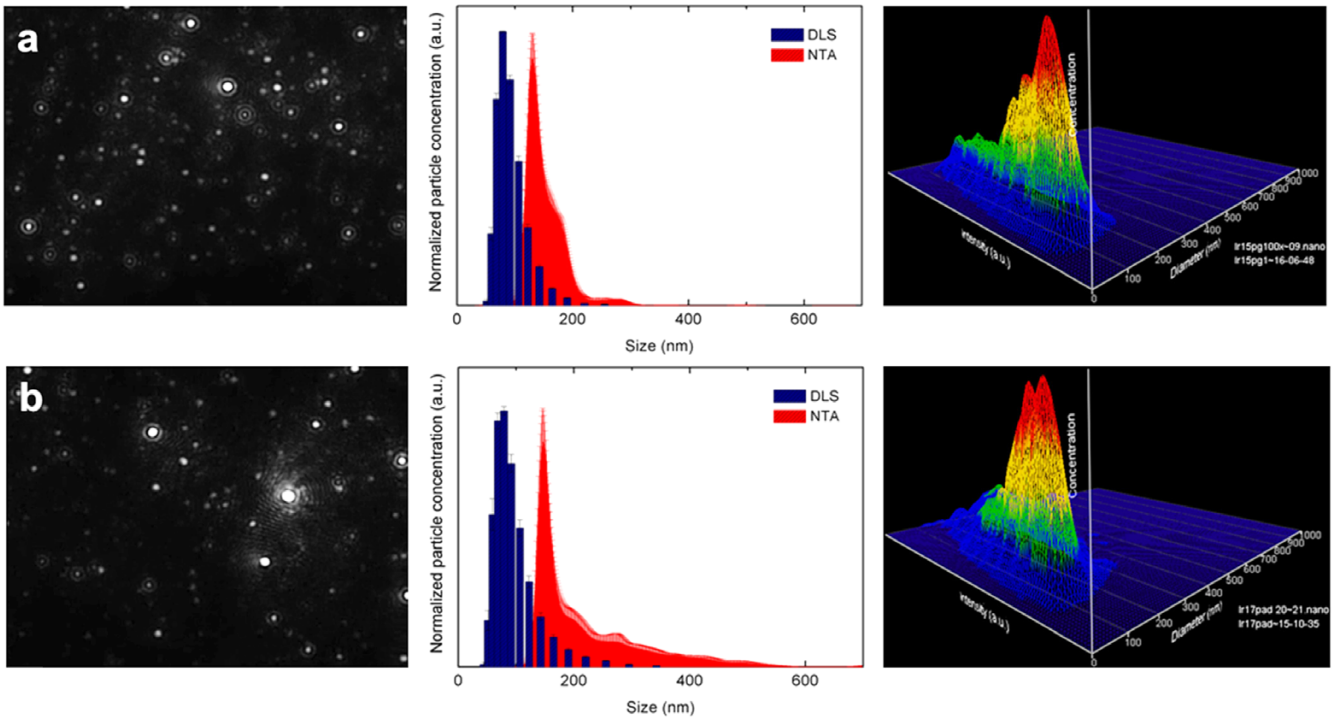

Figure 4. Particle visualization (left), comparison of particle size number distributions obtained by DLS and NTA (center), 3D graph of particle size distribution obtained by NTA (right); (a) 100-fold diluted dispersion of particles made from sample 1; (b) undiluted dispersion of particles from sample 7.

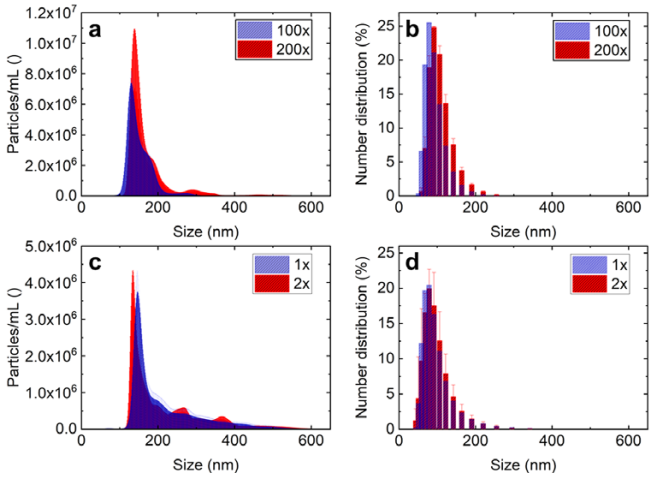

Figure 5. Comparison of particle size distribution obtained before (blue) and after (red) dilution by (a) NTA for sample 1; (b) DLS (number) for sample 1; (c) NTA for sample 7 and (d) DLS (number) for sample 7.

der diffraction methods. Trehalose, a non-reducing disaccharide, was selected as a lyoprotectant.[42] Saccharides are assumed to form amorphous phase immobilizing the copolymer particles to protect them against stress and aggregation during freeze-drying. According to DSC results presented in Table 3 particles made from sample 1 were considered amorphous.

When the particles were left to incubate in water at room temperature for one week and then freeze-dried a slight increase in PTMC crystallinity was observed as the consequence of post-crystallization. As presented in Figure 6 powder diffraction data corresponded well with thermal analysis. For particles made from copolymer 7 with 93% of EO units a crystallization of PEO blocks on the particle surface could be expected during freezing steps.[43] As shown in Table 3, freeze-dried particles from sample 7 had melting transition corresponding to PEO in the copolymer (DSC thermogram is shown in Supporting information). However, the decrease in PEO crystallinity by 50% as compared to starting copolymer 7 could be ascribed to hindered crystallization of PEO chains due to the detrimental effect of trehalose.

Altogether, the obtained results from thermal analysis and X-ray diffraction of starting copolymers were significantly helpful in obtaining information on the phase morphology of dried nanoparticles.

3.3. Model enzymatic hydrolysis

PTMC implants are known to degrade *in vivo* faster than in a buffer due to enzymatic activity. Since these enzymes have not

Table 3. Thermal properties of nanoparticles made from sample 1 and 7

Sample No.	Time (days)	T_g^a (°C)	T_m^b (°C)	ΔH_m^b (J·g^{-1})	$T_m'^c$ (°C)	$\Delta H_m'^c$ (J·g^{-1})
1	0	-34	24	1		
	7	-33	36	6		
7	0	n.d.	39	61	38	52

[a] T_g was determined from the 2nd heating run. [b] The 1st heating run. [c] 2nd heating run at heating rate 5 °C·min^{-1}.

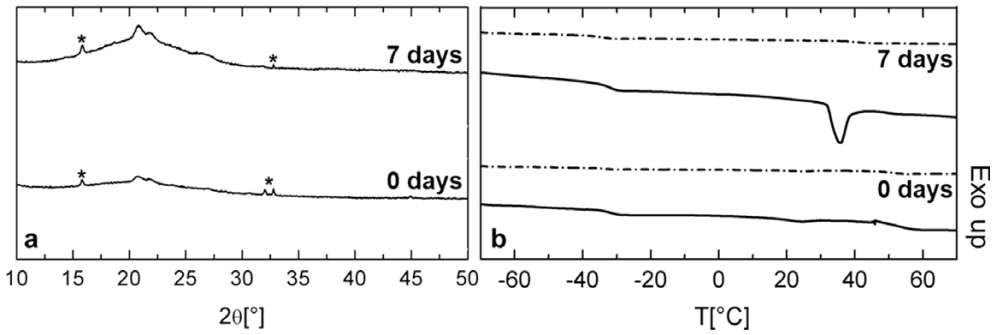

Figure 6. Characterization of physical structure: (a) WAXD patterns of lyophilized particles from sample 1; (b) thermograms of lyophilized particles from sample 1; solid line=1st heating, dash line=2nd heating.

been determined, selecting an appropriate enzyme for degradation experiments *in vitro* represents important task. Moreover, majority of lipolytic enzymes active for polyesters do not function for polycarbonates. Based on screening degradation experiments (data not shown) we selected a lipase from *Mucor miehei* (MM) as a model enzyme for accelerated hydrolytic scission. Particle dispersions were combined with lipase in a measuring cuvette and changes in hydrodynamic diameter and derived count rate (DCR) were monitored. Since DCR ratio could be considered as a measure of particles' concentration in the comparison between various samples, its decrease was assumed as a reduction in particles amount. As shown in Figure 7(a), DCR ratio of particles dispersions with MM lipase dropped within 30-60 min reflecting the occurrence of hydrolytic degradation. The decrease in light scattering intensity appeared faster for particles with shorter PTMC blocks (sample 5, 37 mol% of TMC units) than for particles with longer PTMC blocks (sample 1, 67 mol% of TMC units).

The enzymatic degradation of representative particles made from copolymers with 67, 36, and 7 mol% of TMC units proceeded in equilibrium unimers since DCR ratio declined in time (Figure 7(a)). Lipases, being soluble in water, are expected to diffuse through hydrated PEO shell acting on ester bonds on the surface of hydrophobic PTMC core. Once ester bonds between PEO and PTMC chains were cleaved, the core-shell structure collapsed. Consequently, due to hydrophobic interactions between

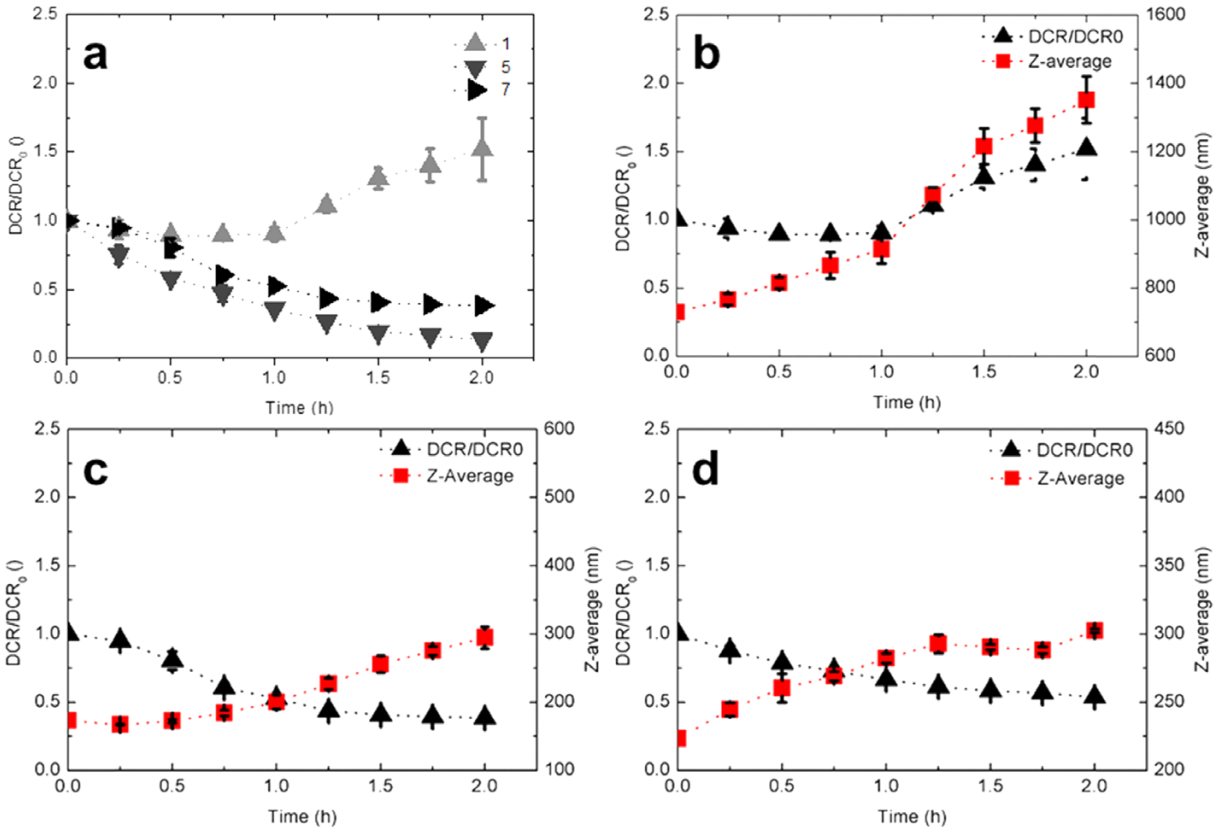

Figure 7. Enzymatic degradation by the action of lipase from *Mucor Miehei*; time profile of DLS measurement for (a) particles made from samples 1, 5, and 7; (b) particles made from sample 1; (c) particles made from sample 7; (d) particles made from PCL_{31}-*b*-PEO_{45}-*b*-PCL_{31} copolymer. The copolymer particles concentration was 1 mg·mL^{-1} and enzyme concentration was 1610 U·mL^{-1}.

PTMC moieties in more or less degraded chains the aggregates were formed as evidenced by an apparent increase in hydrodynamic radius (Figure 7(b)-(c)).

The rate of enzymatic degradation was almost the same for nanoparticles with 67 mol% of TMC units, previously incubated for one week. However, the increase in PTMC core crystallinity was too low to impact bulk degradation behaviour.

To obtain comparison with analogous polyester-based particles, MM lipase was combined with particles made from PCL_{31}-*b*-PEO_{45}-*b*-PCL_{31} copolymer. As seen in Figure 7(d) the course of hydrolytic scission followed the same pattern and thus the same mechanism could be suggested for particles with carbonate units.

3.4. Polymersomes for human genomic DNA encapsulation

As it was proved in previous section, synthesized polycarbonate-based copolymers could assemble into nanosized micelles and spheres with solid, PTMC-based core by solvent displacement method. By changing the preparation method, micrometre-sized polymersomes were prepared to further demonstrate the versatility of studied copolymers. In contrast to nanospheres and micelles, in polymersomes studied copolymer formed membrane surrounding internal cavity with water, which could accommodate hydrophilic drug or nucleic acid. As a-proof-of-concept of designing DNA delivery systems based on aliphatic polycarbonate copolymers we encapsulated human genomic DNA with 70% encapsulation efficiency into polymersomes composed from copolymer 1. The polymersome 3D scans were obtained *via* microscopic tomography (Nanolive SA). Representative images of resulting DNA-polymersome system are depicted in Figure 8. Using the STEVE software, the domains with different refractive indices were each assigned a representative colour indicating their distribution in the polymersome. This colour differentiation allowed distinct localization of genomic DNA within the polymersome cavity. These DNA-loaded polymersomes responsive to enzymes in tissues and cells have potential for genomic DNA transport to antigen-presenting cells *via* internalization,[44] allowing their utilization in immunotherapy.[45-47]

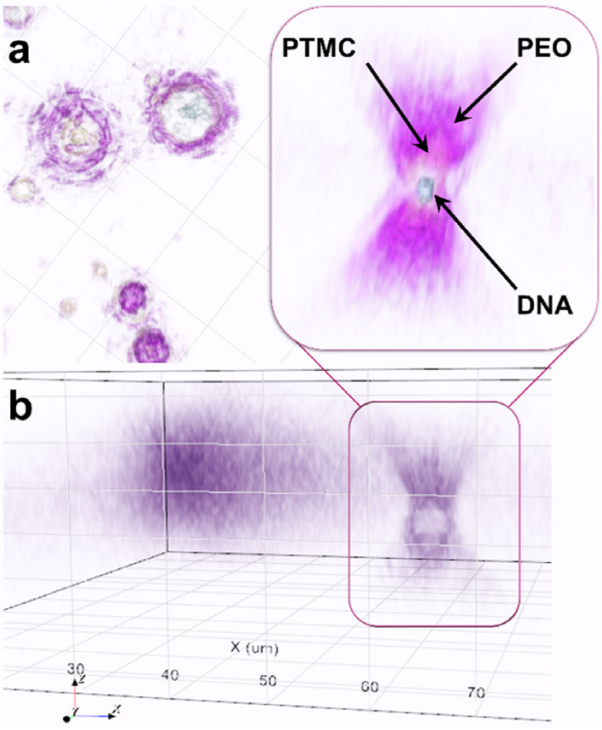

Figure 8. Representative Nanolive 3D scans of DNA-containing polymersomes, colour differentiated as follows: PEO-purple, PTMC-pink, genomic DNA-turquoise; (a) top view, (b) side-view with enlarged polymersome.

4. Conclusions

To develop efficient drug delivery system, an understanding of physicochemical properties and degradation behaviour of copolymer matrix represents an important task. We showed that among PTMC-*b*-PEO-*b*-PTMC copolymers with 67-7 mol% of TMC units those with more than 39 mol% of TMC units were initially amorphous and susceptible to post-crystallization during storage at room temperature. Moreover, rearranging of PTMC chains from disordered to more ordered morphology occurred also in initially amorphous nanoparticles made from copolymer with 67 mol% of TMC units during their one-week incubation at room temperature in water. On the base of *in vitro* experiments, almost all copolymer particles were susceptible to hydrolytic degradation by the action of lipase from *Mucor miehei*. NTA analysis, an advanced method for particle sizing, was applied to evaluate size distributions of various copolymer particles with different concentration affording complementary results to DLS method. We believe that our comprehensive study of the synthesis conditions and behaviour of biodegradable nanoparticles based on polycarbonates with hydrophilic corona will have strong impact on drug delivery applications of such systems. We have also presented a proof-of-concept of the materials' use for human genomic DNA transport.

Supporting information: Information is available regarding NMR spectra of prepared copolymers, DSC curves of cryoprotectant and selected particles, particles size under various NTA settings and temperature optimum of MM lipase. The materials are available *via* the Internet at http://www.springer.com/13233.

References

(1) S. B. Blanquer, S. Sharifi, and D. W. Grijpma, *J. Appl. Biomater. Funct. Mater.*, **10** (2012).
(2) L. Timbart, M. Y. Tse, S. C. Pang, O. Babasola, and B. G. Amsden, *Macromol. Biosci.*, **9**, 786 (2009).
(3) A. D. Messias, K. F. Martins, A. C. Motta, and E. A. d. R. Duek, *Int. J. Biomater.*, **2014** (2014).
(4) A. Leeuwen, H. Yuan, G. Passanisi, J. Meer, J. Bruijn, T. Kooten, D. Grijpma, and R. Bos, *Eur. Cells Mater.*, **27**, 81 (2014).
(5) K. Fukushima, *Biomater. Sci.*, **4**, 9 (2016).
(6) R. R. Vogels, J. W. Bosmans, K. W. van Barneveld, V. Verdoold, S. van Rijn, M. J. Gijbels, J. Penders, S. O. Breukink, D. W. Grijpma, and N. D. Bouvy, *Surgery*, **157**, 1113 (2015).
(7) Z. Zhang, R. Kuijer, S. K. Bulstra, D. W. Grijpma, and J. Feijen, *Biomater-*

ials, **27**, 1741 (2006).
(8) A. C. Albertsson and M. Eklund, *J. Appl. Polym. Sci.*, **57**, 87 (1995).
(9) O. S. Kluin, H. C. van der Mei, H. J. Busscher, and D. Neut, *Biomaterials*, **30**, 4738 (2009).
(10) M. S. Kim, H. Hyun, B. S. Kim, G. Khang, and H. B. Lee, *Current Appl. Phys.*, **8**, 646 (2008).
(11) D. Neut, O. S. Kluin, B. J. Crielaard, H. C. van der Mei, H. J. Busscher, and D. W. Grijpma, *Acta Orthop.*, **80**, 514 (2009).
(12) S. J. Buwalda, L. B. Perez, S. Teixeira, L. Calucci, C. Forte, J. Feijen, and P. J. Dijkstra, *Biomacromolecules*, **12**, 2746 (2011).
(13) F. Nederberg, J. Watanabe, K. Ishihara, J. Hilborn, and T. Bowden, *J. Biomater. Sci., Polym. Ed.*, **17**, 605 (2006).
(14) A.-C. Albertsson, A. Löfgren, C. Sturesson, and M. Sjöling, *Design of New Building Blocks in Resorbable Polymers*, ACS Publications, 1992.
(15) H. Wang, J. H. Dong, A. Y. Qiu, and Z. W. Gu, *J. Macromol. Sci., Part A*, **35**, 811 (1998).
(16) Y. Zhang and R.-X. Zhuo, *Biomaterials*, **26**, 2089 (2005).
(17) Y. Zhang, H. F. Chan, and K. W. Leong, *Adv. Drug Deliv. Rev.*, **65**, 104 (2013).
(18) Y. K. Feng and S. F. Zhang, *J. Polym. Sci., Part A: Polym. Chem.*, **43**, 4819 (2005).
(19) Z. Zhang, D. W. Grijpma, and J. Feijen, *J. Control. Release*, **116**, e28 (2006).
(20) X. Jiang, H. Xin, X. Sha, J. Gu, Y. Jiang, K. Law, Y. Chen, L. Chen, X. Wang, and X. Fang, *Int. J. Pharm.*, **420**, 385 (2011).
(21) G. Mittal, D. K. Sahana, V. Bhardwaj, and M. N. V. Ravi Kumar, *J. Control. Release*, **119**, 77 (2007).
(22) V. Karavelidis, E. Karavas, D. Giliopoulos, S. Papadimitriou, and D. Bikiaris, *Int. J. Nanomedicine*, **6**, 3021 (2011).
(23) H. Hyun, M. S. Kim, G. Khang, and H. B. Lee, *J. Polym. Sci., Part A: Polym. Chem.*, **44**, 4235 (2006).
(24) L. Liao, C. Zhang, and S. Gong, *React. Funct. Polym.*, **68**, 751 (2008).
(25) J. Gross, S. Sayle, A.R. Karow, U. Bakowsky, and P. Garidel, *Eur. J. Pharm. Biopharm.*, **104**, 30 (2016).
(26) C. Perez, A. Sanchez, D. Putnam, D. Ting, R. Langer, and M. J. Alonso, *J. Control. Release*, **75**, 211 (2001).
(27) J. Trousil, S. K. Filippov, M. Hrubý, T. Mazel, Z. Syrová, D. Cmarko, S. Svidenská, J. Matějková, L. Kováčik, B. Porsch, R. Konefał, R. Lund, B. Nyström, I. Raška, and P. Štěpánek, *Nanomedicine*, **13**, 307 (2017).
(28) Y. Wan, Z. Gan, and Z. Li, *Polym. Chem.*, **5**, 1720 (2014).
(29) H. Yao, J. Li, N. Li, K. Wang, X. Li, and J. Wang, *Polymers*, **9**, 598 (2017).
(30) J. Li, X. Li, X. Ni, and K.W. Leong, *Macromolecules*, **36**, 2661 (2003).
(31) A. K. Mohanty, U. Jana, P. K. Manna, and G. P. Mohanta, *Prog. Biomaterials*, **4**, 89 (2015).
(32) S. J. Lee, S. S. Kim, and Y. M. Lee, *Carbohydr. Polym.*, **41**, 197 (2000).
(33) K. J. Zhu, R. W. Hendren, K. Jensen, and C. G. Pitt, *Macromolecules*, **24**, 1736 (1991).
(34) C. He, Y. Hu, L. Yin, C. Tang, and C. Yin, *Biomaterials*, **31**, 3657 (2010).
(35) A. Mayer, M. Vadon, B. Rinner, A. Novak, R. Wintersteiger, and E. Fröhlich, *Toxicology*, **258**, 139 (2009).
(36) K. Letchford and H. M. Burt, *Mol. Pharm.*, **9**, 248 (2012).
(37) J. Logie, S. C. Owen, C. K. McLaughlin, and M. S. Shoichet, *Chem. Mater.*, **26**, 2847 (2014).
(38) R. A. Dragovic, C. Gardiner, A. S. Brooks, D. S. Tannetta, D. J. Ferguson, P. Hole, B. Carr, C. W. Redman, A. L. Harris, and P. J. Dobson, *Nanomedicine*, **7**, 780 (2011).
(39) C. Gardiner, Y. J. Ferreira, R. A. Dragovic, C. W. Redman, and I. L. Sargent, *J. Extracell. Vesicles*, **2**, 19671 (2013).
(40) S. L. N. Maas, J. de Vrij, E. J. van der Vlist, B. Geragousian, L. van Bloois, E. Mastrobattista, R. M. Schiffelers, M. H. M. Wauben, M. L. D. Broekman, and E. N. M. Nolte't Hoen, *J. Control. Release*, **200**, 87 (2015).
(41) B. Carr, P. Hole, A. Malloy, P. Nelson, and J. Smith, *Eur. J. Parenter. Sci. Pharm. Sci.*, **14**, 45 (2009).
(42) F. De Jaeghere, E. Allémann, J.-C. Leroux, W. Stevels, J. Feijen, E. Doelker, and R. Gurny, *Pharm. Res.*, **16**, 859 (1999).
(43) W. Abdelwahed, G. Degobert, S. Stainmesse, and H. Fessi, *Adv. Drug Deliv. Rev.*, **58**, 1688 (2006).
(44) Y. Tabata and Y. Ikada, in *New Polymer Materials*, Springer1990, pp 107-141.
(45) A. Kawashima, K. Tanigawa, T. Akama, H. Wu, M. Sue, A. Yoshihara, Y. Ishido, K. Kobiyama, F. Takeshita, K.J. Ishii, H. Hirano, H. Kimura, T. Sakai, N. Ishii, and K. Suzuki, *Endocrinology*, **152**, 1702 (2011).
(46) H. Abdelkader, B. Pierscionek, and R.G. Alany, *Int. J. Pharm.*, **477**, 631 (2014).
(47) T. L. Whiteside, A. Gambotto, A. Albers, J. Stanson, and E. P. Cohen, *Proc. Natl. Acad. Sci.*, **99**, 9415 (2002).

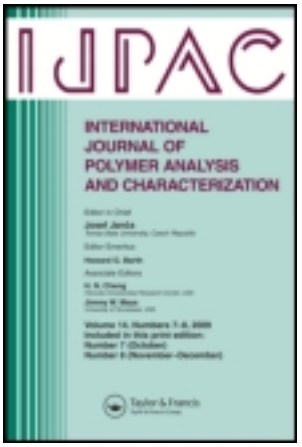

International Journal of Polymer Analysis and Characterization
Publication details, including instructions for authors and subscription information:
http://www.tandfonline.com/loi/gpac20

The Effect of Processing of Polycaprolactone Films on Degradation Process Initiated by Aspergillus Oryzae Lipase

S. Hermanová [a b], J. Omelková [b], S. Voběrková [c], R. Bálková [a d], L. Richtera [a d], L. Mravcová [e] & J. Jančář [a d]

[a] Brno University of Technology, Central European Institute of Technology, Brno, Czech Republic

[b] Institute of Food Science and Biotechnology, Faculty of Chemistry, Brno University of Technology, Brno, Czech Republic

[c] Institute of Chemistry and Biochemistry, Faculty of Agronomy, Mendel University in Brno, Brno, Czech Republic

[d] Institute of Materials Chemistry, Faculty of Chemistry, Brno University of Technology, Brno, Czech Republic

[e] Institute of Chemistry and Technology of Environmental Protection, Faculty of Chemistry, Brno University of Technology, Brno, Czech Republic

Version of record first published: 07 Aug 2012.

To cite this article: S. Hermanová, J. Omelková, S. Voběrková, R. Bálková, L. Richtera, L. Mravcová & J. Jančář (2012): The Effect of Processing of Polycaprolactone Films on Degradation Process Initiated by Aspergillus Oryzae Lipase, International Journal of Polymer Analysis and Characterization, 17:6, 465-475

To link to this article: http://dx.doi.org/10.1080/1023666X.2012.696402

International Journal of Polymer Anal. Charact., 17: 465–475, 2012

ISSN: 1023-666X print/1563-5341 online
DOI: 10.1080/1023666X.2012.696402

Taylor & Francis
Taylor & Francis Group

THE EFFECT OF PROCESSING OF POLYCAPROLACTONE FILMS ON DEGRADATION PROCESS INITIATED BY *ASPERGILLUS ORYZAE* LIPASE

S. Hermanová,[1,2] J. Omelková,[2] S. Voběrková,[3] R. Bálková,[1,4] L. Richtera,[1,4] L. Mravcová,[5] and J. Jančář[1,4]

[1]*Brno University of Technology, Central European Institute of Technology, Brno, Czech Republic*
[2]*Institute of Food Science and Biotechnology, Faculty of Chemistry, Brno University of Technology, Brno, Czech Republic*
[3]*Institute of Chemistry and Biochemistry, Faculty of Agronomy, Mendel University in Brno, Brno, Czech Republic*
[4]*Institute of Materials Chemistry, Faculty of Chemistry, Brno University of Technology, Brno, Czech Republic*
[5]*Institute of Chemistry and Technology of Environmental Protection, Faculty of Chemistry, Brno University of Technology, Brno, Czech Republic*

Poly(ε-caprolactone) (PCL) films with $M_n = 18$ kDa obtained by compression molding (CM) or solution casting (SC) were subjected to Aspergillus oryzae ***(*AO*) lipase action in a phosphate buffer at pH 7 at 37°C. The appearance of randomly oriented cracks on the surface of incubated PCL films accompanied by a decrease of the weight-average molecular weight (M_w) by 10% was observed after 42 days. The increase of crystallinity and surface morphology pattern of PCL samples exposed to*** AO ***lipase action supported the fact that the degradation proceeded in the amorphous phase of the aged films. SC films were degraded faster, probably due to better accessibility of ester bonds in the amorphous phase of spherulites.***

Keywords: *Aspergillus oryzae*; CLSM; Degradation; DSC; Lipase; Poly(ε-caprolactone)

INTRODUCTION

Poly(ε-caprolactone) (PCL), a representative of aliphatic polyesters, is one of the most promising biodegradable and biocompatible semicrystalline polymers.[1] PCL has been used for temporary therapeutic applications such as matrices of sustained drug delivery systems, surgical sutures, scaffolds for tissue regeneration,

Submitted 20 February 2012; accepted 7 April 2012.
This work was supported by the Ministry of Education, Youth and Physical Training of the Czech Republic under the research project no. MSM 0021630501. The authors would like to thank Radka Slavíčková for technical assistance.
Correspondence: S. Hermanová, Faculty of Chemistry, Brno University of Technology, Purkyňova 118, 612 00 Brno, Czech Republic. E-mail: hermanova-s@fch.vutbr.cz

among others.[2,3] PCL has also become an attractive material in environmental applications for biodegradation by the action of microorganisms frequently present in the ecosystem. PCL-based materials have been used as mulch films in agriculture and as packaging material.[4]

Biodegradation of polymers is affected both by the degrading activity of microorganisms and ambient conditions and by the polymer structure and morphology, including molecular weight and initial crystallinity, respectively. It is evident that the rate of biodegradation can be significantly influenced by the polymer surface morphology including the size and type of spherulite and/or lamellar structure. Bikiaris et al.[5] found out that increasing the propylene succinate content in copolymers of poly(butylene-co-propylene succinate) led to faster enzymatic degradation, which correlated with their initial reduced crystallinity and lower melting points. Albertsson et al.[6] reported on the influence of both the microorganism type and initial morphology of PCL films on PCL surface erosion pattern and degradation mechanism. Parallel cracks were observed in film-blown films aged in compost or in mineral medium inoculated with compost microorganisms, while spherulites were formed in film-blown films exposed to *Aspergillus fumigatus* and in melt-pressed films aged in compost.[7]

Extensive studies have been carried out also on the enzymatic chain-cleavage degradation of PCL in vitro by the action of lipase-type enzymes.[8–10] Lipases (triacylglycerol hydrolases, EC 3.1.1.3) are naturally occurring biocatalysts capable of hydrolysis of triacylglycerols into glycerol and fatty acids at a lipid-water interface.[11] The *Aspergillus sp.* lipases appertaining to a group of fungal lipases have attracted considerable research attention due to several properties of immense industrial importance, such as their pH and temperature stability; a few reports regarding the promising degradation capability of PCL and other polyesters have been published.[6,12–19]

The aim of this work was to obtain deeper insight into the influence of different processing on biodegradation behavior of PCL by a simple enzyme system. PCL samples were in the form of disks (Ø 1 cm, 100 μm) prepared by solution casting (SC) or compression molding (CM) from PCL powder of $M_n = 18$ kDa synthesized at our institute. The ^{1}H NMR analyses of neat PCL homopolymer confirmed the presence of both hydroxylic and benzoxylic end groups. The degradation experiment was performed in a phosphate buffer solution at 37°C using a simple enzyme system, i.e., commercially available *Aspergillus oryzae* (*AO*) lipase. The degraded PCL samples were periodically weighted and analyzed by differential scanning calorimetry (DSC), gel permeation chromatography (GPC), and confocal laser scanning microscopy (CLSM) to evaluate eventual changes in PCL structure as a consequence of lipase action. The pH optimum, temperature activity optimum, and temperature stability of *Aspergillus oryzae* lipase were determined spectrophotometrically using p-nitrophenyl-laurate (pNPL) as a substrate before the PCL degradation experiment.

METHODS AND MATERIALS

Assay of Activity of *Aspergillus oryzae* Lipase

Lipase from *Aspergillus oryzae* (WE-Nr. 916028) was obtained from Mucos Pharma. Lipolytic activity, independent of PCL characteristics, was determined by

using a Helios Delta UV/vis spectrophotometer (Thermo Spectronic, U.K.) using p-nitrophenyl-laurate (pNPL) as a substrate, which was dissolved in ethanol. The reaction mixture consisted of 0.25 mL enzyme solution (0.5 mg/mL), 3.25 mL of 50 mM phosphate buffer (pH = 7), and 0.25 mL of 2.5 mM pNPL in ethanol. The hydrolytic reaction was carried out at 37°C for 30 min and afterwards, 0.5 mL of 0.1 M Na_2CO_3 was added to stop the reaction. Subsequently, the absorbance at 420 nm was recorded. One unit of lipase activity (U) was defined as the amount of enzyme that caused the release of 1 μmol of p-nitrophenol from pNPL in one minute under the test conditions.

Determination of pH Optimum, Temperature Activity Optimum, and Temperature Stability

The optimal pH was evaluated by the *AO* lipase activity measurement using pNPL as a substrate as described previously. The effect of pH on the *AO* lipase activity was studied in a pH range of 5.00–11.0 at 37°C using the following 50 mM buffers: citrate-phosphate (pH 5–6), phosphate (pH 7), boric acid-borax (pH 8–9), glycine NaOH (pH 10), and Britton-Robinson (pH 11).

The temperature dependence of lipolytic activity was determined by measuring the *AO* lipase activity in 50 mM phosphate buffer (pH = 7) at different temperatures in the range from 30° to 50°C under the spectrophotometric assay described above.

The temperature stability of the *AO* lipase was determined by spectrophotometry with pNPL as a substrate after incubation for 1 h at different temperatures (30°–55°C). The enzyme samples were diluted in 50 mM phosphate buffer (pH = 7).

Degradation Study

The ^{1}H NMR analyses of PCL homopolymer were performed in a solution of $CDCl_3$. The presence of both hydroxylic and benzoxylic (-CH_2OBn) end groups was confirmed. The observed proton signals were: $\delta = 1.35$ ppm [m, 2H, (-CH_2-)], $\delta = 1.63$ ppm [m, 4H, (-CH_2-)], $\delta = 2.29$ ppm [t, 2H, (-CH_2CO-)], $\delta = 4.04$ ppm [t, 2H, (-CH_2O-)] $\delta = 3.46$ ppm [s, 1H, (-OH)], $\delta = 3.63$ ppm [t, 2H, (-CH_2OH)], $\delta = 5.09$ ppm [s, 2H, (-CH_2OBn)].

PCL samples were prepared for biodegradation tests in the form of circular discs of 10 mm in diameter. The discs were cut from 100 μm thick films produced by casting of PCL dichloromethane solution or by compression molding of PCL powder between poly (ethylene terephtalate) (PET) foils over a period of 6 min at 65°C and a pressure of 300 kN, employing a Fontijne hydraulic press. Afterwards, both types of films were sterilized by UV irradiation for 30 min in an Aura Mini laminar box (BioTech Instruments, Prague, Czech Republic).

The degradation study was carried out in a phosphate buffer solution at pH = 7. PCL films were placed in a test tube containing 3 mL of 50 mM phosphate buffer and a 0.5 mg/mL of *AO* lipase and then incubated at 37°C. The *AO* lipase used for the PCL degradation study showed the highest activity value at pH = 7 and 37°C (0.0347 U/mg), determined spectrophotometrically using pNPL as a substrate, which is why the degradation experiment was performed under these conditions.

The buffer/enzyme system was changed every 72 h in order to maintain the original level of enzymatic activity. After 14, 28, and 42 days of incubation, the films were removed, gently washed with distilled water, and dried to constant weight under vacuum. The control samples were treated in the same way; their incubation was carried out in a buffer without enzyme, but sodium azide 0.02% (w/w) was added to the solution to prevent contamination.

Testing Methods

Melting temperature and crystallinity of PCL samples were determined by DSC using TA Instruments Q 2000 apparatus. The samples of about 1.5 mg were heated at 10°C/min to 100°C.

An Agilent Technologies 1100 Series GPC device equipped with a refractive index (RI) detector, utilizing two PLgel mixed columns, 300 × 7.5 mm, with a particle size of 5 μm, was used to determine molecular weight averages of PCLs against polystyrene standards.

The surface morphology of (bio)degraded PCL samples was studied by CLSM using Olympus Lext OLS 3000 equipment.

RESULTS AND DISCUSSION

It is well known that extracellular enzymes secreted by microorganisms in the presence of PCL (being a lipophilic substrate) act as depolymerases reducing polymer chain length enough to penetrate through cellular membranes.[20] Thus, the degradation of CM and SC PCL films by the action of *AO* lipase was primarily evaluated by weight loss and changes in molecular weight. It can be seen in Table I that the weight loss of both CM and SC PCL samples increased with degradation time up to 3.6 wt.% and 5.8 wt.%, respectively, and the weight-average molecular weight (M_w) of both types of samples gradually decreased by ~10% during 42 days in comparison with the original PCL film. The results are in agreement with a reported biodegradation pattern of PCL proceeding as surface erosion with minor reduction of

Table I. Characteristic data of PCL before and after degradation experiment*

Sample*	Period days	Weight loss%	M_n (GPC)kDa	M_w (GPC) kDa	M_w/M_n	$^{**}X_c^{1st}$ %	$^{**}X_c^{2nd}$ %	T_m^{1st} °C	T_m^{2nd} °C]
SC_PCL	0	—	18.0	47.7	2.7	63.5	52.2	63.0	55.3
CM_PCL	0	—	18.0	47.7	2.7	65.1	48.1	62.6	55.8
SC_14d	14	1.1	18.3	44.5	2.4	67.9	56.5	63.8	55.7
SC_28d	28	3.3	18.5	44.5	2.4	65.0	54.4	63.8	55.5
SC_42d	42	5.8	18.0	42.9	2.4	88.3	73.1	64.5	55.9
CM_14d	14	1.1	17.6	44.5	2.5	67.3	46.1	63.6	55.7
CM_28d	28	2.6	17.8	43.4	2.4	66.9	46.2	62.7	55.8
CM_42d	42	3.6	17.3	43.0	2.5	69.6	47.7	63.2	56.0

*SC: solution casting, CM: compression molding, PCL: poly(ε-caprolactone).

**Crystallinity calculated from the first (1st) and second (2nd) heating as a ratio of $\Delta H_m/\Delta H_m^0$, where ΔH_m^0 of PCL is 139.5 J/g.

molecular weight.[21] Hydrolytic degradation of PCL was excluded due to only negligible weight loss (<1 wt.%) of control samples even after 42 days for both sample types. The representative GPC chromatograms of the original and aged PCL films are presented in Figure 1. The slight shift of high molecular weight peak towards the lower molecular region was observed for both CM and SC samples, suggesting the cleavage of the longest polymer chains during 42 days exposure. The similar character of elution curves as well as the same reduction of M_w leads to the idea that different processing of PCL films did not have significant effect on the enzymatic degradation process.

Since the PCL samples differed in morphology, crystallinity, and probably also inner structure because of different preparation procedures (SC versus CM), the eventual structure changes as a consequence of enzyme action or solely phosphate buffer solution action were studied by DSC, the method designed for indirect observation of polymer morphology.

The DSC data revealed structure variance between studied SC and CM samples as a consequence of the *AO* lipase action due to the different shapes of melting endotherms and different crystallinities (X_c) and crystallization temperatures (T_c) (Table I). In the case of T_c, the original SC sample crystallized at 31°C, whereas the original CM sample crystallized at 34°C. Even after 14 days, the T_c increased to 34°C for SC samples, while it remained the same for CM samples, and no change was shown until the end of the experiment for both sample types (Figures 2 and 3). Thus, it seems that a nucleating effect occurred in SC samples, probably as a result of enzyme-catalyzed chain scission.

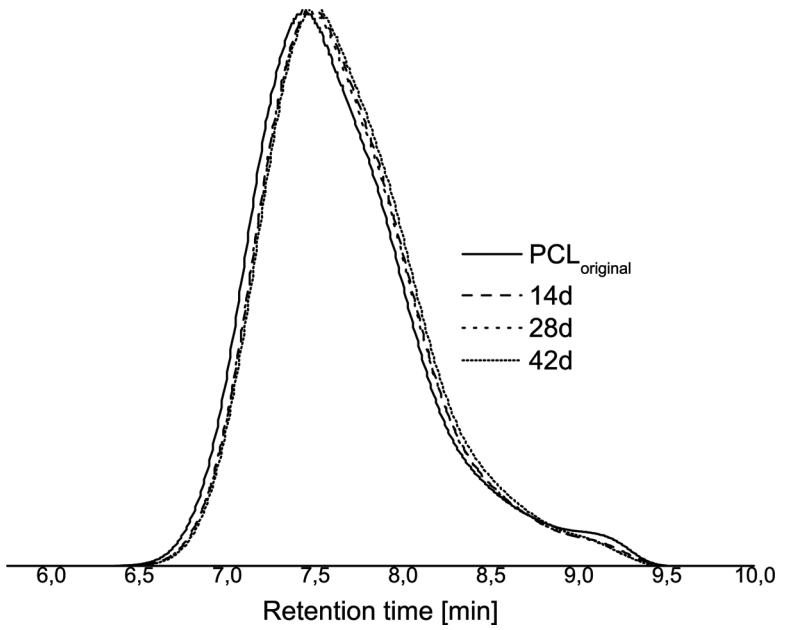

Figure 1. GPC elution curves of SC PCLs films exposed to *AO* in phosphate buffer at pH 7 and 37°C.

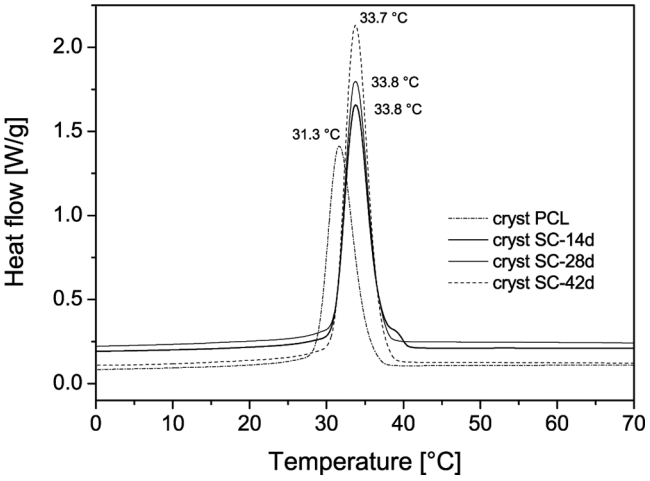

Figure 2. DSC crystallization curves of SC samples unaged (PCL) and aged for 14, 28, and 42 days.

The comparison of the first heating X_c of SC samples exposed to *AO* lipase action with that of control samples revealed that significant change of DSC data occurred only after 42 days since the data after 14 and 28 days were identical (Table I). Thus, during 28 days of the experiment the *AO* lipase action was rather negligible and only the annealing effect of the phosphate buffer solution was responsible for a slight increase of X_c with respect to the original PCL. It should be noted that the degradation experiment was performed at a temperature far above the glass transition temperature of PCL, −60°C, and that is why amorphous chains of PCL were in a rubber-like state and therefore able to crystallize. A significant increase of the first X_c of the SC sample by 40% after 42 days remained the same after the second heating, while no increase was observed for CM samples after the second

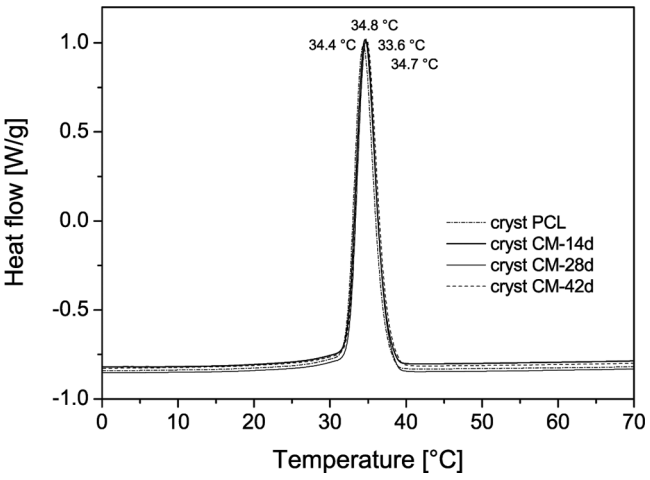

Figure 3. DSC crystallization curves of CM samples control (PCL) and aged for 14, 28, and 42 days.

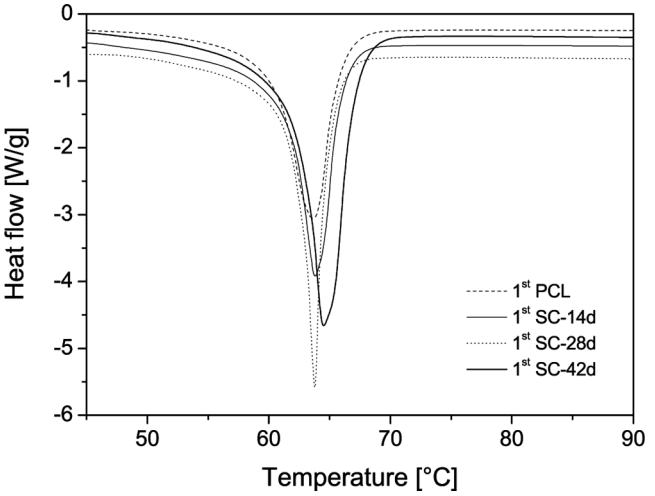

Figure 4. DSC first heating curves of SC samples control (PCL) and aged for 14, 28, and 42 days.

heating (Table I); thus, it must have been a result of the *AO* lipase action. The X_c of controlled samples remained without change as well. The increase of the first X_c of the CM sample by 9% after 42 days is, therefore, attributed only to secondary crystallization of amorphous PCL chains without evident influence of the *AO* lipase.

The X_c data corresponded well with the variance of endotherm shape. The shape of the first endotherms of SC samples the same in aging time (Figure 4) differed from those of CM samples, which revealed shoulders around 49°C (Figure 5) except for the original sample. It is assumed that the shoulder is a consequence of the secondary crystallization because a shoulder of endotherms reflects different lamella thickness and the endotherm width is connected with crystallite size.[22] However,

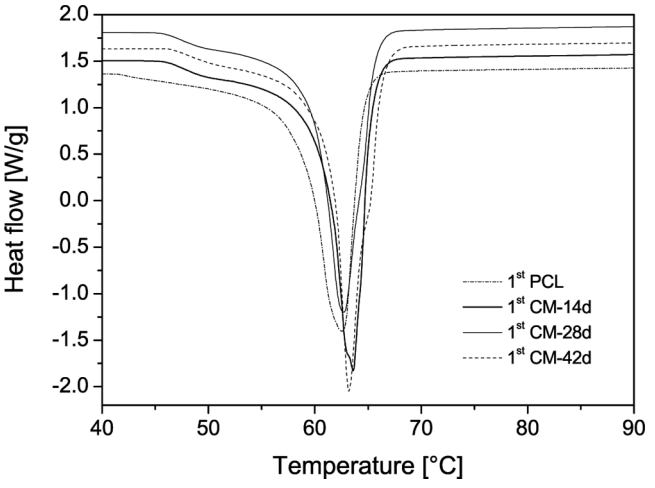

Figure 5. DSC first heating curves of CM samples control (PCL) and aged for 14, 28, and 42 days.

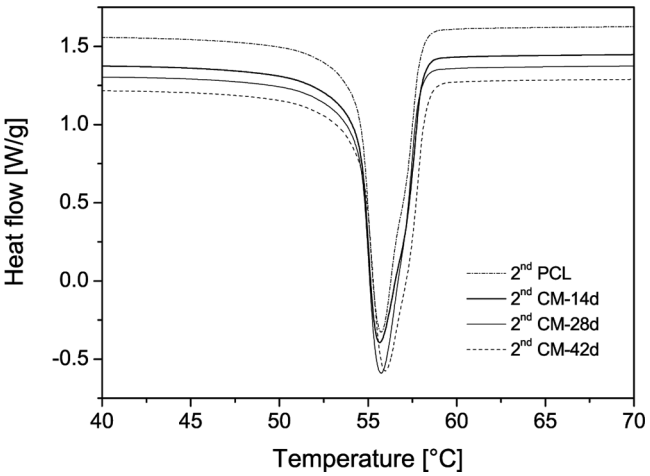

Figure 6. DSC second heating curves of CM samples control (PCL) and aged for 14, 28, and 42 days.

because the shoulder appeared even after 14 days and its position as well as size did not change in time, the ordering of amorphous chains was especially initiated by annealing of the phosphate solution. This also confirmed the second endotherms of CM samples being without shoulders and of the same shape (Figure 6). The inverse situation was observed for SC samples (Figure 7), which was probably also connected with different supramolecular structures of the original SC and CM samples. The shape of the second endotherms differed in time and shoulders were observed on them. Both facts verified chemical degradation of PCL chains (scission) if one takes into account that both thermal and mechanical history should be lost after the first heating and cooling. Although different structures must have been formed after cooling, 25% difference between the second X_c of SC and CM samples

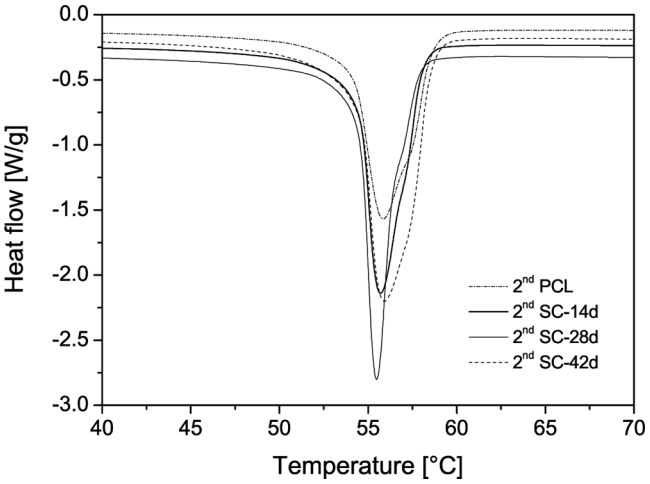

Figure 7. DSC second heating curves of SC samples control (PCL) and aged for 14, 28, and 42 days.

after 42 days adverted to shorter and long chains, respectively, and/or loss of critical amount of low-molecular-weight species, which were rejected from crystallization.

A minor increase of the first T_m (melting temperature) in time, more evident for SC samples, can be explained by physical aging of the solution medium because the T_m of control samples was the same as those of the original and aged samples for both heating cycles (Table I). Nevertheless, chemical degradation occurred not only for SC samples, as the CLSM images show.

It can be assumed that the *AO* lipase preferentially attacked the amorphous phase where the macromolecules are loosely packed and hence are more susceptible to degradation. Further, once the degradation initiated, the accumulation of water-soluble oligomeric species, which were the chain scission products of the polymer, probably caused an osmotic inflow of water, accelerating the degradation process.[23] The formation of oligomeric species possessing carboxylic end groups during the degradation test as evidenced from pH decrease to 6.8 could further contribute to faster chain scission due to autocatalysis. However, the extreme pH changes were excluded by regular changing of buffer solution during the degradation experiment. The decrease of pH was not detected in solution with control samples, which means that simple hydrolysis did not proceed.

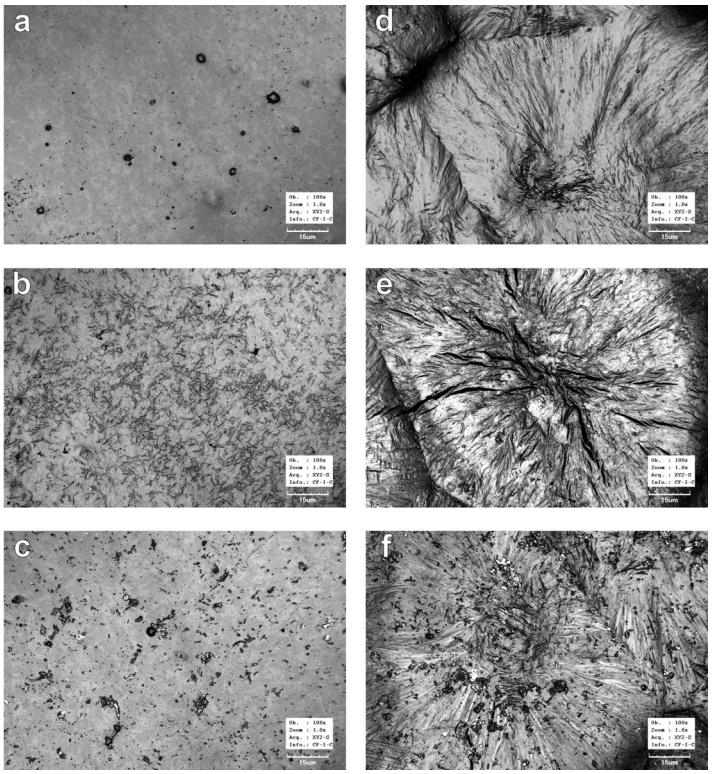

Figure 8. CLSM micrographs showing the PCL surface of (a) original CM film, (b) CM film after 42 days of degradation, (c) control of CM film after 42 days in phosphate buffer solution, (d) original SC film, (e) SC film after 42 days of degradation, and (f) control SC film.

Further, pores formed during the progressive degradation process made possible the release of water-soluble oligomeric and monomeric species, which diffused into the solution; microscopic cracks then started to be visible on sample surfaces exposed to the *AO* lipase (Figure 8). The increase of crack size and number together with gradual weight loss in time confirmed surface erosion of both SC and CM samples as compared with control samples. The initial surface of CM samples was amorphous, while that of SC samples was formed by spherulites. The latter represents ordered structure with amorphous sites only in certain directions among crystallites. Consequently, just the occurrence and the amount of the amorphous region governed the formation of cracks, which were spread homogeneously on CM sample surfaces but spokewise in spherulites of SC samples, where much longer cracks grew up.

CONCLUSION

Based on the results obtained, it can be concluded that PCL sample processing (CM versus SC) had significant influence on the *AO* lipase attack, namely because of different initial structures, on the surface and probably inner as well. Although the *AO* lipase attacked the amorphous phase, suitable sites for PCL chain cleavage seemed to be more available for the *AO* lipase among ordered chains in spherulites, as was observed.

Enzymatic hydrolysis was the surface erosion process where PCL chains were degraded initially by the action of the *AO* lipase, as seen from the drop of weight-average molecular weight, M_w. Subsequently, surface erosion occurred because randomly oriented cracks were formed on surfaces of PCL films obtained by both compression molding and solution casting, and the *AO* lipase action was accompanied by weight loss in comparison with the unchanged control samples.

REFERENCES

1. Tokiwa, Y., T. Ando, T. Suzuki, and K. Takeda. 1990. Biodegration of synthetic polymers containing ester bonds. In *Agricultural and Synthetic Polymers: Biodegradability and Utilization*, eds. J. E. Glass and G. Swift, pp. 136–148. Washington, D.C.: American Chemical Society.
2. Coombes, A. G. A., S. C. Rizzi, M. Williamson, J. E. Barralet, S. Downes, and W. A. Wallace. 2004. Precipitation casting of polycaprolactone for applications in tissue engineering and drug delivery. *Biomaterials* 25: 315–325.
3. Williamson, M. R., and A. G. A. Coombes. 2004. Gravity spinning of polycaprolactone fibres for applications in tissue engineering. *Biomaterials* 25: 459–465.
4. Matzinos, P., V. Tserki, A. Kontoyiannis, and C. Panayitou. 2002. Processing and characterization of starch/polycaprolactone products. *Polym. Degradation Stab.* 77: 17–24.
5. Bikiaris, D. N., and G. Z. Papageorgiou. 2007. Synthesis, cocrystallization and enzymatic degradation of novel poly(butylene-co-propylene succinate) copolymers. *Biomacromolecules* 8: 2437–2449.
6. Albertsson, A. C., C. Eldsater, B. Erlansson, S. Karlsson, and R. Renstad. 1998. Effect of processing additives on (bio)degradability of film-blown poly(ε-caprolactone). *J. Appl. Polym. Sci.* 70: 61–74.

7. Hakkarainen, M., and A. C. Albertsson. (2002). Heterogeneous biodegradation of polycaprolactone - low molecular weight products and surface changes. *Macromol. Chem. Phys.* 203: 1357–1363.
8. Zeng, J., X. Chen, Q. Liang, X. Xu, and X. Jing. 2004. Enzymatic degradation of poly(L-lactide) and poly(ε-caprolactone) electrospun fibers. *Macromol. Biosci.* 4: 1118–1125.
9. Herzog, K., R. J. Muller, and W. D. Deckwer. 2006. Mechanism and kinetics of the enzymatic hydrolysis of polyester nanoparticles by lipases. *Polym. Degradation Stab.* 91: 2486–2498.
10. Sekosan, G., and N. Vasanthan. 2010. Morphological changes of annealed poly-ε-caprolactone by enzymatic degradation with lipase. *J. Polym. Sci. Polm. Phys.* 48: 202–211.
11. Sharma, D., B. Sharma, and A. K. Shukla. 2011. Biotechnological approach of microbial lipase: A review. *Biotechnology* 10(1): 23–40.
12. Contesini, F. J., D. B. Lopes, G. A. Macedo, M. G. Nascimento, and P. O. Carvalho. 2010. *Aspergillus* sp. lipase: Potential biocatalyst for industrial use. *J. Mol. Catal. B Enzym.* 67: 163–171.
13. Renstad, R., S. Karlsson, A. Sandgren, and A. C. Albertsson. 1998. Influence of processing additives on the degradation of melt-pressed films of poly(ε-caprolactone) and poly (lactic acid). *J. Environ. Polym. Degrad.* 6: 209–221.
14. Eldsater, C., B. Erlandsson, R. Rendstad, A. C. Albertsson, and S. Karlsson. 2000. The biodegradation of amorphous and crystalline regions in film-blown poly(ε-caprolactone). *Polymer* 41: 1297–1304.
15. Sanches, J. G., A. Tsuchii, and Y. Tokiwa. 2000. Degradation of polycaprolactone at 50°C by a thermotolerant Aspergillus sp. *Biotechnol. Lett.* 22: 849–853.
16. Hoshino, A., and Y. Isono. 2002. Degradation of aliphatic polyester films by commercially available lipases with special reference to rapid and complete degradation of poly(L-lactide) film by lipase derived from *Alcaligenes sp*. *Biodegradation* 13: 141–147.
17. Maeda, H., Y. Yamagata, K. Abe, F. Hasegawa, M. Machida, R. Ishioka, K. Gomi, and T. Nakajima. 2005. Purification and characterization of a biodegradable plastic-degrading enzyme from *Aspergillus oryzae*. *Appl. Microbiol. Biotechnol.* 67: 778–788.
18. Lovera, D., L. Márquez, V. Balsamo, A. Taddei, C. Castelli, and J. Muller. 2007. Crystallization, morphology and enzymatic degradation of polyhydroxybutyrate/polycaprolactone (PHB/PCL) blends. *Macromol. Chem. Phys.* 208: 924–937.
19. Balmayor, E. R., K. Tuzlakoglu, A. P. Marques, H. S. Azavedo, and R. L. Reis. 2008. A novel enzymatically-mediated drug delivery carrier for bone tissue engineering applications: Combining biodegradable starch-based microparticles and differentiation agents. *J. Mater. Sci. Mater. Med.* 19: 1617–1623.
20. Shah, A. A., F. Hasan, A. Hameed, and S. Ahmed. 2008. Biological degradation of plastics: A comprehensive review. *Biotechnol. Adv.* 26: 246–265.
21. Hakkarainen, M. (2002). Aliphatic polyesters: Abiotic and biotic degradation and degradation products. *Adv. Polym. Sci.* 157: 113–138.
22. Ehrenstein, G. W., G. Riedel, and P. Trawiel. 2004. *Thermal Analysis of Plastics: Theory and Practice*. Munich: Hanser Gardner Publications, p. 368.
23. Xu, H. J., J. C. Sy, and V. P. Shastri. 2006. Towards developing surface eroding poly(α-hydroxy acids). *Biomaterials* 27: 3021–3030.

JOURNAL OF Applied Polymer SCIENCE

Biodegradation Study on Poly(ε-caprolactone) with Bimodal Molecular Weight Distribution

Soňa Hermanová,[1,2] Radka Bálková,[1,2] Stanislava Voběrková,[3] Ivana Chamradová,[2] Jiřina Omelková,[4] Lukáš Richtera,[1,2] Ludmila Mravcová,[1] Josef Jančář[1,2]

[1]Central European Institute of Technology, Brno University of Technology, Technická 3058/10, 616 00 Brno, Czech Republic
[2]Faculty of Chemistry, Institute of Materials Chemistry, Brno University of Technology, Purkyňova 118, 612 00 Brno, Czech Republic
[3]Faculty of Agronomy, Institute of Chemistry and Biochemistry, Mendel University in Brno, Zemědělská 1/1665, 613 00, Czech Republic
[4]Faculty of Chemistry, Institute of Food Science and Biotechnology, Brno University of Technology, Purkyňova 118, 612 00 Brno, Czech Republic
[5]Faculty of Chemistry, Institute of Chemistry and Technology of Environmental Protection, Brno University of Technology, Purkyňova 118, 612 00 Brno, Czech Republic
Correspondence to: S. Hermanová (E-mail: hermanova-s@fch.vutbr.cz)

ABSTRACT: Poly(ε-caprolactone) (PCL) of bimodal molecular weight distribution was exposed to the action of enzymes-lipases from *Aspergillus oryzae* in phosphate buffer at pH 7 and 37°C, and those produced *in situ* by *Bacillus subtilis* in nutrient medium at 30°C for 42 days. The occurrence of biodegradation is proved on the basis of the weight loss, decrease of molecular weight, carbonyl index, crystallinity, and development of cracks on the PCL surfaces. In the case of *Bacillus subtilis*, the degradation (10 wt % loss of PCL) proceeds faster in comparison with lipase from *Aspergillus oryzae* (2.6 wt % loss of PCL), where the degradation process seems to stop during 14 days of experiment. The gel permeation chromatography results reveal that preferential degradation of lower molecular portion did not occur but it is assumed that PCL chains were cleaved in accordance with particular degradation mechanism that depends significantly on biological agent. © 2012 Wiley Periodicals, Inc. J. Appl. Polym. Sci. 000: 000–000, 2012

KEYWORDS: polycaprolactone; degradation; lipase; *Bacillus subtilis; Aspergillus oryzae*; crystallinity; morphology; bimodal molecular weight distribution

Received 31 January 2012; accepted 18 May 2012; published online
DOI: 10.1002/app.38078

INTRODUCTION

Poly(ε-caprolactone) (PCL) has recently returned back into the arena of smart biomaterials due to its good processability related to its superior rheological and viscoelastic properties over many other aliphatic polyesters and development of novel manufacturing technologies.[1]

Biodegradability of PCL-based materials represents other important feature, for example, for food packaging applications because PCL can be decomposed by the action of microorganisms and their enzymes even when the monomer - ε-caprolactone is obtained by chemical synthesis from fossil resources.[2,3] In most cases the polymer degradation begins with deposition, adhesion, and colonization of microorganisms on polymer surface followed by the formation of a biofilm.[4] Then, an excretion of enzymes-lipases into surrounding as a consequence of the presence of lipidic carbon source proceeds.

Biodegradation initiated by enzyme action is assumed to consist basically of the enzyme adsorption on polymer substrate, followed by the formation of transition-state complex between the polymer and enzyme, which leads to specific chain scission of polymer chains.[5]

Three basic processes participating in enzyme-catalyzed ester bonds cleavage were suggested including random chain scission irrespective of chain lengths, specific chain-end scission, and/or synergic participation of both processes.[6]

Up to now, the degradation mechanisms of PCL were confirmed and discussed in details in case of controlled thermal and nonisothermal degradation studies.[7,8,9,10]

Additional Supporting Information may be found in the online version of this article.

It was also found out that the degradation mechanism of PCL-based implants *in vivo* could be attributed to random hydrolytic chain scission of ester bonds in the first step and was identical with *in vitro* hydrolysis at 40°C.[11]

According to number of studies in a variety of different environments, biodegradation of PCL was postulated to be the surface erosion process accompanied by only minor decrease in molecular weight (MW).[12] Furthermore, the rate and pattern of biodegradation is governed by certain principal factors including PCL characteristics (crystallinity, weight-average molecular weight (M_w), surface morphology), type of microorganism or enzyme and last but not least by mode of pretreatment of polymer specimen.[13,14,15,16]

The initial M_w together with crystallinity (X_c) of studied polymer materials represent an important factor influencing the rate of degradation and therefore, they can serve as parameters indicating the degree of degradation. It was found out that extracellular enzymes as triacylglycerol hydrolases (lipases), secreted by microorganism due to the presence of PCL as the lipophilic substrate, act as depolymerases and reduce polymer chain length to be small enough to penetrate through cellular membranes. The reduction of MW was shown to be the rate-limiting factor of degradation of many polymers.[17] The higher the initial MW of polymer the lower the weight loss as it was clearly observed during degradation of series of PCLs (number-average molecular weight (M_n) = 10.0, 43.0, 80.0 kDa) by the action of *Pseudomonas* lipase.[18] Moreover, the MW value is believed to affect the penetration of water molecules and/or enzymes into the polymer matrix and, thus, to influence diffusion phenomena as well. The dependence of the degradation rate on the MW distribution was already revealed in 1974 when Fields et al.[19] found out direct relationship between the degradation rate and the content of low molecular species in bimodal PCL samples exposed to *Aureobasidium pullulans*.

It was shown that enzymatic degradation of monomodal PCL depends on its initial crystallinity which can decrease[16,20] or increase[15,16] during the degradation process. But the influence of medium without microorganisms or enzymes on X_c should also be taken into account.[21] The change of crystallinity is connected with the mechanism of biodegradation and is usually accompanied by the change of surface morphology[16,22] and/or molecular weight.[20,21]

The aim of this work was to study the biodegradation of PCL with bimodal molecular weight distribution, because up to now, there are only a few studies evaluating the effect of the MW distribution on subsequent degradation of polymer. Bimodal PCL was exposed to *Bacillus subtilis* (*BS*) in nutritious medium containing 1 % (v/v) olive oil and 2 % (w/v) glucose at 30°C. Simultaneously, bimodal PCL was incubated in the presence of commercially available lipase from *Aspergillus oryzae* (*AO*) in phosphate buffer at pH 7 and 37°C. The degradation experiment with commercial *AO* lipase with particular substrate specifity carried out under defined conditions (37°C, pH 7) served as a model system which helped understanding the trends observed in case of complex PCL/*BS*/medium system.

PCL samples were in a form of disks (1 cm in a diameter, 100 μm of thickness) and the degradation experiment was performed in a period of 42 days. The degraded PCL samples were periodically weighted (14, 28, 42 days) and analyzed by differential scanning calorimetry (DSC), gel permeation chromatography (GPC), Fourier transform infrared spectroscopy (FTIR), and confocal laser scanning microscopy (CLSM).

EXPERIMENTAL

Materials

Polymer Sample. PCLs were synthesized in the Laboratory of Polymer Synthesis, Brno University of Technology.[23] Two runs were simultaneously performed under the same polymerization conditions to have polymer with tailored bimodal distribution and in a high yield for degradation study. The results of GPC and NMR analyses of PCLs samples denoted as *BS*-PCL and *AO*-PCL are as follows:

GPC characteristics of PCLs

Sample[a]	M_n (kDa)	M_w (kDa)	M_w/M_n
BS-PCL	19.4	132.0	6.8
AO-PCL	25.4	165.0	6.5

NMR spectroscopic analysis confirmed the presence of hydroxylic and benzoxylic end groups, ^{1}H NMR (400 MHz, $CDCl_3$, δ) spectrum in $CHCl_3$ was as follows: 1.37 (m, 2H; CH_2), 1.64 (m, 4H; CH_2), 2.29 (t, $J = 7.5$ Hz, 2H; CH_2CO), 3.64 (t, $J = 6.5$ Hz, 2H; CH_2OH), 4.05 (t, $J = 6.7$ Hz, 2H; CH_2OCO), 5.11 (s, 2H; OCH_2Ph).

PCL powder was processed by dissolving in chloroform (2 wt %). The solution was cast into Petri dishes, air-dried for 2 days and vacuum-dried until constant weight to prepare PCL films. The samples suitable for the degradation study were cut out from PCL films (3 cm in diameter) in a form of circular disks of 1 cm in a diameter and of about 100 μm thickness. All specimens were sterilized by UV irradiation for 30 min in an Aura Mini laminar box, BioTech Instruments, Prague, CZ before degradation experiments.

Biological Agent

BS and culture conditions. The bacterial strain *BS* CCM 1999 was obtained from the culture collection of the Czech Collection of Microorganims, Masaryk University Brno, Faculty of Science. Tested culture was maintained on nutrient agar at 30°C for 3 days before the degradation experiment.

AO. The lipase from *AO* (WE-Nr. 916,028) was obtained from Mucos Pharma.

Assay for lipase activity. Lipolytic activity was determined by *p*-nitrophenyl-laurate (pNPL) as a substrate dissolved in ethanol on UV/VIS HELLIOS spectrophotometer (DELTA Thermospectronic, England).

The reaction mixture consisted of 0.25 mL enzyme solution (0.5 mg mL^{-1} of *AO* lipase), 3.25 mL of phosphate buffer ($c = 0.050$ in water, pH 7) and 0.25 mL of pNPL ($c = 0.0025$ in ethanol).

In the case of *BS*, 0.25 mL of the cell-free culture supernatant containing expected extracellular enzymes was added into the reaction mixture.

Hydrolytic reaction was carried out at 37°C for 30 min and afterward 0.5 mL of Na_2CO_3 ($c = 0.1$ in water) was added to stop the reaction. Subsequently, the absorbance was recorded at 420 nm. One unit of lipase activity (U) was defined as the amount of enzyme that caused the release of 1 μmol of *p*-nitrophenol from pNPL in one minute under the test conditions.

The pH optimum of lipase activity was measured using pNPL as a substrate by incubating 0.25 mL of enzyme solution (*AO*) or 0.25 mL of the cell-free culture supernatant (*BS*) with following buffers ($c = 0.050$ in water): citrate-phosphate (pH 5–6), phosphate (pH 7), boric acid-borax (pH 8–9), glycine NaOH (pH 10), and Britton-Robinson (pH 11) at 37°C for 30 min. The temperature optimum was determined under constant pH of 7 at 30, 35, 37, 40, 45, and 50°C.

The lipase thermal stability was determined spectrophotometrically with pNPL as a substrate by measurement of residual activity after 1 h incubation at different temperatures (30, 40, 50, 60, and 70°C) in phosphate buffer ($c = 0.050$ in water, pH 7).

The initial activity of *BS* lipase, independent of PCL studied, was 0.0643 U mL^{-1} of enzyme at pH 7 and 30°C.

The initial activity of *AO* lipase, independent of PCL studied, was 0.0343 U mL^{-1} of enzyme at pH 7 and 37°C.

Degradation Experiment

Degradation experiment with AO lipase. PCL disks were inserted into vials containing 3 mL of phosphate buffer solution (pH 7) and 1.5 mg of *AO* lipase and placed in a thermostat at 37°C. The enzymatic solution was renewed every 3 days to restore the original level of enzymatic activity.

The control samples were treated in the same way but their incubation was carried out in phosphate buffer without enzyme and sodium azide 0.02 % (w/w) was added into the solution to prevent contamination.

Degradation experiment with BS. For inoculum preparation, 1 mL of distilled sterile water was added into nutrient agar inoculated with *BS*. The colonies were rubbed carefully with a sterile vaccination loop and transferred into 100 mL of nutritious medium in a sterile Erlenmeyer flask (250 mL). The nutritious medium (100 mL) was prepared from peptone (3.0 g), yeast extract (1.0 g), NaCl (0.5 g), glucose (2.0 g), olive oil (1.0 mL), and distilled water. The medium was sterilized in an autoclave at 121°C and 103.4 kPa for 20 min. Inoculated Erlenmeyer flasks were dynamically cultivated (90 rpm) for 1 h. Then, PCL specimens were added into it. The medium was renewed every 4 days to restore the original level of lipase activity.

The control samples were treated in the same way but their incubation was carried out in the absence of bacterial strain and 0.02 % (w/w) sodium azide was added into the solution to prevent contamination.

Methods and Testing

Weight loss measurement. PCL specimens were withdrawn after 14, 28, and 42 days from the degradation medium, washed gently with distilled water and vacuum-dried at lab temperature for 1 week. Then the samples were weighted and the values obtained were compared with those of original and control samples.

DSC. DSC measurements were carried out in two heating runs on calorimeter TA Instruments Q 2000 in the temperature range from -80°C to 90°C under nitrogen (50 mL min^{-1}). The test schedule used was as follows: (i) cooling from room temperature to 0°C, (ii) heating from 0°C to 100°C at 10°C min^{-1}, (iii) 5 min isothermal at 100°C, (iv) cooling down to -80°C at 5°C min^{-1}, (v) 5 min isothermal at -80°C, and (vi) heating from -80°C to 90°C at 5°C min^{-1}. The melting temperature was evaluated from the endothermic peak maximum and melting enthalpy was used to determine PCL samples crystallinity (X_c) both from the first and the second heating scans.

GPC. GPC was used for measurement of the relative molecular weight (M_n, M_w) and polydispersity index (M_w/M_n) of PCLs using an Agilent Technologies 1100 Series device equipped with refractive index (RI) detector and two PLgel MIXED Columns 300 × 7.5 mm with particle size of 5 μm. Tetrahydrofuran (THF) was used as the mobile phase at a flow rate of 1 mL min^{-1} at room temperature. Polystyrene standards were used for calibration (Mp = 316500-162).

FTIR. The change of chemical structure in terms of ester bond cleavage in PCL films was evaluated by FTIR measurement on spectrometer Thermo Scientific Nicolet iS10 in a simple transmission mode. The transmission spectra were recorded in the spectral range of 4000–400 cm^{-1} at the resolution 6 cm^{-1} and 128 scans.

Preweighed amount of PCL film was dissolved in dichloromethane to obtain 3 % solution which was cast on KBr disk. The traces of dichloromethane were subsequently removed under vacuum to yield films for FTIR analysis.

CLSM. Morphology of PCL sample surfaces was analyzed by confocal laser scanning microscope Olympus LEXT OLS 3000.

RESULTS AND DISCUSSION

Degradation study of PCL with bimodal distribution by the action of bacterial and fungi lipase was performed. The degradation experiments were carried out under conditions of the optimum action of both types of lipases. The production of lipase *BS* was stimulated with olive oil added into the cultivation medium because the extracellular lipase produced by *BS* is suggested to have inducible character.[24] Degradation process was evaluated from the weight loss, GPC, FTIR, DSC, and CLSM measurements. PCL molecular characteristics before and after the degradation test are summarized in Table I.

The weight loss of the samples exposed to *BS* gradually increased up to 10 wt % during 42 days of experiment. Significant reduction of number-average molecular weight (M_n) as well as weight-average M_w was observed. The reduction of M_n by 45 % can be explained by preferred interaction of the active enzyme site with ester groups situated near PCL chain ends followed by repeated selective abstraction of segments with the same size such as monomer, dimer, or trimer.[22] The decrease of M_w by 70 % indicates scission of the longest PCL chains. Moreover, the shape of the elution curves changed during the degradation period. Besides shifting of chromatograms to lower

Applied Polymer SCIENCE

Table I. Characteristics of PCL exposed to biological action

Sample[a]	Period (days)	Weight loss (%)	M_n (GPC)[b] (kDa)	M_w (GPC)[b] (kDa)	M_w/M_n
BS-PCL	0	-	19.4	132.0	6.8
BS-14d	14	0.5	12.0	50.0	4.1
BS-28d	28	5.5	11.7	46.7	4.2
BS-42d	42	10	10.6	37.8	3.2
AO-PCL	0	-	25.4	165	6.5
AO-14d	14	2.6	23.5	142	6.2
AO-28d	28	2.6	22.6	143	7.7
AO-42d	42	2.8	19.0	143	7.5

[a]*BS* labels PCL samples exposed to *Bacillus subtilis* while *AO* labels PCL samples exposed to lipase from *Aspergilus oryzae*; the number after the abbreviation denotes aging time in days.
[b]Determined by GPC using polystyren (PS) standards.

molecular region, the elution curve became almost monomodal with a tail in oligomeric region (Figure 1). The amount of smaller low-mass fraction decreased after 42 days probably as a consequence of the diffusion of low MW species into the degradation medium that corresponds with the weight loss. According to the results, one can suggest the synergic process of the chain-end depolymerization and random scission of ester bonds along PCL chains, irrespective of their lengths.[25,26]

PCL samples exposed to *AO* action in phosphate buffer revealed the decrease in M_n by 25 % and M_w by only 13 % and hence lower degradation rate as compared with *BS* aged samples. Similarly, lower weight loss being 2.6 wt % after 14 days did not gradually increase during further degradation period. The observed low level of enzymatic degradation could be explained on the basis of both, substrate binding to fungal lipases and their substrate specifity.[27]

The *AO* lipase could initially interact with hydroxyl end group of PCL chains through hydrophilic binding sites and with PCL segments representing fatty acid chains through aliphatic site to direct the substrate into the right binding mode for catalysis. Subsequently, the depolymerization from PCL chains ends with

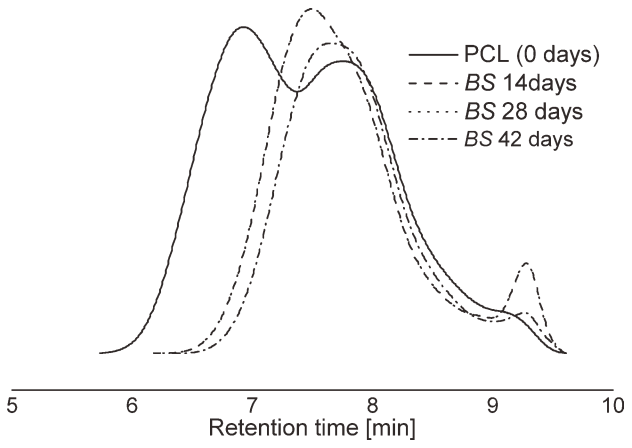

Figure 1. GPC chromatograms of PCLs exposed to *BS* action.

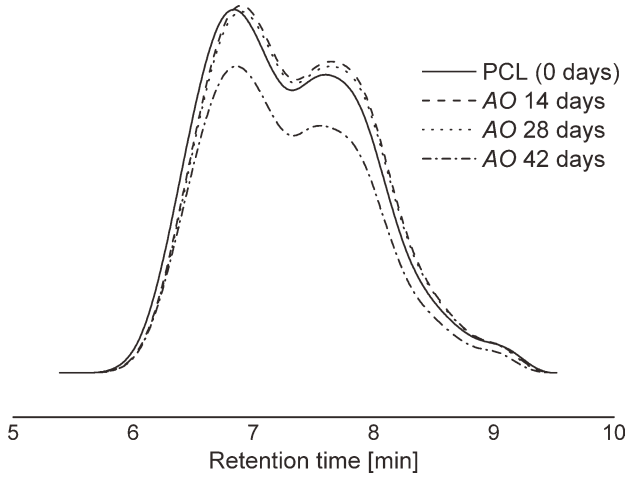

Figure 2. GPC chromatograms of PCLs exposed to *AO* action.

hydroxyl groups toward their centers can be assumed due to the decrease of the area under molecular weight peaks (Figure 2). It is also probable that some conformation defects of PCL segments could terminate the unzipping process after 14 days of the experiment because there was no change in tested parameters at that time observed. Moreover, the acting of *AO* lipase at a specific position on ester bonds of PCL chains, as a consequence of 1,3-regiospecifity of *Aspergillus sp.* lipases reported in literature, could be assumed as well.[28]

It should be mentioned that in the case of *BS* the whole enzyme potential of microbial cells is implemented during the degradation process. This fact together with lower initial molecular weight of studied PCL could contribute to the more rapid degradation process in comparison with lipase from *AO*.

In the case of control samples, the weight loss was negligible, as well as changes in M_w (Figure 3) and thus the occurrence of hydrolytic degradation caused by water solvolysis was excluded. Such finding correlates well with the study of Pitt et al. who did not observe the weight loss until approx. 2.5 years of PCL

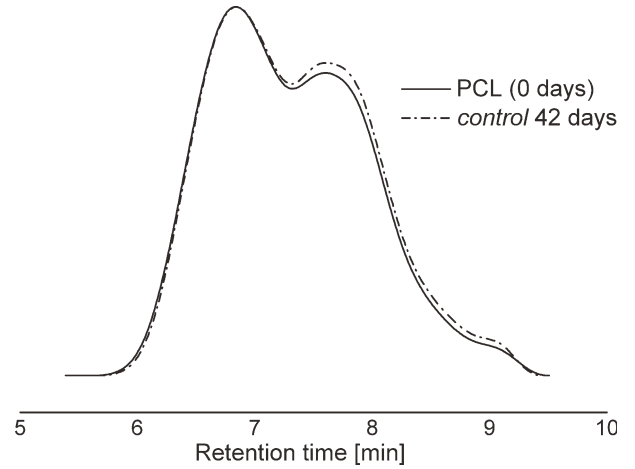

Figure 3. GPC chromatograms of original PCL and PCL immersed in phosphate buffer for 42 days as a control sample (M_n = 23.0 kDa, M_w = 162 kDa, M_w/M_n = 6.9).

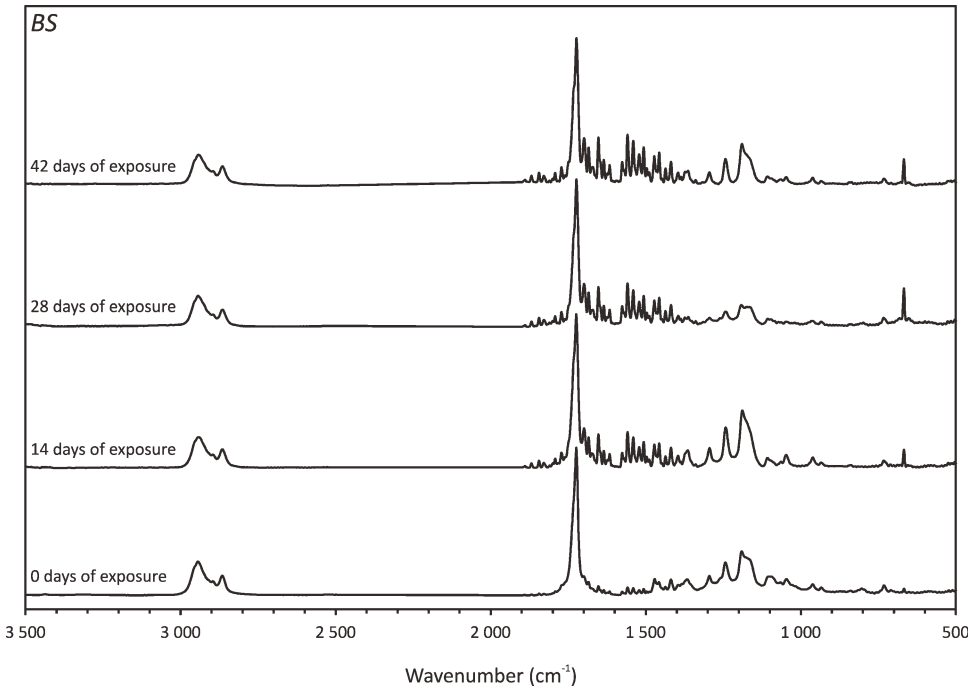

Figure 4. FTIR spectra of PCL films before and after immersion in medium enriched with *BS* in the region of 500–1900 and 2500–3500 cm^{-1} for (a) 0 days, (b) 14 days, (c) 28 days, (d) 42 days.

in vitro degradation test, when the M_w of PCL was reduced to 5000 and thus, PCL oligomers started to diffuse from tested material bulk.[29]

The degradation process through ester bonds cleavage was further confirmed by the decrease of the intensity of the band at 1726 cm^{-1} detected in drop-cast FTIR spectra of incubated PCLs (Figures 4 and 5). The decrease was pronounced in the case of *BS* incubation in accordance with observed higher weight loss. In a similar way, the reduction of carbonyl index calculated as a ratio of 1726/1398 cm^{-1} [15,30] documented different rates of degradation taking place in *AO* and *BS* incubated PCL samples (Table S1, Supporting Information).

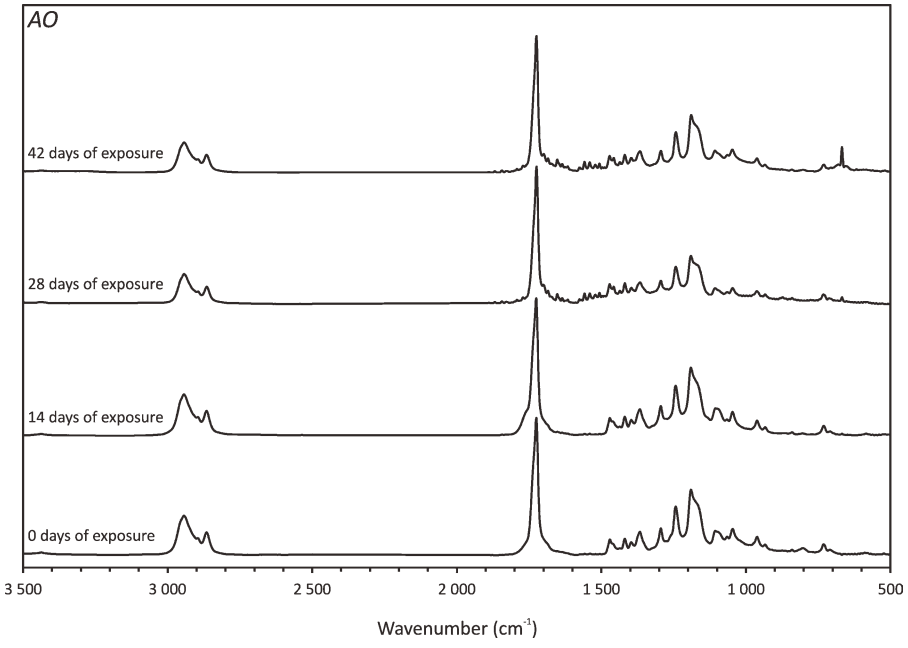

Figure 5. FTIR spectra of PCL films before and after immersion in phosphate buffer enriched with *AO* in the region of 500–1900 and 2500–3500 cm^{-1} for (a) 0 days, (b) 14 days, (c) 28 days, (d) 42 days.

Applied Polymer SCIENCE

Table II. DSC characteristics of PCL exposed to biological action

Sample[a]	Period (days)	$^{1st}X_c$ (%)[b]	$^{2nd}X_c$ (%)[b]	$^{1st}T_m$ (°C)[c]	$^{2nd}T_m$ (°C)[c]
PCL	0	64.1	50.7	63.5	55.8
BS-14d	14	60.8	49.0	63.5	54.1, 56.2
BS-28d	28	59.1	48.5	62.7	54.2
BS-42d	42	53.8	41.1	61.6	52.3, 55.5
AO-PCL	0	63.6	52.2	63.5	55.9
AO-14d	14	53.4	44.7	63.6	56.5
AO-42d	42	54.7	42.1	64.7	56.7

[a]*BS* labels PCL samples exposed to *Bacillus subtilis* while *AO* labels PCL samples exposed to lipase from *Aspergilus oryzae*; the number after the abbreviation denotes aging time in days.
[b]X_c labels crystallinity calculated according to the $\Delta H_m/\Delta H_m^0$ ratio where, ΔH_m^0 of PCL is 139.5 J g^{-1}. 1st, 2nd labels the first and second heating, respectively.
[c]T_m represents melting, temperature, 1st, 2nd labels the first and second heating, respectively.

DSC data confirmed the degradation process of bimodal PCL both by *BS* bacteria and *AO* lipase although the degradation mechanism was evidently different.

The structure change of PCL samples exposed to *BS* bacteria was manifested by the gradual decrease of crystallinity (X_c) that achieved 16 % after 42 days and by the slight decrease of melting (T_m) together with crystallization temperature (T_c; Table II). DSC data of control samples were nearly without change in time suggesting no significant impact of PCL conditioning in nutrient medium without bacterial strain on its structure. It can be seen that the first heating endotherms split from one peak to double one during the second heating, whereas no split was observed for control samples (Figures 6 and 7). It is evident that the original peak gradually shifted to lower T_m and only small peak remained on its place after 42 days. It means that crystallites were predominantly

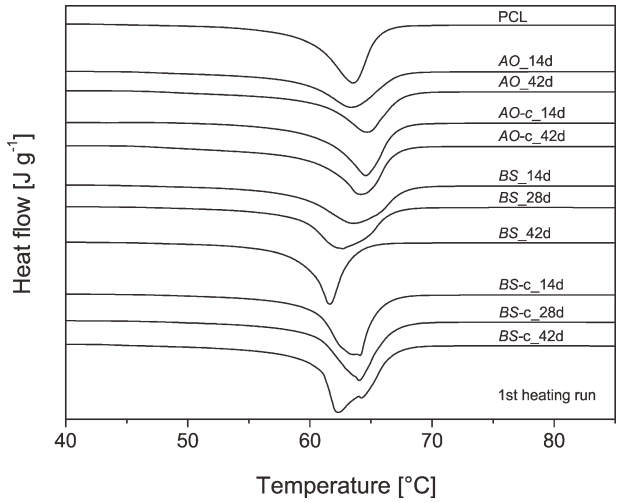

Figure 6. DSC first heating curves of all PCL samples including the control ones (PCL denotes the original polymer, AO_14d denotes PCL exposed to *AO* for 14 days, BS-c_42d denotes control sample for bimodal PCL sample exposed to *BS* for 42 days).

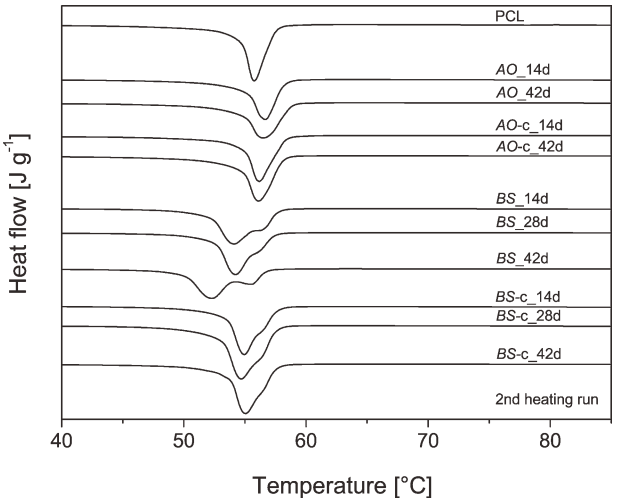

Figure 7. DSC second heating curves of all PCL samples including the control ones (the meaning of DSC curves titles is the same as in Figure 6).

formed by shorter chains produced by scission of the longest ones, as revealed by GPC. Simultaneously, the endotherm shape turning from the narrow one for the original PCL through formation of a shoulder up to double peak reflected gradual bond scission. The scission of PCL bonds was also confirmed by the decrease of the second heating X_c in time with respect to the original PCL, because no decrease of the second heating X_c was measured for control samples. The trend of the second X_c was the same as of the first one (Table II). Thus, the DSC data support the occurrence of enzyme-catalyzed chain cleavage as proved by FTIR measurement.

DSC data of PCL samples exposed to *AO* lipase are summarized in Table II. The samples were measured after 14 and 42 days of experiment. It was shown insignificant change of T_m during 42 days and no change in T_m was observed for control samples. The same situation was observed after the second heating both for degraded and control samples, where no change in endotherm shapes occurred (Figures 6 and 7). These facts imply that the longest PCL chains were not broken and oligomeric species were not formed. However, both the first and the second crystallinity decreased by about 16 % even after 14 days with respect to control PCL and no decrease of X_c was observed for control samples both after the first and the second heating during the same period. Based on the results obtained, the enzyme-catalyzed PCL chain cleavage occurred but under different mechanism compared with the action of *BS* bacteria. The X_c did not change within period 14–42 days which together with the weight loss reflected action of *AO* lipase on PCL substrate only during the first 14 days, even if the *AO*/buffer system was renewed every 72 h. It is supposed that the enzyme-catalyzed cleavage of PCL chains occurred also in crystalline region because both the surface of PCL samples was not amorphous and the original X_c was relatively high (64 %).

The decrease of crystallinity of PCL with monomodal molecular weight distribution exposed to phosphate buffer solution containing lipases was reported by Gan et al. and Sekosan et al.[16,20]

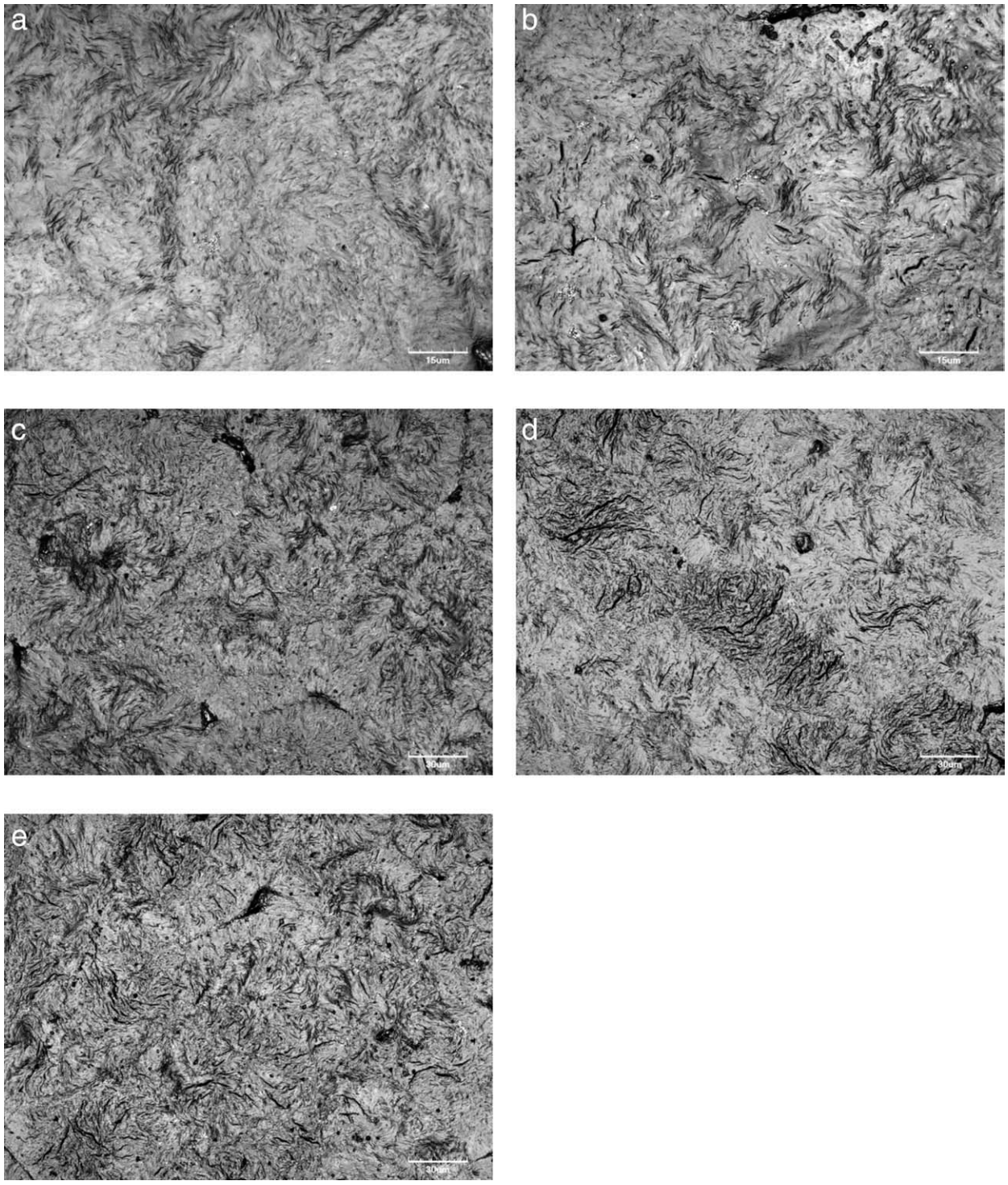

Figure 8. CLSM micrographs of PCL sample surfaces exposed to *BS* (a) original PCL film (scale bar is 15 μm), (b) PCL film aged for 14 days (scale bar is 15 μm), (c) PCL film degraded for 14 days (scale bar is 30 μm), (d) PCL film degraded for 28 days (scale bar is 30 μm), and (e) PCL film degraded for 42 days (scale bar is 30 μm).

Unfortunately, the first did not explain degradation in detail and there are also no data of PCL crystallinity. The latter stated that biodegradation occurred also in crystalline region if X_c of the studied polymer was originally high (more than 45 %). On the other hand, the crystallinity increased during the degradation of PCL with originally low X_c. Yoshioka et al. observed the increase of X_c of monomodal PCL immersed only in phosphate buffer solution by 16 % in 12 weeks without the weight loss and decrease of M_W, although the original X_c of PCL was high (56.5 %).[21] The reason was the fact that amorphous chains were

Applied Polymer SCIENCE

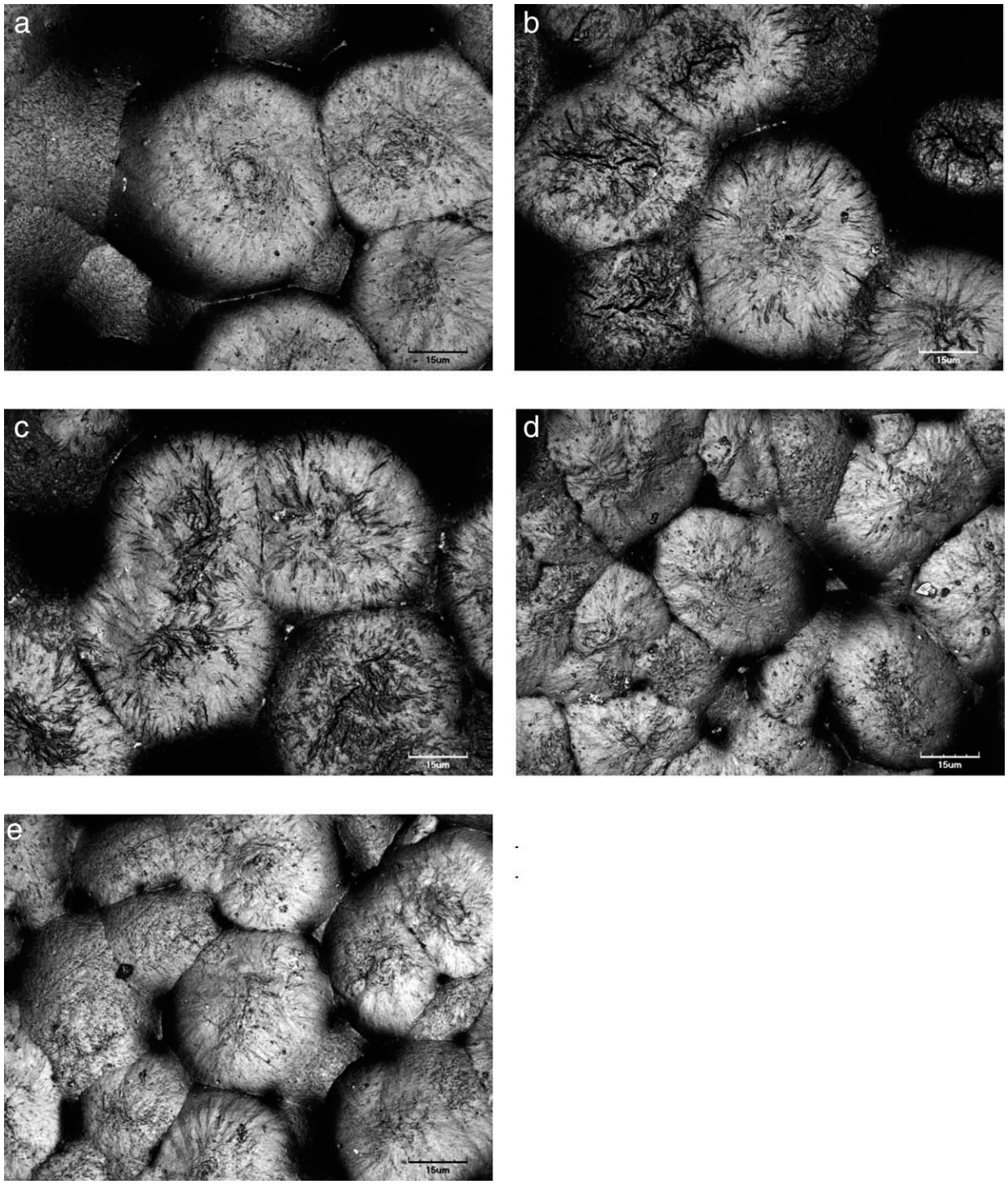

Figure 9. CLSM micrographs of PCL sample surfaces exposed to *AO*. (a) Original PCL film (scale bar is 15 μm), (b) PCL film degraded for 14 days (scale bar is 15 μm), (c) PCL film degraded for 42 days (scale bar is 30 μm), (d) PCL control sample immersed in phosphate buffer for 14 days (scale bar is 30 μm), and (e) PCL control sample immersed in phosphate buffer for 42 days (scale bar is 30 μm).

in rubber-like state under conditions of experiment, and, therefore, able to crystallize.

In this work, PCL amorphous phase was also in rubber-like state but crystallinity of PCL samples degraded by *AO* and *BS* action decreased. It is assumed that the main reason was relatively high initial X_c of the PCL material, which did not increase under given experimental conditions of degradation test. This statement is supported by the fact that in control samples no change of X_c was observed.

It is supposed that microbial biodegradation occurs in amorphous phase. Nevertheless, the ability of microorganism

adhesion on polymer surface and its influence on subsequent biodegradation pattern should be taken into account as well. It is also assumed that the released enzymes will act on available substrate in immediate vicinity. Because of the solution casting, PCL surfaces were formed by spherulites. This means that PCL surface was not amorphous and plain because spherulites have 3D structure, where lamellar units are tilted under different angles. The cracks distributed in certain directions (certain places) were observed on PCL surfaces exposed to *BS* action by CLSM [Figure 8(a–e)]. They could be the consequence of the preferential bacteria adhesion to pits and grooves of 3D surface, where they were protected against friction and shear forces.[31] As the *BS*/degradation medium was renewed every 4 days the compact biofilm was not observed and hence, bacterial adhesion supposed to take place via reversible physicochemical interaction between bacteria and PCL surfaces. Subsequently, the release of depolymerizing enzymes should occur. Based on the results obtained, one can suggest that the enzyme-catalyzed chain cleavage occurred also in crystallites because the polymer crystallinity decreased. However, this statement probably involves the cleavage of bonds in amorphous phase of crystallites.

The cracks were observed on *AO* degraded sample surfaces using CLSM as in previous case reflecting the enzyme action, whereas no cracks were observed on control sample surfaces [Figure 9(a–e)]. Because spherulites covered surfaces of PCL samples the enzyme could attack also crystallites, which corresponds with the decrease of X_c. It is evident that number and size of cracks did not change after 14 days which corresponds well with the observed trends in FTIR spectra, weight loss and molecular weight. It is worth mentioning that both the number and size of cracks were much higher as compared with *BS* exposed samples. The reason could be the synergic action of phosphate buffer solution, where the osmotic inflow of water could accelerate degradation process.

Thus, with no doubt, the biodegradation is a complex process, where both initial characteristics of polymer specimen and its processing, biological agent, degradation medium, and conditions have specific influence.

CONCLUSIONS

PCL of bimodal molecular weight distribution was exposed to the action of enzymes-lipases from *AO* and those produced *in situ* by *BS*. The occurrence of biodegradation was proved on the basis of the weight loss, decrease in molecular weight (M_n, M_w), carbonyl index, and crystallinity together with cracks observed on PCL sample surfaces in comparison with control samples. Random chain scission dominated during the exposition of PCL to *BS* bacteria in nutrient medium. On the contrary, the action of *AO* lipase in phosphate buffer lead to the degradation of PCL chains by the unzipping mechanism. It is assumed that scission of PCL bonds occurred also in amorphous regions of crystallites due to the high crystallinity of the original PCL. This is also supported by crystallinity decrease during degradation and the presence of the cracks observed in spherulites.

ACKNOWLEDGMENTS

This work was supported by the Ministry of Education, Youth and Physical Training of the Czech Republic under the research project no. MSM 0021630501.The authors would like to thank prof. Ing. Ladislav Omelka, DrSc. for fruitful discussion and Radka Slavíčková, and Zdenka Vyroubalová for technical assistance.

REFERENCES

1. Woodruff, M. A.; Hutmacher, D. W. *Prog. Polym. Sci.* **2010,** *35*, 1217.
2. Herrmann, B. G.; Debeer, L.; Wilde, B.; De, K.; Patel, M. K. *Polym. Degrad. Stabil.* **2011,** *96*, 1159.
3. Tokiwa, Y.; Calabia, B. P.; Ugwu, U.; Aiba, S. *Int. J. Mol. Sci.* **2009,** *10*, 3722.
4. Sivan, A. *Curr. Opin. Biotech.* **2011,** *22*, 422.
5. Sivilingham, G.; Chattopadhyay, S.; Madras, G. *Chem. Eng. Sci.* **2003,** *58*, 2911.
6. Ponsart, S.; Coudane, J.; Saulnier, B.; Morgat, J. L.; Vert, M. *Biomacromolecules* **2001,** *2*, 373.
7. Persenaire, O.; Alexandre, M.; Degeé, P.; Dubois, P. *Biomacromolecules* **2001,** *2*, 288.
8. Sivilingham, G.; Madras, G. *Polym. Degrad. Stabil.* **2003,** *80*, 11.
9. Ioshi, P.; Madras, G. *Polym. Degrad. Stabil.* **2008,** *93*, 1901.
10. Aoyagi, Y.; Yamashita, K.; Doi, Y. *Polym. Degrad. Stabil.* **2002,** *76*, 53.
11. Sun, H.; Mei, L.; Song, C.; Cui, X.; Wang, P. *Biomaterials* **2006,** *27*, 1735.
12. Hakkarainen, M. *Adv. Polym. Sci.* **2002,** *157*, 115.
13. Shah, A. A.; Hasan, F.; Hameed, A.; Ahmed, S. *Biotechnol. Adv.* **2008,** *26*, 246.
14. Lucas, N.; Bienaime, C.h; Belloy, C.h; Queneudec, M.; Silvestre, F.; Nava-Saucedo, J. -E. *Chemosphere* **2008,** *73*, 429.
15. Khatiwala, V. K.; Shekkar, N.; Aggarwal, S.; Mandal, U. K. *J. Polym. Environ.* **2008,** *16*, 61.
16. Sekosan, G.; Vasanthan, N. J. *Polym. Sci. Pol. Phys.* **2010,** *48*, 202.
17. Mueller, R. J. *Process Biochem.* **2006,** *41*, 2124.
18. Kulkarni, A.; Reche, J.; Hartmann, J.; Kratz, K.; Lendlein, A. *Eur. J. Pharm. Biopharm.* **2008,** *68*, 46.
19. Fields, R. D.; Rodrigues, F.; Finn, R. K. *J. Appl. Polym. Sci.* **1974,** *18*, 3571.
20. Gan, Z.; Liang, Q.; Zhang, J.; Jing, X. *Polym. Degrad. Stabil.* **1997,** *56*, 209.
21. Yoshioka, T.; Kamada, F.; Kawazoe, N.; Tateishi, T.; Chen, G. *Polym. Eng. Sci.* **2010,** *50*, 1895.
22. Lefebvre, F.; David, C.; Wauven, C. V. *Polym. Degrad. Stabil.* **1994,** *45*, 347.
23. Neumayerová, Z. Polycaprolactone-Synthesis, Characterization and Degradability. Thesis, Brno University of Technology, **2010.**

24. Treichel, H.; De Oliveira, D.; Mazutti, M. A.; Di Luccio, M.; Oliveira, J. V. *Food Bioprocess Tech.* **2010,** *3*, 182.
25. Jarrett, P.; Benedict, C. V.; Bell, J. P.; Cameron, J. A.; Huang, S. J. In Polymers as Biomaterials, Shalaby, S. W.; Hoffman, A. S.; Ratner, B. D.; Horbett, T. A., Eds.; Plenum Press: New York, **1985;** pp 181–192.
26. Reiche, J. *Thin Solid Films* **2008,** *516*, 8821.
27. Norin, M.; Haeffner, F.; Achour, A.; Norin, T.; Hult, K. *Protein. Sci.* **1994,** *3*, 1493.
28. Contesini, F. J.; Lopes, D. B.; Macedo, G. A.; Nascimento, M. G.; Carvalho, P. O. *J. Mol. Catal. B Enzym.* **2010,** *67*, 163.
29. Pitt, C.; Hibionada, F.; Klimas, D.; Schindler, A. J. *Appl. Polym. Sci.* **1981,** *26*, 3779.
30. Hadad, D.; Geresh, S.; Sivan, A. J. *Appl. Microbiol.* **2005,** *98*, 1093.
31. Vu, B.; Chen, M.; Crawford, R. J.; Ivanova, E. P. *Molecules* **2009,** *14*, 2535.

J Polym Environ (2014) 22:190–199
DOI 10.1007/s10924-013-0630-y

ORIGINAL PAPER

Structure and Morphology of Microbial Degraded Poly(ε-caprolactone)/Graphite Oxide Composite

Radka Balkova · Sona Hermanova · Stanislava Voberkova · Pavel Damborsky · Lukas Richtera · Jirina Omelkova · Josef Jancar

Published online: 8 November 2013

Abstract Biodegradation of poly(ε-caprolactone) composite with graphite oxide (GO) by the action of *Bacillus subtilis* (*BS*) was studied in this work. Nanocomposite produced in a form of thin film was exposed to nutrient cultivation medium with *BS* as well as to abiotic nutrient medium (control run) at 30 °C. The matrix itself was exposed to the same conditions for comparison. Biodegradation was demonstrated by the weight loss and the decrease of molecular weight during 21 days of the experiment as well as by changes in the surface morphology and structure. Both degraded and control materials were characterized by confocal laser scanning microscopy, differential scanning calorimetry, thermogravimetry, and Fourier transform infrared spectroscopy with attenuated total reflectance. The bacterial growth expressed as the measure of the optical density/turbidity in McFarland units and pH of medium were measured in situ during the experiment. Lipolytic activity of *BS* was determined by spectrophotometric assay. Degradation process was accompanied by the increase of matrix crystallinity degree. GO served as nucleating agent and facilitated absorption of cultivation media into the composite which led to the increase of the crystallinity degree also for control nanocomposite specimens. It was not evaluated to be promoter of biodegradation. The surface cracks formation was initiated by *BS* action. Large surface cracks were formed on *BS*-degraded composite surfaces while surface erosion was more significant on *BS*-degraded matrix.

Keywords Poly(ε-caprolactone) · Graphite oxide · Biodegradation · Lipase · Structure

R. Balkova (✉) · L. Richtera · J. Jancar
Faculty of Chemistry, Institute of Materials Science, Brno University of Technology, Purkynova 464/118, 612 00 Brno, Czech Republic
e-mail: balkova@fch.vutbr.cz

R. Balkova · L. Richtera · J. Jancar
Central European Institute of Technology, Brno University of Technology, Brno, Czech Republic

S. Hermanova
Department of Polymers, Institute of Chemical Technology Prague, Prague, Czech Republic

S. Voberkova
Faculty of Agronomy, Institute of Chemistry and Biochemistry, Mendel University in Brno, Brno, Czech Republic

P. Damborsky · J. Omelkova
Faculty of Chemistry, Institute of Food Science and Biotechnology, Brno University of Technology, Brno, Czech Republic

Introduction

Poly(ε-caprolactone) (PCL), an aliphatic semicrystalline polyester, is still found for wider applications due to its biocompatibility, non-toxicity, and biodegradability both in human body and environment. PCL was found to be relatively stable against abiotic hydrolysis [1–3] but degraded in many biotic environments including river, lake and seawater, sewage sludge, farm and paddy soil, different types of sediments, compost, sponges, and soil by hydrolysis caused also by enzymes action [1–14]. It was shown that mechanism and rate of PCL degradation varied with molecular weight, crystallinity degree, and morphology [3, 4, 7–10, 14–17] except ambient conditions. Degradation process starts in amorphous phase and is accompanied by the increase in crystallinity degree. Moreover, the crystal size and the amount of loosely chain-packed regions

(crystal defects) in a lamellar crystal are important factors governing the rate of enzyme-catalyzed hydrolysis. It is supposed that aliphatic polyesters such as PCL are degraded by different hydrolases from crystal edges and lateral sides of loosely chain-packed regions [4, 16].

One of the main disadvantages of biodegradable materials for engineering applications including PCL is their poor physical and mechanical performance. Many properties of such materials are usually improved by appropriate blending, filling, reinforcing, and copolymerization. Because fillers and reinforcements change the structure and thus, properties of the polymer matrix, the impact of them on the degradation process could be expected. For example, organoclay/PCL nanocomposites were found both to enhance biodegradability in organic compost together with reduced oxygen permeability [18] and to delay degradation rate in compost with respect to homopolymer PCL [19, 20] but also to have nearly no effect on degradation of PCL matrix by bacteria isolated from compost [20]. Except organoclay, silica and graphene-based polymer composites are produced which found their applications in automobile and aerospace industry and in the electronic industry for thermal management because incorporation of graphene oxide into the polymers greatly improved their thermal stability, electrical, and mechanical properties. But they can find the application also in packaging for food, medicine, electronics and beverages due to low permeability of gas molecules such as N_2, O_2, moisture, and CO_2 [21].

Graphene-based fillers are promising enforcing filler for polymers because functional groups on the surface of graphene sheets can enhance compatibility between them and the polymer matrix. Graphite oxide (GO) was, for example, presented to enhance the Young's modulus and tensile strength in composite with PCL [22]. GO is highly hydrophilic and readily exfoliated in water, yielding stable dispersion consisting mostly of single layered sheets (graphene oxide) [21]. Similar degree of exfoliation of GO was also attained for N,N-dimethylformamide (DMF), tetrahydrofuran (THF), N-methyl-2-pyrrolidone (NMP) and ethylene glycol [21].

Although a lot of work has been done on the synthesis, properties, and characterization of PCL blends, copolymers and composites, little attention has been paid toward biodegradation study of these materials and in case of graphene and graphite/graphene oxide, long term fate, health, and environmental risk assessment is widely lacking [23]. Recent studies of graphene-containing polymer nanocomposites also offer con-tradictory results regarding possible biocompatibility, antimicrobial activity, and toxic effects on a variety of microorganisms [24, 25]. These all are the reasons why biodegradation study of graphene-based PCL composites is an open and useful field to be engaged in.

This work wants to contribute into this field of research with biodegradation study of PCL/GO composite, the material potentially used for packaging, exposed to *Bacillus subtilis* (*BS*) at the optimum growth conditions of this microbial strain. The growth of *BS* was in cultivation medium monitored by the measurement of optical density/turbidity during 21 days of the experiment and the lipolytic activity of cell-free supernatant was determined by standard spectrophotometric method together with the pH measurement of cultivation medium. The effect of *BS* action on the surface morphology, structure and thermal stability of PCL and PCL/GO composite immersed in biotic medium, and for control run in abiotic medium, was determined from the weight loss and molecular weight measurements, by confocal laser scanning microscopy, differential scanning calorimetry, thermogravimetry, and Fourier transform infrared spectroscopy with attenuated total reflectance.

Experimental

Materials

Poly(ε-caprolactone) used was commercial synthetic polyester supplied in a form of pellets by Sigma Aldrich (molecular weights stated by supplier are as follows: $M_w = 14{,}000$, $M_n = 10{,}000$).

Graphite was supplied in a form of square rod by Karbotechnik, Ltd, the Czech Republic.

Bacillus subtilis (*BS*, bacterial strain, CCM 1999), a sporulating rod-shaped Gram-positive bacterium present in almost all ecosystems [26, 27], was obtained from the culture collection of the Czech Collection of Microorganisms (CCM), Masaryk University Brno, Faculty of Science. Bacterial strain was maintained on Meat Peptone Agar medium.

The culture medium for degradation study was nutrient broth medium. The medium consists of peptone (30 g dm^{-3}), yeast extract (10 g dm^{-3}), NaCl (5 g dm^{-3}), and for degradation experiment was supplemented with glucose (20 g dm^{-3}). All other chemicals were used as received.

Preparation

Graphite oxide was prepared by chemical oxidation of graphite in a mixture of H_2SO_4 and $KMnO_4$ according to the simplified Hummer's method described, for example, in [28]. The mixture was stirred for 3 days to ensure complete oxidation accompanied by the color change from dark purplish green to dark brown. To stop the oxidation process, H_2O_2 solution was added and the color of the mixture turned to bright yellow, indicating high oxidation

level of graphite. GO formed was washed 3 times with 1 M of HCl and repeatedly washed with deionized water until pH of 4–5 was achieved using a simple decantation. GO experienced exfoliation during the washing process with deionized water which led to the thickening of GO solution and formation of stable colloid of graphene oxide. This nanomaterial was freeze-dried to obtain solid GO which was analyzed by X-ray diffraction and Fourier-transform infrared spectroscopy with attenuated total reflectance (FTIR–ATR). It was shown that oxidation process breaks graphite crystallites and separate particular sheets (the interplanar spacing increased from 3.37 to 8.50 Å for graphite and GO, respectively, and the average size of crystallites decreased from 60 nm to 30 nm for graphite and GO, respectively). But the obtained GO still remained well-defined layered structure even if more open with respect to graphite. Vibrations of reactive carbonyl together with hydroxyl groups and C–O in ester and C–OH bonds were detected in FTIR-ATR spectra of solid GO. The intensity of the band assigned to the stretching vibration of carboxyl groups on the edges of the layered GO planes or conjugated carbonyl groups was relatively small.

PCL/GO composites were prepared by solution mixing and subsequent compression molding. PCL dissolved in DMF (1.0 g/20 ml) at 90 °C was mixed with GO dispersed in DMF (0.1 g/100 ml) by ultrasound for 24 h at 50 °C. The solid product obtained by vaporization of DMF was dried in vacuum at 90 °C for 3 days and at 25 °C for 1 week as it is also described in [22]. Dissolving of PCL and the addition of GO (2.7 wt%) was performed at inert atmosphere (nitrogen, 99.995 %). The dried composite material was compression molded at 65 °C for 6 min under pressure 300 kN to form films of approximate thickness of 250 μm. PCL pellets were processed in the same way to keep preparation conditions of PCL/GO composite to prepare specimens for comparison. The production of well-dispersed graphene-based polymer nanocomposites depends on GO exfoliation prior to incorporation into a polymer matrix. Direct exfoliation of solid GO in DMF was enhanced with mechanical exfoliation by ultrasound and stirring and colloidal suspension of GO was obtained. But it has not the same character as that of graphene oxide obtained before freeze-drying of is.

Biodegradation

PCL and PCL/GO composite films were sectioned into 10×10 mm^2 specimens, which were sterilized by UV-lamp for 30 min. The sterilized specimens were immersed into 6 ml of nutrient medium with *BS* in L-test tubes to perform biodegradation test (one specimen into one L-test tube). The initial pH was 7, the temperature was kept at 30 °C, and the L-test tubes were continuously agitated at 160 rpm. The biodegradation experiment was performed for 21 days. The control specimens of PCL and PCL/GO were treated in abiotic medium at the same conditions and again one specimen was inserted into one L-test tube.

The antimicrobial effect of GO in PCL/GO composite was examined in Petri dishes with meat peptone agar medium in the presence of bacterium *BS* for 24 h as it is also described in [29]. The test was done as a preliminary screening before biodegradation study to exclude inhibition action of tested material on the growth of utilized microorganism.

The specimens' code system used in this work is explained in Table 1.

Table 1 The specimens' code system used in the work

Code	Material
PCL	Original poly(ε-caprolactone) thin film
PCL-*BS*, PCL+BS	PCL degraded by the action of *Bacillus subtilis*
PCL_7d	PCL degraded by the action of *Bacillus subtilis* for 7 days
PCL-c	Control sample of PCL aged in abiotic medium
PCL-c_7d	Control PCL aged in abiotic medium for 7 days
GO	Graphite oxide
PCL/GO	Original composite of PCL with GO—thin film
PCL/GO-*BS*, PCL/GO+BS	PCL/GO composite degraded by the action of *Bacillus subtilis*
PCL/GO_7d	PCL/GO composite degraded by the action of *Bacillus subtilis* for 7 days
PCL/GO-c	Control composite material aged in abiotic medium
PCL/GO-c_7d	Control composite material aged in abiotic medium for 7 days

Characterization

Optical density/turbidity and pH of nutrient medium was measured in situ during the biodegradation test. The densitometer used was McFarland DEN-1B, CZ. The lipase activity of the cell-free culture supernatant, prepared after the particular degradation test (7, 14 and 21 days) was determined. Lipolytic activity was determined using colorimetric assay system with *p*-nitrophenyl laurate (*p*NPL) as the substrate. The absorbance of *p*-nitrophenol formed after 30 min of reaction of lipases with *p*NPL at 37 °C and pH 7.2 was measured at 420 nm using UV/VIS HELIOS DELTA spectrophotometer Thermospectronic, United Kingdom. One unit of activity is the amount of enzyme, which released one μmol *p*-nitrophenol from *p*NPL per minute under the assay conditions. Lipolytic activity measurement was done six times and other experiments

were run in triplicate to determine mean values and standard deviations.

SEC–MALLS

Molecular weight averages (M_n, number-average molecular weight and M_w, weight-average molecular weight) were determined by size exclusion chromatography (SEC–MALLS) on Waters Breeze chromatographic system equipped with RI detector operating at 880 nm and multi-angle laser light scattering miniDawn TREOS from Waytt with laser wavelength 658 nm, using dn/dc = 0.079 ml/g according to [30]. The system consists of Waters 2,410 refractive index detector, Waters 1,515 pump, Waters 717 plus Autosampler, and column heater. Separation was performed on one Polymer Laboratories Mixed column at 35 °C in THF at an elution rate of 0.8 ml/min. Polymer/composite sample (15–20 mg) was dissolved in 5 ml of THF. Before analysis, the prepared solution was filtered through 0.45 μm PTFE microfilters. Different conditions of SEC analysis and solid state of the specimens tested is the reason for the difference in the initial molecular weight of PCL film and that of PCL pellets.

Weight loss

Both control and degraded specimens were after 7, 14, and 21 days of the exposition to *BS* and abiotic medium removed from the medium, washed with distilled water and dried to constant weight. The specimens were stored in a desiccator before morphology and structure characterization.

DSC

Calorimetric (DSC) measurements were performed on DSC 204 F1, Netzsch using specimens of the weight 2.2–4.7 mg sealed in standard aluminum pans. The specimens were heated at 10 °C/min in nitrogen (40 ml/min) from laboratory temperature to 90 °C. Three measurements were done for neat PCL and PCL/GO specimens and two ones for control specimens after 21 days.

TGA

Thermogravimetric (TGA) measurements were done on TGA Q500, TA Instruments in nitrogen (60 ml/min). The specimens weighting 1.1–3.5 mg were heated at 5 °C/min from laboratory temperature to 650 °C.

FTIR–ATR

The surface functional groups of solid specimens were identified using spectrophotometer Tensor 27, Bruker with ATR using diamond crystal. The spectra were recorded at room temperature in the spectral range 4,000–600 cm^{-1} at the resolution 2 cm^{-1}. One spectrum was the result of 128 scans. The spectra were recorded from three surface points of each specimen. The FTIR-ATR spectra were studied in the range 1,800–1,600 cm^{-1} upon normalization on the signal corresponding to the [–(CH_2)n–] stretching group at 1,466 and 1,398 cm^{-1} (carbonyl index determination) in order to evaluate changes on the peak corresponding to ester groups of polymer chains (1,723 cm^{-1}) as it is described also in [6].

CLSM

The surface morphology of PCL and PCL/GO specimens was studied on confocal laser scanning microscope (CLSM) LEXT OLS 3000, Olympus at laboratory temperature using the laser beam of 408 nm. Both surfaces of each specimen were observed.

Results and discussion

Microbial activity on PCL, PCL/GO and GO materials

The screening of potential antimicrobial effect of GO in melt-pressed PCL/GO composite against selected bacterium *BS* revealed no zone of inhibition on the composite specimen surfaces as well as on the control ones under tested conditions. The similar effect was observed by Ruiz et al. [31] but was not reported in other papers dealing with similar material systems [24, 25, 29].

The systematic study of microbial degradation was performed at the optimum growth conditions of *BS* from the viewpoint of aeration (agitation), nutritional factors, pH, and temperature. The measurement of the optical density showed that exponential growth of *BS* proceeding occurred during the first day of the experiment at the same rate in all types of media (nutrient medium, medium and PCL, medium and PCL/GO) as it is seen in Fig. 1. Afterwards, the growth curve became horizontal as a consequence of the stationary phase. The time profile of *BS* growth in nutrient medium reflects prolonged stationary phase and slight decline occurring in the population during lag phase. *BS* started to grow again after 5 days of the experiment in the presence of PCL and PCL/GO, which indicates the effect of *diauxie*. At first, *BS* utilized glucose as a simple carbon source together with peptone and then started to utilize more complicated substrate, probably scission products released from the polymer as a result of its degradation.

Lipolytic activity of *BS* was monitored supposing that lipases play dominant role in enzyme-catalyzed PCL chain

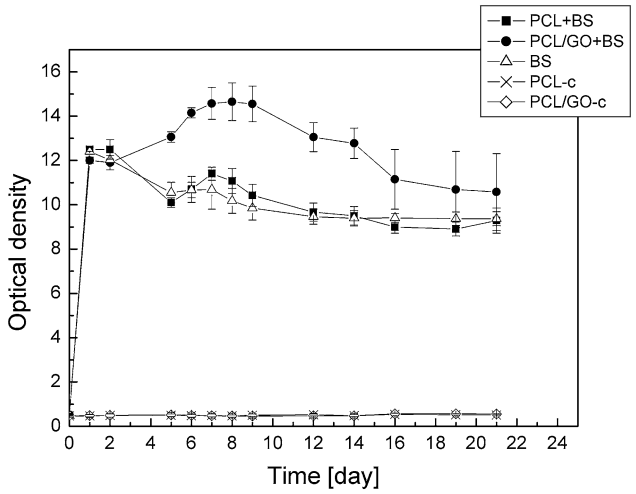

Fig. 1 Time profile of *BS* bacterial growth (expressed as optical density in McFarland units) in cultivation media and the optical density of control abiotic nutrient medium

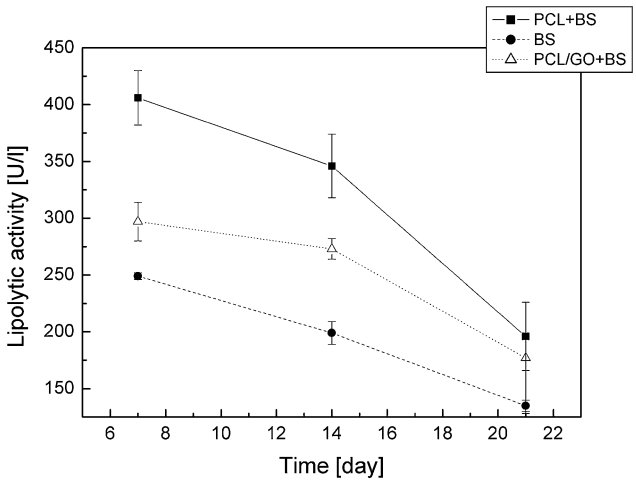

Fig. 2 Lipolytic activity of *BS* in nutrient cultivation medium and that enriched with PCL and PCL/GO specimens measured after 7, 14, and 21 days of the experiment

scission. The highest values of lipolytic activity of *BS* were measured in the presence of PCL in nutrient medium. This fact demonstrates stimulating effect of oligomeric chains gradually released into the medium during the degradation process on the the lipases production (Fig. 2). The presence of GO in PCL supported good cell growth but extracellular lipase production was lower than only in nutrient medium (Fig. 2). This phenomenon will be further studied.

Almost identical pH profiles of *BS*-inoculated media were observed, which can reflect utilization of similar substrates and hence, only little metabolic changes in the presence of polymer or GO. The pH of medium increased from 7.0 to 8.5–9.0 both in the presence of PCL and PCL/GO after 14 days of the experiment and the value was always slightly higher as compared to medium inoculated with *BS* (8.5). This fact could consequently contribute to faster degradation of PCL chains, previously partially degraded by the action of enzymes, in alkaline environment [17]. The value of pH of control abiotic nutrient medium with PCL-based specimens was constant *i.e.* 7 during the experiment.

Molecular weight and weight loss of PCL and PCL/GO materials

Both PCL and PCL/GO specimens exposed to *BS* gradually lost the weight contrary to control specimens as can be seen in Table 2. There was no difference between PCL and PCL/GO specimens after 7 days but then the matrix itself became more prone to degradation and lost nearly three times higher mass after 21 days compared to nanocomposite. The shift of the chromatograms peeks maxima observed both for PCL and PCL/GO specimens supports random cleavage of the longest chains as a consequence of *BS* action after 14 days (Fig. 3a). Small tails developed on the lower molecular side of elution curves become visible already after 14 days and were pronounced after 21 days of degradation experiment (Fig. 3b). The tails indicated the formation of lower molecular chains entrapped in the polymer matrix. Since pH values of *BS*-innoculated medium increased to alkaline region after 14 days of the experiment due to metabolites production, the contribution of base-catalyzed abiotic hydrolysis is assumed after 21 days as well. The number-average molecular weight (M_n) decreased by 33 % in case of PCL and by 28 % in case of PCL/GO nanocomposite degraded for 21 days so we can assume that degradation of ester bonds close to the polymer chain ends also occurred (Fig. 3b). Abiotic hydrolysis to PCL chains of control specimens immersed in abiotic medium at constant pH of 7.0 did not proceed significantly since negligible changes in molecular weight and its distribution were measured (Table 2).

Thermal properties of PCL and PCL/GO materials

Slight increase of crystallinity of *BS*-degraded PCL after 14 and 21 days (Table 2) corresponds with the weight loss and molecular weight increase as a consequence of the release of low molecular species formed by PCL chain scission. Secondary crystallization of loosen and cleaved PCL chains is supposed to occur onto the preexisting crystals after 21 days due to the appearance of the right shoulder on the melting peak as it is seen in Fig. 4a. Random scission of small amount of the longest PCL chains evidenced by SEC–MALLS is responsible for the stable melting temperature of PCL. The crystallinity of control PCL remained the same and no change in supramolecular structure is evident from DSC curve shapes shown in Fig. 4a.

Table 2 Molecular characteristic, weight loss and DSC data of the original, control and *BS*-degraded PCL and PCL/GO materials

Material	Aging [day]	Weight loss [%]	M_n	Đ	Melting temperature		Crystallinity [%]
					T_{m1} [°C]	T_{m2} [°C]	
PCL	0	–	18	1.5	58.8 ± 0.3	60.0 ± 0.3	70 ± 3
PCL-*BS*	7	2.9 ± 0.1	16	1.5	58.7 ± 0.3	59.4 ± 0.3	69 ± 3
PCL-*BS*	14	8.6 ± 0.9	15	1.6	58.7 ± 0.3		76 ± 2
PCL-*BS*	21	12.0 ± 0.9	12	1.8	59.4 ± 0.3	Right shoulder	75 ± 3
PCL-c	7	0.5 ± 0.01	16	1.6	59.8 ± 0.3		71 ± 3
PCL-c	14	0.4 ± 0.6	16	1.5	59.8 ± 0.3		68 ± 3
PCL-c*	21	0.0 ± 0.0	17	1.4	58.3 ± 0.3		69 ± 2
PCL/GO	0	–			61.0 ± 1.7		65 ± 3
PCL/GO-*BS*	7	2.7 ± 0.9	15	1.5	60.2 ± 1.2		72 ± 2
PCL/GO-*BS*	14	5.1 ± 0.5	15	1.5	58.6 ± 1.4		76 ± 3
PCL/GO-*BS*	21	4.7 ± 0.4	13	1.7	58.9 ± 0.9		75 ± 2
PCL/GO-c	7	0.2 ± 0.2	17	1.4	58.9 ± 1.1		75 ± 2
PCL/GO-c	14	0.8 ± 0.6	17	1.5	59.3 ± 0.8		72 ± 2
PCL/GO-c*	21	0.4 ± 0.0	17	1.4	60.7 ± 0.9		72 ± 3

M_n is number average molecular weight; $Đ$ is molecular weight dispersity; T_{m1} and T_{m2} represents melting temperature evaluated as the maximum of endothermic peaks of specimens heated once and twice, respectively; the degree of crystallinity was determined with $\Delta H_m^0 = 139.5$ J/g [3, 14] for 100 % PCL; *c* in the material title means control

[a] the control PCL and PCL/GO samples were maintained at constant pH of 7.0

GO particles act as nucleating agent because PCL crystallization temperature increased from (24.9 ± 0.3) °C to (28.8 ± 0.1) °C for the original PCL and PCL/GO, respectively, and thus, they are responsible for lower degree of crystallinity and higher melting temperature with respect to the original PCL. Nanocomposites degraded by *BS (BS*-degraded*)* revealed higher crystallinity with respect to the original one, however, nanocomposite control specimens revealed the increase of crystallinity as well. This is prescribed to the action of cultivation medium penetrating into nanocomposite specimens easily at PCL/GO interface due to the polar surface of GO. The medium is supposed to be preferentially absorbed into the amorphous phase improving motion of loosely packed polymer chains and their ordering because biodegradation test was performed highly above PCL glass transition region. But, if one takes into account the scatter of crystallinity results, the PCL crystallinity degree was always higher in PCL/GO composites exposed to biotic medium with respect to control ones exposed to abiotic medium, which corresponds with the fact that PCL chains scission occurred too as detected by SEC–MALLS. The degree of the chain scission is lower compared to PCL specimens exposed to biotic medium due to GO supporting microbial growth (Fig. 1) and lowering lipolytic activity in comparison with original PCL (Fig. 2). The decrease in the activity of lipases-extracellular hydrolases being known to catalyze PCL chains scission could have the impact on degradation kinetics. Secondary crystallization together with PCL bond scission in PCL/GO composites is reflected by the variance of their DSC curve shapes in time (Fig. 4b).

Although the melt of PCL decomposes in thermogravimeter during heating and thus, it is without direct connection to supramolecular structure of solid materials, *BS*-action and the presence of GO changed decomposition process of PCL as it is shown in Fig. 5 on the example of the original and *BS*-degraded PCL and PCL/GO materials after 21 days. Decomposition process of PCL shifted to lower temperature after 21 days in biotic medium and GO contributed to less gradual weight loss up to 360 °C compared to the original PCL. The first decomposition step of PCL/GO forgoing the main decomposition step disappeared after 21 days in biotic medium and the main decomposition step shifted to lower temperature. The main difference is obvious between *BS*-degraded PCL and *BS*-degraded PCL/GO where the first decomposition onset temperature shifted from 284 to 349 °C, respectively. The reason is very probably specific interaction of PCL chains with GO in all nanocomposites together with different rate of washing out/erosion of low molecular chains and random scission of the longest PCL chains can be prescribed to lower temperature of the main decomposition step of PCL.

FTIR–ATR analysis of PCL and PCL/GO materials

The FTIR–ATR spectra of all tested specimens, control and *BS*-degraded, PCL and PCL/GO, were nearly the same and also the intensity of the band at 1,722 cm^{-1} belonging to

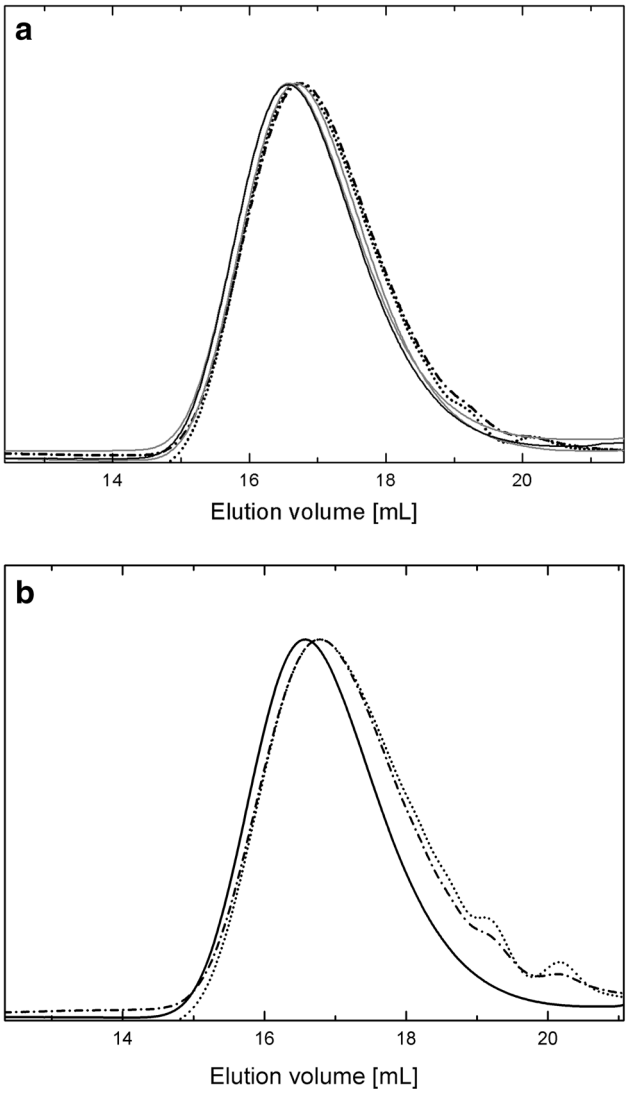

Fig. 3 **a** SEC chromatograms of the original PCL (*solid line*), PCL-*BS* and PCL/GO-*BS* (*dot* and *dash-dot*, respectively), control PCL and control PCL/GO (*grey*, *solid line*) after 14 days. **b** SEC chromatograms of the original PCL (*solid line*), PCL-*BS* and PCL/GO-*BS* after 21 days (*dot* and *dash-dot*, respectively)

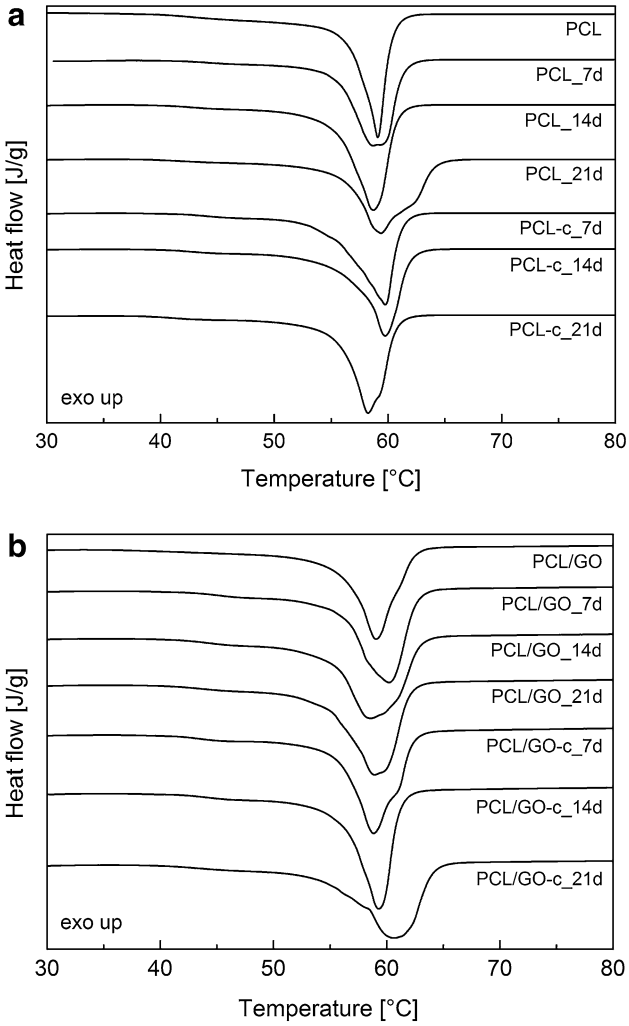

Fig. 4 **a** First heating *DSC curves* (endothermic response, exo up) of the original, *BS*-degraded and control PCL aged for 7, 14, and 21 days. **b** First heating *DSC curves* (endothermic response, exo up) of the original, *BS*-degraded and control PCL/GO aged for 7, 14, and 21 days

carbonyl group in ester bonds did not change. The PCL bonds of all specimens exposed to *BS* are supposed to be cleaved by enzyme-catalyzed hydrolysis which results in the presence of intensive carbonyl peak in time. The change of the FTIR carbonyl peak intensity is observed if microorganisms, enzymes, and by-products of the degradation survive water washing prior to characterization [20] or the molecules with other than carbonyl groups are formed [6]. These changes are usually described by the change of carbonyl index. In this work, carbonyl index of *BS*-degraded PCL and *BS*-degraded PCL/GO materials was nearly without change.

The fact that PCL was of high crystallinity degree also in GO nanocomposites was verified by the presence of the intensive band at 1,722 cm^{-1}, by the band of medium intensity at 1,297 cm^{-1}, and the broad band at around 1,172 cm^{-1} splitting into the other one at 1,186 cm^{-1}, which all are associated with ordered conformations of PCL chains [6, 32, 33]. The presence of PCL amorphous phase is indicated by broadening the band at 1,722 to 1,737 cm^{-1} and the broad band at 1,172 cm^{-1}, which also hides the band of amorphous PCL phase occurring at 1,161 cm^{-1}.

The second-order derivatives of carbonyl peaks [34] show that the amount of crystalline phase on *BS*-degraded surfaces decreased with the degradation time and this decrease is higher for PCL. No change is seen for control materials (Fig. 6). It corresponds with the surface degradation and erosion of *BS*-degraded specimens, especially PCL ones. The second-order derivatives of carbonyl peaks

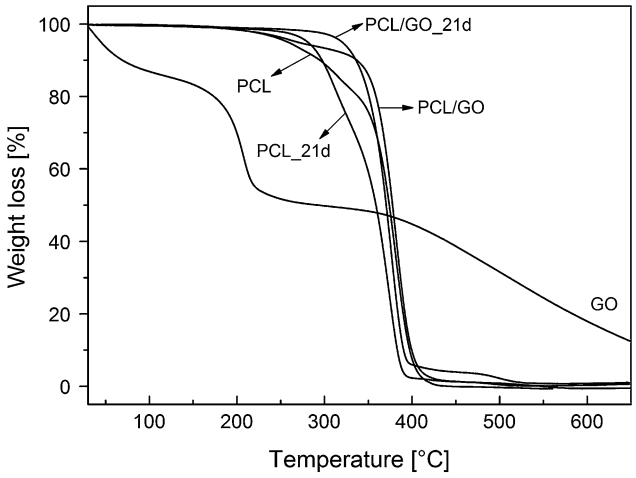

Fig. 5 *TGA curves* of the original and *BS*-degraded PCL and PCL/GO materials after 21 days together with *TGA curve* of GO

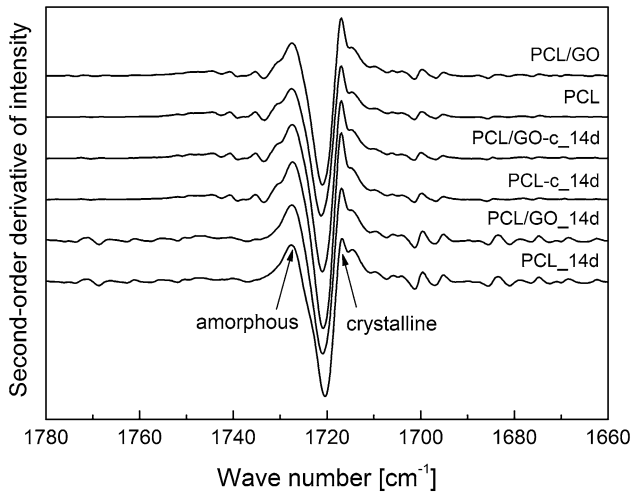

Fig. 6 Second-order derivatives of carbonyl peak of the original, control, and *BS*-degraded PCL and PCL/GO after 14 days

of *BS*-degraded PCL and *BS*-degraded PCL/GO materials for 14 and 21 days did not differ much which reflects the same mechanism of degradation together with washing of low molecular species out of the surface.

CLSM imaging of PCL and PCL/GO materials

Even if pressed, morphology of small spherulites was nicely visible on the original PCL specimen surfaces. The surface cracks regularly spread on PCL surfaces were the result of seven-day *BS*-degradation (Fig. 7a). The cracks observed after 14 days were not so sharp and were in less numbering but the surface itself became rougher as a consequence of surface erosion (8.6 % weight loss). The process of the surface degradation continued during other week (12.0 % weight loss) by erosion together with new crack formation (Fig. 7b). The erosion process is assumed to occur in the vicinity of the chain-ends due to SEC-MALL. The surface cracks were not formed in any stage of aging of PCL control specimens in biotic medium. Several spherulites on the surface of PCL control specimens aged for 21 days seemed to be uncovered due to reorganization of loosely packed chains in the surface amorphous region.

The addition of GO caused on composite surfaces formation of less developed spherulites looking twice larger with respect to neat matrix. The surface cracks were produced on PCL/GO specimen as a consequence of *BS* action whereas the size and depth of them increased gradually with time of degradation (Figs. 7c, d) but no cracks were formed on PCL/GO control specimens.

Surface erosion and formation of cracks, voids, and cavities are signs of the action induced by enzymes followed by medium penetration into the surface micropores. It is evident that the formation of surface cracks was in both types of specimens (PCL and PCL/GO) initiated only by *BS* action because no cracks were formed on surfaces of control specimens. Cultivation medium diffusion into the nanocomposite specimens is mainly responsible for the formation of large cracks compared to PCL. It is also very probable that final drying contributed to the enlargement of the cracks as well. The development of tensile residual stresses that reduce toughness and induce premature failure of the polymer exposed to microbial action was reported in [15]. The action of enzymes was not in case of PCL/GO specimens as significant as in case of PCL ones because the surface erosion was not so extensive and also the weight loss was nearly three times lower.

Conclusion

The biodegradation of PCL and its nanocomposite with GO by *BS* was demonstrated by the weight loss and the decrease of molecular weight even after 14 days of the experiment. PCL degradation was initiated by *BS* because control materials were not degraded however at constant pH of 7.0. During the last period of the experiment, the base-catalyzed abiotic hydrolysis could contribute to the whole degradation process because pH of medium increased up to 8.5–9.0. Since the control samples were maintained at constant pH of 7.0 the biotic and abiotic degradation could not be distinguished. Higher amount of low molecular chains were formed in PCL than in PCL/GO as the consequence of scission of ester bonds close to the PCL chain-ends in preference and random cleavage of the longest chains occurred both in neat matrix and nanocomposites. The latter is responsible for unchanged melting temperature of PCL in both *BS*-degraded material types.

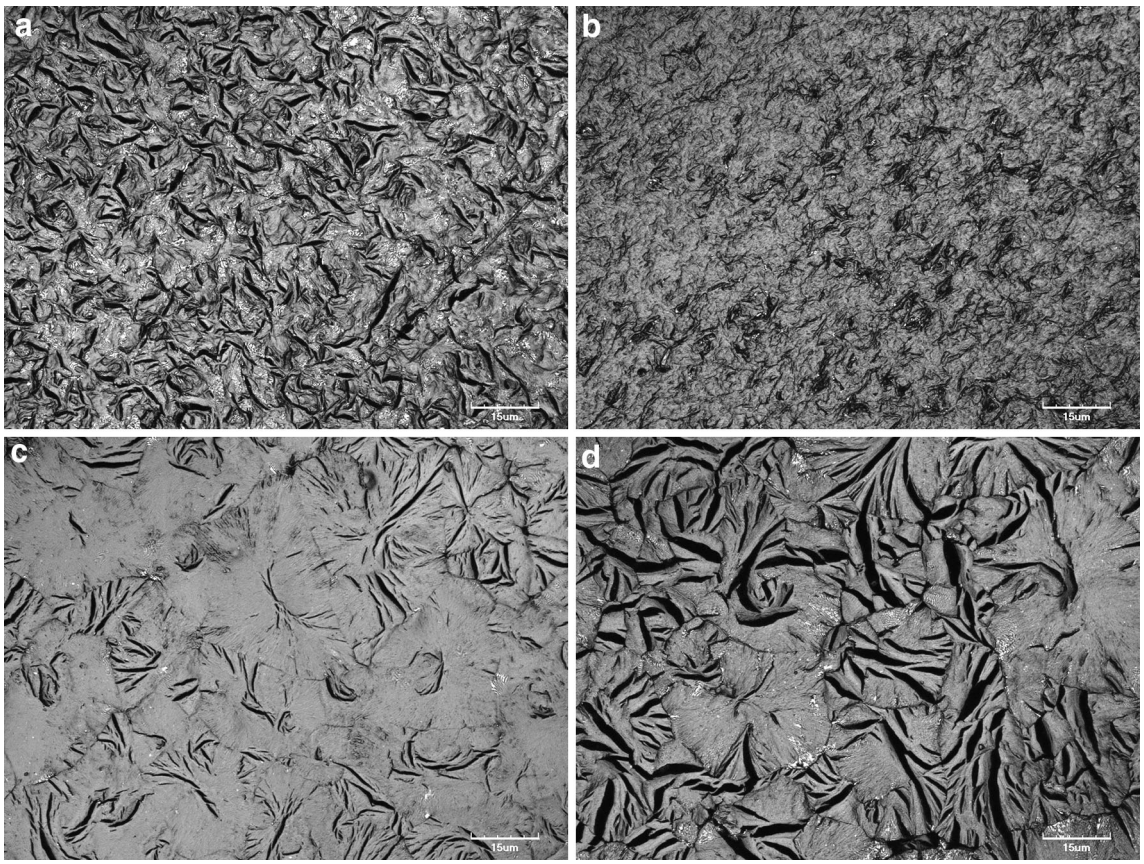

Fig. 7 **a** CLSM image of cracks on PCL-*BS* surface after 7 days. **b** CLSM image of PCL-*BS* surface after 21 days. **c** CLSM image of cracks on PCL/GO-*BS* surface after 7 days. **d** CLSM image of cracks on PCL/GO-*BS* surface after 21 days

BS-degradation is assumed to occur in amorphous phase because the degree of crystallinity increased both in PCL and PCL/GO accompanied by the washing out of low molecular chains as seen from the weight loss. *BS*-degradation became evident by surface erosion and surface cracks formation (no cracks were observed on any control specimen). Extensive surface erosion was observed on PCL specimens even after 14 days while large cracks were formed on nanocomposite surfaces. Easy diffusion of cultivation media through PCL/GO interface was caused by polar GO surface supported formation of large cracks together with the second crystallization of PCL also in nanocomposite control specimens, which revealed only negligible weight loss. GO acts as nucleating agent and caused the increase of decomposition onset temperature of PCL together with washed out/eroded low molecular species. GO was not evaluated to be promoter of biodegradation.

Acknowledgments R.B., L.R., J.J. were supported by the project "CEITEC—Central European Institute of Technology" (CZ.1.05/1.1.00/02.0068) from European Regional Development Fund, by the project MATERIS—CZ.1.07/2.3.00/20.0029 from European Social Fund. J.O, S.V., P.D. were supported by specific research (FCH-S-13-1912) from the Ministry of Education, Youth and Sports of Czech Republic. S.H. would like to thank Dr. Jan Merna from Institute of Chemical Technology, Prague, Faculty of Chemical Technology, CZ for SEC analysis. Authors thank Dr. Jiří Másilko from Materials Research Centre, Faculty of Chemistry, Brno University of Technology, CZ for X-ray diffraction analysis and Karbotechnik, Ltd, the CZ for graphite.

References

1. Yoshioka T, Kamada F, Kawazoe N, Tateishi T, Chen G (2010) Structural changes and biodegradation of PLLA, PCL, and PLGA sponges during in vitro incubation. Polym Eng Sci 50(10):1895–1903
2. Hakkarainen M, Albertsson AC (2002) Heterogeneous biodegradation of polycaprolactone—Low molecular weight products and surface changes. Macromol Chem Phys 203(10/11):1357–1363
3. Hakkarainen M (2002) Aliphatic polyesters: abiotic and biotic degradation and degradation products. Adv Polym Sci 157:113–138
4. Iwata T, Doi Y (2002) Morphology and enzymatic degradation of poly(epsilon -caprolactone) single crystals: does a polymer single crystal consist of micro-crystals? Polym Int 51:852–858
5. Lefevre C, Tidjani A, Wauven CV, David C (2002) The interaction mechanism between microorganisms and substrate in the biodegradation of polycaprolactone. J Appl Polym Sci 83:1334–1340
6. Khatiwala VK, Shekhar N, Aggarwal S, Mandal UK (2008) Biodegradation of poly(epsilon-caprolactone) (PCL) film by alcaligenes faecalis. J Polym Environ 16(1):61–67

7. Jenkins MJ, Harrison KL (2008) The effect of crystalline morphology on the degradation of polycaprolactone in a solution of phosphate buffer and lipase. Polym Adv Technol 19:1901–1906
8. Gu JD (2003) Microbiological deterioration and degradation of synthetic polymeric materials: recent research advances. Int Biodeterioration Biodeg 52:69–91
9. Hermanova S, Balkova R, Voberkova S, Chamradova I, Omelkova J, Richtera L, Mravcova L, Jancar J (2013) Biodegradation study on poly(epsilon-caprolactone) with bimodal molecular weight distribution. J Appl Polym Sci 127(6):4726–4735
10. Hermanova S, Omelkova J, Voberkova S, Balkova R, Richtera L, Mravcova L, Jancar J (2012) The Effect of processing of polycaprolactone films on degradation process initiated by aspergillus Oryzae lipase. Int J Polym Anal Charact 17(6):465–475
11. Sekonsan G, Vasanthan N (2010) Morphological changes of annealed poly-epsilon-caprolactone by enzymatic degradation with lipase. J Polym Sci, Part B: Polym Phys 48:202–211
12. Gan ZH, Liang QZ, Zhang J, Jing XB (1997) Enzymatic degradation of poly(epsilon-caprolactone) film in phosphate buffer solution containing lipases. Polym Degrad Stab 56:209–213
13. Rutkowska M, Krasowska K, Heimowska A, Steinka IL, Janik H, Haponiuk J, Karlsson S (2002) Biodegradation of modified poly(ε-caprolactone) in different environments. Pol J Environ Stud 11(4):413–420
14. Michell RM, Müller AJ, Castelletto V, Hamley I, Deshayes G, Dubois P (2009) Effect of sequence distribution on the morphology, crystallization, melting, and biodegradation of poly(epsilon-caprolactone-co-epsilon-caprolactam) copolymers. Macromolecules 42:6671–6681
15. Martins-Franchetti SM, Egerton TA, White JR (2010) Morphological changes of poly(carpolactone)/poly(vinyl chloride) blends caused by biodegradation. J Polym Environ 18:79–83
16. Mochizukiw M, Hirami M (1997) Structural effects on the biodegradation of aliphatic polyesters. Polym Adv Technol 8:203–209
17. Göpferich A (1996) Mechanisms of polymer degradation and erosion. Biomaterials 17:103–114
18. Sabet SS, Katbab AA (2009) Interfacially compatibilized poly(lactic acid) and poly(lactic acid)/polycaprolactone/organoclay nanocomposites with improved biodegradability and barrier properties: effects of the compatibilizer structural parameters and feeding route. J Appl Polym Sci 111:1954–1963
19. Neppalli R, Causin V, Marega C, Saini R, Mba M, Marigo A (2011) Structure, morphology, and biodegradability of poly(ε-caprolactone)-based nanocomposites. Polym Eng Sci 51(8):1389–1496
20. Fukushima K, Abbate C, Tabuani D, Gennari M, Rizzarelli P, Camino G (2010) Biodegradation trend of poly(ε-caprolactone) and nanocomposites. Mater Sci Eng, C C30:566–574
21. Singh V, Joung D, Zhai L, Das S, Khondaker SI, Seal S (2011) Graphene based materials: past, present and future. Progress Mat Sci 56:1178–1271
22. Kai WH, Hirota Y, Hua L, Inoue Y (2008) Thermal and mechanical properties of a poly(epsilon-caprolactone)/graphite oxide composite. J Appl Polym Sci 107:1395–1400
23. Wu YH, Yu T, Shen ZX (2010) Two-dimensional carbon nanostructures: fundamental properties, synthesis, characterization, and potential applications. J Appl Phys 108:071301
24. Carpio IEM, Santos CM, Wei X, Rodriguez DF (2012) Toxicity of a polymer-graphene oxide composite against bacterial planktonic cells, biofilms, and mammalian cells. Nanoscale 4:4746–4756
25. Liu SB, Zeng TH, Hofmann M, Burcombe E, Wei J, Jiang RR, Kong J, Chen Y (2011) Antibacterial activity of graphite, graphite oxide, graphene oxide, and reduced graphene oxide: membrane and oxidative stress. ACS Nano 5(9):6971–6980
26. Kearns DB, Chu F, Branda SS, Kolter R, Losick R (2005) A master regulator for biofilm formation by Bacillus subtilis. Mol Microbiol 55(3):739–749
27. Marvasi M, Visscher PT, Martinez LC (2010) Exopolymeric substances (EPS) from Bacillus subtilis:polymers and genes encoding their synthesis. FEMS Microbiol Lett 313(1):1–9
28. Lim HN, Huang NM, Loo CH (2012) Facile preparation of graphene-based chitosan films: enhanced thermal, mechanical and antibacterial properties. J Non-Cryst Solids 358:525–530
29. Tai ZX, Ma HB, Liu B, Yan XB, Xue QJ (2012) Facile synthesis of Ag/GNS-g-PAA nanohybrids for antimicrobial applications. Colloids Surf B 89:147–151
30. Wu C, Woo KF, Luo XL, Ma DZ (1994) A modified light-scattering method for the characterization of the segmented copolymer poly(ethylene terephthalate-co-caprolactone). Macromolecules 27:6055
31. Ruiz ON, Fernando KAS, Wang BJ, Brown NA, Luo PG, McNamara ND, Vangsness M, Sun YP, Bunker CE (2011) Graphene oxide: a nonspecific enhancer of cellular growth. ACS Nano 5:8100–8107
32. Coleman MM, Zarian J (1979) Fourier-transform infrared studies of the polymer blends. II. poly(epsilon-caprolactone)-Poly(vinyl Chloride) systems. J Polymer Sci Polymer Phys Ed 17:837–850
33. Rohindra D, Sharma P, Khurma J (2005) Soil and microbial degradation study of poly(epsilon-caprolactone)-poly(vinyl butyral) blends. Macromol Symp 224:323–331
34. Gupta KK, Kundan A, Mishra PK, Srivastava P, Mohanty S, Singh N, Mishra A, Maiti P (2012) Polycaprolactone composites with TiO_2 for potential nanobiomaterials: tunable properties using different phases. Phys Chem Chem Phys 14(37):12844–12853

Nanoscale

PAPER

View Article Online
View Journal | View Issue

Cite this: *Nanoscale*, 2019, **11**, 12124

Proteinase-sculptured 3D-printed graphene/polylactic acid electrodes as potential biosensing platforms: towards enzymatic modeling of 3D-printed structures†

Carmen Lorena Manzanares-Palenzuela,[a] Sona Hermanova,[a,b] Zdenek Sofer[a] and Martin Pumera*[a,c,d]

3D printing technologies are currently appealing for the research community due to their demonstrated versatility for different scientific applications. One of the most commonly used materials for 3D printing is polylactic acid (PLA), a biodegradable polymer that can be fully or partially digested by enzymes such as proteinase K. This work seeks to exploit PLA's biodegradability to selectively and reproducibly sculpt 3D-printed graphene/PLA surfaces to turn them into sensitive electroactive platforms. Proteinase K-catalyzed digestion of 3D-printed graphene/PLA electrodes is proposed as an environmentally friendly, highly controllable, and reproducible activation procedure of 3D-printed electrodes. Proteinase K digests PLA in a controllable fashion, exposing electroactive graphene sheets embedded within the 3D-printed structures to the solution and therefore achieving a tailorable electrode performance. A proof-of-concept biosensing application is proposed, based on the immobilization of enzyme alkaline phosphatase at the sculptured electrodes with the subsequent electrochemical detection of 1-naphthol in aqueous media. This work attempts to continue demonstrating the potential of 3D printing in electroanalytical applications, as well as to explore the exciting possibilities arising from merging biotechnological processes with these manufacturing procedures.

Received 30th March 2019,
Accepted 3rd June 2019

DOI: 10.1039/c9nr02754h

rsc.li/nanoscale

Introduction

The number of 3D printing applications in scientific research has been rapidly increasing in the last few years.[1,2] 3D printing technologies have found their way into research laboratories as affordable and fast tools to create scale models or prototypes and objects for routinely laboratory use.[2,3] The rising variety of printable materials, together with the possibility of shape customization without design constraints, has gained the interest of a wide research community, especially in biomedical sciences.[2,4] However, micro and nanoscale sculpting of the surfaces of large objects remains a challenge.

With the advent of conductive printable materials, 3D printing has entered the field of electrochemistry at a fast pace with the fabrication of 3D-printed electrodes for energy storage[5] and sensors.[2,6] Of particular significance for the field is the manufacture of low cost metal-free objects, utilizing desktop 3D printers based on Fused Deposition Modelling (FDM).[7–10] The availability of conductive filaments made from carbon/polymer composites for FDM, such as the commercial graphene/polylactic acid (PLA) filament, has recently been exploited in different electrochemical systems.[8,11–17] Our group recently reported 3D-printed electrodes made from this composite to detect picric acid and ascorbic acid.[8] There is a significant drawback of the "as printed" 3D graphene/PLA electrodes as they show no electroactivity and they need to be activated by the organic solvent method or electrochemical pretreatment.[8,12,13] This problem arises from the high bulk content of the thermoplastic polymer concealing the electrodes after 3D printing, hindering the conductive and electroactive carbon-based part from exposition to the electrolyte.

The common objective of the activation methods proposed so far is to uncover the graphene embedded within 3D-printed objects without disrupting their structural and mechanical properties. We herein propose a distinct approach based on an

[a]*Center for Advanced Functional Nanorobots, Department of Inorganic Chemistry, University of Chemistry and Technology Prague, Technická 5, 166 28, Czech Republic. E-mail: pumera.research@gmail.com*
[b]*Department of Polymers, Faculty of Chemical Technology, University of Chemistry and Technology Prague, Technická 5, 16628, Czech Republic*
[c]*Department of Chemical and Biomolecular Engineering, Yonsei University, 50 Yonsei-ro, Seodaemun-gu, Seoul 03722, Korea*
[d]*Future Energy and Innovation Laboratory, Central European Institute of Technology, Brno University of Technology, Purkyňova 656/123, Brno, CZ-616 00, Czech Republic*
† Electronic supplementary information (ESI) available: SEM images, XPS spectra and a table on method comparison. See DOI: 10.1039/c9nr02754h

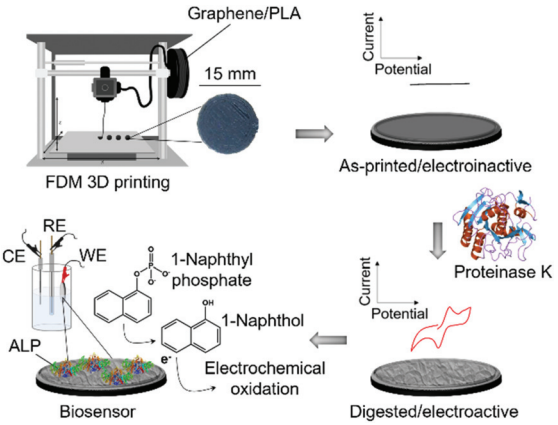

Scheme 1 Representation of the 3D-printed graphene/PLA electrodes' fabrication, digestion/activation and application: first, coin-shaped electrodes from the graphene/PLA composite filament are 3D-printed with a Fused Deposition Modelling printer. The as-printed electrodes are electrochemically irresponsive towards the ferro/ferricyanide redox pair. After proteinase K-mediated PLA digestion, the electrodes' surface becomes eroded and electroactive. The resulting activated surface is used to immobilize alkaline phosphatase (ALP) enzyme *via* adsorption. ALP catalyzes the conversion of 1-naphthyl phosphate into 1-naphthol, which is electrochemically oxidized at the surface of 3D-printed electrodes.

environmentally friendly, highly controllable biocatalytic process consisting of partial digestion of 3D-printed electrodes by proteinase K-mediated PLA hydrolysis. PLA's widespread use in 3D printing technologies, particularly FDM, brings up the advantages of its biodegradability: PLA belongs to a family of polyesters called "biodegradable plastics".[18] It undergoes abiotic hydrolysis, which is significantly accelerated by extracellular enzymes produced by microorganisms naturally occurring in a soil environment. Among enzymes hydrolyzing protein-like substrates, serine proteases such as proteinase K play an important role.[19] Proteinase K-catalyzed degradation of PLA is a topic that dates back to 1981 and has been thoroughly reviewed in the literature.[20] We seek to apply this well-characterized, nature-inspired process to achieve controlled patterning of 3D-printed surfaces to be used as working electrodes. We explore the application of the digested surfaces not just as electrodes but also as biosensors, showing that these enzymatically sculptured 3D-printed objects can serve as immobilization platforms for biomolecules and electrochemical transducers (Scheme 1).

Experimental

Chemicals

Potassium ferrocyanide and ferricyanide, magnesium chloride hexahydrate and potassium chloride were purchased from Lach-Ner (Neratovice, Czech Republic). Proteinase K from *Tritirachium album* (≥30 units per mg protein), tris(hydroxymethyl)aminomethane hydrochloride (Tris-HCl), alkaline phosphatase, 1-naphthyl phosphate monosodium salt monohydrate, phosphate buffered saline tablets and calcium dichloride were acquired from Sigma-Aldrich. Milli-Q water was used in all experiments.

3D printing and proteinase K-mediated digestion/activation

The graphene/PLA filament was acquired from Black Magic 3D (New York, USA). The electrodes were designed with sketch-up 3D modeling open-source software and printed with Fused Deposition Modeling (FDM) technology, using a TRILAB 3D printer (DeltiX, Czech Republic). Each 3D-printed specimen (coin-shaped, for specific dimensions see disc-shaped electrodes in ref. 8) was immersed in a proteinase K 0.2 mg mL^{-1} solution prepared in Tris-HCl buffer (Tris 100 mM, $CaCl_2$ 1 mM, pH 8) and incubated at 37 °C for 28 or 72 h. The enzyme/buffer was replaced every 24 h to restore enzymatic activity, avoiding the pH value decrease. Afterwards, the degraded samples were rinsed thoroughly with distilled water at 4 °C to stop further degradation and then dried under vacuum until constant mass. Mass loss (%) was calculated according to $(m_0 - m_t)/m_0$, where m_0 and m_t represent the dry weights of the specimens before and after degradation, respectively. For the purpose of water uptake determination, wet specimens were periodically withdrawn, gently dried with filter paper and their mass was taken. Water uptake (%) was determined according to $(m_W - m_0)/m_0$, with m_W representing the wet weight of the specimens taken at specific times during degradation.

Characterization

The morphology and elemental mapping of the 3D-printed objects were examined by scanning electron microscopy (SEM) using a FEG electron source (Tescan Lyra dual beam microscope) coupled with an energy dispersive spectrometer (Oxford Instruments, UK). An optical microscope (Olympus IX73, equipped with 10×, 20× and 50× objective lens, and a high-speed camera (Retiga R1™ CCD) was also used to investigate the morphological characteristics of the electrodes before and after degradation. Carbon composition of the electrodes before and after digestion was assessed with X-ray photoelectron spectroscopy (XPS) by performing high-resolution scans of the C 1s region. The XPS system was based on an XR-50-MF X-ray source with a μ-Focus monochromator and Phoibos 150 2D CCD hemispherical detector (SPECS, Germany). An iS50R FTIR spectrometer (Thermo Scientific, USA) was used to carry out Fourier-transform infrared spectroscopy (FTIR) measurements. The measurement was performed using a diamond ATR crystal, DLaTGS detector and KBr beamsplitter in the 4000–400 cm^{-1} range at a resolution of 4 cm^{-1}.

Biosensor

The digested 3D-printed electrodes were immersed in 3 mL of solution containing ALP fragments (1.25 U mL^{-1}) prepared in PBS 1× (137 mM NaCl, 2.7 mM KCl and 10 mM phosphate buffer solution, pH 7.4) and were incubated for 30 min at room temperature. A control experiment was carried out by

incubating a digested 3D-printed electrode in PBS 1× without ALP for the same period of time. After rinsing the specimens with the same buffer, the electrodes were carefully dried under a nitrogen flow and placed in an electrochemical cell containing 1-naphthyl phosphate 12 mM prepared in Tris buffer (Tris-HCl 0.5 M, $MgCl_2$ 0.5 mM, KCl 0.1 M, pH 9.8).[21] After 3 min of enzymatic reaction, the measurement was carried out *via* cyclic voltammetry in the potential range 0 to 0.6 V at a scan rate of 100 mV s^{-1}. After extensive rinsing with water, subsequent measurements were carried out to assess whether ALP remained physiosorbed on the 3D-printed surfaces.

Electrochemical measurements

Cyclic voltammetry (CV) experiments were carried out at a scan rate of 100 mV s^{-1} at room temperature using a three-electrode configuration. The supporting electrolyte was KCl 0.1 M for the ferro/ferricyanide redox pair ($K_6Fe(CN)_6$: $K_4Fe(CN)_6$) 1 mM and Tris buffer (Tris HCl 0.5 M, $MgCl_2$ 0.5 mM, KCl 0.1 M, pH 9.8) for 1-naphthol detection. KCl 1 M Ag/AgCl was used as the reference electrode and a platinum wire was used as the counter electrode, both purchased from CH Instruments (Texas, USA). The measurements were performed with an Autolab PGSTAT 204 (Metrohm Autolab, Switzerland), controlled by Nova 2.1 software (Metrohm Autolab, Switzerland). The 3D-printed graphene electrodes were directly held by a crocodile clip and placed in a 5 mL electrochemical cell. A glassy carbon (GC) electrode (geometrical surface area: 0.0707 cm^2), purchased from CH Instruments, was employed for comparison. 1.98 cm^2 was the estimated geometrical surface area of the 3D-printed electrodes based on the region immersed in the electrolyte.

Results and discussion

Coin-shaped 3D-printed electrodes were printed from a graphene/PLA filament using an FDM printer. A biocatalytic method for activation consisting of proteinase K-mediated hydrolysis of PLA fragments was performed on these electrodes. Here, the terms "proteinase K-treatment", "degradation" and "digestion" are interchangeably used to refer to this activation process. The terms "as-printed" and "blanks" refer to the specimens or electrodes used after 3D printing without any treatment and to those samples exposed to an enzyme-free solution under exactly the same conditions as those with proteinase K activity, respectively. Enzymatic digestion of 3D printed electrodes was characterized in terms of morphological changes (by SEM and optical microscopy), bulk analysis during enzymatic hydrolysis (water uptake, mass loss), surface chemistry (FTIR and XPS) and electrochemical response towards an electroactive redox species.

Fig. 1 shows the morphological changes of 3D printed electrodes induced by the enzymatic digestion process. The representative SEM images reveal that the treatment with proteinase K results in an increased exposition of graphene-based structures at the surface (wire-like[8,13] and sheet morphologies can be seen in Fig. 1C and D, respectively), significantly differing from the morphological characteristics of the as-3D-printed electrodes (Fig. 1A) and the blank specimens (Fig. 1B). A close-up look on the wrinkled features of the exposed graphene sheets can be seen in Fig. S1.† The blanks represent an important control experiment that evaluates the contribution of abiotic hydrolysis occurring at pH 8 and 37 °C. A broader overview of the surfaces (optical microscopy) shows that the blank specimens display a plastic-like "sealed" appearance (Fig. 1E–G), whereas the digested electrodes present an eroded aspect with pores of substantial size (Fig. 1H–J), resembling the degradation pattern observed for proteinase K-degraded PLA films.[22] Fig. S2† shows low-magnification SEM images coupled with EDS mapping, displaying surface features and carbon/oxygen composition after 3, 6 and 28 h of proteinase K treatment. As the digestion reaction progresses, the PLA regions (shown as dark spots rich in oxygen) seem to decrease while the contrast of the overall micrograph increases. The clearer areas (less oxygen-rich) represent the conductive regions being further exposed with longer digestion times.

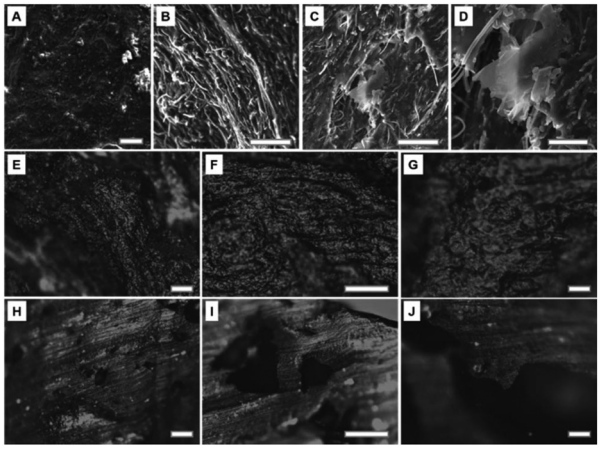

Fig. 1 Morphology of 3D-printed graphene/PLA electrodes before and after treatment with proteinase K: typical SEM images of (A) as-printed electrodes; (B) blank specimen*; (C and D) proteinase K-treated electrodes. Scale bars: 5 μm (grey-lined) and 2 μm (blue-lined). Optical microscopy images taken with 10×, 20× and 50× objective lens of (E–G) blank electrodes* and (H–J) proteinase-treated electrodes. Scale bars: 100 μm (grey-lined) and 20 μm (blue-lined). *Blanks refer to 3D-printed specimens subjected to the same digestion conditions but in the absence of proteinase K.

To gain further insight into the degradation process, water uptake/mass variation of the blanks and the proteinase K-treated electrodes was monitored throughout 28 h (Fig. 2A). It is desirable to be able to digest the 3D-printed electrodes in a well-controlled and timely manner, thus the process was monitored for 28 h. Longer digestion times were also tested: 72 h of degradation time resulted in disintegration of the 3D-printed specimens. After 28 h, the mechanical properties were maintained, while achieving significant PLA loss at the surface, as will be discussed later. The process begins with water gradually diffusing into the polymer matrix during the

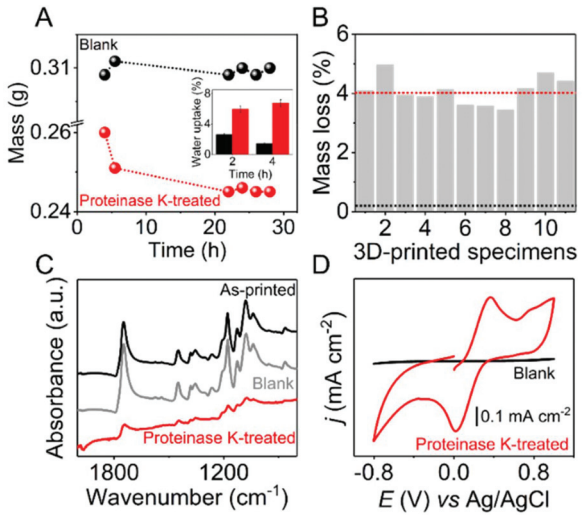

Fig. 2 Characterization of the proteinase-K digestion process and electrode activation: (A) mass variation during proteinase K treatment of 3D-printed electrodes (inset: initial water uptake of the blanks* and the proteinase K-treated specimens shown in black and red bars, respectively); (B) mass loss value distribution (reproducibility) of the enzymatic degraded samples (the dotted line represents average mass loss: red for proteinase K-treated and black for blanks*); (C) FTIR spectra of the as-printed, blank* and proteinase K-treated specimens; (D) electrochemical characterization of blank* and proteinase-K digested 3D-printed electrodes *via* cyclic voltammograms (CVs) of the ferro/ferricyanide pair ($[Fe(CN)_6]^{4-} \leftrightarrow [Fe(CN)_6]^{3-}$); scan rate: 100 mV s^{-1}, supporting electrolyte: KCl 0.1 M. *Blanks refer to 3D-printed specimens subjected to the same digestion conditions but in the absence of proteinase K.

initial phase of degradation. Formation of hydroxyl and carboxylic groups by starting chain scission contributed to an increase of water uptake (*i.e.* increased hydrophilicity), which at the same time favors the proceeding degradation process due to faster diffusion of the enzyme into the hydrophilic polymer network.[23,24] The next stage of the degradation is characterized by a significant mass loss due to proteinase K-catalyzed chain scission and diffusion of oligomeric fragments to the solution. Progressive surface erosion increased the porosity of the matrix.[23] The inset in Fig. 2A shows that the specimens start to take up water up to *ca.* 7% after 4 h. From this point on, a progressive mass decrease (from 4 h to 28 h) was recorded for the proteinase K-treated samples as proof of degradation, whereas the blanks presented negligible mass variation in both 0–4 h (water uptake) and 4–28 h (mass loss) time windows (Fig. 2A). The pH of the degradation media was also monitored up to 48 h (data not shown), given that PLA degradation products are acidic and thus pH slightly decreases during the digestion process. After 24 h and 48 h, the pH decreased by 0.1 and 0.3 units, respectively, whereas for the blank specimen the pH remained unaltered. pH decrease during degradation can reduce the enzymatic efficiency, thus the enzyme/buffer system should be exchanged every 24 h.

The average mass loss, determined in the dry state, was 4.1% (n = 11) (Fig. 2B), with a relative standard deviation (RSD) of 11.6%. Considering the specimen-to-specimen variations inherent to the FDM fabrication technology (the initial mass of the as-printed electrodes presented an RSD value of *ca.* 6%), the digestion process can be considered highly reproducible due to the fine control of degradation conditions. The blanks presented a mass loss average of 0.2%, confirming that abiotic hydrolytic cleavage is negligible as compared to highly efficient enzymatic degradation.

Fig. 2C shows the FTIR spectra of the as-printed, blank and proteinase K-treated 3D-printed specimens, in the region between 2000 and 800 cm^{-1} showing characteristic bands of the active ester and methyl groups of PLA. The weak absorption bands located at ~1540 cm^{-1} and ~1575 cm^{-1} can be assigned to the carboxylate –O–C=O– groups and skeletal vibrations of the graphene sheets, respectively.[25,26] Strong absorption at ~1746 and ~1080 cm^{-1}, ascribed to the symmetrical stretching of the C=O and –C–O– groups of the ester bonds of PLA, respectively, can be seen for the three samples. A shift to lower frequency (~5 cm^{-1}) was evidenced for the degraded specimen due to hydrolysis of the –C–O– ester bond, whereas the carbonyl group C=O band attributed to the ester bond did not shift.[27] Further changes in the structure of PLA due to the chain-scission of polyester bonds in the hydrolysis reaction were noted in the ~1449 cm^{-1} (C–H bending vibration of CH_3), ~1264 cm^{-1}, ~1178 cm^{-1} and ~1080 cm^{-1} (C–O stretching vibrations), ~954 cm^{-1} and ~914 cm^{-1} (crystallinity-related ring skeletal vibrations) absorptions.[27–32] The amide I band near 1650 cm^{-1}, characteristic of proteins, is not observed in the spectrum collected for the proteinase K-treated specimen,[33] suggesting that most of the enzyme is successfully washed off the surface of the 3D-printed samples after treatment. However, small traces of protein can be present (see electrochemical results later).

Further characterization was performed with XPS to examine the carbon functional groups before and after proteinase-K treatment. Fig. S3† shows the C 1s regions of the as-printed (S3-A) and proteinase-K-treated electrodes (S4-B) taken at four different sites of the surface. The as-printed electrodes show the contributions of C=O moieties (~289.2 eV) from the PLA structure, as well as C–O (~287 eV) and C–C (~284–285 eV) bonds accounting for the presence of graphitic carbon as well. The presence of carbides is also evidenced at lower binding energies,[13] which can be associated with the presence of impurities.[8,16] After enzymatic digestion, the XPS showed a significantly decreased intensity of the C–O and C=O peaks, indicating that most of the PLA has been cleaved off the surface. The four different C 1s spectra of the treated electrodes systematically point to the C–C graphitic nature of the surface with stronger sp^2 contributions and a higher degree of uniformity after digestion.[13]

Up to this point, the digestion process of 3D-printed electrodes has been characterized in terms of morphology, mass variation related to the activity of proteinase K and changes in surface chemistry before and after digestion. The next step was aimed at performing electrochemical characterization of these electrodes by means of cyclic voltammetry (CV) measurements

in the presence of a surface-sensitive redox molecule, *i.e.* ferro/ferricyanide redox pair. Fig. 2D shows the CVs of graphene/PLA 3D-printed electrodes in the presence of this redox pair, where it can be seen that these surfaces become highly electroactive after enzymatic digestion. A typical quasi-reversible redox process, characteristic of the well-known ferro/ferricyanide system, was obtained with a peak separation of *ca.* 350 mV. This signifies an ~40% improvement of the heterogeneous electron transfer rate compared to our previous activation method, based on dimethylformamide-assisted PLA dissolution.[8] However, the rate dramatically improves when the DMF method is followed by electrochemical pre-treatment, as recently shown by Browne *et al.*,[13] outperforming what we have obtained after proteinase-K treatment in terms of peak separation (*ca.* 180 mV). dos Santos *et al.*[12] also showed that electrochemical activation works well with these electrodes, reaching *ca.* 250 mV of peak separation with the ferro/ferricyanide pair. These findings suggest that incorporating an electrochemical activation step can be beneficial after PLA digestion. We show in Fig. S4† the typical SEM images of different treatments, where the different contrasts/porosities rendered after each treatment can be appreciated.

Fig. 2D also shows that blank specimens were not electrochemically responsive towards the ferro/ferricyanide system, despite the morphological changes these electrodes underwent compared to the as-printed ones (Fig. 1A and B). Such morphological features, together with the mass loss recorded for the blanks (0.2%), indicate that a small degree of PLA degradation takes place in water medium after 28 h. However, the mass loss of the digested electrodes was *ca.* 20 times higher than that of the blank specimens, which can account for this marked difference in the electrochemical performance.

A shoulder peak located at *ca.* 0.76 V seen in ferro/ferricyanide voltammograms (Fig. 2D, 1st scan) can be assigned to the inherent protein electroactivity due to electro-oxidized amino acid residues (tyrosine, tryptophan, and cystine).[34] Traces of adsorbed proteinase K are thus present on the surface of 3D-printed electrodes after digestion, even after extensive washing. The peak is no longer seen at a second voltammetric scan (data not shown), as will be discussed below for 1-naphthol's system.

Once confirmed that 3D-printed graphene/PLA structures are electrochemically active after the proteinase K-mediated digestion, we proceeded to look into their electroanalytical applications. Graphene-based materials are beneficial for the adsorption of certain aromatic molecules (*e.g.* phenolic compounds) mainly *via* π–π interaction.[35,36] We focused on the detection of 1-naphthol as a model analyte due to its widespread use as an enzymatic product in biosensing schemes.[37–42] This molecule is also analytically relevant as an industrial phenolic contaminant found in wastewaters and as a biomarker for the assessment of occupational and environmental exposure to carbaryl and naphthalene pollutants.[43] We investigated the electrooxidation of 1-naphthol directly on the 3D-printed surfaces and glassy carbon electrode (GC) as the reference substrate (Fig. 3A). The cyclic voltammetric response

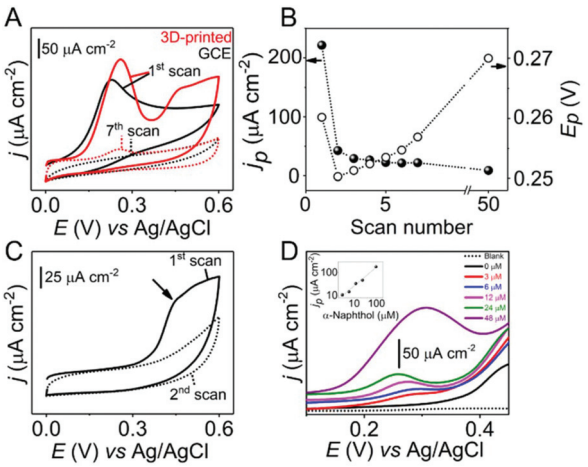

Fig. 3 Electrooxidation of 1-naphthol at the digested 3D-printed surfaces: (A) CVs performed on the activated 3D-printed electrodes and glassy carbon electrode (GCE) in the presence of 1-naphthol (60 μM); (B) progression of maximum current density (j_p) and peak potential (E_p) with the number of scans, on activated 3D-printed surfaces; (C) CV measurements carried out in the supporting electrolyte, without 1-naphthol, on activated 3D-printed surfaces; (D) enlarged region of the forward CV scans showing the oxidation peak of 1-naphthol at increasing concentration levels on 3D-printed electrodes (the dotted line represents the highest 1-naphthol concentration at non-activated blank electrodes). The inset shows the calibration plot of current density peak *versus* concentration. Scan rate: 100 mV s^{-1}, supporting electrolyte: Tris buffer (Tris-HCl 0.5 M, $MgCl_2$ 0.5 mM, KCl 0.1 M, pH 9.8).

obtained for the GC electrode diminished for repeated cycles with a marked potential peak shift (data not shown) and the complete absence of redox peaks from the third scan, indicating passivation of the electrode surface.[44] It is well known that naphthol easily undergoes electrochemical polymerization analogously to phenol. The resulting polymer film, poly (naphthalene oxide), forms a passivating layer on the surface of the electrode,[45] a process reported before for screen-printed and carbon paste electrodes.[42,44] This is seemingly consistent with the continuous insulating films formed on platinum electrodes, free from bulky pinholes or defects, not allowing electroactive molecules to reach the electrode surface.[46] In contrast, the voltammetric behavior of 1-naphthol on 3D-printed electrodes suggests that the surface is not fully passivated under the same conditions. The peak potential (E_p) (Fig. 3B) initially decreases after the first scan (from 260 to 250 mV), possibly as a result of an electrochemical activation.[13] Subsequently, E_p shifts towards more positive potentials after the second scan, which together with the gradual decrease in maximum current density, j_p, indicates that surface passivation is taking place, although not reaching completion even after 50 scans. We attribute the incomplete passivation to the large surface area and porous features of the eroded 3D-printed surfaces. Although passivating films have shown interesting properties for corrosion protection,[47–49] catalysis[50] and as permselective membranes in biosensor research,[46] the formation of such films has its drawbacks for electrochemistry.

A few examples include the interference of electrode passivation with the electrochemical treatment of phenolic wastes, as well as with electrochemical immunoassay schemes.[51,52]

The shoulder peak associated with intrinsic protein electrochemistry, previously seen for the ferro/ferricyanide system, was also observed in the cyclic voltammograms of 1-naphthol-containing samples. Its disappearance with the second scan was confirmed with CV measurements done in the supporting electrolyte without 1-naphthol, suggesting that the protein may be desorbed off the surface (Fig. 3C) or underwent irreversible changes. We assessed the analytical response of the 3D-printed electrodes towards different concentrations of 1-naphthol (Fig. 3D). Differences in E_p up to 50 mV can be seen, attributed to the previously mentioned FDM-related inter-electrode variation. The calibration plot shown as the inset spans over two orders of magnitude starting from 3 μm ($R^2 > 0.98$), demonstrating the potential of these 3D-printed platforms for the electrochemical detection of phenolic compounds, *e.g.* in contaminated wastewaters, with the added advantage of not undergoing complete electrode passivation after a few voltammetric cycles. Table S1† shows a comparison of different electrochemical methods for the detection of naphthol.

We carried out a proof-of-concept evaluation of the biosensing capabilities of these 3D-printed structures by immobilizing an enzyme *via* physical adsorption and utilizing 1-naphthol as an enzymatic redox product. The enzyme, alkaline phosphatase (ALP), can convert a specific electroinactive substrate, 1-naphthyl phosphate, into the electroactive 1-naphthol. In routine clinical laboratory tests, the activity of ALP is usually monitored for the diagnosis and therapeutic observation of bone and hepatobiliary diseases.[53] The detection of ALP activity is typically based on measuring its ability to catalyze the hydrolysis and transphosphorylation of phosphomonoesters usually by detecting the final product of the enzymatic conversion. ALP is also one of the most commonly used labeling tracers in immunological[52,54] and DNA hybridization assays.[21,41] Fig. 4 shows the voltammetric response of the ALP-based 3D-printed biosensing system. Before carrying out these experiments, we pre-treated the electrodes with one voltammetric scan in a supporting electrolyte in order to eliminate the potential interference of the proteinase K-related oxidation peak seen before in the blanks (Fig. 3C). The oxidation of 1-naphthol on ALP-modified electrodes takes place at a higher potential than that of bare electrodes due to its hindered diffusion through a layer of physiosorbed ALP enzymes. Fig. 4A shows the response of ALP-modified digested 3D-printed electrodes where the oxidation peak of 1-naphthol is detected at 365 mV. In bare electrodes, 1-naphthyl phosphate is not converted to 1-naphthol, thus there is no electrochemical response in that potential window (Fig. 4B). Physisorption of the enzyme is quite strong on these surfaces, as shown in Fig. 4C, where it is noted that after two subsequent washing cycles, the presence of ALP is still detected on the surface of the electrode.

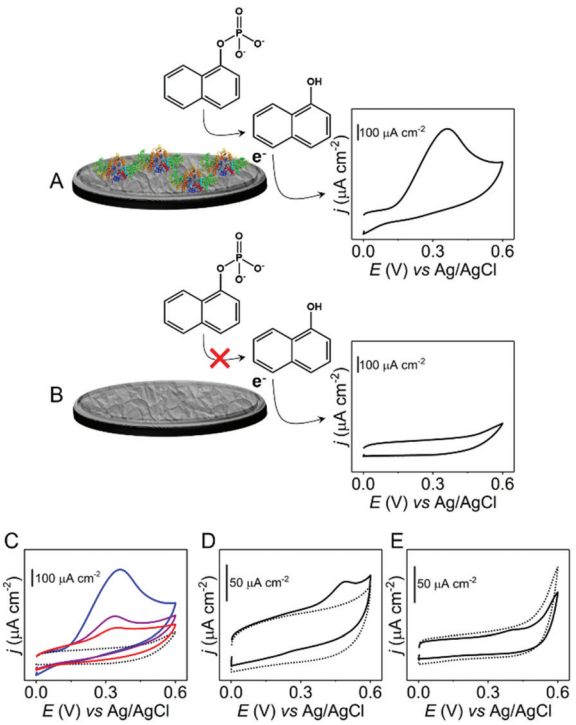

Fig. 4 Electrochemical response of the digested 3D-printed biosensor: (A) detection of 1-naphthol as the enzymatic product of 1-naphthyl phosphate conversion on ALP-modified electrodes; (B) absence of the oxidation peak of 1-naphthol in the presence of 1-naphthyl phosphate at bare electrodes; electrochemical response of ALP-modified electrodes in the presence of 1-naphthyl phosphate: (C) initially, after the first wash and after the second wash (blue, purple and red lines, respectively); (D) in neutral pH and (E) in neutral pH without co-factor Mg^{2+} (dotted lines represent the response of bare electrodes). Scan rate: 100 mV s^{-1}. Supporting electrolyte: tris buffer (Tris-HCl 0.5 M, $MgCl_2$ 0.5 mM, KCl 0.1 M, pH 9.8 or 7.4 and Tris-HCl 0.5 M KCl 0.1 M, pH 7.4).

To further confirm that the electrochemical response is merely due to the presence of the immobilized ALP, the activity of this enzyme was investigated under suboptimal conditions. The dephosphorylation activity of ALP relies on: (1) an alkaline environment and (2) the presence of a co-factor, *i.e.* Mg^{2+}. We assessed the effect of other reaction buffers where ALP activity is expected to be considerably lower, *i.e.* neutral pH and neutral pH in the absence of the co-factor. Fig. 4D and E show that ALP's activity is significantly compromised in a neutral reaction medium and in the absence of the metallic co-factor.

The enzyme-sculptured and digested 3D-printed surfaces show great promise for aqueous-based sensing and biosensing applications. Its graphene-based composition is beneficial for strong immobilization of biomolecules, as well as for the detection of aromatic molecules that are active in the anodic potential window. The large surface area and porosity of these electrodes seem to prevent complete electrode passivation after many voltammetric scans, which represents an important advantage for electroanalytical applications where the adherence of such insulating films interferes with the measurements.

Conclusions

We have demonstrated a conceptually novel method of activation of 3D-printed electrodes made from a graphene/PLA composite based on the proteinase K-mediated partial digestion of the PLA filament and the exposure of active graphene edges. The process results in the electrochemical activation of these surfaces, exposing graphene structures after reducing the amount of PLA concealing the 3D-printed objects. We demonstrated that this biotechnological activation process turns electrically irresponsive 3D-printed structures into actual active electrodes, turning them into sensitive platforms for electroanalysis. We carried out electrochemical detection of 1-naphthol, either directly or *via* a biosensing approach, by immobilizing alkaline phosphatase, capable of converting 1-naphthyl phosphate into 1-naphthol. Our findings should revolutionize the way 3D-printed polymer structures are post-processed.

Conflicts of interest

There are no conflicts to declare.

Acknowledgements

This work was supported by the project Advanced Functional Nanorobots (reg. no. CZ.02.1.01/0.0/0.0/15_003/0000444 financed by the EFRR). C. L. M. P. acknowledges the financial support of the European Union's Horizon 2020 Research and innovation programme under the Marie Skłodowska-Curie Actions IF grant agreement no. 795347. Z. S. was supported by the Czech Science Foundation (GACR no. 17-05421S). This work was created with the financial support of the Neuron Foundation for Science.

References

1 A. N. Raluca Marinescu Repanovici, presented in part at the 22nd International Conference on Innovative Manufacturing Engineering and Energy - IManE&E 2018, 2018.
2 C. L. Manzanares Palenzuela and M. Pumera, *TrAC, Trends Anal. Chem.*, 2018, **103**, 110–118.
3 M. Coakley and D. E. Hurt, *JALA*, 2016, **21**, 489–495.
4 U. Ghosh, S. Ning, Y. Z. Wang and Y. L. Kong, *Adv. Healthcare Mater.*, 2018, **7**, DOI: 10.1002/adhm.201800417.
5 S. H. Park, M. Kaur, D. Yun and W. S. Kim, *Langmuir*, 2018, **34**, 10897–10904.
6 H. H. Hamzah, S. A. Shafiee, A. Abdalla and B. A. Patel, *Electrochem. Commun.*, 2018, **96**, 27–31.
7 Z. Rymansaib, P. Iravani, E. Emslie, M. Medvidovic-Kosanovic, M. Sak-Bosnar, R. Verdejo and F. Marken, *Electroanalysis*, 2016, **28**, 1517–1523.
8 C. L. Manzanares Palenzuela, F. Novotny, P. Krupicka, Z. Sofer and M. Pumera, *Anal. Chem.*, 2018, **90**, 5753–5757.
9 R. M. Cardoso, D. M. H. Mendonça, W. P. Silva, M. N. T. Silva, E. Nossol, R. A. B. da Silva, E. M. Richter and R. A. A. Muñoz, *Anal. Chim. Acta*, 2018, **1033**, 49–57.
10 K. C. Honeychurch, Z. Rymansaib and P. Iravani, *Sens. Actuators, B*, 2018, **267**, 476–482.
11 C. Foo, H. N. Lim, M. A. Mahdi, M. HaniffWahid and N. M. Huang, *Sci. Rep.*, 2018, **8**, 7399.
12 V. K. Pãmyla, L. dos Santos, H. C. Loureiro, M. F. dos Santos, D. P. dos Santos, A. L. B. Formiga and J. A. Bonacin, *Sens. Actuators, B*, 2019, **281**, 837–848.
13 F. N. Michelle, P. Browne, Z. Sofer and M. Pumera, *ACS Appl. Mater. Interfaces*, 2018, **10**, 40294.
14 D. Vernardou, K. C. Vasilopoulos and G. Kenanakis, *Appl. Phys. A: Mater. Sci. Process.*, 2017, **123**, 623.
15 S. A. Baskakov, Y. V. Baskakova, N. V. Lyskov, N. N. Dremova and Y. M. Shul'ga, *Russ. J. Phys. Chem. A*, 2017, **91**, 1966–1970.
16 C. W. Foster, M. P. Down, Y. Zhang, X. B. Ji, S. J. Rowley-Neale, G. C. Smith, P. J. Kelly and C. E. Banks, *Sci. Rep.*, 2017, **7**, 42233.
17 D. M. Wirth, M. J. Sheaff, J. V. Waldman, M. P. Symcox, H. D. Whitehead, J. D. Sharp, J. R. Doerfler, A. A. Lamar and G. LeBlanc, *Anal. Chem.*, 2019, **91**, 5553–5557.
18 N. Deoray and B. Kandasubramanian, *Polym.-Plast. Technol. Eng.*, 2018, **57**, 860–874.
19 F. Kawai, *ACS Symp. Ser.*, 2010, **1043**, 405–414.
20 Y. Tokiwa and B. P. Calabia, *Appl. Microbiol. Biotechnol.*, 2006, **72**, 244–251.
21 C. L. Manzanares-Palenzuela, N. de-los-Santos-Alvarez, M. J. Lobo-Castanon and B. Lopez-Ruiz, *Biosens. Bioelectron.*, 2015, **68**, 259–265.
22 L. Liu, S. Li, H. Garreau and M. Vert, *Biomacromolecules*, 2000, **1**, 350–359.
23 R. L. R. Helena and S. Azevedo, in *Biodegradable Systems in Tissue Engineering and Regenerative Medicine*, ed. J. S. R. and Ruis L. Reis, CRC Press, Boca Raton, 1st edn, 2004, pp. 177–201.
24 K. R. Miller and M. D. Soucek, *J. Appl. Polym. Sci.*, 2014, **131**, 40475.
25 C. Sellitti, J. L. Koenig and H. Ishida, *Carbon*, 1990, **28**, 221–228.
26 V. Tucureanu, A. Matei and A. M. Avram, *Crit. Rev. Anal. Chem.*, 2016, **46**, 502–520.
27 B. S. Ndazi and S. Karlsson, *eXPRESS Polym. Lett.*, 2011, **5**, 119–131.
28 H. T. Zou, C. H. Yi, L. X. Wang, H. T. Liu and W. L. Xu, *J. Therm. Anal. Calorim.*, 2009, **97**, 929–935.
29 E. Meaurio, N. Lopez-Rodriguez and J. R. Sarasua, *Macromolecules*, 2006, **39**, 9291–9301.
30 S. Inkinen, M. Hakkarainen, A. C. Albertsson and A. Sodergard, *Biomacromolecules*, 2011, **12**, 523–532.
31 D. Cam, S. H. Hyon and Y. Ikada, *Biomaterials*, 1995, **16**, 833–843.
32 N. Vasanthan and O. Ly, *Polym. Degrad. Stab.*, 2009, **94**, 1364–1372.

33 S. Hermanova, M. Zarevucka, D. Bousa, M. Pumera and Z. Sofer, *Nanoscale*, 2015, **7**, 5852–5858.
34 E. V. Suprun, V. V. Shumyantseva and A. I. Archakov, *Electrochim. Acta*, 2014, **140**, 72–82.
35 Y. H. Pang, Y. Zhang, W. Y. Li, H. L. Ding and X. F. Shen, *J. Electroanal. Chem.*, 2016, **769**, 89–96.
36 X. B. Wang, Y. H. Hu, J. H. Min, S. J. Li, X. Y. Deng, S. D. Yuan and X. H. Zuo, *Appl. Sci.*, 2018, **8**, 1950.
37 M. Moreno-Guzman, M. Eguilaz, S. Campuzano, A. Gonzalez-Cortes, P. Yanez-Sedeno and J. M. Pingarron, *Analyst*, 2010, **135**, 1926–1933.
38 F. G. Sanchez, A. N. Diaz, M. C. R. Peinado and C. Belledone, *Anal. Chim. Acta*, 2003, **484**, 45–51.
39 R. Miranda-Castro, P. De-Los-Santos-Alvarez, M. J. Lobo-Castanon, A. J. Miranda-Ordieres and P. Tunon-Blanco, *Anal. Chem.*, 2007, **79**, 4050–4055.
40 M. Plucnara, E. Eksin, A. Erdem and M. Fojta, *Electroanalysis*, 2018, **30**, 2321–2329.
41 C. L. Manzanares-Palenzuela, J. P. Martin-Clemente, M. J. Lobo-Castanon and B. Lopez-Ruiz, *Talanta*, 2017, **164**, 261–267.
42 C. Fernandez-Sanchez and A. Costa-Garcia, *Biosens. Bioelectron.*, 1997, **12**, 403–413.
43 C. Sams, *Toxics*, 2017, **5**, 3.
44 R. M. Pemberton, J. P. Hart and T. T. Mottram, *Analyst*, 2001, **126**, 1866–1871.
45 M. C. Pham, A. Hachemi and M. Delamar, *J. Electroanal. Chem.*, 1985, **184**, 197–203.
46 R. Ciriello, T. R. I. Cataldi, D. Centonze and A. Guerrieri, *Electroanalysis*, 2000, **12**, 825–830.
47 A. Meneguzzi, C. A. Ferreira, M. C. Pham, M. Delamar and P. C. Lacaze, *Electrochim. Acta*, 1999, **44**, 2149–2156.
48 S. Fletcher and V. J. Black, *J. Phys. Chem. C*, 2016, **120**, 8014–8022.
49 G. Mengoli and M. M. Musiani, *J. Electrochem. Soc.*, 1987, **134**, C643–C652.
50 M. C. Pham and J. E. Dubois, *J. Electrochem. Soc.*, 1986, **199**, 153–164.
51 H. Al-Maznai and B. E. Conway, *J. Serb. Chem. Soc.*, 2001, **66**, 765–784.
52 M. P. Kreuzer, C. K. O'Sullivan and G. G. Guilbault, *Anal. Chim. Acta*, 1999, **393**, 95–102.
53 W. Meyersabellek, P. Sinha and E. Kottgen, *J. Chromatogr.*, 1988, **429**, 419–444.
54 Y. L. Xianyu, Z. Wang and X. Y. Jiang, *ACS Nano*, 2014, **8**, 12741–12747.

Polymer Degradation and Stability 111 (2015) 176–184

Contents lists available at ScienceDirect

Polymer Degradation and Stability

journal homepage: www.elsevier.com/locate/polydegstab

Biodegradation of waste PET based copolyesters in thermophilic anaerobic sludge

Soňa Hermanová [a, *], Pavla Šmejkalová [b], Jan Merna [a], Marie Zarevúcka [c]

[a] Institute of Chemical Technology, Prague, Department of Polymers, Technická 5, 166 28 Prague 6, Czech Republic
[b] Institute of Chemical Technology, Prague, Department of Water Technology and Environmental Engineering, Technická 5, 166 28 Prague 6, Czech Republic
[c] Institute of Organic Chemistry and Biochemistry ASCR, v.v.i. Flemingovo nám. 2, 166 10 Prague 6, Czech Republic

ARTICLE INFO

Article history:
Received 20 August 2014
Received in revised form
6 November 2014
Accepted 14 November 2014
Available online 26 November 2014

Keywords:
Poly(ethylene terephthalate)
Copolymers
Sludge
Biodegradation
Hydrolysis
Waste

ABSTRACT

A series of poly(ethylene terephthalate-*co*-lactate) copolyesters with random microstructure was prepared from PET waste beverage bottles and L-lactic acid. Square specimens, sectioned from melt-pressed film, were incubated in thermophilic sludge (55 °C, alkaline environment) for 394 days. The biodegradability of the samples, determined from biogas yield, reached 34–69 % depending on the starting aromatic to aliphatic units' ratio.

Water uptake study in sludge and abiotic buffers at 55 °C showed sharp border around 57% of aromatic units in copolyester composition between polymers susceptible and resistant to both hydrolytic attack by hydrolases and the abiotic hydrolysis. Samples biodegraded in sludge and those abiotically aged in buffers were characterized by ^{1}H NMR, ATR-FTIR, SEC, DSC, and TGA analysis to gain an insight into the chain scission mechanism.

Aromatic oligomers as model of copolyester degradation intermediates were prepared and proved to biodegrade in sludge as well.

1. Introduction

Poly(ethylene terephthalate), PET, represents the highest-volume produced polyester with a broad range of applications. Excellent properties of this material are accompanied with its high resistance to degradation. Up to now enormous research effort was paid on the development of PET waste recycling technologies. With chemical recycling approach, monomer, bis(2-hydroxyethyl terephthalate), BHET, could be obtained from PET waste [1,2]. Another way consists in transesterification reactions of PET and aliphatic polyesters or copolymerization of PET depolymerisation products and aliphatic co-monomers [3–9].

The incorporation of aliphatic units in principle causes the decrease in ethylene terephthalate units sequence length and thus improves the flexibility of rigid aromatic chains. Aliphatic ester linkages introduced were proved to be more susceptible to abiotic and enzyme-catalysed hydrolytic scission under different environmental conditions [4,10–12]. The advantage of the plastics biodegradation in sludge over that in compost, landfill, and soil consists in the production of biogas, which is composed of methane as energy recovery along with carbon dioxide and water vapour. The measured amount of biogas evolved gives polymer biodegradability under certain test conditions. For the BTA polyester (50 mol % of 1,4-butanediol, 30 mol % of adipic acid, and 20 mol % of terephthalic acid) a biogas formation of about 11% was calculated after 42-day cultivation at 37 °C in anaerobic sludge [13].

It is well known that the aliphatic-aromatic copolyesters with blocky or random microstructure undergo the hydrolytic scission at reasonable rate when the experiment is performed at temperatures close to their melting or glass transition temperatures. Hydrolytic degradation of poly(ethylene terephthalate-*co*-lactate)s was considerably accelerated at 60 °C in phosphate buffer solution (pH 7.40) in comparison with that at 45 °C [10]. The overall thermal properties of the copolymer matrix are proposed to control the biodegradability as documented by the biodegradation studies on defined model copolyesters containing terephthalate units [14]. At elevated temperatures an increased mobility of polymer chains both arranged in crystalline regions and embedded in amorphous glassy matrix is supposed to liberate hindered ester bonds in the vicinity to aromatic moiety to be available for hydrolytic scission. Enhanced polyester degradation rate at higher temperatures is also

* Corresponding author. Tel.: +420 2 2044 3189/3192; fax: +420 2 2044 3175.
E-mail address: sona.hermanova@vscht.cz (S. Hermanová).

http://dx.doi.org/10.1016/j.polymdegradstab.2014.11.007
0141-3910/

caused by different microbial community occurring at thermophilic (50–60 °C) conditions in comparison with that at mesophilic (~37 °C) ones [15]. The blends containing poly(ethylene terephtalate-*co*-lactate) with 35 mol % of aromatic ester units and thermoplastic starch (25 and 35 wt. %) were completely disintegrated in sludge under thermophilic conditions (55 °C) within four months accompanied with an intensive biogas production with the yield up to 350 ml per g of substrate [16].

In this study, we report on the synthesis of poly(ethylene terephthalate-*co*-lactate) copolyesters with aromatic to aliphatic molar ratio of 41:59–60:40 from PET waste and their biodegradation under thermophilic conditions in digested sludge. Aromatic oligomers were prepared as models of possible degradation residues rich in ethylene terephthalate sequences. Their biodegradation was also studied in separate runs.

2. Experimental part

2.1. Materials

L-lactic acid (85% aqueous solution), bis(2-hydroxyethyl terephthalate) from Sigma–Aldrich, zinc octanoate, zinc acetate dihydrate (99%) from Fluka AG, and ethylene glycol from Lachema Neratovice were used as received. Poly(ethylene terephthalate) was obtained from colourless beverage bottles, which were carefully washed and cut into flakes.

Digested sludge from thermophilic digesters of the Central Waste Water Treatment Plant (CWWTP) in Prague, Czech Republic was used as the inoculum (Table 1). For the purpose of water uptake test the digested sludge was heated at 160 °C at a pressure of about 4 bar for 2 h (deactivated sludge). As control buffer solutions sodium borate buffer (pH 8.0) and phosphate buffer (pH 7.5) were used.

Total solids (TS), volatile solids (VS), total suspended solids (TSS), and volatile suspended solids (VSS) were determined according to APHA/AWA/WPCF (1998) [17].

Chemical oxygen demand (COD) was determined according to ISO 15705 Internal standard [18].

2.2. Methods

2.2.1. Preparation of the copolyester samples and model aromatic oligomers

PET flakes (25 g) were treated with lactic acid (30, 25, 15, and 10 ml of 85% aqueous solution for sample A, B, C, and D) in the presence of zinc acetate (0.075 g for each synthesis) at 250 °C for 30 min [16]. The acidolysis product, a mixture of low-molar-mass aromatic-aliphatic esters, was then polycondensed in a melt (250 °C) at a pressure gradually decreasing from 133 Pa to 1 Pa for certain time period. Total reaction time was 3 h for sample A, 2.5 h for B, 2 h for C, and 1.5 h for D. The virgin samples, which have character of glassy yellowish solids, were processed by melt pressing (temperature 105 °C, 3 min, pressure 0.35 MPa) into film form. Square specimens with dimension of 10 × 10 × 0.7 mm, sectioned from films, were used for the degradation study. Films were subjected to ^{1}H NMR, DSC, SEC, and ATR-FTIR analysis.

Glycolysis of PET waste (20 g) with ethylene glycol (7.5 g), catalysed by zinc octanoate (0.024 g), was conducted at 220 °C under argon atmosphere for 40 min. The glycosylate, crushed into the powder, was extracted with distilled water to eliminate remaining ethylene glycol. Further extraction of PET glycolyzate in methanol yields fractions rich in aromatic trimer and dimer, respectively, since majority of BHET was extracted off by distilled water. After that, glycolysate was dissolved in boiling methanol and insoluble fraction was filtered off. Hot filtrate was cooled to room temperature to precipitate the first fraction comprising dimer and trimer. An evaporation of the cold methanol solution afforded the second fraction, composed of monomer and dimer.

Correlation experiments (COSY, HMQC) were done to assign ^{1}H NMR signals to monomer, dimer, and trimer structures.

^{1}H NMR spectrum of cold methanol soluble fraction comprised following signals: (δ, DMSO) 8.1 ppm (q, 4H, aromatic $C_6\mathbf{H}_4$), 5.0 ppm (t, 1H, O**H**), 4.7 ppm (s, 0.97H, internal), δ 4.3 ppm (q, 2H, CO–C$\mathbf{H}_2$), 3.7 ppm (m, 2H, C$\mathbf{H}_2$–OH), corresponding to 50:50 mol/mol % of monomer to dimer.

^{1}H NMR spectrum of cold methanol insoluble fraction comprised following signals: (δ, DMSO) 8.1 ppm (m, 4H, aromatic $C_6\mathbf{H}_4$), 5.0 ppm (t, 1H, O**H**), 4.7 ppm (d, 2.34H, internal), δ 4.3 ppm (t, 2H, CO–C$\mathbf{H}_2$), 3.7 ppm (q, 2H, C$\mathbf{H}_2$–OH)), corresponding to 85:15 mol/mol % of dimer to trimer.

2.2.2. Biodegradation, abiotic control test, and water absorption test

Batch test was carried out in 120 ml serum bottles at the temperature of 55 ± 1 °C under the nitrogen atmosphere. Thermophilic digested sludge from operating digesters at CWWTP in Prague, Czech Republic was used as the inoculum (digested sludge) or as the culture medium after its deactivation (deactivated sludge). The copolyester samples (two specimens with total mass approximately 0.2 g) were fixed in the frames to be easily withdrawn and then placed into the serum bottle with 80 ml of sludge. For the abiotic degradation study, copolyester was immersed (two specimens) in 80 ml of phosphate buffer and borate with sodium azide (0.03%). The flasks were incubated at the same temperature as that for degradation experiment.

The biogas production was measured volumetrically at regular time intervals using a gas-tight burette with NaCl saturated solution as a stop liquid. The bottles were stirred before each measurement. The gas composition was analysed by a gas chromatograph (Fisons Instruments GC 8000Top) equipped with a thermal conductivity detector HWD 800 and a Separon AE (200–300 μm) glass column (2.5 m, 3 mm inside diameter). Argon was used as a carrier gas at a pressure of 100 kPa.

Biodegradability of the copolyester samples is expressed as an achieved percentage of the theoretical biogas yield calculated according to Buswell equation [19]. Lag phase time is reported for the period with no biogas production. Start of fast biogas production was evaluated as an intersection of maximal slope of biogas production curve with time axis.

All samples were after the incubation in sludge washed with distilled water several times, vacuum dried, and subjected to analyses. The mass loss of the films was calculated according to the relationship as follows:

$$\text{mass loss}\ (\%) = (m_0 - m_d)/m_0 \times 100,$$

where m_0 means initial mass of the film, and m_d denotes the mass of the dried degraded film.

Table 1
Properties of the inoculum used (thermophilic digested sludge).

TS	VS	TSS	VSS	COD_T	COD_f
[g/l]	[g/l]	[g/l]	[g/l]	[g/l]	[g/l]
28.56	14.67	26.71	13.54	22.70	1.90

TS total solids, VS volatile solids, TSS total suspended solids, and VSS volatile suspended solids were determined according to APHA/AWA/WPCF (1998) [17].
COD chemical oxygen demand was determined according to ISO 15705 Internal standard [18].

Water absorption test was conducted by immersing the specimens in sludge (initial pH 8.0), deactivated sludge (initial pH 8.9), sodium borate buffer (initial pH 8.0) and phosphate buffer (initial pH 7.5) at 55 °C for nine days. Specimens were removed at regular intervals, carefully blotted with filtration paper and weighed. The final results were obtained by averaging three separate runs. The water absorption was calculated according to the weight difference as follows:

$$\text{water uptake } (\%) = (m_w - m_0)/m_0 \times 100,$$

where m_0 denotes the initial mass of the film and m_w means mass of wet sample.

2.3. Characterization methods

Molar masses were determined using SEC with RI detection (Watrex P102 pump, Schambeck RI2000 detector). Separation was performed on one PL Mixed C column 8*300 mm, 5 μm in $CHCl_3$ as a mobile phase at flow rate 1 ml/min. Sample concentration was cca. 1 mg/ml, injection volume 20 μl. Relative calibration using narrow PS standards (580–3,250,000 g/mol) was used to calculate apparent molar masses. Data were evaluated using Clarity 5.0 data processing software.

FTIR spectra were collected on FTIR spectrometer Nicolet 6700 (Thermo Scientific, USA) equipped with a diamond crystal GladiATR (PIKE Technologies, USA). ATR-FTIR spectra were measured with a resolution of 4 cm^{-1} in the range of 4000–400 cm^{-1} (64 scans) and corrected against the background spectrum of air.

^{1}H NMR spectra were measured on NMR Spectrometer Bruker Avance DRX 500 in $CDCl_3$ and DMSO, respectively, at lab temperature and tetramethylsilane (TMS) was used as the internal standard. The assignment of proton signals (see Supporting information) observed in measured ^{1}H NMR spectra was performed according to the study of Olewnik [6].

For the DSC experiments, DSC Q100 (TA Instruments) was used. Samples were encapsulated in hermetic aluminium pans, typically 4 mg of sample. The samples were heated and cooled at a rate of 5 °C/min under a nitrogen gas flow (50 ml/min). The measurement was started by heating the samples from 0 °C to 300 °C and then cooling to 0 °C. A thermal analyser TGA Q500 (TA Instruments, USA) was used to measure the sample mass loss under nitrogen atmosphere up to 800 °C at the heating rate of 20 °C/min.

Surface morphology was evaluated by Vega Tescan SEM microscope.

3. Results

3.1. Synthesized copolyesters and aromatic oligomers

For the purpose of biodegradation study model aliphatic-aromatic copolyesters were prepared by the acidolysis and subsequent melt-polycondensation of waste PET with L-lactic acid. Concretely, four poly(ethylene terephthalate-*co*-lactate) copolyesters consisted in 41 mol % (sample A), 43 mol % (sample B), 57 mol % (sample C), and 60 mol % (sample D) of aromatic T units and corresponding aliphatic L units were prepared and subjected to the biodegradation study. The sequential length, number-average sequential length, and the degree of randomness were determined by adopting the calculation method of Tessier and Fradet [20] (for calculation details see Supporting info). The co-monomer composition, microstructure characteristics, and thermal properties of the samples under investigation are summarized in Table 2. Both the degree of randomness in the range of 0.8–0.9 and single T_g along with no melting endotherm support almost random microstructure of the obtained copolyesters. The single glass transition temperature, which was for all samples below T_g of both reference PLA and PET, also evidences that the copolyesters do not exhibit phase segregation phenomenon.

Aromatic oligomer mixtures serving as model degradation intermediates were separated by methanol extraction from PET waste glycolysate and were subjected to the incubation in sludge. The thermal and spectroscopic characteristics of these oligomers were in accordance with published literature (Fig. 1) [2,21]. Fraction insoluble in cold methanol consisted in aromatic dimer and corresponding trimer (85:15 mol %) and is denoted as d + t. The fraction soluble in cold methanol comprised BHET and its dimer, (50:50 mol %) and is denoted as m + d.

3.2. Copolyester biodegradation under anaerobic conditions in sludge

Studied copolyester samples A–D were incubated at comparable initial organic loading rate of inoculum in the range of 0.18–0.25 g COD/g VSS. To determine the appropriate ratio of polymer specimen to sludge, COD of the copolyester samples was estimated to be 1.24–1.34 g/g.

For all samples (A–D) the occurrence of an initial lag phase without the biogas production is apparent (Fig. 2, Table 3). It is also evident that the increased starting content of aliphatic L units in the molecular structure reduced the length of the lag phase. The first indication of the initiated biodegradation, *i.e.* slow biogas production, was detected already after 3 days of incubation for sample A, after 14 days for B and C, and after 44 days for sample D.

The rate and extent of the copolyester decomposition increased with increasing starting aliphatic content in the original material. Biodegradability declines from the maximum of 69% for sample A to 34% for D. The biogas yield is up to 663 ml/g of original material (sample A) (under standard conditions). Biogas contains 63–67 % of energy-rich methane (Fig. 2) as the product of copolyester mineralization beside carbon dioxide, water vapour, and other minor

Table 2
Composition (^{1}H NMR) and thermal properties (DSC) of synthesized PET/LA copolyesters and bio/degraded representatives.

Sample denotation	T:L[a]	Sequential length		Number-average sequential length		Degree of randomness	T_g (°C)	T_m (°C)
		Y_L	X_{ET}	$L_{n,L}$	$L_{n,ET}$	B		
A 0d	41:59	2.0	2.0	2.2	3.0	0.79	63.4	–
A 29 d buffer	45:55	1.9	2.1	2.0	3.3	0.79	57.7	–
A 29 d sludge	37:63	1.9	1.8	2.6	3.1	0.70	61.2	–
B 0d	43:57	1.9	1.9	1.9	2.8	0.90	62.2	–
C 0d	57:43	1.8	2.9	1.6	4.2	0.86	64.7	–
D 0d	60:40	1.7	3.5	1.4	4.2	0.94	67.4	–
D 29 d buffer	64:36	1.4	3.6	1.8	6.5	0.70	65.7	180.4 (10.6 J/g)
D 29 d sludge	68:32	1.4	3.6	1.5	6.1	0.85	66.2	175 (17.7 J/g)

[a] T:L molar ratio of aromatic and aliphatic units in copolyesters.

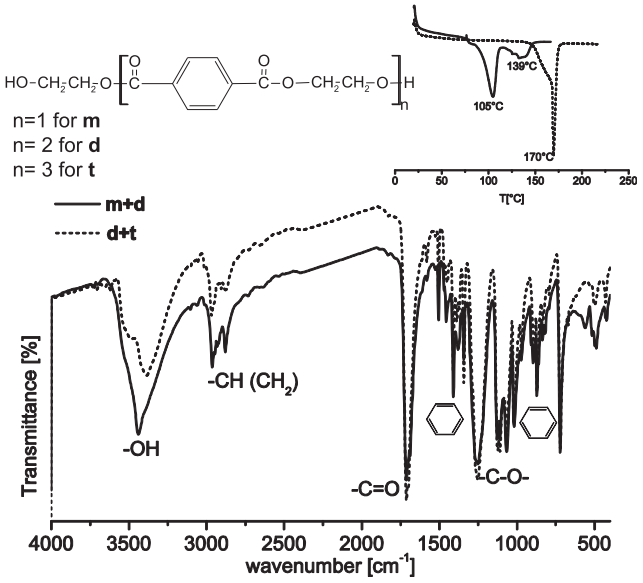

Fig. 1. ATR-FTIR and DSC (endothermic response, exo up) of aromatic oligomers (m + d, monomer and dimer; d + t, dimer and trimer).

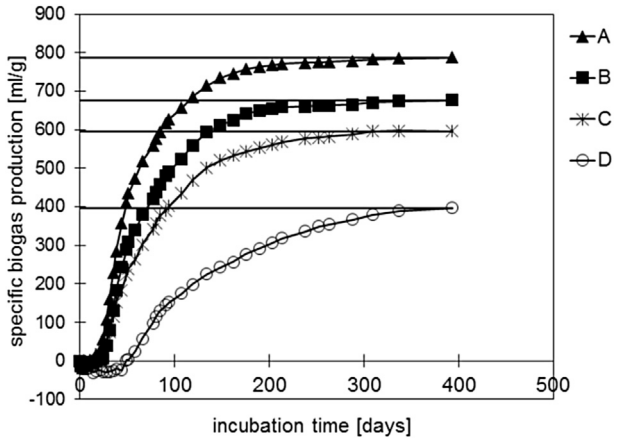

Fig. 2. Specific biogas production related to sample mass (TS) in anaerobic biodegradation test of samples A – D in sludge at 55 °C. Theoretical (100% biodegradation) specific biogas production is from 1150 (sample A) to 1200 ml/g (sample D).

Table 3
Biodegradability, biogas, and methane production.

	Biodegradability[a]	Time of 90% decomposition	Biogas yield[b]	CH_4 yield[b]	Lag phase	Start of fast biogas production
	[%]	[day]	[ml/g]	[ml/g]	[day]	[day]
A	69	130	663	420	3	22
B	59	145	573	365	14	24
C	51	165	506	340	14	22
D	34	265	340	228	44	44
d + t	58	90	611	–	2	0
m + d	82	43	865	–	0	0

[a] Biodegradability of the copolyester samples is expressed as an achieved percentage of the theoretical biogas yield calculated according to Buswell equation [19].
[b] To sample mass (TS), under standard conditions (STP- temperature of 273.15 K and pressure (10^5 Pa).

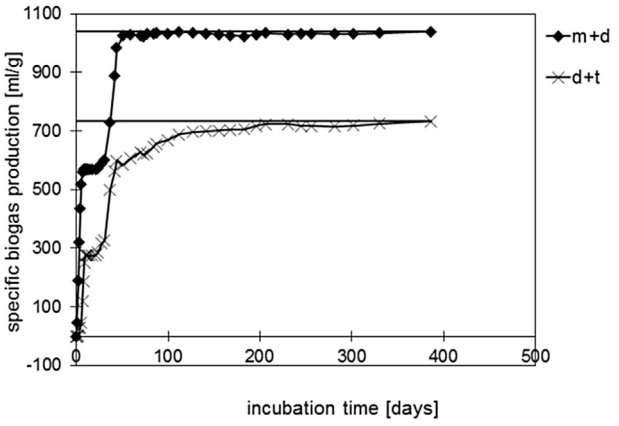

Fig. 3. Specific biogas production related to sample mass (TS) in anaerobic biodegradation test of samples m + d and d + t in sludge at 55 °C. Theoretical (100% biodegradation) specific biogas production is about 1270 ml/g for both samples.

gases. During incubation of unmodified PET no release of biogas was detected.

The degradation behaviour of aromatic oligomers, respectively mixtures of them (m + d, d + t) was studied in separate run to prove their biodegradability. The decomposition of both oligomeric samples starts almost at the same time within the first few days of incubation. It is worth mentioning that three-week lag phase was observed after 8 days of the initiated biodegradation. Afterwards the decomposition continued at the same rate as before lag phase (Fig. 3). The decomposition of both these aromatic oligomers (m + d, d + t) is significantly faster than those of samples A–D, as evidenced by the time of 90% decomposition (Table 3). Intensive biodegradation and higher biogas yield was achieved for sample m + d (BHET and dimer, 50/50 mol %), for which biogas yield significantly exceeds the values determined for all copolyester samples A–D. This could be ascribed to higher availability of water-soluble BHET as a substrate.

3.3. Water uptake study

The emphasis was paid on water absorption study in order to evaluate the extent of abiotic and the enzyme-catalysed hydrolysis occurring during the initial phase of the samples incubation in sludge. For this purpose borate and phosphate buffers with alkalinity close to those measured initially or during sludge incubation were selected as comparative abiotic media. The deactivated sludge was supposed to mimic abiotic environment with the same alkalinity and namely buffering capacity as digested sludge. During digested sludge thermal pre-treatment the changes in NH_3/NH_4^+ and HCO_3^-/CO_3^{2-} equilibrium resulted in a pH value shift from 8.0 to 8.9 and also low enzymatic activity was retained. In deactivated sludge all hydrolases activities were considerably decreased due to the reduction in microbial community. Evidently, the autoclaving under pressure caused the protein denaturation and microorganism growth inhibition. However, hydrolytic microorganisms and their spores are very resistant to certain stressful conditions including damaging temperature. This could be supported by the biogas production detected after the incubation of sludge, previously conditioned at 100 °C and atmospheric pressure for 20 min. Free extracellular hydrolase activities together with biogas production profiles in digested and deactivated sludge are depicted in Supporting info.

Low water uptake values measured within 3 and 4 days of all copolyester samples' immersion reflected slow water diffusion into the glassy and mostly hydrophobic matrix (Fig. 4).

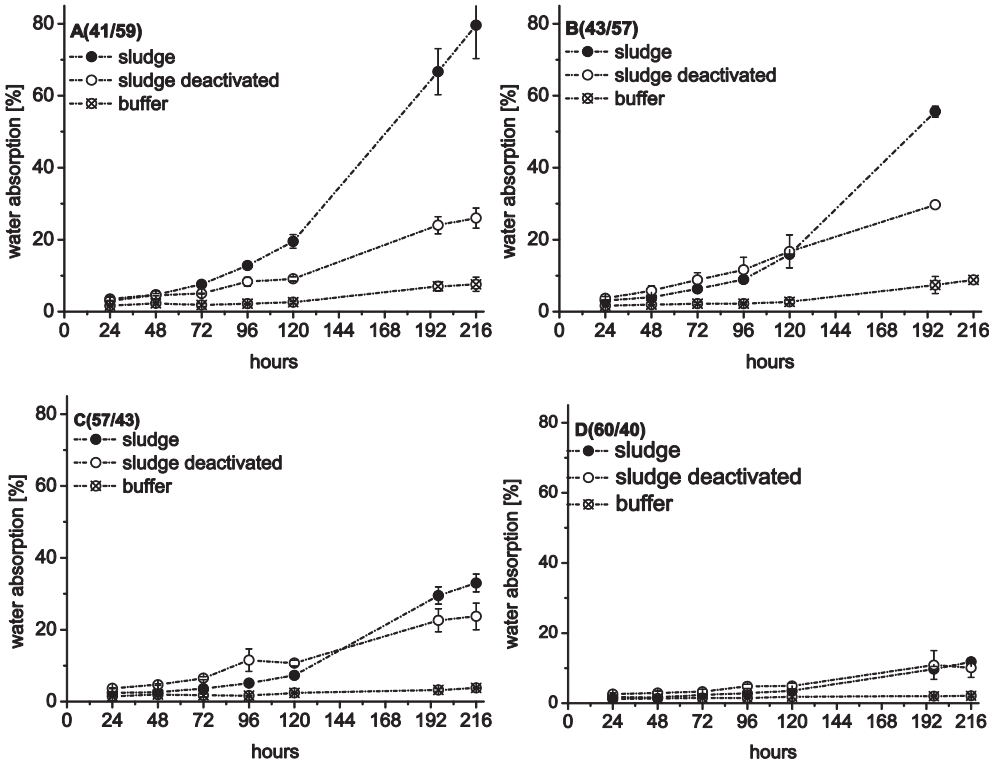

Fig. 4. Water uptake profile for copolyesters A–D immersed in sludge, deactivated sludge, and borate buffer.

During this initial period the hydrolytic scission of accessible ester bonds is supposed to take place mainly at the copolyesters films surface. Increasing amount of generated carboxylic and hydroxyl end groups enhanced hydrophilic character of the specimen and due to the surface micro-cracking water penetrated into the specimen causing its swelling. Such swelling contributes significantly to the formation of channels in the copolymer bulk. In the case of samples A and B high swelling (60–80 % water uptake) led to their rubbery appearance.

Surface micro-cracking is documented by the surface changes of dried sample A, where microporous character was seen for the film aged in buffer (Fig. 5) in comparison with smooth surface of non-hydrolysed sample. Larger pores along with cracks were observed on the surface of samples exposed to sludge after the same 9-day period confirming intensive erosion and degradation extending from the surface deep into the matrix (Fig. 5, cross section). Proceeding bulk degradation accompanied with incubated specimens' mass loss and disintegration caused poorly reproducible results with high standard deviations after 10 days.

It was found that the increase in water uptake values corresponded with the starting content of aliphatic L units within the copolyester series and was strongly dependent on the particular environment (Fig. 4). The sample D with the highest starting content of aromatic T units (60 mol %) was the most resistant to abiotic hydrolysis and also enzyme attack under all incubation conditions.

The abiotic hydrolysis induced by the attack of hydroxide ions in borate buffer (pH 8.0) proceeded most slowly with the maximum values of 8% reached for both copolyesters A and B after eight days. Almost the same values and trends were received for samples immersed in phosphate buffer with starting pH 7.5.

Water uptake values of samples with 59, 57, and even 43 mol % of aliphatic L units (A, B, C) considerably increased in digested sludge in comparison with those measured in abiotic buffers. Such trend could be ascribed to intensive enzymatic activity on the copolyester surface, which prevails over abiotic base-catalysed hydrolytic scission. This could be also evidenced by water uptake values of samples incubated in deactivated sludge, where more alkaline environment considerably accelerates abiotic chain scission process but still not in the same extent as in digested sludge.

3.4. Determination of mass loss and molar masses

Measured mass losses of degraded copolyester films in this study are connected with the sample disintegration due to the hydrolytic scission occurring initially on the surface and then namely in the specimen bulk. Photographs illustrating the macroscopic visual evaluation of the specimens' changes and disintegration in time are presented in Fig. 6.

To get more insight into the impact of abiotic (base-catalysed) hydrolysis on the copolyesters' chain degradation the disintegration rate and molar mass of abiotically aged samples was compared with characteristics of those incubated for 29 days in sludge. The results are summarized in Tables 2 and 4. The hydrolysis rate of the copolyesters (A-D) in abiotic phosphate buffer dropped with decreasing starting lactate units' content and the presence of longer ethylene terephthalate sequences as documented by respective mass losses (Table 4).

In sludge, the hydrolysis rate was significantly accelerated in the case of samples with 41–57 mol % of aromatic T units (A–C) in comparison with buffer ageing. Measurable mass loss means that degradation process occurred in whole copolyester specimen bulk and not only at the surface as initially.

SEC analysis revealed significant decrease in molar masses of all degraded samples supporting the occurrence of intensive chain scission as the result of abiotic and enzyme-catalysed hydrolysis (Table 4). Higher drop in molar mass is observed for samples aged in both types of buffers in comparison with those biodegraded in sludge.

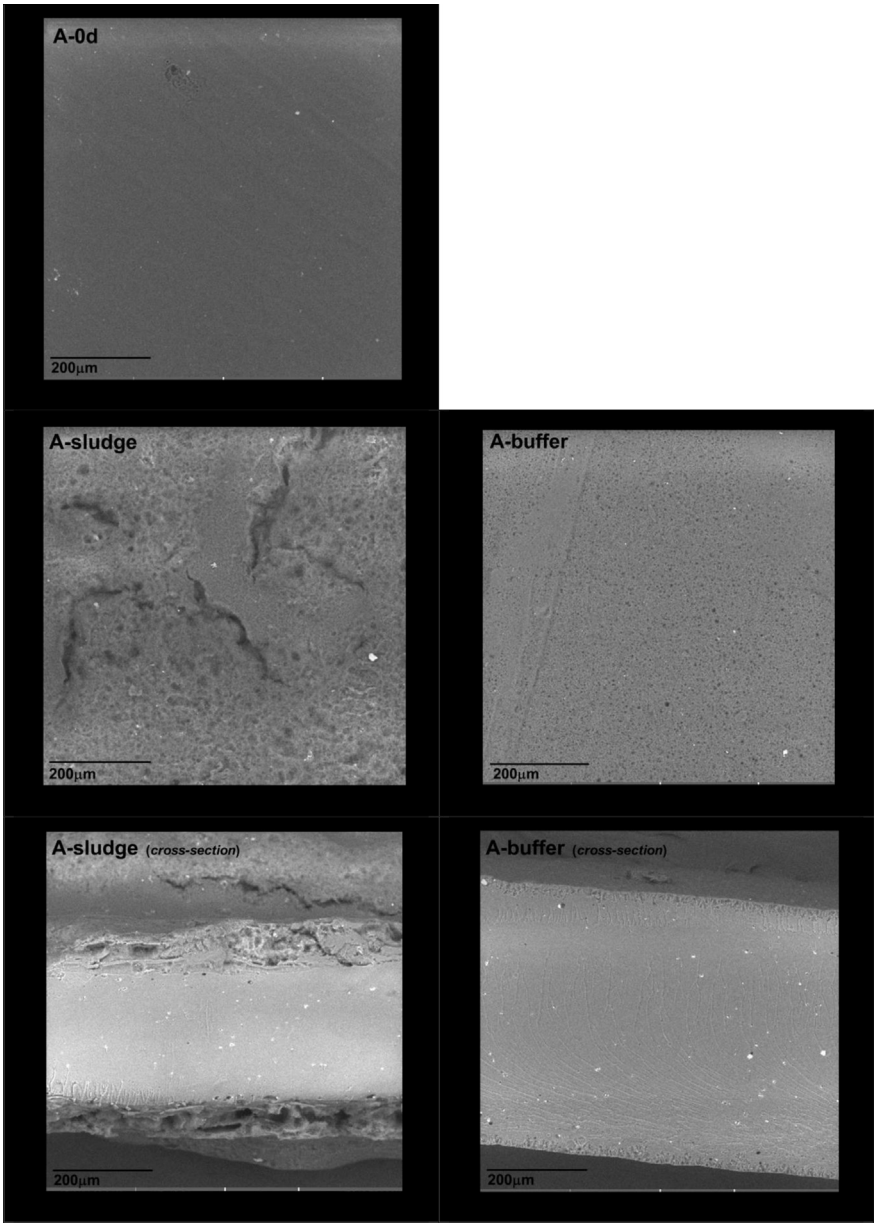

Fig. 5. Representative SEM images of dried copolyester A surface before (A-0d) and after the 9-day incubation in sludge and phosphate buffer.

We suggest that during extracellular enzyme-catalysed hydrolysis the chain-unzipping mechanism dominated during which shorter water-soluble degradation intermediates were released into the aqueous environment and hence were not involved in SEC distribution curves. Their diffusion out from the samples is documented by high mass loss (79–90 wt%) of biodegraded samples A–C. During this rapid process accessible ester bonds of copolyesters were cleaved yielding solid residues rich in hindered ester bonds which in turn become more resistant to enzymatic and also abiotic hydrolysis. In both buffer types random abiotic hydrolysis occurred in aliphatic ester bonds yielding shorter chain length species. These are insoluble and hence not contributing to mass loss whereas significantly decreasing average molar mass values.

Given that during ester bonds scission species ended with carboxylic groups are formed, their accumulation could influence the microenvironment surrounding copolyester matrix and degradation process. These groups dissociate to generate H^+ ions which in dependence of their increasing concentration up to medium buffer capacity cause drop in pH value [22]. In our case the bulk alkalinity of digested sludge decreased after 29 days relatively in a small extent which implies its high buffer capacity [23] and also involvement of degradation products into complex anaerobic digestion process. It means that during methanogenic fermentation the consumption of H^+ occurred.

3.4.1. Composition and microstructure analysis

The characteristic peaks location in ^{1}H NMR spectra of all degraded samples was the same as for those of the samples before the degradation. New signals attributed to protons of hydroxyethyl terephthalate (3.97 ppm) and hydroxyethyl lactate (3.82 ppm) end group documented the lower molecular character of degraded samples.

During the bio/degradation aliphatic L sequences degraded more rapidly than the aromatic ones and consequently aromatic

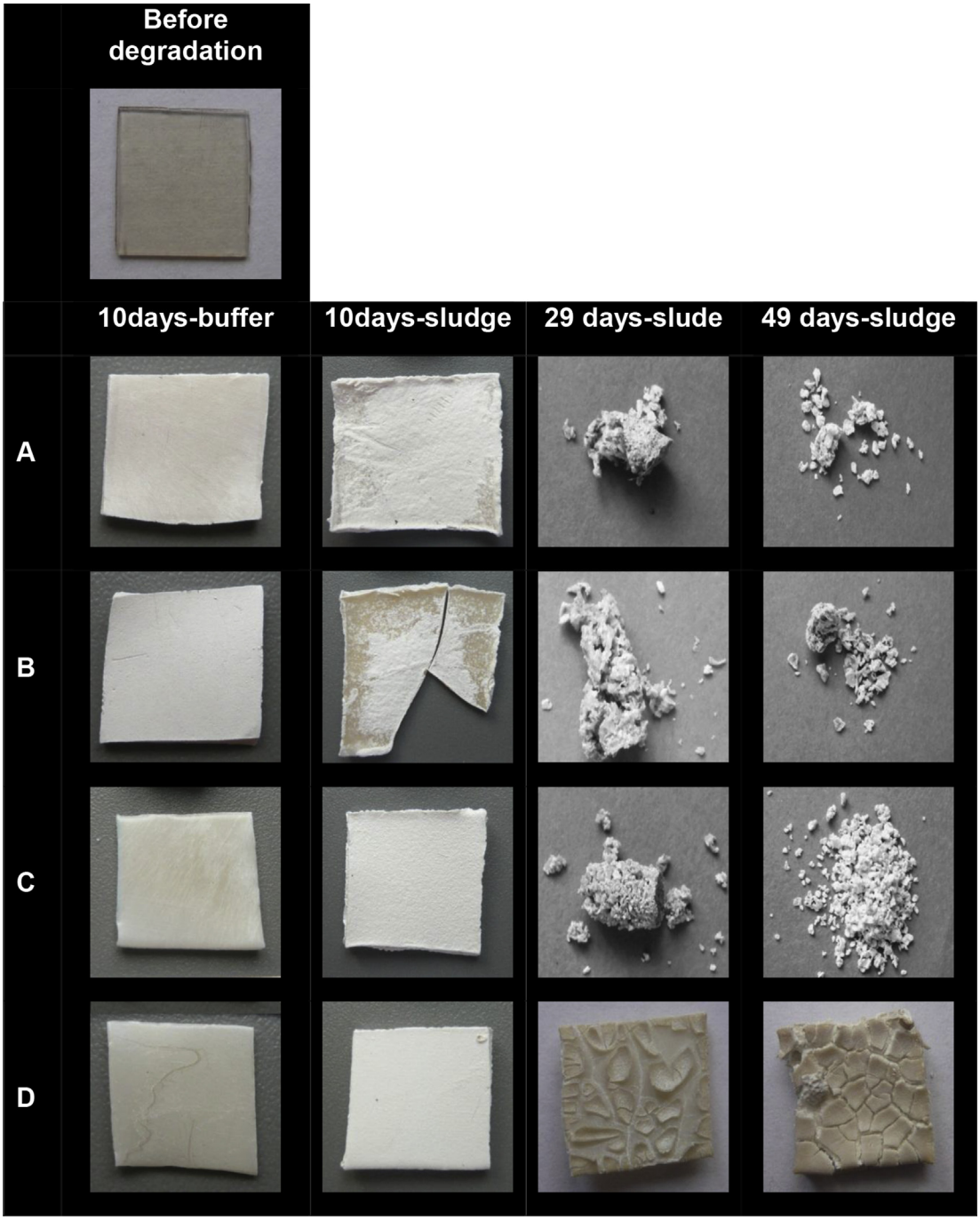

Fig. 6. Photographs of dried copolyester specimens before and after the degradation in sludge and phosphate buffer.

units' content and length increases (Table 2). Only the sample A, which was immersed for 29 days in sludge, showed reversely slight decrease in aromatic content from 59 to 63 mol % which could be caused by its limited solubility in chloroform used for NMR measurement.

To evaluate the changes in the structure of insoluble copolyesters obtained during long-term scale biodegradation in digested sludge (29, 49, and 78 days), solids remaining were characterized by ATR-FTIR analysis [3] (Fig. 7). Hydrolytic scission is again observed mainly in aliphatic L units as documented by a gradual decrease in intensity of the bands at 1750 (stretching vibrations of C═O of lactate aliphatic units), 1451 (bending vibrations of CH_3 of lactate units), and 1190 cm^{-1} (stretching vibrations of O–CO of lactate units) in the spectra of all copolyester samples, which were incubated in sludge for 29, 49, and 78 days.

Gradual increase in the intensity of peaks attributed to carboxyl (1612 cm^{-1}) and carboxylate (1580 cm^{-1}) end groups supported the occurrence of the ester bonds scission and lower molecular character of almost all samples incubated for 29 days and in the case of sample D for 78 days.

3.4.2. Thermal properties

The DTGA curve of original PET waste and reference PLLA, shows that the polymer decomposes in a single step with the maximum decomposition rate (T_{dm}) at 451 °C and 387 °C, respectively. As expected the incorporation of 59 and 40 mol % of L units into the

Table 4
Mass loss and molar masses of copolyesters after the incubation in digested sludge (29, 49, and 78 days) and phosphate buffer (29 days).[a]

Sample	Days	wt. loss (%)	pH change	M_n[b] (kg/mol)	Đ[b]	M_p[b](kg/mol)
A	0			11.0	3.6	35.2
	29-buffer	11	7.3	1.1	4.3	3.5
	29	90	7.5	2.8	3.1	7.5
	49	95	7.7	ins		
	78	96	7.7	ins		
B	0			9.4	3.3	29.8
	29-buffer	16	7.2	1.2	3.6	3.5
	29	79	7.5	2.6	3.6	8.4
	49	91	7.7	ins		
	78	97	7.6	ins		
C	0			9.3	3.2	28.1
	29-buffer	0	7.4	2.4	3.1	6.4
	29	82	7.6	4.2	3.4	12.5
	49	92	7.7	ins		
	78	93	7.6	ins		
D	0			10.7	3.2	32.7
	29-buffer	0	7.4	6.0	3.3	21.1
	29	16	7.7	3.9	4.0	15.9
	49	27	7.7	ins		
	78	31	7.7	ins		

[a] Conditions: abiotic phosphate buffer, initial pH 7.5, 55 °C, 29 days; digested sludge, initial pH 8.0, 55 °C, 29, 49, and 78 days.
[b] Number-average molar mass (M_n), molar mass at peak maximum (M_p), and dispersity ($Đ = M_w/M_n$) were determined by SEC according to the PS calibration; ins means insoluble sample in chloroform.

rigid PET chains influenced considerably their thermal degradation. Both resulting PET-*co*-PLA copolymers A and D exhibited two overlapping decomposition processes (Fig. 8). The first decomposition step, observed at temperature T_{dm1} 382 °C, is attributed to L units' degradation and the second one at temperature Td_{m2} 447 and 450 °C, respectively, is associated with *T* units' degradation.

Thermal stability of copolyester A in buffer and D in both buffer and sludge decreased as documented by the drop in $T_{5\%}$, $T_{10\%}$, and $T_{50\%}$ in comparison with original samples (Table 5). For sample D the changes in thermal behaviour induced by bio/degradation were relatively low in accordance with low mass loss. In the case of the sample A, degraded in sludge, shift in $T_{50\%}$ to higher temperature proves improved thermal stability in this temperature range.

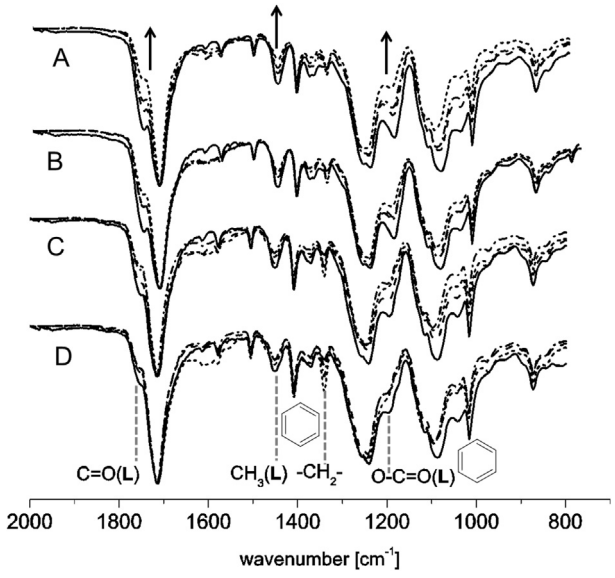

Fig. 7. ATR-FTIR spectra of copolyesters A–D before (solid) and after the biodegradation in sludge for 29 (dash), 49 (dash dot), and 78 days (short dash).

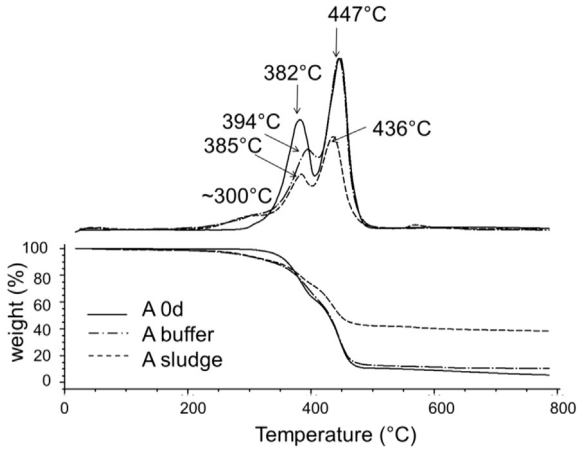

Fig. 8. TGA thermograms and the first derivatives (DTGA) of copolyester A before the degradation and those exposed to sludge and buffer for 29 days.

Table 5
The temperature range of representative copolyesters decomposition before and after their incubation in digested sludge and phosphate buffer.

Sample	Time of degradation (days)	$T_{5\%}$	$T_{10\%}$	$T_{50\%}$	Residue (%) at 800 °C
PET	0d	413	422	450	11
PLLA	0d	347	357	381	0
A	0d	346	361	429	10
	29d sludge	293	341	447	39
	29d buffer	290	335	430	12
D	0d	361	377	444	14
	29d sludge	352	375	442	14
	29d buffer	358	377	442	13

The three -step thermal decomposition was revealed for sample A degraded in both buffer and sludge. Probably low-molar-mass degradation products rich in L units thermally decompose already at 279 °C (sludge) and 318 °C (buffer) with 8 wt% loss. Thermal decomposition of L sequences in longer copolyesters' chains remaining after the biodegradation is observed at 385 °C, which are present in half proportion than in the sample before the degradation (19% *vs*. 38% wt. loss). Consequently, increased number of T–T linkages resulted in higher thermal stability of aromatic domains as documented by the shift in $T_{50\%}$ to higher temperature. Relatively high residue at 800 °C for biodegraded sample A (39%) is due to inorganic sludge particles which penetrated into the porous and swollen sample during incubation.

4. Conclusion

With the PET waste modification by L-lactic acid a random sequence distribution of the co-monomeric units along the polymeric chains was produced. Resulting copolyesters, in which aromatic units are linked to the aliphatic ones, were proved as materials more susceptible to hydrolytic degradation and/or biodegradation than PET waste. Copolyester mineralization yielded methane-rich biogas in 69% of theoretical amount for sample A and 34% for D. The anaerobic biodegradation rate of studied copolyesters decreased with higher starting content of aromatic sequences and their length in chains. It is worth mentioning, that beside soluble degradation intermediates, the formation of insoluble ones is also assumed. The biodegradability of these species based on aromatic trimers and higher *T* units' content oligomers is a matter of time necessary for their hydrolysis to dimers and

monomers. The biodegradability of aromatic oligomers and monomer mixtures was proved under sludge conditions.

Acknowledgement

The research was financially supported by the Ministry of Education of the Czech Republic, under the project no. MSM 6046137302 and MSM6046137308. The authors thank Lenka Malinová from the Department of Polymers, ICT Prague for the microscope imaging and Linda Mišková from Central laboratories, ICT Prague for IR spectra measurement. We also thank Veronika Kužníková and Lucie Větrovcová, ICT Prague for their help during the laboratory work.

Appendix A. Supplementary data

Supplementary data related to this article can be found at http://dx.doi.org/10.1016/j.polymdegradstab.2014.11.007.

References

[1] Sinha V, Patel M, Patel J. Pet waste management by chemical recycling: a review. J Polym Environ 2010;18:8–25.
[2] Ptiček Siročić A, Fijačko A, Hrnjak-Murgić Z. Chemical recycling of postconsumer poly(ethylene-terephthalate) bottles – depolymerization study. Chem Biochem Eng Q 2013;27:65–71.
[3] Grzebieniak K, Wesołowski J. Glycolysis of PET waste and the use of glycolysis products in the synthesis of degradable co-polyesters. FIBRES Text East Eur 2004;12:19–22.
[4] Acar I, Kaşgöz A, Özgümüş S, Orbay M. Modification of waste poly(Ethylene terephthalate) (PET) by using poly(L-lactic acid) (PLA) and hydrolytic stability. Polymer-Plastics Technol Eng 2006;45:351–9.
[5] Opaprakasit M, Petchsuk A, Opaprakasit P, Chongprakobkit S. Effects of synthesis conditions on chemical structures and physical properties of copolyesters from lactic acid, ethylene glycol and dimethyl terephthalate. eXPRESS Polym Lett 2009;3:458–68.
[6] Namkajorn M, AP, Opaprakasit M, Opaprakasit P. Synthesis and characterizations of degradable aliphatic-aromatic copolyesters from lactic acid, dimethyl terephthalate and diol: effects of diol type and monomer feed ratio. EXPRESS Polym Lett 2010;4:415–22.
[7] Olewnik E, Czerwiński W, Nowaczyk J, Sepulchre M-O, Tessier M, Salhi S, et al. Synthesis and structural study of copolymers of l-lactic acid and bis(2-hydroxyethyl terephthalate). Eur Polym J 2007;43:1009–19.
[8] Acar I, Pozan GS, Özgümüş S. Thermal oxidative degradation kinetics and thermal properties of poly(ethylene terephthalate) modified with poly(lactic acid). J Appl Polym Sci 2008;109:2747–55.
[9] Vitásek J, Šašek V, Prokopová I. PET from used beverage bottles: a material for preparation of biologically degradable copolyesters. J Polym Environ 2012;20:618–25.
[10] Olewnik E, Czerwiński W, Nowaczyk J. Hydrolytic degradation of copolymers based on l-lactic acid and bis-2-hydroxyethyl terephthalate. Polym Degrad Stab 2007;92:24–31.
[11] Prokopová I, Vlčková E, Šašek V, Náhlík J, Soukupová-Chaloupková V, Skolil J. Aromatic-aliphatic copolyesters based on waste poly(ethylene terephthalate) and their biodegradability. e-Polymers 2008;052:1–9.
[12] Tan L, Chen Y, Zhou W, Li F, Chen L, He X. Preparation and biodegradation of copolyesters based on poly(ethylene terephthalate) and poly(ethylene glycol)/oligo(lactic acid) by transesterification. Polym Eng Sci 2010;50:76–83.
[13] Abou-Zeid D-M, Müller R-J, Deckwer W-D. Biodegradation of aliphatic homopolyesters and aliphatic–aromatic copolyesters by anaerobic microorganisms. Biomacromolecules 2004;5:1687–97.
[14] Marten E, Müller R-J, Deckwer W-D. Studies on the enzymatic hydrolysis of polyesters. II. Aliphatic–aromatic copolyesters. Polym Degrad Stab 2005;88:371–81.
[15] Kleeberg I, Welzel K, VandenHeuvel J, Müller RJ, Deckwer WD. Characterization of a new extracellular hydrolase from thermobifida fusca degrading aliphatic–aromatic copolyesters. Biomacromolecules 2004;6:262–70.
[16] Turečková J, Prokopová I, Niklová P, Šimek J, Šmejkalová P, Keclík F. Biodegradable copolyester/starch blends—preparation, mechanical properties, wettability, biodegradation course. Polimery 2008;53:639–43.
[17] APHA-AWA-WPFC. Standard methods for the examination of water and wastewater. 20th ed. 1998. Washington D.C.
[18] Standardization IOf. Water quality — determination of the chemical oxygen demand index (ST-COD) — small-scale sealed-tube method. 2002.
[19] Buswell AM, Mueller HF. Mechanism of methane fermentation. Industrial Eng Chem 1952;44:550–2.
[20] Tessier M, Fradet A. Determination of the degree of randomness in condensation copolymers containing both symmetrical and unsymmetrical monomer units: a theoretical study. e-Polymers 2003;030:1–7.
[21] Wang H, Liu Y, Li Z, Zhang X, Zhang S, Zhang Y. Glycolysis of poly(ethylene terephthalate) catalyzed by ionic liquids. Eur Polym J 2009;45:1535–44.
[22] Sriromreun P, Petchsuk A, Opaprakasit M, Opaprakasit P. Standard methods for characterizations of structure and hydrolytic degradation of aliphatic/aromatic copolyesters. Polym Degrad Stab 2013;98:169–76.
[23] Venkata Mohan S, Lalit Babu V, Sarma PN. Anaerobic biohydrogen production from dairy wastewater treatment in sequencing batch reactor (AnSBR): effect of organic loading rate. Enzyme Microb Technol 2007;41:506–15.

J Mater Cycles Waste Manag (2018) 20:414–420
https://doi.org/10.1007/s10163-017-0595-3

ORIGINAL ARTICLE

Degradation of pet copolyesters under real and laboratory composting conditions

Magdalena Vaverková[1] · Dana Adamcová[1] · Lenka Kotrchová[2] · Jan Merna[2] · Soňa Hermanová[2]

Received: 10 February 2016 / Accepted: 31 January 2017 / Published online: 22 February 2017

Abstract The present work is aimed on the study of degradation of poly(ethylene terephthalate-*co*-lactate) copolyesters, prepared by chemical modification of PET waste beverage bottles using L-lactic acid, under laboratory (bioreactor) and natural (Central Composting Plant in Brno, Czech Republic) composting conditions. The structure of solid residues after degradation was analyzed by IR, NMR, thermogravimetric (TGA) methods, and size exclusion chromatography in chloroform and the residues rich on aromatic units were analyzed in $CHCl_3$/HFIP solutions. Sample with 57 mol% of aliphatic units showed the highest degree of degradation with mass loss of about 90% independently of composting conditions. The samples with 57 and 60 mol% of aromatic units reached 68 and 51% degradation in the compost pile and only 39 and 5% in laboratory bioreactor. Gravimetric analysis along with molar mass distribution measurement showed that laboratory-level composting study provides more consistent and defined results. However, it should be accompanied with tests performed under real conditions for the purpose of biodegradability evaluation of polymeric materials with varying composition.

Keywords PET waste · Copolyesters · Hydrolysis · Composting

Introduction

Aromatic polyester poly(ethylene terephthalate), PET, can be found in beverage plastic bottles, packaging films, fibers, and moulded articles with annual manufacture capacity over 50 Mtpy. The wide use of this material (along with a very slow rate of degradation) has resulted in the demand for the development of effective recycling and reprocessing technologies [1–3]. The chemical recycling approach, which is more sensitive to the contaminants in plastic waste, could lead to original feedstock monomers [4–6].

The transesterification reactions of PET with L-lactic acid, oligo(L-lactic acid), poly(L-lactic acid), PLA, or cyclic esters (lactones, lactides) resulted in materials, which possess acceptable mechanical properties and enhanced susceptibility to hydrolytic scission [7, 8]. Logically, the overall rate of degradation in resulting aliphatic–aromatic copolyester is governed by both the ratio of aliphatic to aromatic units, their distribution along the chain, the sequences' length, temperature and the environment. Increasing PLA, amount in the feed from 10 to 90 wt% with respect to PET afforded PET-*co*-PLA copolyesters prone to more extensive hydrolytic degradation with mass loss from 1.3 to 49.0% during samples' 28-day incubation in phosphate buffer (pH 7.2) at 60 °C [8]. Random copolyesters obtained by modification of PET waste with L-lactic acid were found to be susceptible to biodegradation and hydrolytic scission under thermophilic sludge conditions

This paper is dedicated to the memory of the late Assoc. Prof. Irena Prokopová.

Electronic supplementary material The online version of this article (doi:10.1007/s10163-017-0595-3) contains supplementary material, which is available to authorized users.

✉ Soňa Hermanová
sona.hermanova@vscht.cz

[1] Department of Applied and Landscape Ecology, Faculty of Agronomy, Mendel University in Brno, Zemědělská 1, 613 00 Brno, Czech Republic

[2] Department of Polymers, Faculty of Chemical Technology, University of Chemistry and Technology Prague, Technická 5, 16628 Prague, Czech Republic

[9]. The presence and activity of thermophilic extracellular hydrolyses significantly contributed to hydrolytic scission in chains which has positive impact on the biodegradation of degradation products with the evolution of biogas.

To obtain more comprehensive picture of degradation behavior, poly(ethylene terephthalate-*co*-lactate) samples were incubated under real and laboratory composting conditions and the solid residues were subjected to structural and thermal analysis. The study of (bio)degradation of modified PET waste is important for understanding mechanisms operating in various biological environments and also for evaluating laboratory tests, which asses degradability of polymeric materials. PET waste was proved as a material inert to a degradation under composting conditions [10].

Experimental part

Materials

Three poly(ethylene terephthalate-*co*-lactate) samples with aromatic T units content of 43, 57, and 60 mol% were prepared according to published procedure [11]. For the purpose of degradation study, the square specimens with a dimension of 50 × 50 × 0.9 mm were sectioned from films. These films were obtained by neat samples pressing at softening temperature (temperature 105 °C, 3 min, pressure 0.35 MPa).

Composting

Composting was performed in the Central Composting Plant in Brno, Czech Republic (details about the composting clamps are given in Online Resource 1). The sum of daily precipitation amounts for this period was 75.9 mm (daily precipitation amounts for the experimental period is presented in Online Resource 2). The data were kindly provided by the branch of the Czech Hydrometeorological Institute (CHMI) in Brno-Tuřany. The pH value of soil in the compost pile was measured at different locations at the beginning of composting experiment and was in the range of 6–9. For the purpose of pH measurement, water extracts of the compost soil were prepared by shaking the fresh sample with distilled water (1:10 w/v) for 1 h, and then filtered. The pH value of extracts was measured by pH meter with a standard electrode.

Composting (aerobic degradation experiment) in the laboratory scale was performed according to ČSN EN 14,806 Norm [12] in an air circulation oven (composting bioreactor—ECOCELL 22) at a constant temperature of 58.0 °C (±2 °C) [13, 14]. Concretely, polypropylene vessels (300 mm × 200 mm × 100 mm) were filled with composting mass to 90% of their volume. The compost used corresponded to 3-month-old mature compost, which was provided by a full-scale aerobic composting plant located in Brno-Černovice (Czech Republic). The characteristics of the compost are summarized in Table 1.

After 3 weeks all samples were removed from the compost, carefully rinsed with distilled water and dried until constant weight under vacuum.

Incubation in abiotic buffer

Preliminary aging test of the specimens in the phosphate buffer (pH 7.0) at 58 °C for 21 days did not result in measurable mass loss or decrease in molar mass distribution. Considering alkaline sensitivity of polyesters, alkaline borate buffer was used as aging medium to accelerate abiotic hydrolysis process. The copolyesters' specimen was immersed in alkaline borate buffer (pH 8.0) at 58 °C for 21 days. After incubation, samples were rinsed with distilled water and dried under vacuum until constant mass.

Characterization of the samples

For the DSC experiments, DSC Q100 (TA Instruments) was used. The samples were heated from 0 to 300 °C and cooled to 0 °C at a rate of 5 °C/min under nitrogen (50 mL/min). Thermogravimetric analysis was carried out using a thermal analyzer TGA Q500 (TA Instruments, USA). The samples were scanned from room temperature to 800 °C at heating rate of 20 °C/min under nitrogen atmosphere.

Table 1 Characteristics of the compost before the beginning of laboratory composting experiment

Parameters	Value	Unit
Moisture	30–65	(%)
Combustibles	Min. 20	(%)
Total nitrogen	Min. 0.6	(% DM)
pH	6.0–8.5	
Undecomposable ingredients	Max. 2.0	(%)
C:N	Max. 30	
Cd	2	(mg kg^{-1})
Pb	100	
Hg	1	
As	20	
Cr	100	
Mo	20	
Ni	50	
Cu	150	
Zn	600	

DM dry matter

ATR-FTIR spectra were collected on FTIR spectrometer Nicolet 6700 (Thermo Scientific, USA) equipped with a diamond crystal GladiATR (PIKE Technologies, USA). The spectra were measured with a resolution of 4 cm^{-1} in the range of 4000–400 cm^{-1} (64 scans) and corrected against a background spectrum of air.

^{1}H NMR spectra were measured on NMR Spectrometer Bruker Avance DRX 500, with $CDCl_3$ and DMSO, respectively, as the solvent and tetramethylsilane (TMS) as the internal standard. For copolyesters, insoluble in $CDCl_3$, $CDCl_3/CF_3COOH$ was used as the solvent. The character of structures present in copolyesters agreed with the respective monomeric units reported in the study of Olewnik et al. [15].

The apparent average molar masses (M_n, M_w) and dispersities ($Đ$) of polyesters soluble in $CHCl_3$ were determined by a size exclusion chromatograph (SEC chromatograph) with RI detector (P102 pump, Watrex; RI2000, Schambeck). Separation was performed on one Polymer Laboratories Mixed C column (5 µm, 7.8 × 300 mm) at 35 °C in chloroform at an elution rate of 1 mL/min. Copolyesters insoluble in $CHCl_3$ were analyzed using SEC with UV detection (Waters 515 pump, ECOM LCD 2082 UV detector, PL Mixed C column 8 × 300 mm) in $CHCl_3$/1,1,1,3,3,3-hexafluoroisopropylalcohol (HFIP) 98/2 v/v as a mobile phase at flow rate 1 mL/min according to literature [16]. Samples solutions were prepared by dissolution of about 3 mg of copolyester in 60 µl of neat HFIP followed by dilution to 3 mL with $CHCl_3$ (sample concentration was approx. 1 mg/mL) and filtration through 0.45 µm PTFE filter. Injection volume was 20 µL. In both SEC methods relative calibration using narrow PS standards (580–3,250,000 g/mol) was used to calculate apparent molar masses. Data were evaluated using Clarity 5.0 data processing software.

Surface morphology of polyesters coated by 5 nm gold was evaluated by Vega Tescan SEM microscope.

The mass loss of degraded films was calculated according to the relationship as follows:

Mass loss (%) $= (m_0 - m_d)/m_0 \times 100$, where m_0 means initial mass of the film, and m_d denotes the mass of the dried film after the degradation study. The results are expressed as averages of mass losses determined for three composted samples with the same composition.

Results and discussion

The rate of copolyesters specimens' hydrolysis and biodegradation

In composting conditions, abiotic factors including elevated temperature, moisture, and pH value are supposed to favor random abiotic hydrolytic scission of copolyesters' chains. To reveal the impact of such hydrolytic scission on whole degradation process the specimens were incubated in borate buffer for 3 weeks. During this period namely the longest chains were cleaved as documented by the reduction in M_w from 17 (60 mol% of aromatic units) to 50% (43 mol% of aromatic units) along with narrowing of molar mass distribution (Table 2).

Table 2 Mass loss and changes in molar mass of PET copolyesters after 21 days of composting and immersion in buffer

Copolymer[a]	Mass loss[b] (%)	M_n[c] (g/mol)	$Đ$[c]
T:L (43:57)	–	9400	3.3
Compost pile	92 ± 11	NA	NA
Lab compost	89 ± 1	2900	3.4
Buffer	6	5400	2.8
T:L (57:43)	–	9300	3.2
Compost pile	68 ± 17	790[d]	3.2[d]
Lab compost	39 ± 4	3900	2.8
Buffer	0.2	8300	2.8
T:L (60:40)	–	10,700	3.2
Compost pile	51 ± 10	920[d]	3.6[d]
Lab compost	5 ± 1	5600	2.9
Buffer	0.1	10,200	2.8

NA not analyzed due to insufficient amount of sample

[a]Composition of a copolymer: *T* terephthalate units, *L* lactate units

[b]Mass loss is calculated according to the equation as follows: $\left(\frac{m_0 - m_d}{m_0}\right) \times 100$, where m_0 means mass of the film before experiment and m_d means mass of the dried sample after the composting

[c]Apparent number-average molar mass and dispersity (M_w/M_n) determined by SEC analysis in $CHCl_3$

[d]Determined by SEC analysis in HFIP/$CHCl_3$

The samples composted under lab conditions showed higher reduction in molar mass followed by the samples buried in compost pile. Comparable reduction in M_n and M_w by 50 (60 mol% of aromatic units) to 70% (43 mol% of aromatic units) suggests that the degradation took place both randomly and from the end of the copolyesters chains.

Direct comparison of molar mass changes was complicated in the case of solid residues after the incubation in compost pile since they become insoluble in chloroform. Consequently, HFIP/chloroform mixture was examined as the solvent for these samples and the eluent to perform SEC analysis. Despite possible influence of the used SEC method on obtained molar mass values (and therefore their higher scattering), both M_n and M_w were comparably reduced by about 90% (samples with 57 and 60 mol% of aromatic units). Similar pattern of molar mass reduction of samples composted in the laboratory and in the pile could indicate similar processes of hydrolytic scission in copolyesters chains, which is reasonably faster in compost pile.

The mass loss of composted specimens, providing indirect information on the degradation rate, generally increased with a decrease in the starting content of aromatic units in the copolyesters' chains under all incubation conditions. Considerable higher mass losses of composted samples in comparison with those exposed to abiotic aging are ascribed to microbial and enzymatic activity in addition to abiotic hydrolysis. The sample rich in aliphatic units (57 mol%), which was found as the most prone to abiotic hydrolysis, was seemingly degraded in the same extent under both composting conditions with mass loss of about 90%.

On the other hand, the degradability of samples rich in aromatic units (57 and 60 mol%) was significantly dependent on composting conditions.

It is well known, that various microbial communities prevail during the different phases of composting [17]. Composting phases, occurring naturally under real conditions, impacted the abundance and activity of specific microbial community in comparison with that grown in laboratory compost, where constant abiotic conditions (temperature, humidity and aeration) were maintained during the whole incubation. On the base of our results, the biotic factors acting in real compost are suggested to accelerate the hydrolytic scission of resistant copolyesters, rich in aromatic units, more than those in laboratory compost. On the other hand the test performed under laboratory conditions yielded more reproducible results.

Structural and thermal analysis of remaining solids

To reveal the changes in composted copolyesters' microstructure, the *T:L* composition, average sequence lengths (Y_L, X_{ET}), number-average sequence length ($L_{n,L}$, $L_{n,ET}$), and degree of randomness (B) were calculated according to ^{1}H NMR spectra of samples by applying the method of Tessier and Fradet [18]. Results on the copolyesters' composition are summarized in the Table 3.

After 21-day composting the content of lactate units (L) was reduced for all composted samples, which implies that the hydrolysis of ester bonds occurred mainly in L units. Correspondingly, the values of Y_L and $L_{n,L}$ dropped, whereas the aromatic units' sequence length (X_{ET}) increased. The presence of long aromatic sequences interrupted by only one L unit or very short L sequences in the chains led to the insolubility of degraded solids with 75 mol% of T units in chloroform, therefore their NMR spectra were acquired in $CDCl_3/CF_3COOH$ mixture. It is worth noting that the analysis was performed immediately after the samples dissolving to avoid esterification between hydroxyl end groups and CF_3COOH acid.

ATR-FTIR spectroscopic analysis of the solid residues confirmed considerable changes in copolyesters' microstructure induced by hydrolytic scission. The intensity of lactate units signals (1750, 1451, 1190 cm^{-1}) dropped and the decrease was pronounced for samples degraded in real conditions, for which a new band at 1614 cm^{-1} (asymmetric un-protonated carboxylate group stretching) evidenced their low-molar-mass character (Fig. 1a).

To gain a better insight on the microstructure of solid residues remaining after composting ATR-FTIR spectra were normalized in the region from 1500 to 1300 cm^{-1} taking the band at 1409 cm^{-1} (aromatic ring vibrations) as the reference one (Fig. 1b). On comparing the spectra it is clearly seen that after the incubation of all samples the intensity of the band at 1340 cm^{-1} grown, whereas the intensity of the band at 1370 cm^{-1} (or 1386/1370 cm^{-1}) decreased.

The band at 1340 cm^{-1} is ascribed to the vibrations of ethylene glycol unit (CH_2 wagging) adopting *trans*

Table 3 Changes in the *T:L* composition, average sequence lengths, number-average sequence length, and degree of randomness of PET copolyesters before and after composting

Sample denotation	Composition[a]	Sequential length[b]		Number-average sequential length[b]		Degree of randomness[b]
	(*T:L*)	Y_L	X_{ET}	$L_{n,L}$	$L_{n,ET}$	B
T:L (43:57)	43:57	1.9	1.9	1.9	2.8	0.90
Compost pile	59:41	1.7	2.7	1.4	4.0	0.95
Lab compost	59:41	1.7	3.1	1.7	5.0	0.78
T:L (57:43)	57:43	1.8	2.9	1.6	4.2	0.86
Compost pile	75:25	1.3	5.5	1.0	5.9	1.19
Lab compost	58:42	1.7	3.1	1.7	4.8	0.81
T:L (60:40)	60:40	1.7	3.5	1.4	4.2	0.94
Compost pile	75:25	1.2	5.5	1.0	6.0	1.16
Lab compost	66:34	1.6	3.6	1.6	6.0	0.81

21 days of composting

[a]Determined by ^{1}H NMR spectroscopic analysis; *T* terephthalate units, *L* lactate units

[b]Calculated according to literature from ^{1}H NMR data [18]

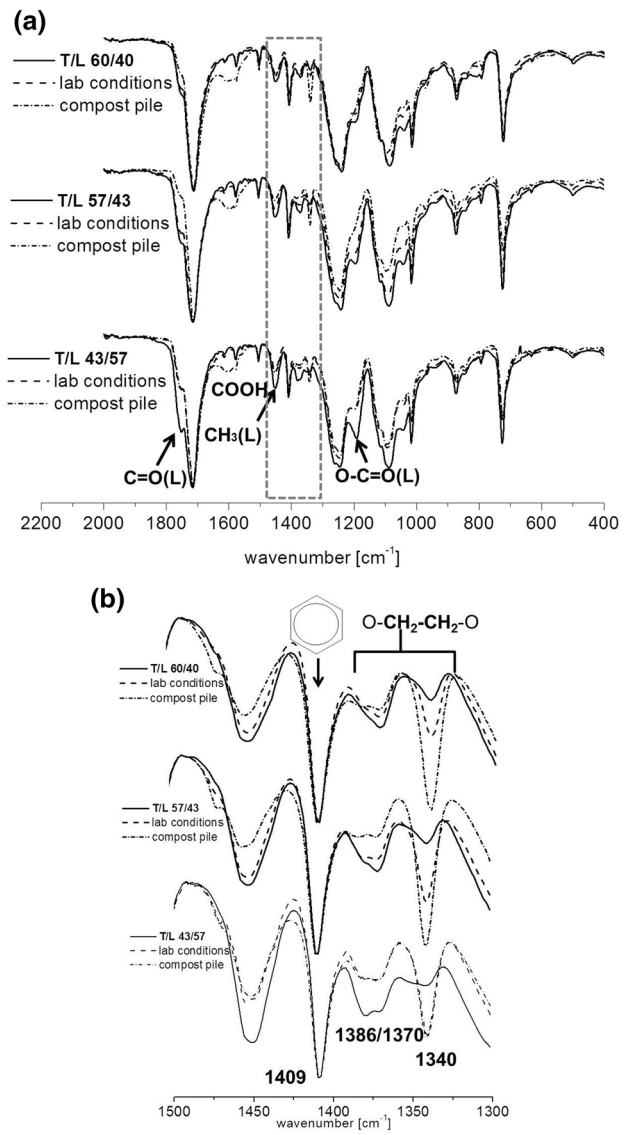

Fig. 1 ATR-FTIR spectra of copolyesters before and after performing the composting test (**a**) ATR-FTIR spectra in the 1500–1300 cm^{-1} region normalized to the band at 1409 cm^{-1} (**b**)

conformation, whereas that at 1370 cm^{-1} corresponds to the vibration of the same unit in gauche conformation. The changes in the intensity of these bands were reported to be connected with the reorientation of PET chains and a generation of crystalline domains from the amorphous ones [19]. Thus, the formation of crystalline domains due to resulting longer T sequences, approaching the structure of original PET waste, could be the reason for the insolubility of the particular degraded samples.

In addition to changes in samples' microstructure, the occurrence of degradation process was evidenced also by the surface defect of composted samples in comparison with smooth surface of the sample before composting (SEM micrographs of representative samples are presented in Online resource 3).

Changes in copolymers' thermal properties induced during the incubation in compost were studied by DSC and TGA analyses. Almost all composted copolyesters displayed broad endothermic peaks with maxima around 100 °C (43 mol% of aliphatic units) and between 150 and 200 °C (57 and 60 mol% of aromatic units) (Thermal properties of copolyesters and reference polyesters are summarized in Online Resource 4). In accordance with IR spectroscopic interpretation this documents the presence of crystallizable domains, which amount is dependent on the sample actual composition induced by the degradation conditions.

TGA analysis revealed that all prepared copolymers show a two-step decomposition with the remaining mass of about 5–14% at 800 °C. Thermal degradation of sequences rich in aliphatic units was observed at the temperature range 381–384 °C as for the reference PLA the main degradation occurred at 387 °C. The second degradation step, which took place in the temperature range 446–450 °C, is attributed to domains consisting mainly of T units. TGA thermograms and their first derivatives (DTGA) of representative copolyester and reference homopolymers are shown in Fig. 2a.

Temperatures corresponding to 5% mass loss ($T_{5\%}$), 10% mass loss ($T_{10\%}$) and 50% mass loss ($T_{50\%}$) were determined from the TGA curves and are presented in the Table 4.

For all composted samples an initial mass loss temperature ($T_{5\%}$) is shifted to lower temperatures. This could be ascribed to the thermal degradation of low-molar-mass fractions of degraded samples. Consistently with previous spectroscopic results a drop in L units' mass percentage was considerably higher in the samples buried in compost pile as compared to those incubated under laboratory conditions. The most significant reduction of aliphatic units was documented by almost one-step decomposition pattern of degraded samples with starting 57 and 60 mol% of aromatic units (Fig. 2b). For all composted samples the increase in remaining mass at 800 °C is suggested to be due to the presence of soil particles from compost media embedded in the copolymer bulk.

It could be concluded that considerable changes in the samples' microstructure and thermal properties bring evidence on the preferential cleavage of aliphatic ester bonds in copolyesters' chains.

Conclusion

Laboratory compostability testing, used in this study, enabled reproducible evaluation of degradation of poly(ethylene terephthalate-*co*-lactate) copolyesters with

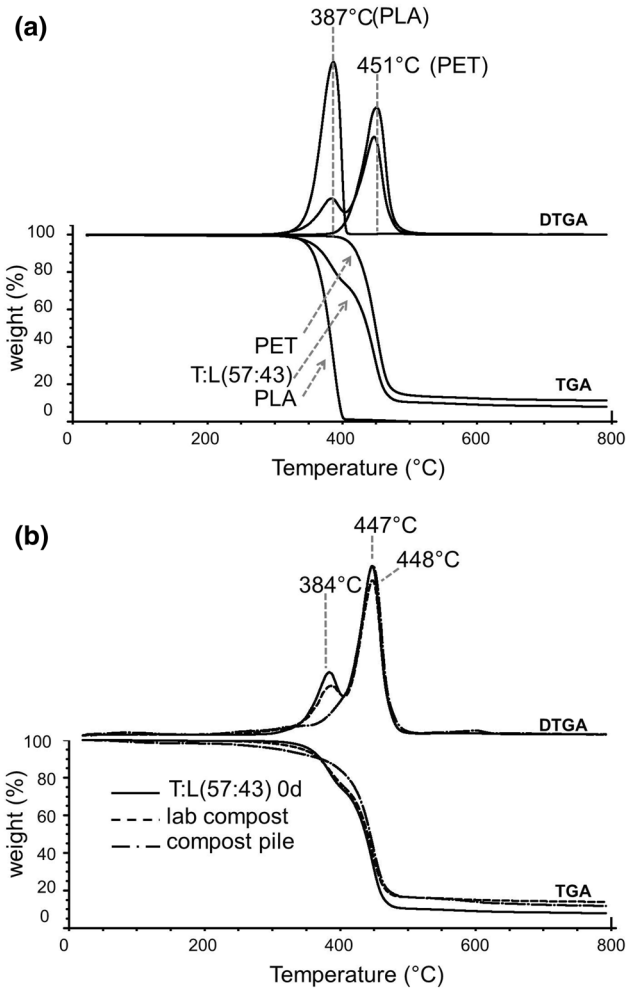

Fig. 2 TGA thermograms and their first derivatives of representative copolyester with 57 mol% of aromatic units and reference homopolymers (**a**), of this copolymer and the solid residues after incubation in compost (**b**)

Table 4 The temperature range of the copolyesters' decomposition

Sample[a]	$T_{5\%}$	$T_{10\%}$	$T_{50\%}$	Residue (%) at 800 °C
T:L (43:57)	346	361	428	5
Compost pile	342	367	439	5
Lab compost	340	367	440	12
T:L (57:43)	356	371	438	8
Compost pile	311	369	445	12
Lab compost	345	369	441	14
T:L (60:40)	361	377	444	14
Compost pile	315	376	445	16
Lab compost	352	373	441	12

[a]Copolyester composition: *T* terephthalate units, *L* lactate units

43, 57, and 60 mol% of aromatic units. In the compost pile, where real environmental conditions and treatment period play an important role, the degradation of resistant copolyesters (i.e. those with 57 and 60 mol% of aromatic units) proceeded to much higher degree than in the composting bioreactor.

Principally, hydrolytic scission of preferentially aliphatic ester bonds in the copolyesters' chains was the main degradation mechanism taking place during the samples incubation at both composting conditions. Solid residues remained, typically in the compost pile, had increased aromatic character resulting in their insolubility in chloroform. However, the molar mass of these residues was significantly decreased as determined by SEC in $CHCl_3$/1,1,1,3,3,3-hexafluoroisopropylalcohol.

Acknowledgements Authors thank to specific University Research No. 20/2015 for financial support.

References

1. Burat F, Güney A, Olgaç Kangal M (2009) Selective separation of virgin and post-consumer polymers (PET and PVC) by flotation method. Waste Manag 29:1807–1813. doi:10.1016/j.wasman.2008.12.018
2. Sinha V, Patel M, Patel J (2010) Pet waste management by chemical recycling: a review. J Polym Environ 18:8–25. doi:10.1007/s10924-008-0106-7
3. Zhang H, Wen Z-G (2014) The consumption and recycling collection system of PET bottles: a case study of Beijing, China. Waste Manag 34:987–998. doi:10.1016/j.wasman.2013.07.015
4. Khoonkari M, Haghighi AH, Sefidbakht Y, Shekoohi K, Ghaderian A (2015) Chemical recycling of PET wastes with different catalysts. Int J Polym Sci 2015:1–11. doi:10.1155/2015/124524
5. Shukla SR, Harad AM, Jawale LS (2008) Recycling of waste PET into useful textile auxiliaries. Waste Manag 28:51–56. doi:10.1016/j.wasman.2006.11.002
6. George N, Kurian T (2014) Recent developments in the chemical recycling of postconsumer poly(ethylene terephthalate) waste. Ind Eng Chem Res 53:14185–14198. doi:10.1021/ie501995m
7. Vitásek J, Šašek V, Prokopová I (2012) PET from used beverage bottles: a material for preparation of biologically degradable copolyesters. J Polym Environ 20:618–625. doi:10.1007/s10924-012-0423-8
8. Acar I, Kaşgöz A, Özgümüş S, Orbay M (2006) Modification of waste poly(ethylene terephthalate) (PET) by using poly(l-lactic acid) (PLA) and hydrolytic stability. Polym Plast Technol Eng 45:351–359. doi:10.1080/03602550600553267
9. Hermanová S, Šmejkalová P, Merna J, Zarevúcka M (2015) Biodegradation of waste PET based copolyesters in thermophilic anaerobic sludge. Polym Degrad Stab 111:176–184. doi:10.1016/j.polymdegradstab.2014.11.007
10. Ki HC, Ok Park O (2001) Synthesis, characterization and biodegradability of the biodegradable aliphatic–aromatic random copolyesters. Polymer 42:1849–1861. doi:10.1016/S0032-3861(00)00466-3
11. Turečková J, Prokopová I, Niklová P, Šimek J, Šmejkalová P, Keclík F (2008) Biodegradable copolyester/starch blends—preparation, mechanical properties, wettability, biodegradation course. Polimery 53:639–643

12. Standardization IOf. ČSN EN 14806 Norm (2006) Packaging—preliminary evaluation of the disintegration of the packaging materials under simulated composting conditions in a laboratory scale test
13. Vaverková M, Toman F, Adamcová D, Kotovicová J (2012) Study of the biodegrability of degradable/biodegradable plastic material in a controlled composting environment. Ecol Chem Eng S 19:347–358. doi:10.2478/v10216-011-0025-8
14. Adamcová D, Vaverková M, Daria, Hermanová S, Voběrková S (2015) Ecotoxicity of composts containing aliphatic–aromatic copolyesters. Pol J Environ Stud 24:1497–1505. doi:10.15244/pjoes/31227
15. Olewnik E, Czerwiński W, Nowaczyk J, Sepulchre M-O, Tessier M, Salhi S et al (2007) Synthesis and structural study of copolymers of l-lactic acid and bis(2-hydroxyethyl terephthalate). Eur Polym J 43:1009–1019. doi:10.1016/j.eurpolymj.2006.11.025
16. Weisskopf K (1988) Characterization of polyethylene terephthalate by gel permeation chromatography (GPC). J Polym Sci Part A Polym Chem 26:1919–1935. doi:10.1002/pola.1988.080260718
17. Bågstam G (1978) Population changes in microorganisms during composting of spruce-bark. Eur J Appl Microbiol 5:315–330
18. Tessier M, Fradet A (2003) Determination of the degree of randomness in condensation copolymers containing both symmetrical and unsymmetrical monomer units: a theoretical study. e-Polymers 030:1–7. doi:10.1515/epoly.2003.3.1.391
19. Rusu E, Drobota M, Barboiu V (2008) Structural investigations of amines treated polyester thin films by FTIR-ATR spectroscopy. J Optoelectron Adv M 10:377–381

Pol. J. Environ. Stud. Vol. 24, No. 4 (2015), 1497-1505
DOI: *10.15244/pjoes/31227*

Original Research

Ecotoxicity of Composts Containing Aliphatic-Aromatic Copolyesters

Dana Adamcová[1], Magdalena Daria Vaverková[1]*, Soňa Hermanová[2], Stanislava Voběrková[3]

[1]Department of Applied and Landscape Ecology, Faculty of Agronomy, Mendel University in Brno, Zemědělská 1, 61300 Brno, Czech Republic
[2]Department of Polymers, Faculty of Chemical Technology, University of Chemistry and Technology Prague, Technická 5, 16628 Prague, Czech Republic
[3]Institute of Chemistry and Biochemistry, Faculty of Agronomy, Mendel University in Brno, Zemědělská 1, 61300, Czech Republic

Received: 6 August 2014
Accepted: 23 September 2014

Abstract

The eco-toxicological impact of copolyesters during composting was evaluated by plant growth tests with cress (*Lepidium sativum*) and barley (*Hordeum vulgare*). The research was conducted to determine if PET beverage bottles modified by lactic acid (copolyesters) and products of their biodegradation would affect compost. The results demonstrate that the composts on which the examined materials were degrading were not toxic to the plants. Compared to the reference sample, the germination and growth of plants were stimulated. The plants showed an increase in plant biomass. Changes in appearance, retarded growth, or necrotic changes were not observed. The resulting compost did not exhibit any unfavorable influence on compost quality, and the products of degradation affected the growth and development of plants positively.

Keywords: biodegradable plastics, compost, phytotoxicity, *Lepidium sativum*, *Hordeum vulgare*

Introduction

Synthetic polymers are recognized as major solid waste environmental pollutants. Many synthetic polymers, resistant to chemical and physical degradation, are produced and utilized. They present disposal problems when their usefulness ceases. For plastic wastes, an alternative method of disposal is biodegradation [1]. Biodegradation concerns specially designed so-called biodegradable polymers [2]. Increasing amounts of synthetic polymers produce results in increasing interest in polymer biodegradation. The recent incorporation of biological waste treatment in an integrated approach to solid waste management has resulted in a growing commercial interest in the development of biodegradable materials for consumer products [1, 3]. Biodegradable plastics can decompose into carbon dioxide, methane, water, inorganic compounds, or biomass via microbial activities within the natural environment [4]. Biodegradable plastics are designed to degrade under environmental conditions or in municipal and industrial biological waste treatment facilities [5].

Biodegradation of plastics depends on both the environment in which they are placed and the chemical nature of the polymer. There are different mechanisms of polymer biodegradation. The process of polymer biodegradation is affected by many factors [6].

The problem of degradation of biodegradable plastics in environmental conditions has aroused increasing interest, thereby forcing new studies on the behavior of many materials in different environments [7-11].

Composting is one of the oldest methods for processing organic waste, and today this process is more and more

*e-mail: magda.vaverkova@uake.cz

often taken into consideration in waste management strategies [12]. In many European countries the controlled biological treatment of solid waste is considered to be a suitable waste management method. Space for landfill is scarce and therefore expensive in many industrial countries, and biotreatment is a much cheaper alternative. Not only green waste from gardens or biowaste from kitchens can be treated, but any compostable material is in principle suitable, e.g., waste from the food industry or packaging materials made from paper, cardboard, wood, or biodegradable plastics, when not recyclable in other ways. Besides natural materials, synthetic material also can be recycled through composting, if its compatibility with this system is proved [13].

Interest in the ecological effects of composting has been growing recently [13]. Compost is the immediate substrate for cultivated plants, and its properties may limit or stimulate plant development, particularly at the early stages of their growth [12].

International and national quality requirements define that compost shall not contain any environmentally harmful substances. Quality requirements for the compostability of biodegradable materials presuppose that the product does not include any harmful substances or degradation products derived from composted materials. The relative environmental safety of biodegradable plastic materials should be an important consideration during the development stages of these products [13].

Research on ecotoxicity of compost make use of organisms belonging to various taxonomic groups and representing all links of the trophic chain, i.e. bacteria (destructans), plants (producers), and invertebrates (consumers) [13]. Investigations conducted using biotests allow for a general assessment of quality of compost on the basis of a living organism's (bioindicator) response. The response comprises aggregate activities of all substances contained in a given material and shows interactions between them. Such an approach allows us to determine the potential influence of composts on the soil environment. The use of an appropriate set of biotests enables assessment of environmental risks connected with the application of composts prepared from various wastes.

Biological and chemical properties of composts are modified through components used for their preparation and processes occurring during preparation. Especially the use of waste components entails a risk of inappropriate course of the composting process or obtaining a poor-quality product. Therefore, biodegradable polymer wastes introduced into the environment should raise interest. Supporting substances used for their production or compounds formed during the composting process may either inhibit or stimulate plant growth. The degree of hazard may be different and, as in the case of compost salinity, some of the unfavorable effects of such material applications may be eliminated by dissolving them in soil [14]. However, it requires knowledge of not only the level of biodegradability of polymers but also other outcomes of their application, including those resulting from their biological properties.

It is clearly important to study the impact of biodegradable polymers on waste management so as to realize the truth benefit and the need to establish an adequate waste management system and legislation. The research was conducted to determine if PET beverage bottles modified by lactic acid (copolyesters with random microstructure) would affect select biological properties of compost. Research works on the use of biotest set for the estimation of compost toxicity are scarce [12, 15-17]. On the other hand, there are numerous papers dealing with the use of various plant species in estimation of compost phytotoxicity [18-21]. Measurement of seed germination and root growth are the parameters most often used in the assessment of compost toxicity [13]. In the presented investigations the phytotoxicity of compost was estimated by means of a set of biotests using two test organisms. The eco-toxicological impact of model aliphatic-aromatic copolyesters-poly(ethylene terephthalate-co-lactate)s during composting was evaluated by plant growth tests with cress (*Lepidium sativum*) and barley (*Hordeum vulgare*).

Experimental Procedures

Materials

Poly(ethylene terephthalate) was obtained from colorless beverage bottles, which were carefully washed and cut into flakes. L-lactic acid (85 % aqueous solution) obtained from Sigma-Aldrich and zinc acetate dihydrate from Fluka AG were used as received.

The investigated materials were prepared according to published procedure [22]. ^{1}H NMR analysis confirmed the random microstructure of copolyesters prepared. Concretely, four synthesized poly(ethylene terephthalate-*co*-lactate) copolyesters consisted in 41 mol % (sample A), 43 mol % (sample B), 57 mol % (sample C), and 60 mol % (sample D) of aromatic T units, and corresponding aliphatic L units were selected. Films were prepared by pressing of copolyester samples at the temperature of material softening. Square specimens with dimension of 50×50×0.9 mm, sectioned from films, were used for the phytotoxicity experiment.

Disintegration Tests

The disintegration degree of the copolyester specimens obtained was evaluated following modified version of ČSN EN 14806 Norm "Packaging – Preliminary evaluation of the disintegration of packaging materials under simulated composting conditions in a laboratory scale test" and a modified version of ČSN EN ISO 20200 "Plastics – Determination of the degree of disintegration of plastic materials under simulated composting conditions in a laboratory-scale test" (ISO 20200:2004). The materials were mixed with compost and subjected to aerobic degradation. This modification was undertaken in order to bring the test nearer to real conditions.

Table 1. Characteristics of the compost [9].

Parameters	Value	Unit
Moisture	30-65	%
Combustibles	min. 20	%
Total nitrogen	min. 0.6	% DM*
pH	6.0-8.5	-
Undecomposable ingredients	max. 2.0	%
C:N	max. 30	-
Cd	2	mg/kg
Pb	100	mg/kg
Hg	1	mg/kg
As	20	mg/kg
Cr	100	mg/kg
Mo	20	mg/kg
Ni	50	mg/kg
Cu	150	mg/kg
Zn	600	mg/kg

* %DM – % dry matter

For each tested material two reactors were prepared. The authors modified the procedure stated in the Norm and filter paper was used in order to safeguard the presence of suitable conditions for biodegradation. The compost used corresponded to three-month-old mature compost, which was provided by a full-scale aerobic composting plant located in Brno-Černovice (Czech Republic). The characteristics of the compost used are shown in Table 1.

The disintegration experiments were carried out with four types of samples: copolyesters A, B, C, and D. In addition, a reactor containing compost without plastic pieces but with cellulose filter paper was prepared (reference mixture).

The copolyesters and reference materials were used for degradation experiments in the same form as square specimens with dimensions of 50×50×0.9 mm. Copolyester specimens (2.206 g of copolyester A, 3.024 g of copolyester B, 3.099 g of copolyester C and 3.208 g of copolyester D) were mixed with $500 \cdot 10^{-3}$ kg of compost and put into a polypropylene reactor. The polypropylene vessels of 300 mm×200 mm×100 mm (length, width, height) were sealed to avoid excessive evaporation and 5 mm diameter holes at the center of each 100 mm side served for air exchange.

The aerobic degradation was carried out in an air circulation oven (composting bioreactor) at a constant temperature of 58.0ºC (±2ºC). The duration of the incubation was three weeks. During this time, moisture, mixing, and aeration of the samples were periodically controlled. The sample weight loss was calculated as follows:

$$100 \times (m_0\text{-}m_d)/m_0$$

...where m_0 means weight of the film before the experiment and m_d means weight of the dried sample after the experiment.

Water Absorption Test

Previously dried copolyester films were immersed in a Tris-HCl buffer solution (pH 8.50, 0.1 M) and in compost soil at 58ºC for 21 days in the laboratory. For each run, one specimen per tube with 10 ml of Tris-HCl solution or with 43 g of regularly wetted compost soil was maintained. Specimens were periodically removed and dried with filter paper before recording their weight gains. The specimens were reweighed and inserted back into the soil. Experiments were run in triplicate to determine mean values and standard deviations. The relationship used for calculation was as follows:

$$\textit{water uptake}\ (\%) = (m_w - m_0)/m_0 \times 100$$

...where m_0 denotes the initial weight of the film, and m_w denotes the weight of the film after exposure to water or soil.

Plant Material

Seeds used as plant material for testing were commercial seeds of cress (*Lepidium sativum*) and barley (*Hordeum vulgare*). Seeds were surface-sterilized by soaking for 2 min in a commercial sodium hypochlorite (2%) solution with a few drops of Tween-20. Then they were rinsed twice in sterile distilled water.

Phytotoxicity Test

Phytotoxicity of compost was investigated by means of a set of biotests using two test plants: cress (*Lepidium sativum*) and barley (*Hordeum vulgare*). The possible toxicological effect of soluble degradation products, which were released to the environment during copolyester composting, was assessed according to CSN EN 13432 on the growth of dicotyledonous plants. The medium was specialized soil for germination and plant growth, enriched with compost (25%, 50% w/w). Reference soil was composed of peat and silica sand. Each pot was filled with 200 g of medium, then 100 seeds were placed on the top and covered with a thin layer of silica sand. Plants were grown under controlled conditions for 21 days. Humidity at 70-100% of water absorption capacity, low light intensity, and the laboratory temperature were maintained to be constant. Values obtained from three simultaneously conducted experiments were averaged and presented (germination capacity, plant biomass).

Results and Discussion

The low water uptake was observed for all tested copolyester samples within the first few days of immersion both in the buffer and in the compost soil (Figs. 1a, b). During this period, the low absorption of water was related to the low rate of its diffusion into a copolyester matrix in a glassy state. The subsequent significant increase measured for copolymers A and B was ascribed to the increase in the

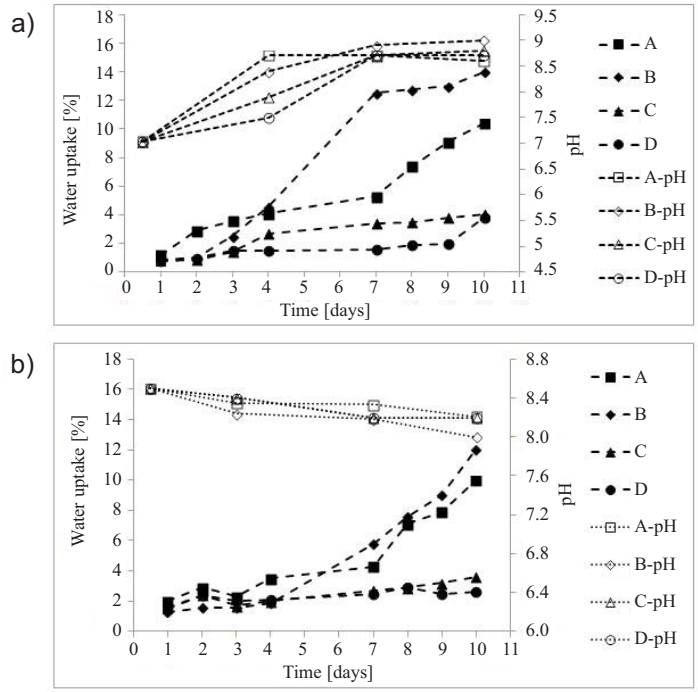

Fig. 1. Weight gained due to water absorption vs pH profile in compost soil (a) and in a Tris-HCl buffer (b); standard error was within 1%.

hydrophilic character of their surfaces due to the generation of hydroxyl and carboxylic groups as products of ester bonds hydrolysis.

The water uptake measured for samples C and D slightly increased over time, which reflects the occurrence of a hydrolytic scission even to a low extent. The development of acidic carboxylic groups was also confirmed by the decrease of pH value from 8.5 to about 8.0 in the Tris-HCl buffer. However, the pH value of compost soil reflected more microbial metabolism changes than the character of degradation products. This was due to its gradual increase from 7.0 to 9.0 during the experiment. Based on these results, copolyester samples with a higher initial content of L units (A, B) were proved to be more susceptible to hydrolytic scission than their counterparts rich in aromatic T units (C, D). The water uptake values of samples were almost the same independent of the incubation environment (soil vs. buffer) and thus the abiotic hydrolysis is supposed to occur dominantly during the initial period of composting.

The photographs (Fig. 2) document the extent of the copolyester specimen's disintegration after 21 days of composting. Hydrolytic scission of ester bonds resulted in the copolyester chains' degradation and loss of specimen integrity.

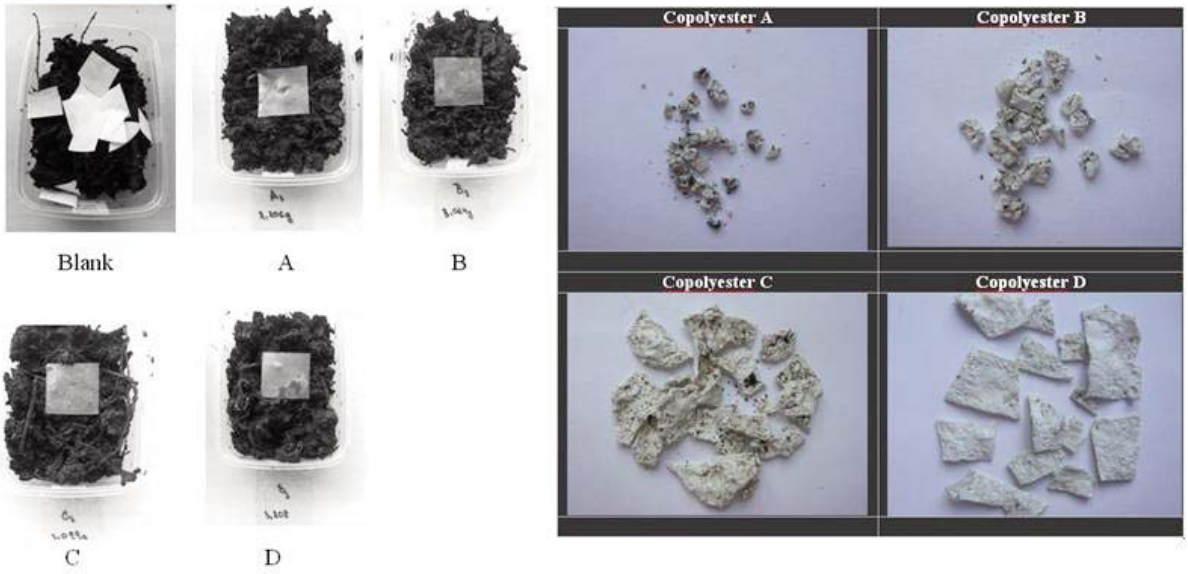

Fig. 2. Examined (composted) samples (A, B, C, and D) and one reference standard at the beginning (left photo) and at the end of the experiment (right photo).

Fig. 3. Layout of the phytotoxicity test.

After the disintegration test the weight losses of copolyesters with prevailing initial L units (A, B) corresponded to each other and were about 90%. The biodegradation rate of copolyesters decreased for sample C (weight loss of 39%) and dramatically for D (weight loss of 5%). These both possessed a dominant portion of aromatic T units with lower accessible ester bonds.

Degradation products released into the surrounding environment are supposed to be based on lactic acid. This was supported by the presence of lactic acid identified in buffer, where copolyesters were abiotically incubated for 21 days.

Phytotoxicity was performed according to instructions given in the standard ČSN EN 13432. Test layout: all dishes were filled with 200 g of the sample (mixture of reference substrate and compost after decomposition of the examined material) and 100 seeds were placed on the surface. The seeds were subsequently covered with a thin layer of inert material (quartz sand) (Fig. 3).

Three parallel determinations were made for each mixture. To prepared samples an amount of water was added to reach 70-100% of moisture-holding capacity. Photographs were taken to document the establishment of the trial (Figs. 3, 4). During the experiment, evaporated water was regularly added as needed. The dishes were kept in a dark place in the laboratory and were covered during the germination period.

Fourteen days after the establishment of the experiment, sprouts and the number of growing plants occurring in the dishes were counted. The data were plotted into tables and

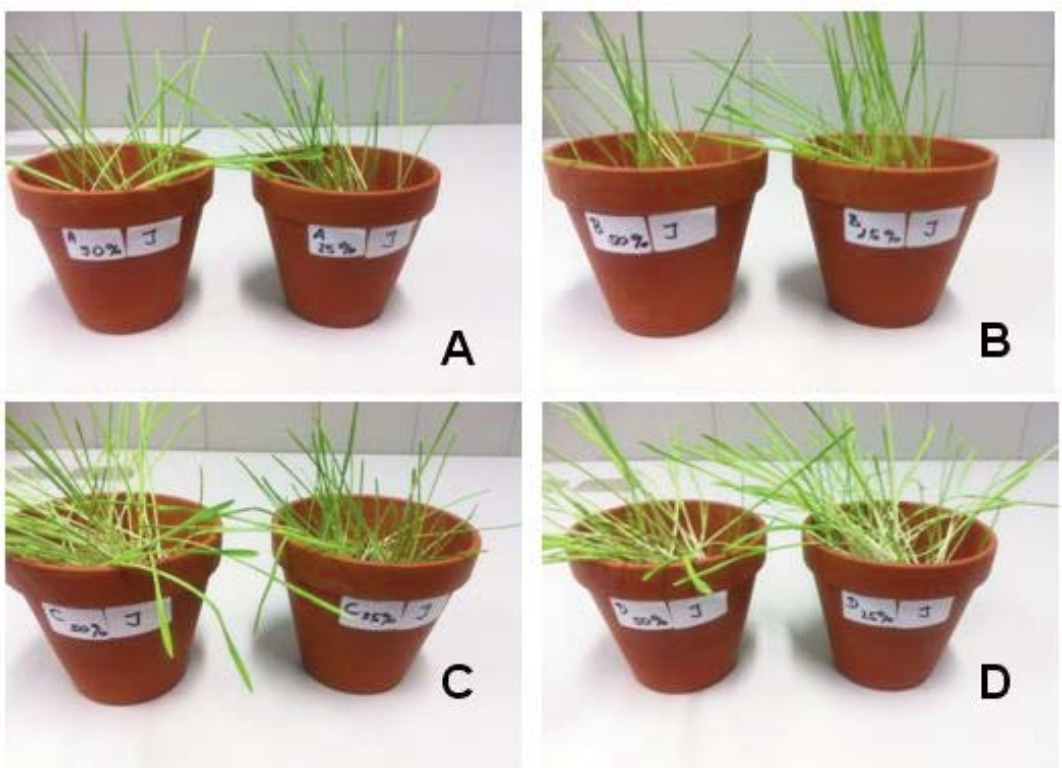

Fig. 4. Samples of *Hordeum vulgare* after 14 days.

Table 2. Germinating capacity of seeds – *Hordeum vulgare*.

Sample 25% (50 g)	14 days REF	21 days REF	Number of seeds sown	Number of seeds germinated		% of seeds germinated	
				14 days	21 days	14 days	21 days
A	50	59	100	37	51	74	86
B	50	59	100	45	63	90	107
C	50	59	100	54	85	108	144
D	50	59	100	56	78	112	132
Sample 50% (100 g)	14 days REF	21 days REF	Number of seeds sown	Number of seeds germinated		% of seeds germinated	
				14 days	21 days	14 days	21 days
A	50	59	100	35	41	70	69
B	50	59	100	36	44	72	74
C	50	59	100	44	88	88	149
D	50	59	100	46	71	92	120

Table 3. Germinating capacity of seeds – *Lepidium sativum*.

Sample 25% (50 g)	14 days REF	21 days REF	Number of seeds sown	Number of seeds germinated		% of seeds germinated	
				14 days	21 days	14 days	21 days
A	60	66	100	60	80	100	121
B	60	66	100	48	86	80	130
C	60	66	100	58	95	97	144
D	60	66	100	62	48	103	73
Sample 50% (100 g)	14 days REF	21 days REF	Number of seeds sown	Number of seeds germinated		% of seeds germinated	
				14 days	21 days	14 days	21 days
A	60	66	100	85	99	142	150
B	60	66	100	60	90	100	136
C	60	66	100	65	53	108	80
D	60	66	100	62	88	103	133

photographs were taken to document the course of the experiment. Germinating capacity and growth of *Hordeum vulgare* is shown in Fig. 4. Twenty-one days from the establishment of the experiment, the counting of sprouts and growing plants was repeated, the results were recorded, and photographs were taken.

The experiment was brought to an end after determination of results, and subsequent establishment of plant biomass. All plant biomass from the individual dishes was removed and weighed. Then it was desiccated in the Ecocell drier at 60ºC, and weighed on analytic digital scales Precisa 4000C; the measured values were recorded.

Results were evaluated from the acquired data. The number of sprouts (number of growing plants) and plant biomass on the compost samples and on the compost from the blank experiment were compared for all mixing ratios. Germinating capacity and plant biomass were calculated as a percentage share of corresponding values obtained from the compost in the blank experiment (see Table 2 – *Hordeum vulgare* and Table 3 – *Lepidium sativum*). Results in the tables (germinating capacity of seeds and plant biomass for the two plant species) are mean values obtained from the conducted experiment results.

The highest germinating capacity of *Hordeum vulgare* seeds (%) with a 25% proportion of compost upon the decomposition of samples after the elapse of 21 days was exhibited by sample C (144%), and the highest germinating capacity of seeds (%) with a 50% proportion of compost after the elapse of 21 days also was shown by sample C (149%).

The highest germinating capacity of *Lepidium sativum* seeds (%) with a 25% proportion of compost upon the decomposition of samples after the elapse of 21 days was

Table 4. Plant biomass – *Hordeum vulgare*.

Sample 25% (50 g)	Biomass weight REF [g]	Fresh biomass [g]	Fresh biomass against REF %	Dry biomass REF [g]	Dry biomass [g]	Dry biomass %
A	4.32	3.35	78	0.48	0.4	83
B	4.32	4.05	94	0.48	0.49	103
C	4.32	4.12	95	0.48	0.57	119
D	4.32	7.5	174	0.48	0.81	169
Sample 50% (100 g)	Biomass weight REF [g]	Fresh biomass [g]	Fresh biomass against REF %	Dry biomass REF [g]	Dry biomass [g]	Dry biomass %
A	4.32	3.31	77	0.48	0.39	81
B	4.32	2.58	60	0.48	0.34	71
C	4.32	8.17	189	0.48	0.84	175
D	4.32	6.22	144	0.48	0.63	131

Table 5. Plant biomass – *Lepidium sativum.*

Sample 25% (50 g)	Biomass weight REF [g]	Fresh biomass [g]	Fresh biomass against REF %	Dry biomass REF [g]	Dry biomass [g]	Dry biomass %
A	0.86	1.16	135	0.19	0.19	100
B	0.86	1.59	185	0.19	0.34	180
C	0.86	1.69	196	0.19	0.35	184
D	0.86	0.79	92	0.19	0.3	158
Sample 50% (100 g)	Biomass weight REF [g]	Fresh biomass [g]	Fresh biomass against REF %	Dry biomass REF [g]	Dry biomass [g]	Dry biomass %
A	0.86	1.56	181	0.19	0.28	147
B	0.86	1.23	143	0.19	0.29	153
C	0.86	1.03	120	0.19	0.3	158
D	0.86	1.06	123	0.19	0.26	137

exhibited by sample C (144%), and the highest germination capacity of seeds (%) with a 50% proportion of compost after the elapse of 21 days was shown by sample A (150%).

Fig. 5 shows the percentage expression of the germination capacity of *Lepidium sativum* (compost shares 25% and 50%) and *Hordeum vulgare* (compost shares 25% and 50%) after 14 days from the beginning of the experiment and after 21 days (end of the experiment).

Data about individual plant biomass weights of *Hordeum vulgare* and *Lepidium sativum* after the elapse of 21 days are summarized in Tables 4 and 5.

The weight of fresh biomass in the 25% and 50% samples of *Hordeum vulgare* ranged from 3.35 to 7.5 g and from 2.58 to 8.17 g, respectively. In the case of dry biomass, the values ranged from 0.4 to 0.81 g in sample 25% from 0.34 to 0.84 g in sample 50% of dry biomass.

The highest value of dry biomass (%) in *Hordeum vulgare* with a 25% proportion of compost upon the decomposition of samples after the elapse of 21 days was exhibited by sample D (169%), and the highest value of dry biomass in *Hordeum vulgare* with a 50% proportion of compost after the decomposition of samples was shown by sample C (175%).

The weight of fresh biomass in the 25% and 50% samples of *Lepidium sativum* ranged from 0.79 to 1.69 g and from 1.03 to 1.56 g, respectively. In the case of dry biomass, the values ranged from 0.19 to 0.35 g in a sample containing 25% and from 0.26 to 0.3 g in a sample containing 50% of dry biomass.

Sample C exhibited the highest values of dry biomass (%) in *Lepidium sativum* with a 25% and 50% proportion of compost upon the decomposition of samples after the elapse of 21 days in both cases (184% and 158%).

Fig. 6 presents a percentage expression of biomass weight for the seeds of *Lepidium sativum* (compost share 25% and 50%) and *Hordeum vulgare* (compost share 25% and 50%) 14 days from the beginning of the experiment and after 21 days (end of the experiment).

Conclusion

The standard EN 13432:2000: Packaging. Requirements for packaging recoverable through composting and biodegradation stipulates that the examined compost does not exhibit phytotoxicity if the indicator of germinated seeds and the increase of plant biomass are not lower than 90% as compared with plants growing on the control sample. The obtained results clearly demonstrate that the tested copolyesters buried in the compost have no toxic effect on plants. It can be stated that, compared to the reference sample, the germination and growth of plants

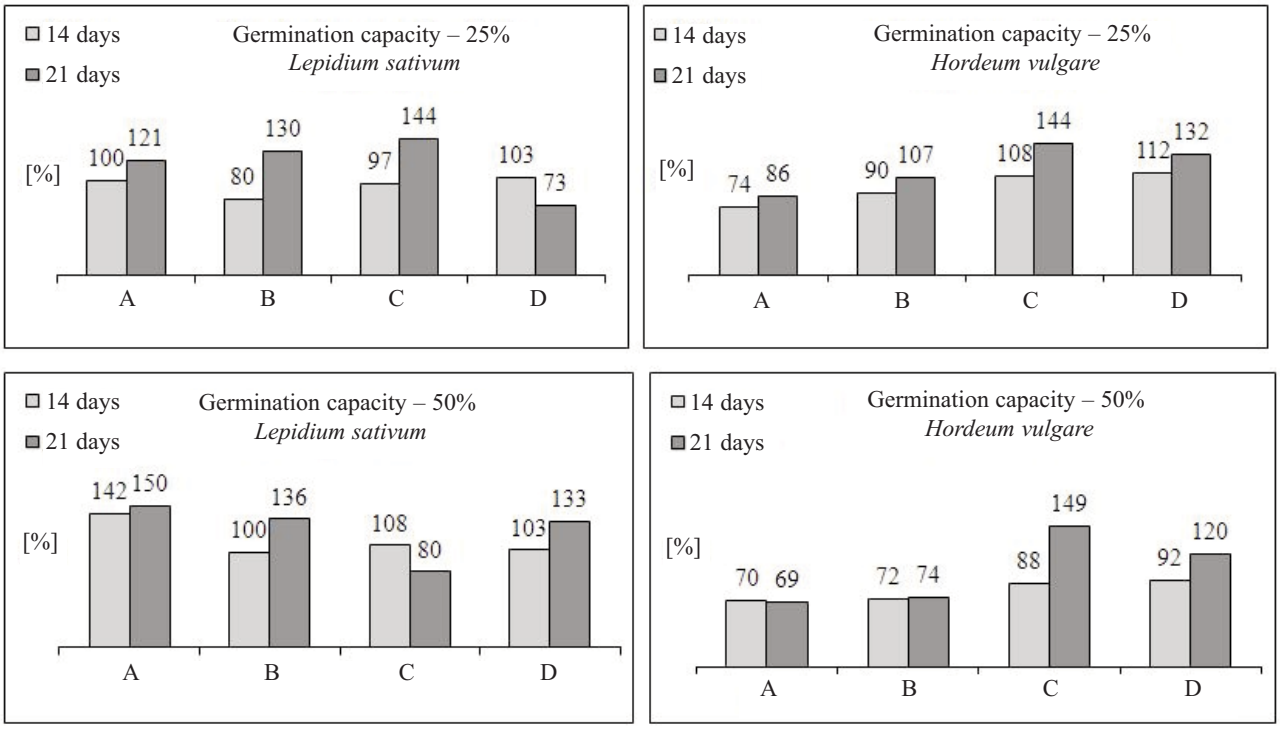

Fig. 5. Comparison of the germination capacity of *Lepidium sativum* and *Hordeum vulgare* seeds.

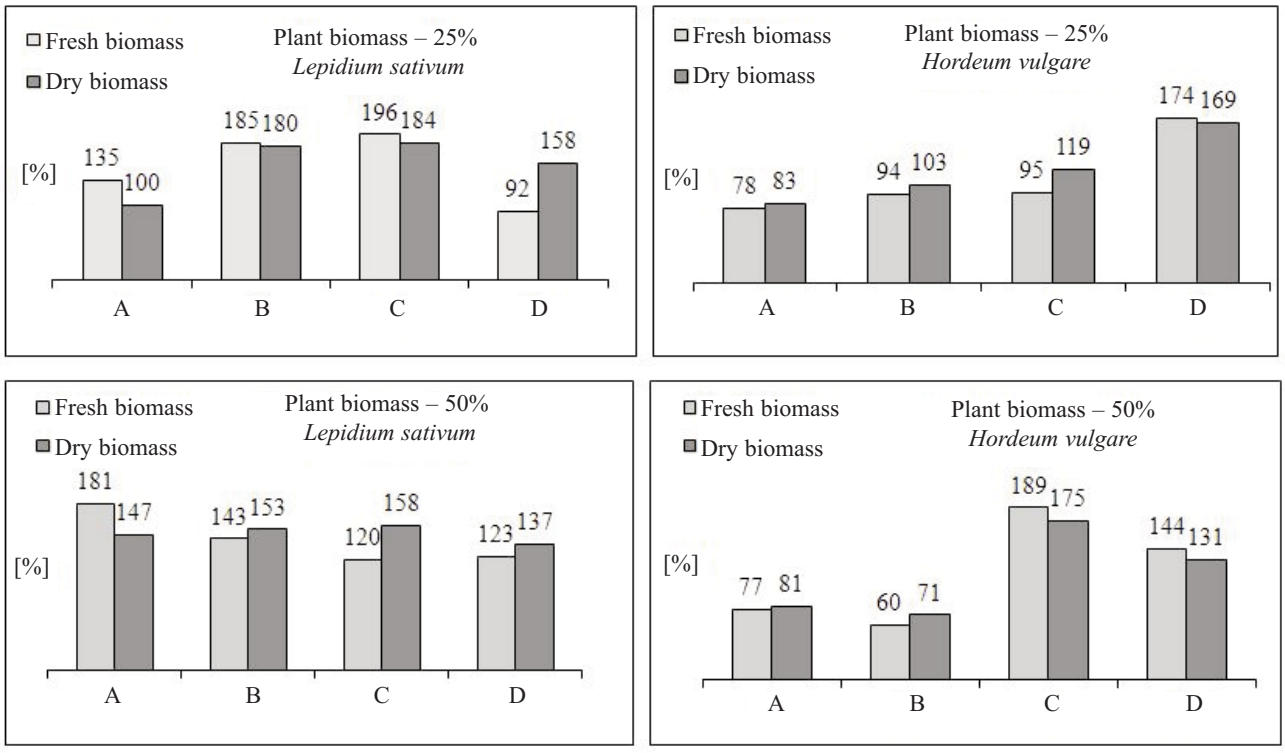

Fig. 6. Comparison of the biomass of *Lepidium sativum* and *Hordeum vulgare*.

were stimulated. The plants growing in the dishes with the compost samples showed an increase in plant biomass. Changes in appearance, retarded growth, or necrotic changes were not recorded.

After the decomposition of the examined materials, the resulting compost did not exhibit any unfavourable influence on the process of composting or compost quality, and the products of degradation affected the growth and development of plants (general biomass increase) positively, too.

References

1. LEJA K., LEWANDOWICZ G. Polymer Biodegradation and Biodegradable Polymers – a Review. Pol. J. Environ. Stud. **19**, (2), 255, **2010**.
2. YRIKOU J., BRIASSOULIS D. Biodegradation of Agricultural Plastic Films: A Critical Review. J. Polym. Environ. **15**, (2), 125, **2007**.
3. WHITE P., FRANKE M., HINDLE P. Integrated solid waste management: a lifecycle inventory. Chapmann & Hall. pp. 368, **1994**.
4. CHO HS., MOON HS., KIM M., NAM K., KIM JY. Biodegradability and biodegradation rate of poly(caprolactone)-starch blend and poly(butylene succinate) biodegradable polymer under aerobic and anaerobic environment. Waste Manage. **31**, (3), 475, **2010**.
5. ABOU-ZEID D-M., MÜLLER R-J., DECKWER W-D. Degradation of natural and synthetic polyesters under anaerobic conditions. J. Biotechnol. **86**, (2), 113, **2001**.
6. CZAJA-JAGIELSKA N., MELSKI K. Biodegradation of Starch-Based Films in Conditions of Nonindustrial Composting. Pol. J. Environ. Stud. **22**, (4) 1039, **2013**.
7. RUTKOWSKA M., KRASOWSKA K., HEINOWSKA A., STEINKA I. JANIK H., HAPONIUK J., KARLSSON S. Biodegradation of Modified Poly(ε-caprolactone) in Different Environments. Pol. J. Environ. Stud. **11**, (4), 413, **2002**.
8. DOMKA L., MALICKA A., JAGŁA K., KOZAK A. Biodegradation of Starch-Modified Foil in Natural Conditions. Pol. J. Environ. Stud., **18**, (2), 191, **2009**.
9. VAVERKOVÁ M., TOMAN F., ADAMCOVÁ D., KOTVICOVÁ, J. Study of the biodegrability of degradable/biodegradable plastic material in a controlled composting environment. Ecol. Chem. Eng. **19**, (3), 347, **2012**.
10. VAVERKOVÁ M., ADAMCOVÁ D., KOTVICOVÁ J., TOMAN F. Evaluation of biodegradability of plastics bags in composting conditions. Ecol. Chem. Eng. **21**, (1), 45, **2014**.
11. ADAMCOVÁ D., VAVERKOVÁ M., TOMAN F. Repeated research of biodegradability of plastics materials in real composting conditions. Acta Univ. Agric. et Silvic. Mendel. Brun. **61**, (6), 1557, **2013**.
12. KOPEĆ M., GONDEK K., BARAN A. Assessment of respiration activity and ecotoxicity of composts containing biopolymers. Ecotox. Environ. Safe. **89**, (1), 137, **2013**.
13. KAPANEN A., ITÄVAARA M. Ecotoxicity Tests for Compost Applications. Ecotox. Environ. Safe. **49**, (1), 1, **2001**.
14. DIAZ L.F., DE BERTOLDI M., BIDLINGMAIER W., STENTIFORD E. Compost science and technology. Waste Management Series; V. **8**, 364, **2007**.
15. DUBOVA L., ZARINA D. Application of toxkit microbiotest for toxicity assessment in soil and compost. Environ Toxicol. **19**, 274, **2004**.
16. OLESZCZUK P. The toxicity of compost from sewage sludges evaluated by direct contact tests Phytotoxkit and Ostracodotoxkit. Waste Manage. **28**, 1645, **2008**.
17. OLESZCZUK P. Toxicity of light soil fertilized by sewage sludge or compost in relation to PAHs kontent. Water Air Soil Poll. **210**, 347, **2010**.
18. WARMAN P.R. Evaluation of seed germination and growth test for assessing compost maturity. Compost Sci Util. **7**, 33, **1999**.
19. HADAM A., OBIDOWSKA G. Phytotoxicity and gentoxicity of heavy metals in composts produced from urban wastes. Environ Prot Nat Resour. **41**, 332, **2009** [In Polish].
20. ARAUJO A.S.F., MONTEIRO R.T.R. Plant bioassays to assess toxicity of textile sludge kompost. Sci Agri. **62**, (3), 286, **2005**.
21. MITELUT A.C., POPA M.E. Seed germination bioassay for toxicity evaluation of different composting biodegradable materials. Rom Biotech Lett. **16**, (1), 121, **2011**.
22. PROKOPOVÁ I. TUREČKOVÁ J., NIKLOVÁ P., ŠIMEK J., ŠMEJKALOVÁ P., KECLÍK F., Biodegradable copolyester/starch blends-preparation, mechanical properties, wettability, biodegradation course. Polimery, **53**, 639, **2008**.